Key Enzymes of Sphingolipid Biosynthesis

Beverley A. Yard

A Thesis Submitted for the Degree of Doctor of Philosophy

The University of Edinburgh 2008

Contents

Acknowledgements

Firstly, I would like to thank my supervisors: Dr Dominic Campopiano for his help and advice throughout the course of my PhD and Professor Bob Baxter for his advice and critical reading of my work. Secondly, I would like to thank all of Lab 229 both past and present for making the last 3 years "interesting" to say the least. In particular, Dr. Dave Clarke and Dr. Paul Bilton for answering my numerous questions with patience and Josefin for keeping me sane!

I would also like to thank Prof. Jim Naismith, Dr. Lester Carter and Dr. Ken Johnson at the SSPF, St. Andrews for all their help with the SPT structure, Dr. Andy Corran and Dr Shradha Singh (Syngenta) for their help with Aur1p project and Syngenta for funding and last but not least, Dr Kevin Hardwick (Wellcome Trust Centre for Cell Biology, University of Edinburgh) for help and advice on yeast transformations.

Finally, I would like to thank my family for their constant support throughout my PhD (in particular Garry, who can now pronounce sphingolipid biosynthesis) but most of all, I would like to dedicate this work to my Pa, who would have been so proud.

Abstract

Sphingolipids are not only ubiquitous structural components of the plasma membrane they are also involved in many important cellular process such as cell signalling, signal transduction and the immune response. Serine palmitoyltransferase (SPT) catalyses the first and rate limiting step of sphingolipid biosynthesis; a decarboxylative, Claisen condensation of the amino acid L-serine and the long chain fatty acid palmitoyl CoA to produce the first sphingolipid precursor 3-ketosphinganine (KDS). SPT is a membrane-associated heterodimer in eukaryotes making its isolation and characterisation challenging. However, a cytoplasmic, homodimeric homologue has been identified from the Gram-negative bacterium *Sphingomonas paucimobilis*. This organism has a unique outer membrane structure that contains glycosphingolipid (GSL) instead of lipopolysaccharide (LPS, endotoxin) as found in most other Gram-negative bacteria. As yet, no bacterial sphingolipid pathway has been characterised in detail, so we propose *S. paucimobilis* as a model organism for the characterisation of sphingolipid biosynthesis.

SPT belongs to the α-oxoamine synthase family, which are a small group of pyridoxal 5'-phosphate (PLP)-dependent enzymes. This thesis describes spectroscopic studies of recombinant SPT and reports high-resolution crystal structures of the PLP-, L-serine- (substrate) and L-cycloserine- (inhibitor) bound forms of *S. paucimobilis* SPT (1.3, 1.5 and 1.45 Å respectively). These structures are the first of an SPT from any organism and provide an insight into the mechanisms of catalysis and inhibition that take place at the active site of this important enzyme.

Another interesting sphingolipid biosynthetic enzyme is Inositol Phosphorylceramide Synthase (IPCS; also known as AUR1p) which, is encoded by the *aur1* gene and catalyses the transfer of phospho-inositol onto phytoceramide to produce inositol phosphorylceramide (IPC). Deletion or mutation of this gene in *S. cerevisiae* was found to be lethal, therefore highlighting the importance of this enzyme and since it is unique to fungi, AUR1p provides

an attractive target for the development of novel anti-fungal agents. However, it is an integral membrane protein of the Golgi apparatus, with 6 predicted transmembrane domains which means that to date, no structural information is available. Expression of a recombinant, soluble, affinity-tagged AUR1p now paves the way for full characterisation of this important enzyme.

Figures

Tables

Abbreviations

Å	Angstrom
°C	Degrees Celsius
λ_{max}	Absorbance maximum
AAT	Aspartate amino transferase
AbA	Aureobasidin A
ABC	ATP binding cassette
ALAS	5-aminolevulinic acid synthase
AON	8-amino-7-oxononanoate
AONS	8-amino-7-oxononanoate synthase
AOS	Alpha oxoamine synthase
AOX	Alcohol oxidase
AUR1	Wild type gene encoding Aur1 protein
AUR1-C	Gene encoding Aur1 protein containing double point mutations F158Y and A240C
Aur1p	Protein encoded by the *AUR1* gene
Aur1-C	Protein encoded by the *AUR1-C* gene
BCA	Bicinchoninic acid
BLAST	Basic Local Alignment Search Tool
bp	Base pair(s)
Bq	Bequerel
µCi	Micro-Curie
C_6-NBD-Cer	C_6-NBD-Ceramide, N-[6-[(7-nitro-2-1,3-benzoxadiazol-4-yl)amino]hexanoyl]-D-*erythro*-sphingosine
CD_4	Cluster of differentiation 4 (a glycoprotein expressed on the surface of T helper/regulatory cells, monocytes, macrophages and dendritic cells
CFTR	Cystic fibrosis transmembrane receptor
CHO	Chinese hamster ovary
CoA	Co-enzyme A
CTTL	Cytotoxic T cell line
Da	Daltons
DAG	Diacylglycerol
DCS	D-cycloserine

DHS	Dihydrosphinganine
DNA, cDNA	Deoxyribonucleic acid, clone DNA derived from complementary DNA
EDTA	Ethylene diaminetetracetic acid
ER	Endoplasmic reticulum
FLAG	Polypeptide protein tag (N-DYKDDDDK-C)
g, mg, mg	Gram, milligram, microgram
α-GalCer	α-Galactosylceramide
Gal	Galactose
GalCer	Galactosylceramide
GFP	Green fluorescent protein
GlcA	Glucuronic acid
GlcN	Glucosamine
GluCer	Glucosylceramide
GM_1	Monosialotetrahexosylganglioside
GSL	Glycosphingolipid
GSL-1	Glycosphingolipid modified by the addition of a monosaccharide
GSL-4A	Glycosphingolipid modified by the addition of a tetrasaccharide
GST	Glutathione-S-transferase
His_6	Six consecutive histidine residues
HIV	Human immunodeficiency virus
HSAN1	Hereditary sensory and autonomic neuropathy type-I
IC_{50}	The concentration of inhibitor required to inhibit 50% activity of an enzyme
IFN-γ	Interferon-γ
IgG	Immunoglobulin G
IL-1/2/4/6	Interleukin-1/2/4/6
INVSc1	Invitrogen *S. cerevisiae* strain auxotrophic for uracil
IPC	Inositol phosphorylceramide
IPTG	Isopropyl β-D-1-thiogalactopyranoside
K_1	Dissociation constant for L-serine binding
K_2	Dissociation constant for external aldimine formation
k_{app}	Apparent rate constant
K_{obs}	Observed rate constant
K_d^{app}	Apparent dissociation constant

KBL	2-amino-3-ketobutyrate-CoA ligase
kDa	kilodalton
KDS	3-ketosphinganine
KPhos	Potassium phosphate buffer containing both the monobasic and dibasic salts
L, ml, ml	Litre, millilitre, microlitre
LB	Luria Bertani
lcb1/lcb2	Genes encoding LCB1/LCB2 protein subunits
LCB1/LCB2	Proteins encoded by *lcb1/lcb2* genes
LCB	Long chain base
LC-MS	Liquid chromatography mass spectrometry
LCS	L-cycloserine
LPS	Lipopolysaccharide
M, mM, mM, nM	Molar, millimolar, micromolar, nanomolar
MALDI-ToF	Matrix Assisted Laser Desorption Ionization Time-of-Flight
Man	Mannose
MDR	Multi drug resistance
MGY	Minimal glycerol medium
MIC	Minimal inhibitory concentration, the lowest concentration of antimicrobial agent that inhibits the growth of a microorganism
MM	Minimal methanol medium
MOPS	3-(N-morpholino)propanesulfonic acid
nm	Nanometre
Ni	Nickel
NKT cells	Natural Killer T cells
NTA	Nitrilotriacetic acid
OD	Optical density
ORF(s)	Open reading frame(s)
PBS	Phosphate buffered saline
PBST	Phosphate buffered saline, Tween-20
PBSTM	Phosphate buffered saline, Tween-20, milk
PCR	Polymerase chain reaction
PI	Phosphatidyl inositol
PLP	Pyridoxal 5'-phosphate

PMP	Pyridoxamine 5'-phosphate
R_f	The retention factor, the distance travelled by the compound divided by the distance travelled by the solvent in TLC.
RNA, mRNA	Ribonucleic acid; messenger RNA
rpm	Rotations per minute
S-1-P	Sphingosine-1-phosphate
Sc	*Saccharomyces cerevisiae*
SDS-PAGE	Sodium dodecyl sulphate polyacrylamide gel electrophoresis
SM	Sphingomyelin
SMase	Sphingomyelinase
SPT	Serine palmitoyl transferase
TAP	Tandem affinity purification
TEMED	N,N,N',N'-tetramethylethylenediamine
TEV	Tobacco etch virus
TLC	Thin layer chromatography
TMH	Trans membrane helix
Tris	Tris (hydroxymethyl) aminomethane
Tris-Cl	Tris (hydroxymethyl) aminomethane, pH obtained with hydrochloric acid
Triton X-100	Octylphenolpoly(ethyleneglycolether)$_n$
UV	Ultraviolet
v/v	Volume to volume
w/v	Weight to volume
YPD	Yeast extract peptone dextrose medium

Chapter 1: Sphingolipid Biosynthesis

1.1 Sphingolipid Structure

During his studies in the field of brain chemistry in the 1800's, the German scientist J.L.W. Thudichum examined the presence of a mixture of substances within the matter of the brain. He showed that this mixture consisted of lecithins, cephalins and myelins and also correctly classified the latter two as phosphatides. Moreover, he identified sphingomyelin, the sulphatides and the cerebrosides (*1, 2*). He characterised the molecule sphingosine, **7** suggesting that the structure contained an amino acid and that it had basic properties. Following Thudichum's death, Levine and co-workers confirmed the structure of sphingosine as an unsaturated monoaminodihydroxyalcohol (*3*). Subsequently, Carter *et al.* elucidated the structure of sphingine to be 1-hydroxy-2-aminooctadecane and the O-methyl esters of sphingosine to be 1-hydroxy-2-amino-3-methoxyoctadec-4-ene (*4, 5*). This early pioneering work, together with the development of various methodologies for the isolation and characterization of sphingolipids, has provided the basic structure upon which all sphingolipids are based (**Fig. 1**) (*6*). The basic sphingolipid structure consists of a sphingoid base (1, 3-dihydroxy-2-amino-alkane and its derivatives) attached to a long chain fatty acid through an *N*-acyl linkage.

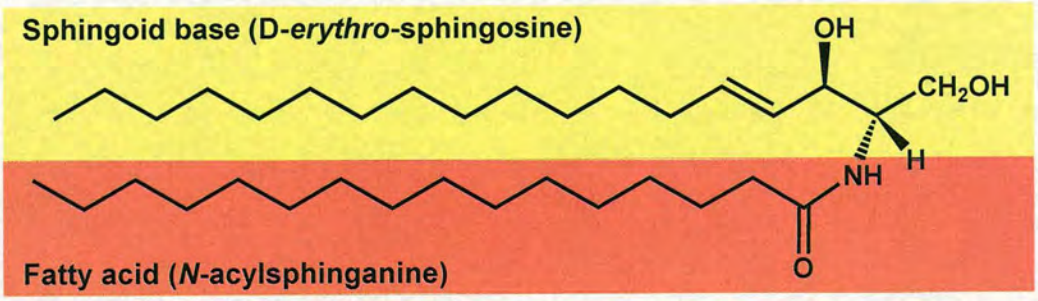

Figure 1: Basic Sphingolipid Structure
The basic sphingolipid structure is derived from a sphingoid base joined by a *N*-acyl linkage to a long chain fatty acid (*7*). The addition of a polar head group onto the 1-hydroxy position gives the molecule distinctive properties e.g. addition of phosphate produces sphingosine-1-phosphate, a potent anti-apoptotic molecule (*8, 9*).

The sphingoid base moiety differs between species, for example in mammals, it is commonly D-*erythro*-sphingosine (a C18 hydroxylated alkene), in *S. cerevisiae* 4-hydroxysphinganine

(phytosphingosine, a linear C18 or C20 alkane) is the main sphingoid base whereas in plants this portion varies due to the synthesis of a diverse composition of unsaturated D-*erythro*-sphingosine derivatives (*10, 11*).

The moiety (R) attached to the 1-hydroxy position of the sphingoid base varies (**Fig. 1**), resulting in a high level of heterogeneity amongst sphingolipid molecules. For example, in mammals a phosphate may be added by sphingosine kinase to form sphingosine-1-phosphate or phospho-choline by sphingomyelin synthase to form sphingomyelin (*12*). In contrast, inositol-phosphate is attached to phytoceramide to produce inositol phosphorylceramide (IPC) in fungi, thus creating a difference between the eukaryotic sphingolipid pathways (*10*).

1.2 The Sphingolipid Pathway

Sphingolipid biosynthesis begins with the decarboxylative condensation of the amino acid L-serine and the long chain fatty acid palmitoyl CoA. This step, which has been found to be rate limiting, produces the first sphingolipid precursor 3-ketosphinganine (KDS) and is catalysed by serine palmitoyltransferase (SPT) (*13*). KDS is subsequently reduced to form dihydrosphinganine, **7** and it is at this stage where the two eukaryotic pathways diverge (**Fig. 2**). In mammals, phospho-choline is attached to ceramide to form sphingomyelin whereas in fungi, inositol-phosphate is added to phytoceramide forming inositol phosphorylceramide. These molecules are modified further by the addition of one or more carbohydrate moieties to produce the glycosphingolipids which include the cerebrosides and gangliosides.

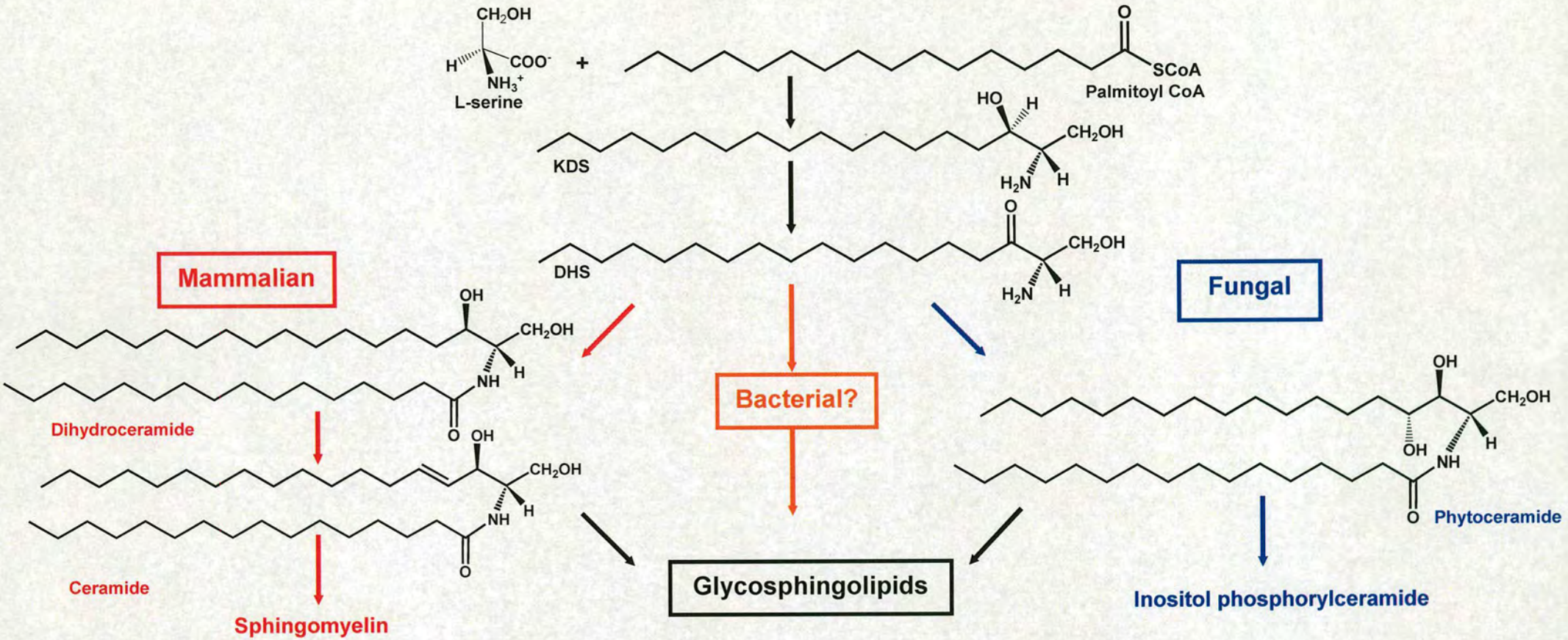

Figure 2: The Sphingolipid Pathway

Sphingolipid biosynthesis commences with the decarboxylative, Claisen condensation of L-serine and palmitoyl-CoA to produce the first sphingolipid precursor 3-ketosphinganine (KDS). KDS is subsequently reduced to form dihydrosphinganine (DHS) and it is, at this point, that the pathway diverges amongst eukaryotes. In mammals the addition of phospho-choline onto ceramide forms sphingomyelin (see **fig. 3** for structure) whereas in fungi, phospho-inositol is added to phytoceramide forming inositol phosphorylceramide (see **fig. X** for structure). Ceramide may also be glycosylated to form the glycosphingolipids, which can be further modified by the addition of more carbohydrate molecules. To date, no bacterial sphingolipid pathway has been identified however the studies discussed in this thesis suggest the existence of such a pathway. All structures are sourced from http://www.lipidmaps.org.

1.3 Sphingolipid Metabolism

Sphingolipids and their metabolites play important roles not only in cell signalling and signal transduction, but also in the immune response and in pathological conditions such as neurodegeneration and cancer. Sphingomyelin, for example, is an important lipid located in the plasma membrane of mammalian cells. Not only does it provide structural support within the membrane but it also takes part in the ubiquitous signalling system referred to as the "sphingomyelin cycle" (*14, 15*). Together with cholesterol, alterations in sphingomyelin levels have been associated with Alzheimer's disease. This occurs when amyloid beta peptide 42 activates sphingomyelinase (SMase) leading to the reduction of sphingomyelin levels (*16*). Extracellular inducers, such as tumour necrosis factor alpha (TNFα), have been shown to activate SMase in HL-60 human promyelocytic leukaemia cells causing hydrolysis of membrane sphingomyelin to produce phosphocholine and ceramide (*17*).

Ceramide is another important cellular lipid and might be thought of as the central molecule in sphingolipid metabolism as it is the first biosynthetic precursor of all glyco- and phospho-sphingolipids such as galactosylceramide and sphingomyelin. It has been proposed that a delicate and finely balanced equilibrium exists between ceramide and its metabolites in the control of cellular functions such as signal transduction (**Fig. 3**) (*18*).

The implication of ceramide in programmed cell death has been discussed extensively and its involvement in pathological processes such as neurodegeneration and cancer have been highlighted (*18-20*). For example, by studying the conversion of ceramide to ceramide-1-phosphate using diacylglycerol kinase and radiolabelled ATP, Riboni *et al.* showed that decreased levels of ceramide in association with human astrocytoma tissue in comparison with levels found in the surrounding peritumoural tissue. This suggests a reduction of the cellular ceramide levels in the progression of human astrocytomas which may be advantageous to the cancer cell as it may prevent apoptosis thereby allowing rapid tumour growth (*21*).

In contrast, Huang *et al.* observed increased expression of acid ceramidase in Alzheimer's diseased brain (*22*). They noted an association of acid ceramidase with the pathological neurofibrillary tangles, however the relative levels of the substrate ceramide and the hydrolysis product sphingosine were not determined. Acid ceramidase catalyses the catabolism of ceramide to produce sphingosine, high levels of which are cytotoxic, hence the enzyme is maintained at low levels within the cell. Sphingosine has a direct effect on cellular sphingolipid content as this molecule can be *N*-acylated to form ceramide or phosphorylated to produce sphingosine-1-phosphate. In contrast to ceramide, sphingosine-1-phosphate (S-1-P) is an anti-apoptotic signalling molecule. It has been identified as a component of the intracellular second messenger system involved in calcium mobilisation and the regulation of sphingosine induced cell growth (*8, 9*). Olivera *et al.* found that sphingosine kinase expression altered the balance of sphingolipid metabolites causing elevated levels of S-1-P with a concomitant decrease in the levels of sphingosine and ceramide (*23, 24*). Their results showed that sphingosine kinase expression in HEK293 and Jurkat T cells, as well as 3T3 fibroblasts, suppressed serum deprived apoptosis which is known to result in elevated ceramide levels.

As with all signalling molecules, cellular levels of S-1-P are tightly regulated and its production and degradation can be rapidly induced. For example, the expression of sphingosine kinase, to produce S-1-P in response to signal transduction pathways, is activated by the potent mitogens platelet derived growth factor and foetal calf serum and by the rapid production of S-1-P in response to mitogenic concentrations of sphingosine (*24, 25*).

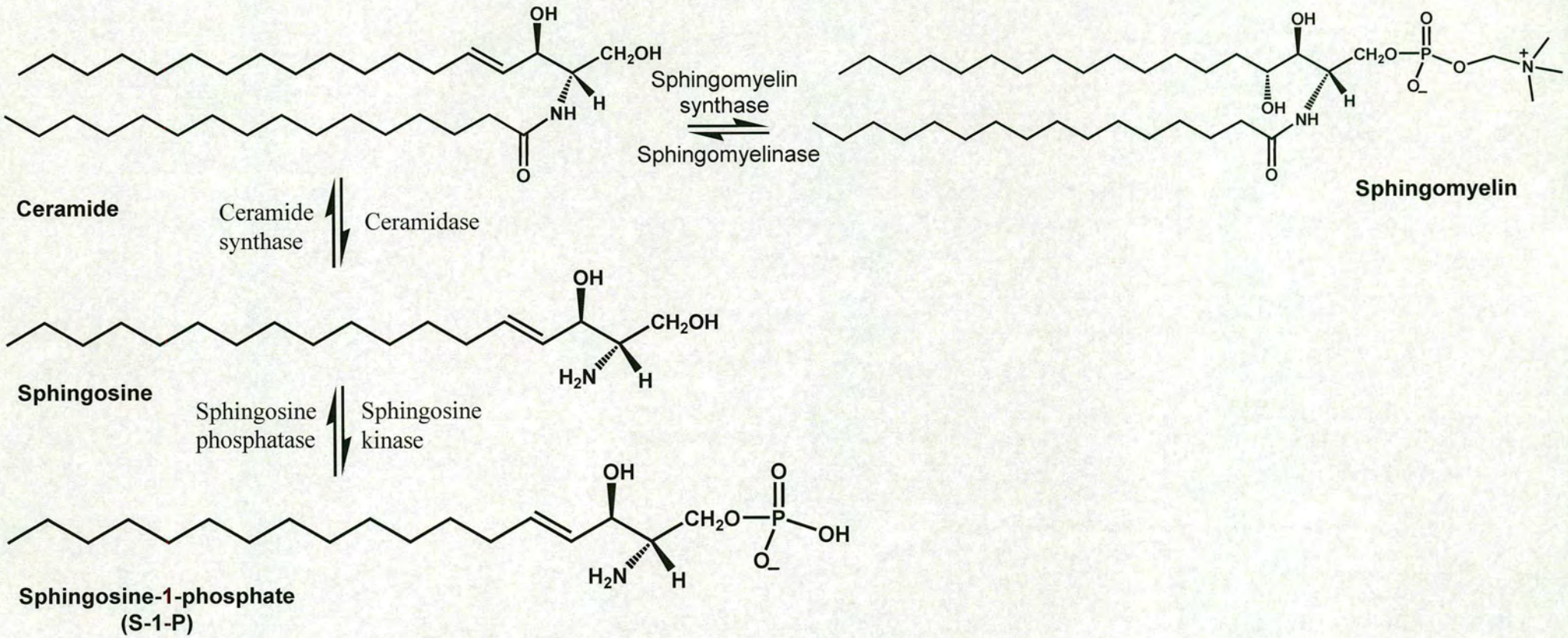

Figure 3: Ceramide Metabolism

Ceramide and its metabolites (sphingomyelin and sphingosine-1-phosphate, S-1-P) are important signalling molecules and exist in a tightly controlled equilibrium. Disruption of this equilibrium has been implicated in numerous pathological diseases such as neurodegeneration and cancer (*18-20*).

1.4 Glycosphingolipids

Glycosphingolipids form an extremely diverse group of complex sphingolipids and are exploited by many bacteria, viruses, parasites and microbial toxins when binding to host organisms (*26*). This diversity arises from variations in sugar type, number, linkage and modifications. For example, the most simple glycosphingolipids are the cerebrosides which consist of a ceramide moiety with a single sugar residue (glucose or galactose) attached at the 1-hydroxyl position. Two examples are galactosylceramide, **1** which, in mammals, is typically found in neural tissue and glucosylceramide, **2** which is common in most other tissues (**Fig. 4**). Galactosylceramides are restricted to animals and fungi whereas glucosylceramides are commonly found in plants, animals and fungi (*27*).

Both of these molecules are important for cellular function as it has been shown that alterations to their concentrations lead to pathogenic disorders. For example, the accumulation of glucosylceramide, due to an autosomally inherited deficiency of glucocerebrosidase, causes the rare lysosomal storage disorder known as Gaucher disease (*28*). Autosomally recessive inherited mutations of the galactocerebrosidase gene cause an accumulation of galactosylceramide resulting in segmental demyelination of peripheral nerves. (*29*). This is followed by the onset of Krabbe's disease which is characterised by diffuse leukodystrohphy; the severe degeneration of mental and motor skills (*30*).

In addition to the cerebrosides, there are more the complex glycosphingolipids known as gangliosides which were originally isolated and identified from brain tissue by Ernst Klenk in the 1940's, however the heterogeneity amongst brain gangliosides was not demonstrated until a decade later by Svennerholm (*31*). Although they are most abundant in neural tissue, gangliosides are also found at low levels in all animal tissues where they are concentrated, together with other glycosphingolipids, into lipid rafts. Structurally, they consist of ceramide, an oligosaccharide moiety and one or more sialic acid constituents. The structure of the prototypic ganglioside, GM1 (monosialotetrahexosylganglioside, **3**) is shown in **figure 4**.

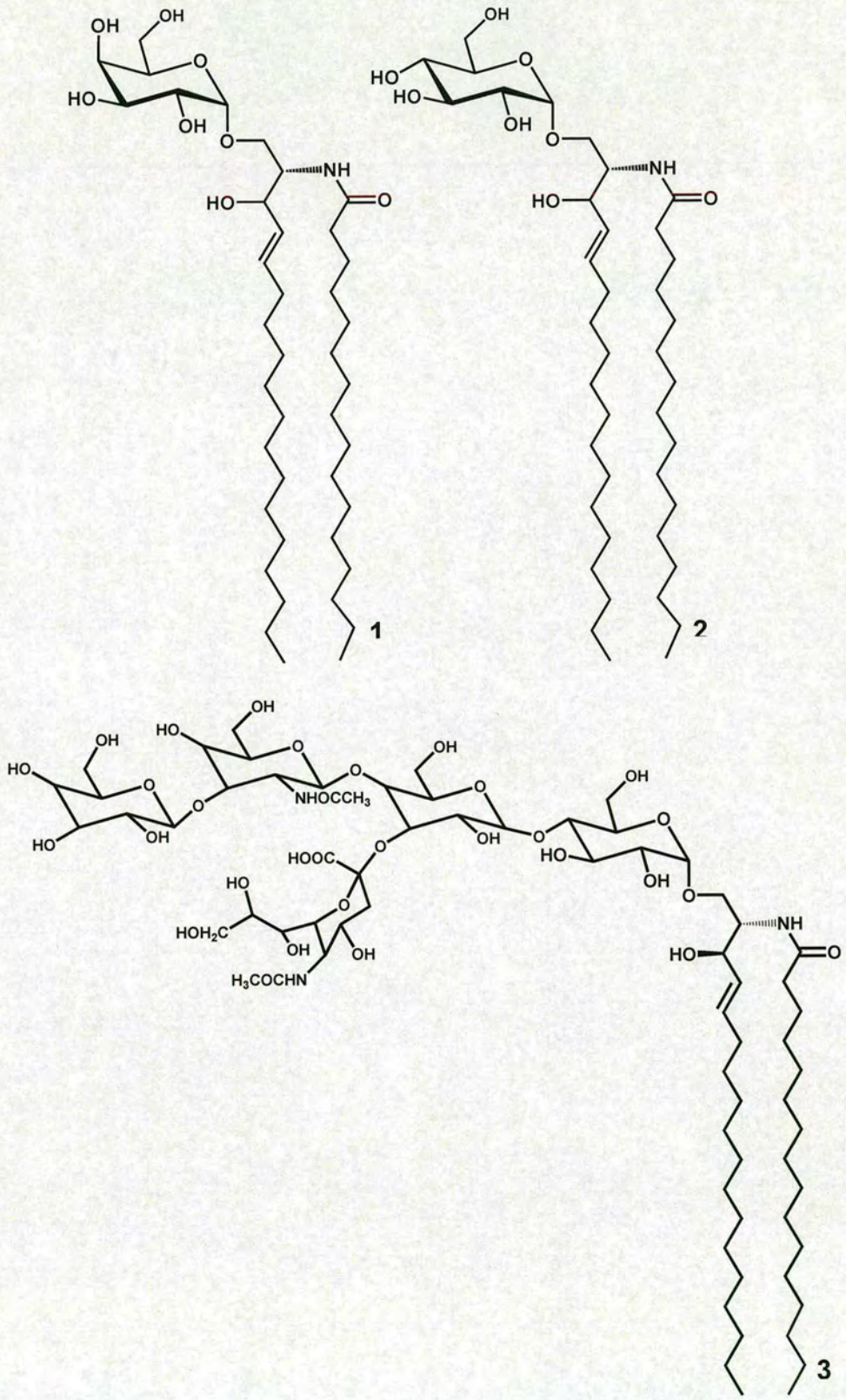

Figure 4: Structures of the Cerebrosides GalCer and GluCer and the Ganglioside GM1 The sugar group is attached in the α-anomeric position in the cerebrosides GalCer, **1** and GluCer, **2** to produce biologically active molecules. The prototypic ganglioside GM1 (monosialotetrahexosylganglioside, **3**) is a more complex tetrasaccharide.

1.5 The Role of Sphingolipids in Lipid Rafts and The Immune Response

In addition to their involvement in neurodegeneration and cancer, sphingolipids also play a role in infectious disease, as they can be exploited by various pathogens in order to gain access into the host cell. The plasma membrane is a crucial element during host-pathogen interactions and contains primarily sphingolipids, cholesterol and phospholipids which interact within the membrane to form different domains. Sphingolipids and cholesterol preferentially associate to form mobile membrane microdomains known as lipid "rafts". These rafts have been referred to as "detergent resistant" in comparison to phospholipids which are "detergent soluble" and their presence creates different environments within the membrane (*32-34*). It has been suggested that these rafts allow the attachment of specific proteins within the lipid bilayer and that the lipid microdomains are organized such that proteins can be selectively included or excluded. This allows the transport of selected membrane components and can potentially act as a platform for intracellular signalling (*35*). It has been proposed that viral entry through mucosal epithelial cells requires the presence of lipid rafts, in particular, the sphingolipid component of the raft. This has been studied for human immunodeficiency virus (HIV) where it has been shown that the treatment of virus-producing cells or virus particles with raft-disrupting agents significantly impairs virus infectivity (*36*). In addition, it has been observed that CD4-negative cell lines are still susceptible to infection with various HIV strains, therefore, although it is the major cellular receptor for HIV, CD4 appears not to be the only mode of infection. Studies by Harouse *et al.* have shown that antibodies raised against galactosylceramide (GalCer) inhibited viral internalization and infection in two CD4-negative cell lines derived from the nervous system, U373-MG and SK-N-MC, suggesting that GalC may play a role in HIV infection of neural cells (*37*).

In addition to viral recognition, their actions as agonists in the immune response have also been documented. Wu *et al.* and Kinjo *et al.* have described the ability of bacterial glycosphingolipids to activate human and murine Natural Killer T (NKT) cells (*38, 39*). Alpha-galactosyl ceramide (α-GalCer) is a well known NKT cell agonist which acts by binding to CD1 receptors which are antigen-presenting proteins that bind and display various lipids to T-lymphocytes. Wu *et al.* found that microbial derived α-GalCer from *Sphingomonas wittichii* activated NKT cells causing cytokine IFN-γ and IL-4 release. By CD1d dimer/glycolipid staining of the NKT cell line they also showed NKT cell reactivity toward bacterial glycosphingolipids *(39)*.

Krziwon *et al.* compared the activation of monokine release by the common Gram-negative bacterial membrane constituent lipopolysaccharide (LPS) with glycosphingolipids from the unusual LPS lacking Gram-negative bacterium *Sphingomonas paucimobilis*. Two forms of glycosphingolipid were isolated from *S. paucimobilis* by Kawahara *et al.*, the tetrasaccharide GSL-4A and the monosaccharide GSL-1 (*40*). Studies show that the tetrasaccharide GSL-4A activates monokine production whereas GSL-1 does not. In comparison to LPS, a 10,000 fold higher concentration of GSL-4A was required to induce the release of the cytokines TNF, IL-6 and IL-1 (*41*).

1.6 *Sphingomonas paucimobilis*

Sphingomonas paucimobilis is an opportunistic pathogen that often causes nosocomial infections in immuno-compromised individuals. It is often found in hospital environments and has been isolated from water systems and ventilation equipment (*42, 43*). This Gram-negative bacterium was originally classed as a *Flavobacterium* in the 1970's. It later assumed the genus *Pseudomonas paucimobilis*, however the taxonomical genus was revised in 1990 to *Sphingomonas paucimobilis* (type strain) in light of accumulating data suggesting features that distinguished this organism from other *Pseudomonas* species (*44, 45*). Early

work carried out on *Flavobacterium devorans* by Yamamoto *et al.* showed that it produced a novel sphingoglycolipid containing glucuronic acid and a 2-hydroxy fatty acid (*44, 45*). Further work on the outer membrane of *S. paucimobilis* by Kawahara *et al.* found that they could not isolate LPS using the common "hot-phenol" extraction method. Instead they isolated the lipids by chloroform/methanol extraction and found that they contained 2-hydroxy myristic acid rather than the 3-hydroxylated fatty acids found in the Lipid A portion of LPS (*46*). This "Lipid A type" molecule was subsequently shown to be an equimolar mixture of two glycolipids. The structures of these were determined by Kawahara *et al.* and are shown in **figure 5** (*40*).

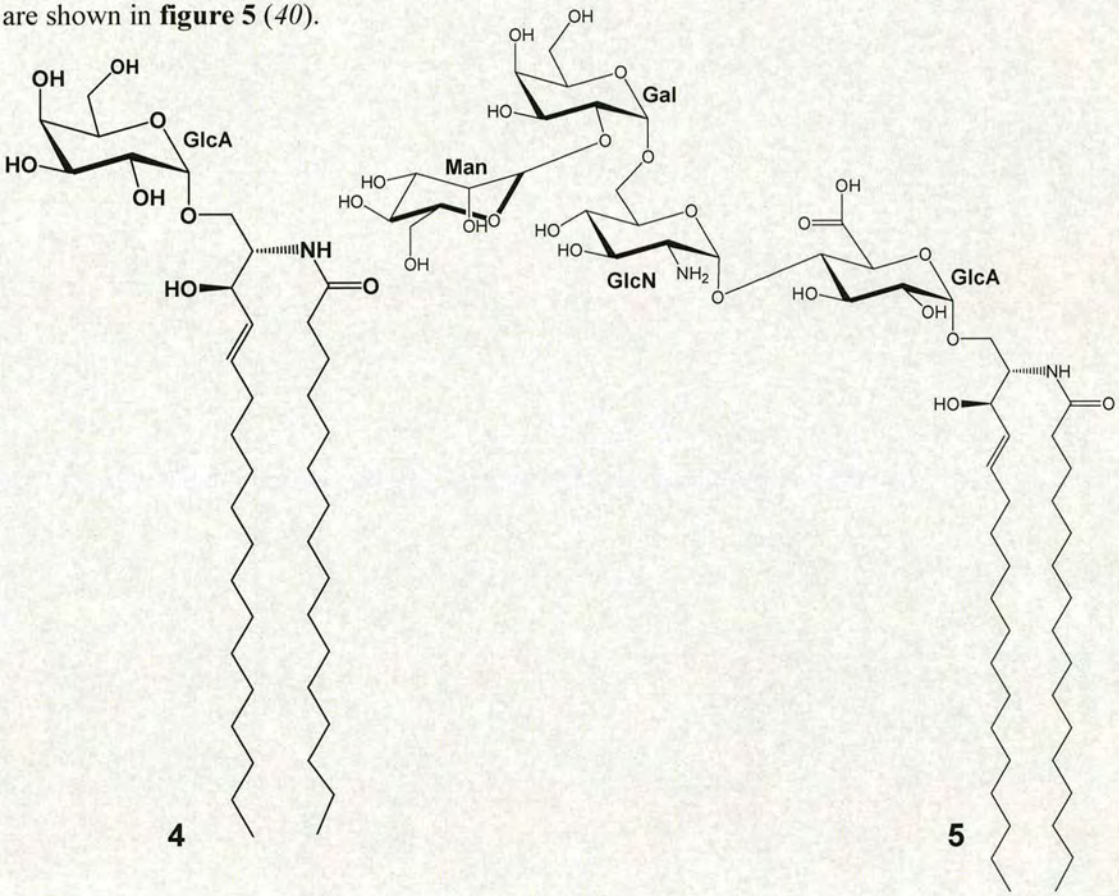

Figure 5: Structures of the Major Glycosphingolipids from *S. paucimobilis*
Two distinct glycolipids have been identified from the outer membrane of *S. paucimobilis*. The monosaccharide GSL-1, **4** (glucuronic acid + fatty acid) and the tetrasaccharide GSL-4A, **5** (mannose (Man), galactose (Gal), glucosamine (GlcN), glucuronic acid (GlcA) + fatty acid) (*40*).

These glycosphingolipids were later designated as GSL-1, **4** and GSL-4A, **5** and were found to be localised in the outer leaflet of the outer membrane of *S. paucimobilis* as shown by biochemical and immuno-electron microscopic analyses (*47*). These analyses also showed that the outer membrane of this organism was less dense than that of *E. coli*. This is likely since the LPS constituent of *E. coli* outer membranes contains more fatty acid components compared with GSL, which contain only dihydrosphingosine and 2-hydroxy myristic acid. Models of the outer membranes of *E. coli* and *S. paucimobilis* (**Fig. 6**) highlight this distinct difference in lipid complexity (*47*).

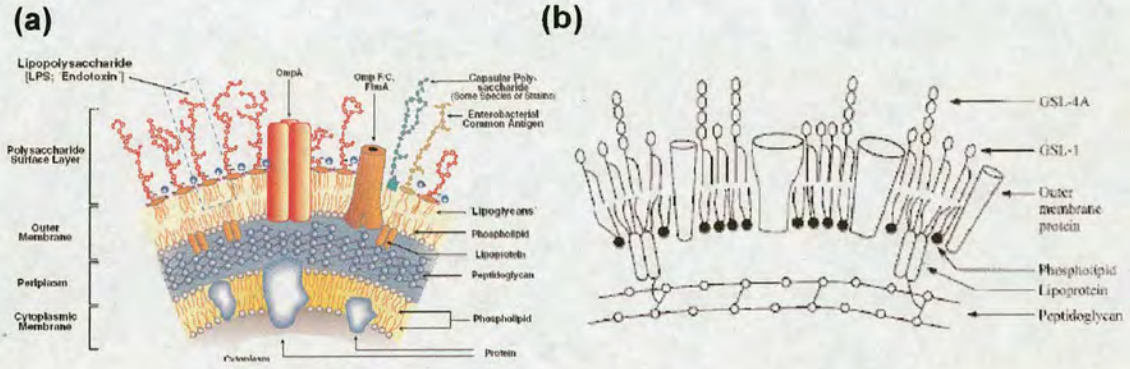

Figure 6: Models of the Outer Membranes of *E. coli* and *S. paucimobilis*
(a) Illustration of the outer membrane structure of *E. coli* highlighting the complexity of the LPS molecules (*48*). (b) Illustration of a proposed outer membrane structure of *S. paucimobilis* highlighting the less complex glycosphingolipids. Over all, the membrane of *S. paucimobilis* is less dense due to its less complex glycolipid composition compared with that of *E. coli* (*47*).

The first step of (glyco-)sphingolipid biosynthesis in any organism commences with the condensation of the amino acid L-serine and the long chain fatty acid palmitoyl-CoA to produce the first sphingolipid precursor 3-ketosphinganine (KDS). This reaction is catalysed by the enzyme serine palmitoyltransferase (SPT). It is logical therefore to propose that *S. paucimobilis* contains SPT and indeed, a water soluble, homodimeric SPT has been characterised from this organism (*49*). Unsuccessful attempts at the crystallisation of *S. paucimobilis* SPT led Ikushiro *et al.* to look for alternative candidates in other sphingolipid-containing bacteria (*50*). As a result, they have identified three novel SPT genes from

Sphingobacterium and *Bdellvibrio* spp are unusual bacteria. Like *Sphingomonas*, they lack lipopolysaccharide and instead produce glycosphingolipids. Ikushiro *et al.* have successfully over-produced SPTs from both organisms, in *E. coli*, and have shown that unlike SPT from *S. paucimobilis*, they are peripheral membrane proteins (*50*).

1.7 Serine Palmitoyltransferase (SPT)

To date, the genes encoding serine palmitoyltransferase (SPT) have been identified from an extremely wide variety of organisms. In addition to mammalian, murine and fungal sources, SPT has also been identified from bacteria, plants and a marine virus thus highlighting the ubiquitous nature of this enzyme and suggesting the importance of sphingolipid biosynthesis in a plethora of organisms (*49, 51-55*).

1.7.1 Isolation and Characterisation of LCB1 and LCB2

1.7.1.1 Human, Fungal and Murine Sources

In work by Wells and Lester a mutant form of *Saccharomyces cerevisiae* was reported to be unable to synthesise phospho-inositol containing lipids in the absence of long chain bases. This mutant strain was viable and similar to wild type cells in the production of phospholipids when cultured in the presence of *D*-L-erythrodihydrosphingosine however, in the absence of exogenous long chain bases, cell growth was affected (*56*). This suggested an important role for one or more yeast sphingolipid(s) in cell viability.

Eukaryotic SPT consists of two hetorologous sub-units encoded by the genes *lcb1* and *lcb2*. Early studies in this field identified mutant *S. cerevisiae* cells that exhibited decreased or even negligible SPT activity when either *lcb1* or *lcb2* was absent, suggesting that both gene products are essential for SPT function. (*52, 53, 57*). In addition to yeast *lcb1* and *lcb2*, the complete cDNA sequences of genes encoding mammalian and murine SPT have now been identified and cloned (*51*).

The extensive work by Hanada *et al.*, with mutagenised chinese hamster ovary (CHO) cells lacking the *lcb1* gene, showed that no SPT activity could be obtained unless both *lcb1* and *lcb2* genes were expressed. Furthermore, the tagging of LCB1 protein wih a FLAG and His_6 tag confirmed that LCB1 interacted with LCB2 since LCB2 could be co-purified and co-immunoprecipitated with tagged LCB1 (*13*). This also led them to propose that the stoicheometry of LCB1 and LCB2 was 1:1, again suggesting that they are two monomers which interact to form an active SPT heterodimer (*13*). Additionally, Yasuda *et al.* demonstrated that LCB1 is essential for the maintenace of LCB2 and that it is crucial for the formation of active SPT in mammalian cells (*58*).

A novel 80 amino acid protein has been identified in association with LCB1 and LCB2 from *S. cerevisiae (59)*. This small protein, Tsc3p, does not influence the expression or membrane localisation of LCB1/2 however SPT activity decreases in mutant cells lacking Tsc3p, suggesting that this protein is required for optimal SPT activity. Tsc3p can also be solubilised from the microsomes in a similar fashion to LCB1 and LCB2 suggesting that it is also membrane bound. Gable *et al.* showed that co-immunoprecipitation of Tsc3p with LCB1 and/or LCB2 can be achieved at NaCl concentrations up to 300 mM. However, above this concentration only LCB1 and LCB2 co-immunoprecipitate together. This suggests that the interaction between Tsc3p and LCB1/2 is weaker than that between the two monomers.

To date however, no mammalian homologue of Tsc3p has been identified. Therefore it is not clear if an additional sub-unit is required for optimal SPT activity in mammals.

1.7.1.2 Viral and Plant Sources

In the last decade the number of organisms known to express SPT has increased and now this includes a group of marine viruses of the genus *Coccolithovirus*. The genome of this viral genus has recently been sequenced and was found to contain a cluster of sphingolipid biosynthetic genes, in particular, the single open reading frame ehv050, which appears to encode a protein similar in sequence to eukaryotic LCB1 and LCB2. Further analysis has shown that this gene encodes two tandemly-repeated α-oxoamine synthase domains within a single polypeptide chain, with an N-terminal portion similar to LCB2 and a C-terminus similar to LCB1. When cloned into a *S. cerevisiae* double *Δlcb1/ Δlcb2* mutant, lacking endogenous SPT activity, viral SPT was able to rescue KDS production suggesting it encodes an SPT (*55, 60*).

One way in which viral SPT differs from eukaryotic SPT is in its substrate specificity. An increased proportion of longer C-16 sphingoid bases was observed in *S. cerevisiae* cells expressing viral SPT. This alteration in substrate specificity, for myristol-CoA compared to palmitoyl-CoA, suggests that viral SPT may be capable of catalysing various condensation reactions of long chain fatty acids (*55, 60*).

The significance of sphingolipid biosynthesis has also been demonstrated in plants, where sphingolipids contribute to growth and development. Work by Tamura *et al.* identified cDNA from *Arabidopsis thaliana* encoding a protein homologous to yeast and mammalian LCB2 (*At*LCB2) and showed that expression of the gene encoding *At*LCB2 (*Atlcb2*)caused increased sphinganine production in mutant *S. cerevisiae* cells deficient in SPT activity (*54, 61*). More recently, Chen *et al.* have identified a LCB1 homologue from *A. thaliana* and also demonstrated that LCB auxotrophy could be rescued from mutant *S. cerevisiae* cells by co-expression of *Atlcb1* with *Atlcb2*. Furthermore, partial RNA interference suppression of *lcb1* in *A. thaliana* leads to altered levels of saturated long chain bases which ultimatly, causes a decrease in plant size and altered leaf morphology (*62*).

1.7.1.3 Bacterial SPT

As mentioned in section 1.6, the Gram-negative bacterium *Sphingomonas paucimobilis* expresses a water soluble, homodimeric SPT, unlike the eukaryotic enzyme which is a membrane bound heterodimer. BLAST sequence alignment of *S. paucimobilis* SPT showed 48% and 49% similarity to mouse LCB1 and LCB2 respectively *(49)*. Surprisingly however, *S. paucimobilis* SPT displayed higher similarity to the other enzymes of the α-oxoamine synthase family of which SPT is a member e.g. 56% similarity with 8-amino-7-oxononanoate synthase (AONS) of *Bacillus sphaerious*, 54% with 2-amino-3-ketobutyrate-CoA ligase (KBL) of *Bacillus subtilis*, and 55% with 5-aminolevulinic acid synthase (ALAS) of *Agrobacterium radiobacter (49)*.

Recombinant *S. paucimobilis* SPT was over-expressed in *E. coli* and purified to homogeneity by Ikushiro *et al.* and they demonstrated that it was active in the conversion of L-serine and palmitoyl-CoA to produce KDS *(49)*. In their discussion Ikushiro and colleagues concluded that although their preparations of recombinant, untagged SPT were suitable for x-ray crystallography analysis. No structural data was deposited in the PDB between 2001 and 2004. Since, unlike its eukaryotic counterparts, this protein is water soluble, a procedure for its characterisation and crystallisation was optimised and is the subject of this thesis (*63*).

1.7.2 Identification of an Additional LCB Sub-unit (LCB3)

As discussed earlier, the small 80 amino acid protein Tsc3p was identified by Gable *et al.* as a requirement for optimal SPT activity in yeast. To date, no mammalian homologue has been identified. However, using a systematic screen of the genomic data base for sequences homologous to human *lcb1* (SPTLC1) and *lcb2* (SPTLC2) Hornemann *et al.* identified a short open reading frame encoding 134 amino acids that showed 86% similarity with the C-terminus of LCB2. Further analysis revealed an open reading frame encoding a polypeptide

with an overall similarity of 84% to the LCB2 subunit of SPT. The similarity to LCB1 was less at 45%.

Based on its homology to LCB2, this new protein was named SPTLC3 and was proposed to be an isoform of SPTLC2 since it is located on a different chromosome (*64*). Further work showed that SPTLC3 co-immuno-precipitated with SPTLC1 and SPTLC2 from human placenta extracts and human embryonic kidney (HEK) 293 cells. Non-denaturing PAGE and size exclusion chromatography suggests that all three protein sub-units interact to form a single SPT complex of approximately 480 kDa, suggesting that SPT is not a heterodimer but in fact a high molecular weight complex. The stoichiometry of SPTLC2 and SPTLC3 in the complex appears to be variable, suggesting a possible tissue specific mechanism of SPT activity which changes to suit the sphingolipid requirements of a particular cell type (*65*).

1.7.3 Hereditary Sensory and Autonomic Neuropathy Type I

Hereditary sensory and autonomic neuropathy type I (HSAN1) is an autosomal dominant disorder which is the most common group of degenerative disorders of sensory neurons. The disease involves a progressive degeneration of dorsal root ganglion and motor neurons, leading to distal sensory loss and consequent distal muscle wasting. Sensory impairments include loss of sensation to pain and temperature.

Nicholson *et al.* showed that the gene responsible for HSAN1 was located on chromosome 9q22.1-q22.3 (*66*). Subsequently, the gene encoding SPT (SPTLC1) was mapped to this locus and mutational screening identified 3 three missense mutations resulting in a change to two amino acids within the protein structure (*67, 68*). Two of these mutations involve two different nucleotides in codon 133 which normally encodes a cysteine residue. The first, A398G, causes an amino acid change from cysteine to tyrosine and the second, G399T causes a change to tryptophan (*67, 68*). The third mutation T431A, within codon 144, causes a change of valine to aspartic acid (*68*).

In addition to identifying the mutations responsible for HSAN1, Bejaoui *et al.* have examined the effects of the C133 mutations on SPT function. They observed a 50% reduction of SPT activity in microsomal preparations, obtained from the lymphoblasts of HSAN1 patients with C133 mutations, compared to preparations from healthy individuals. LCB1 and LCB2 appeared to be present in similar concentrations in both preparations suggesting that the mutations do not affect the stability of the LCB1 protein. They postulate that an alteration of LCB1 may affect either; the formation of the active site upon dimerisation of LCB1 with LCB2, or the overall geometry of the active site (*69*).

Sequence alignment of SPTLC1 and *S. paucimobilis* SPT maps residue C133 of SPTLC1 to N100 of the bacterial enzyme (**Fig. 7**).

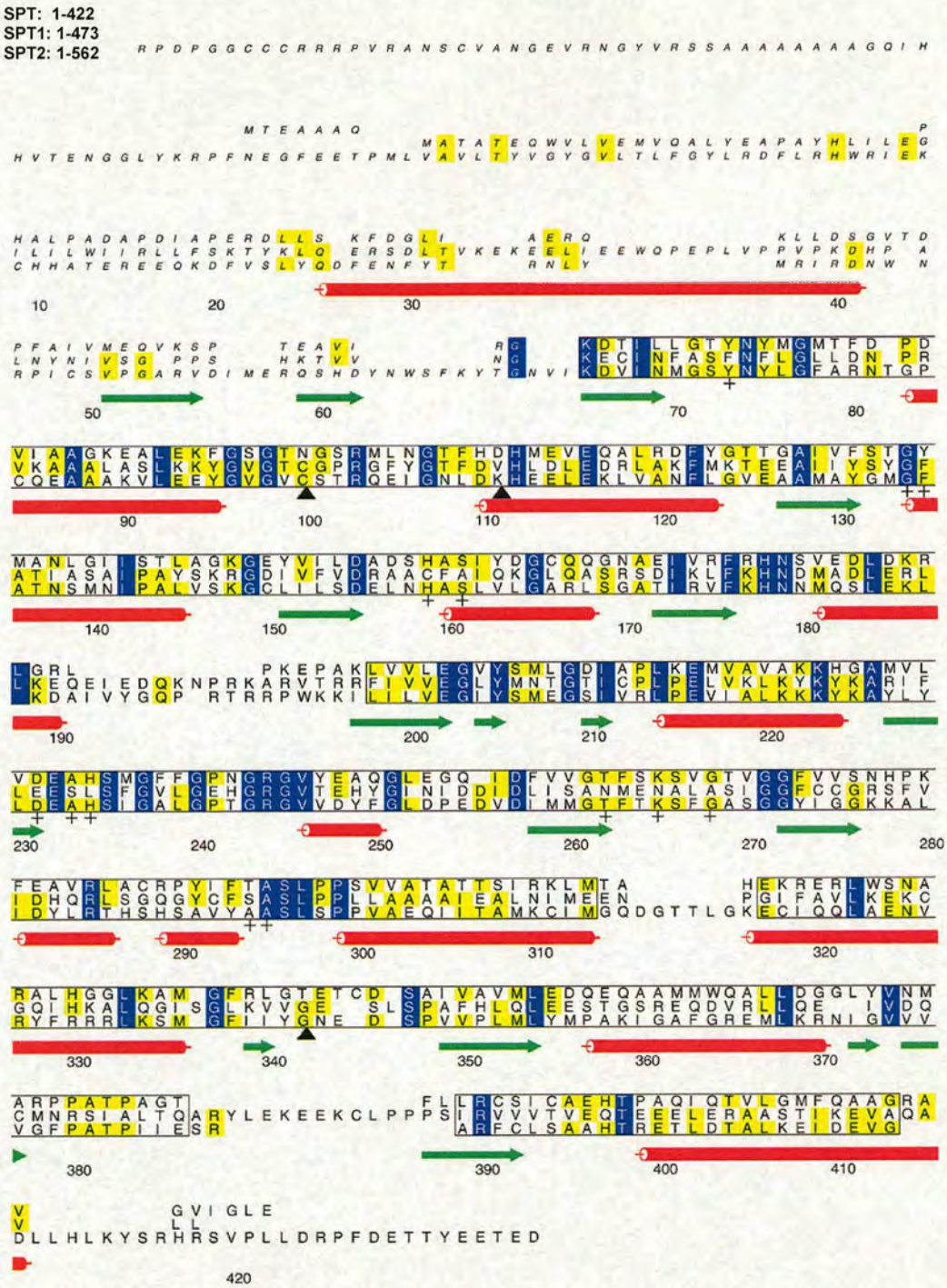

Figure 7: Sequence Alignment of *S. paucimobilis* SPT with Human SPT1 and SPT2

Residues are coloured to indicate conservation and numbering refers to the *S. paucimobilis* SPT sequence. "+" symbols denote important active site residues identified by examination of the SPT structure (see **table 1,** section 2.5.1). The secondary structure elements of *S. paucimobilis* SPT are indicated above the sequence with red barrels representing an α-helix and the green arrow, β-sheets. Regions considered to be relatively well aligned are boxed. Conserved residues (3/3) are highlighted in blue, 2/3 in yellow and regions considered to be relatively well aligned are boxed.

The crystal structure of *S. paucimobilis* SPT was used as a model for the eukaryotic enzyme, and locates N100 within hydrogen bonding distance to the backbone carbonyl oxygen of the active site lysine residue (**fig. 8**, see section 2.5 for more detail). It is fair to suggest from this, that substitution of N100 to a larger more hydrophobic residue (tryptophan or tyrosine) would cause disturbance of the active site geometry (*63*).

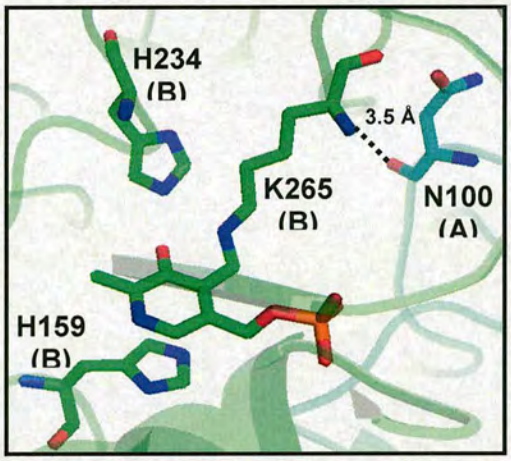

Figure 8: Active Site of *S. paucimobilis* SPT
The distance between N100, monomer A (blue) and the backbone carbonyl oxygen from the active site lysine residue K265, monomer B (green) is highlighted.

There have however, been cases of sensory neuropathy reported where there is no apparent mutation of SPTLC1. Analysis of patients carried out by Dawkins *et al.*, where SPTLC1 mutations have been excluded, did not show any alterations to the SPTLC2 sequence. This suggests that, in rare cases, other protein(s) may be involved in the onset of HSAN1 (*70*).

1.7.4 The α-oxoamine Synthase (AOS) Family

The α-oxoamine synthase family is a group of pyridoxal-5'-phosphate (PLP)-dependent enzymes which commonly catalyse the decarboxylative condensation between an amino acid and a fatty acid thioester. These include 8-amino-7-oxononanoate Synthase (AONS) which catalyses the first step of biotin biosynthesis, 5-aminolevulinate synthase (ALAS) which catalyses the first step of tetrapyrrole biosynthesis, 2-amino-3-ketobutyrate CoA Ligase

(KBL) which plays a role in threonine degradation, and serine palmitoyltransferase (SPT) which catalyses the first and rate limiting step of sphingolipid biosynthesis (*71-73*). Interestingly, two proteins involved in the biosynthesis of prodiginine antibiotics contain AOS-like domains in addition to acyl carrier protein domains. These are RedN and RedL from *Streptomyces coelicolor* and PigH from *Serratia marcescens* (*74, 75*).

Due to low sequence homology within the family of PLP-dependent enzymes, classification is difficult. Initially, this is normally based upon reaction specificity - which carbon (C-R) bond of the amino acid is targeted for cleavage (α, β or γ) (*76*). Reactions that occur at the α-carbon include transamination, decarboxylation, racemisation, condensation and elimination of a side group. Reactions that occur on the β- or γ-carbons are less common and include the replacement of a side group and elimination.

More recently, PLP-dependent enzymes have been divided into five groups based upon their three-dimensional fold-type: Fold type I, the aspartate amino transferase superfamily, which is sub-divided into a further 5 classes and contains enzymes previously classified under the α and γ family as described by Alexander *et al.* (*76*). Fold types II-V are typified by enzymes of a specific fold. For example, fold type II is typified by tryptophan synthase, fold type III by alanine racemase, fold type IV by the D-alanine aminotransferase family and fold type V is based upon the lactate dehydrogenase fold superfamily (*77, 78*).

There are two significant structural features within the sequences of the enzymes classified under fold type I. Firstly, the positioning of the conserved active site lysine residue which is located closer to the C-terminus directly following a hydrophobic β-strand and secondly, the positioning of the conserved aspartic acid residue that provides hydrogen bonding contact to the pyridoxal ring nitrogen, preceding the active site lysine residue by 20-50 amino acids. ALAS, AONS and SPT are classified under class II of the fold type I aspartate amino transferase family.

1.7.5 PLP-dependent Reaction Mechanism of the AOS Family

A general reaction mechanism may be postulated for the AOS family, which constitutes class II (fold type I) within the PLP-dependent enzyme superfamily. The PLP co-factor is bound to these enzymes via a conserved, active site, lysine residue forming an internal aldimine/Schiff base. Generally, the initial steps of catalysis commence with a transaldimination reaction, where the internal aldimine complex is displaced by the incoming amino acid substrate, to form an external aldimine (**Fig. 9a(i)**). The PLP exists in two tautomeric forms in the external aldimine: the enolimine and ketoenamine. These tautomers have different absorbance maxima (336nm and 425nm respectively) which are responsible for the characteristic spectroscopic properties associated with PLP-dependent enzymes (**Fig. 9a (ii)**) (*79*).

External aldimine formation is followed by the heterolytic cleavage of a CR bond of the amino acid. Several studies indicate that the conserved active site lysine residue acts as the catalytic base during deprotonation in fold type I enzymes (*80-82*). Cleavage of the amino acid CR bond is postulated to generate a resonance-stabilized quinonoid intermediate (**Fig. 9b**) which has been observed, spectroscopically, in the case of AONS (486nm), ALAS (510nm) and AAT (525 nm) (*80, 83, 84*). In addition, the formation of a quinonoid species in AONS was also demonstrated by deuterium exchange. Using ^{1}H NMR, Ploux *et al.* observed from the spectra of the AON product (formed from either L-[2-^{2}H]alanine in H_2O or L-alanine in D_2O) that the C2-H proton of alanine was lost during the reaction and that the C8-H proton of 8-amino-7-oxononanoate was solvent derived (*85*).

The quinonoid is consequently presumed to react with the other substrate, commonly a thioester (palmitoyl-CoA in the case of SPT), in a Claisen-type condensation to form a putative β-ketoacid aldimine intermediate (**Fig. 9c**). Such an intermediate has been observed in the case of AONS, when incubated in the presence of alanine methyl ester and pimeloyl

CoA (*86*). Subsequently, the next step is presumed to be the decarboxylation and reprotonation of the resultant β-ketoacid (**Fig. 9d**) to form the product external aldimine.

A further transaldimination reaction by the active site lysine allows product release and regeneration of the enzyme-PLP internal aldimine moiety (**Fig. 9e**). In ALAS the last steps, those of transamination and product release, are known to be rate determining.

Intriguingly, unlike LCB2, the LCB1 sub-unit of eukaryotic SPT does not contain the active site lysine residue common to all other members of the AOS family. It is therefore suggested to play a regulatory role in the dimerisation with LCB2 facilitating the function of an active heterodimeric enzyme with a single catalytic site (*53*).

(a) i

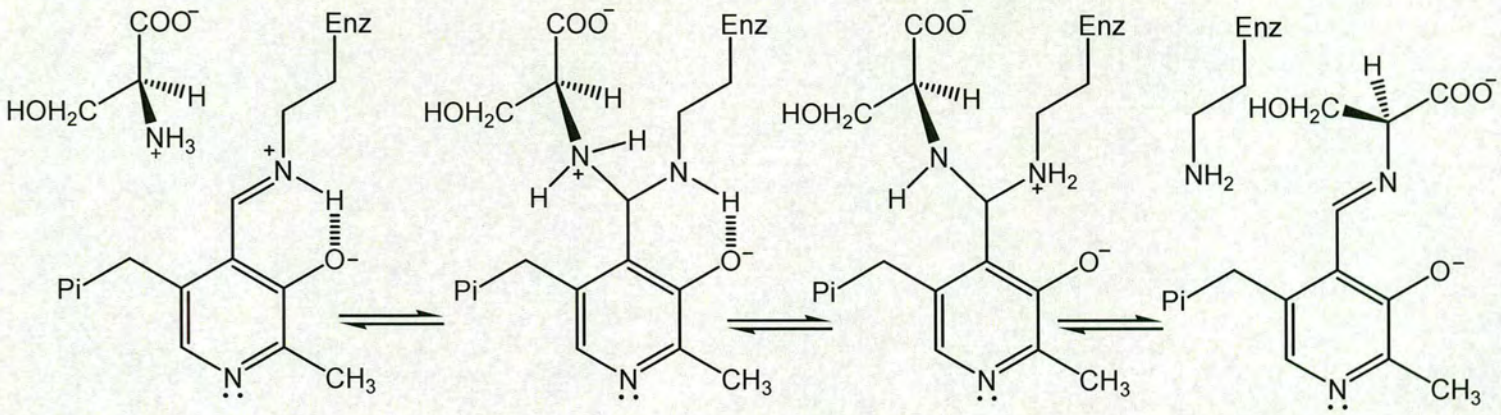

(a) ii

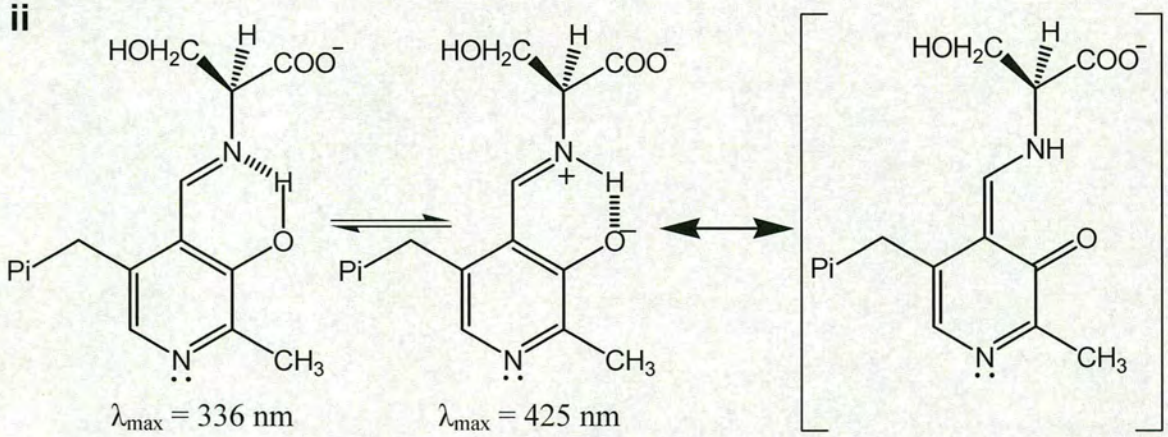

λ_{max} = 336 nm λ_{max} = 425 nm

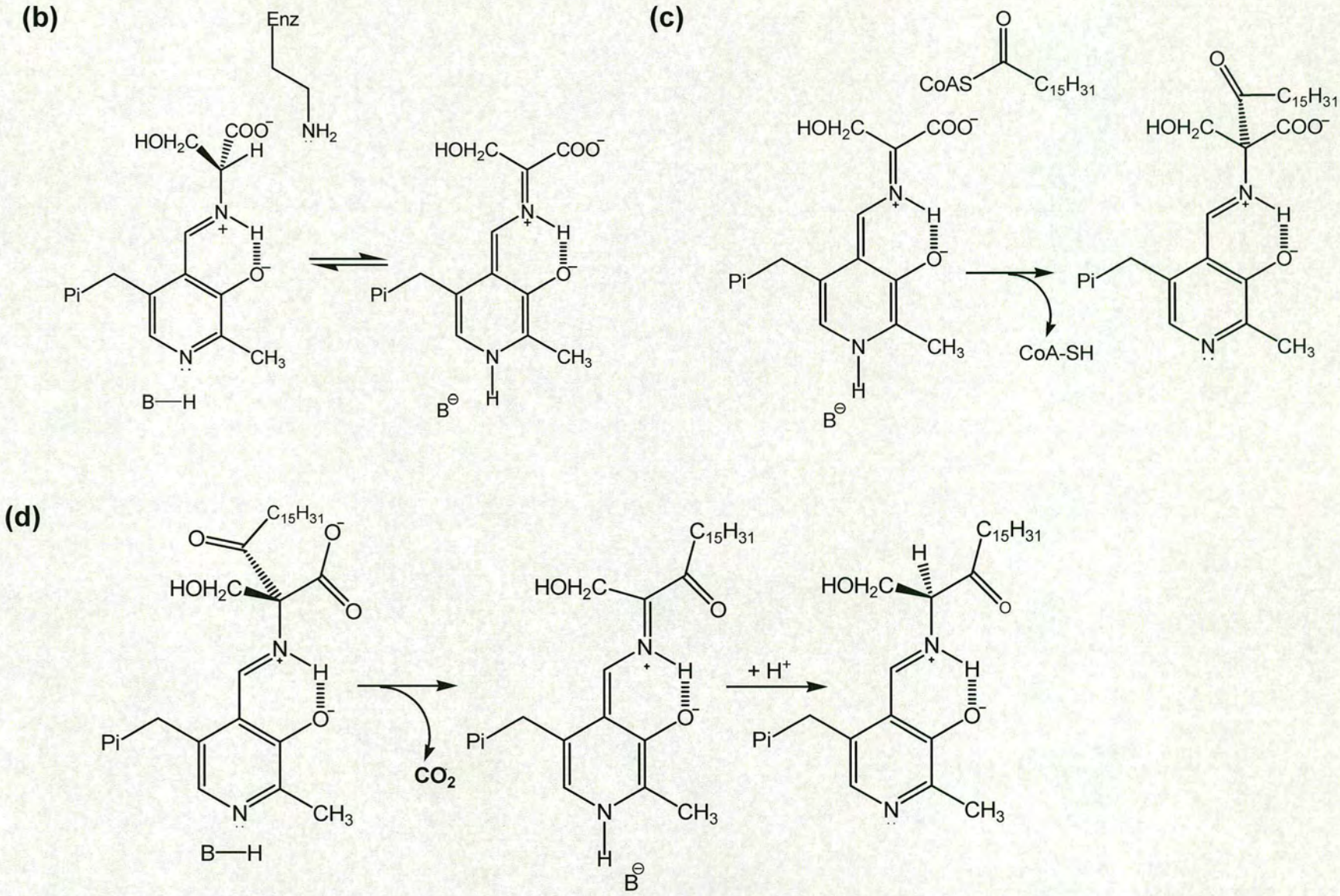
(b)
Enz
NH2
HOH2C
COO−
H
N
H
O−
Pi
N
CH3
B—H
B⊖
(c)
O
CoAS
C15H31
CoA-SH
(d)
C15H31
O
O−
HOH2C
CO2
+ H+

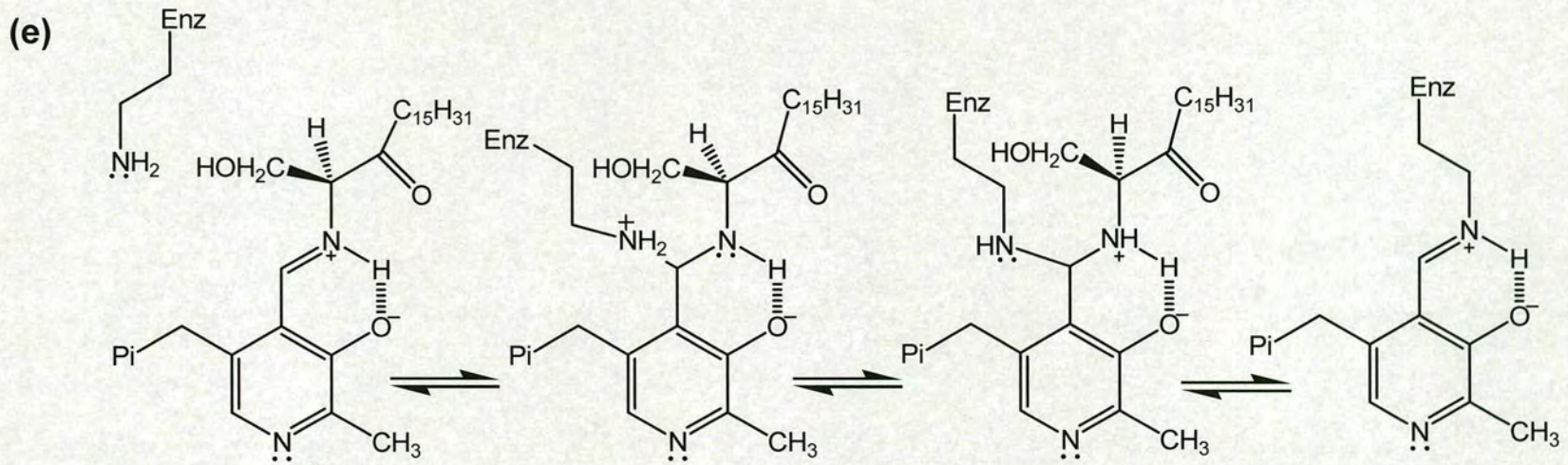

Figure 9: PLP-dependent Reactions of Serine palmitoyltransferase (SPT)

(a) L-serine External Aldimine Formation: (i) A transaldimation reaction occurs between the alpha amino group of L-serine and the imine bond of the Lys-PLP internal aldimine to form the PLP-L-serine external aldimine. **(ii)** The PLP moiety exists in two tautomeric forms (enolimine and ketoenamine) which give the enzyme characteristic absorbance maxima at 336 and 425 nm respectively. **(b) Deprotonation and Quinonoid Formation:** Deprotonation occurs to form a resonance stabilized (quinonoid) intermediate. It is postulated that the active site lysine acts as the catalytic base during deprotonation. Quinonoid intermediates observed to date have characteristic absorbance maxima between 480-530 nm. **(c) Product External Aldimine Formation:** The incoming palmitoyl-CoA substrate undergoes nucleophilic attack by the quinonoid intermediate, causing CoA release and the formation of a condensation intermediate. **(d) Decarboxylation and Reprotonation:** Decarboxylation is then thought to take place to form the product quinonoid. This is subsequently reprotonated, possibly by the active site lysine, to form the 3-ketosphinganine (KDS) product external aldimine. **(e) Product Release and Internal Aldimine Regeneration:** The active site lysine residue initiates a transaldimination reaction to release KDS and regenerate the Lys-PLP internal aldimine.

1.8 Inositol Phosphorylceramide Synthase

Inositol phosphorylceramide synthase (IPC synthase, IPCS), also known as Aureobasidin resistance protein (Aur1p), catalyses the transfer of *myo*-phosphoinositol from phosphatidyl inositol (PI) onto phytoceramide to yield inositol phosphorylceramide (IPC) and diacylglycerol (DAG) (*87*). This reaction is shown in **figure 10** below. To date, IPC synthase and its orthologues have been identified from a wide variety of sources from protozoan parasites and pathogenic fungi to bean plant microsomes (*88-90*). Down-regulation of *C. neoformans* IPC synthase activity in J774.16 murine macrophage-like cells, significantly decreased the intracellular growth of this pathogenic fungus indicating that inhibition of Aur1p activity could be a strategy for fungicidal action (*91*). Aur1p is not present in mammalian cells thus the enzyme is a potential target for the development of novel anti-fungal agents.

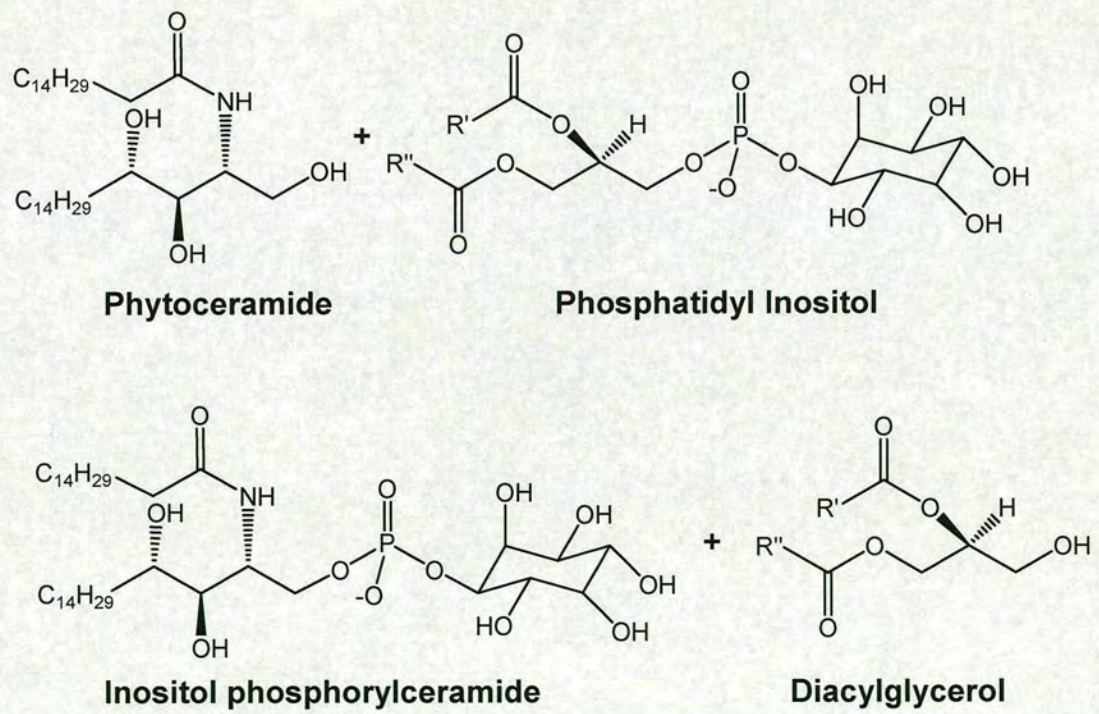

Figure 10: IPC synthase Catalysed Transfer of Inositol-phosphate
IPC synthase catalyses the transfer of inositol phosphate onto phytoceramide to produce inositol phosphorylceramide (IPC).

1.8.1 IPC synthase Homologues

Using a combination of bioinformatic and functional genetic approaches Denny *et al.* identified a functional *AUR1* orthologue from the protozoan parasite *Leishmania major*. Despite having the same function as fungal IPC synthase and having the ability to rescue Aur1p null mutants, it shares more sequence similarity with its human orthologue sphingomyelin synthase. This suggests the presence of a novel class of protozoan IPC synthases and since there is no functional equivalent in mammalian cells, it offers a potential target for the development of anti-protozoan inhibitors. Such compounds could help combat a number of human diseases such as leishmanaises, Chagas disease and African sleeping sickness (*88*).

Bromley *et al.* have examined IPC synthase activity from the microsomes of a variety of plant tissues by monitoring the incorporation of [^{3}H]-inositolphosphate. From the seven tissue samples analysed it was found that the highest IPC synthase activity came from bean leaf and hypocotyl samples. Bean microsomal IPC synthase is also inhibited by aureobasidin A and rustmicin, which are two known inhibitors of the fungal IPC synthase (*90*).

Homologues of *S. cerevisiae AUR1* have also been identified from a number of human pathogenic fungi including *Candida glabrata* and *Cryptococcus neoformans*. Sequence alignment of the proteins encoded by these genes with other homologues from *Candida albicans*, *Aspergillus fumigatus*, *Aspergillus nidulans*, *Saccharomyces cerevisiae* and *Schizosaccharomyces pombe* showed a high degree of homology within the central 250 amino acids. Two domains within this region are highly conserved suggesting that they may play a role in transferase activity (*89*).

The mammalian contrapart of IPC synthase is sphingomyelin synthase (SM synthase) which catalyses the transfer of phosphocholine onto ceramide to produce sphingomyelin (SM), a major component of the mammalian plasma membrane (**Fig.3**). Two forms of human SM synthase have been identified by Huitema *et al.* as integral membrane proteins located in the

Golgi lumen (SMS1) and the plasma membrane (SMS2) (*12*). V5-tagged versions of SMS1 and SMS2 were transfected into HeLa cells and monitored by immuno-flourescence microscopy. SMS1 co-localised with sialyltransferase, a trans Golgi marker protein, whereas SMS2 was associated mainly with the plasma membrane. Additionally, protease protection analysis showed that the C-termini of both enzymes were located on the cytosolic side of the membrane with the active site facing the exoplasmic leaflet, which is where SM synthesis takes place (*12, 92*).

1.8.2 Inositol; An Essential Growth Factor

It was discovered as early as 1928 by Eastcott that a substance essential for yeast growth and survival (originally termed "bios") was in fact inositol (*93*). Later, in the 1940's and 50's it became apparent that inositol was an essential growth requirement for both bacterial and eukaryotic cells. Pennington *et al.* investigated the growth requirements of *S. cerevisiae* for inositol and noted that the rate of growth of inositol-deficient cultures was less than the rate of growth of cells in a medium containing excess inositol (5 μg/ml) (*94*). Similarly Ghosh *et al.* demonstrated that inositol deficiency in the yeast *Saccharomyces carlsbergensis* resulted in the formation of abnormal cell walls leading to failure of separation of daughter cells from parent cells causing the formation of large cellular aggregates (*95*). Myo-inositol was shown by Eagle *et al.* to be an essential growth factor for a variety of normal and malignant human cells; as growth of cell lines in inositol-deficient media was lethal and only a few myo-inositol analogues such as inositol monophosphate were capable of sustaining cell growth and survival (*96*).

Inositol containing lipids and glycolipids have also been isolated from *S. cerevisiae* by Steiner *et al.* who have shown that the major inositol containing lipid is mannosyl di-inositolphosphate ceramide. This lipid can also incorporate deoxyglucose to form a glycolipid with identical chromatographic properties as the previously identified inositol-

phospholipids (*97, 98*). Inositol containing sphingolipids ($(IP)_2$ ceramide) and glycolipids (tetrahexoside sphingolipid) have also been identified from the fungus *Neurospora crassa* (*99*).

1.8.3 Characterisation of *AUR1*

Work by three independent groups identified a gene responsible for the resistance of *S. cerevisiae* to the antifungal agent aureobasidin A (AbA, **18**) (*100-102*). Originally named *ABR1* by Heidler and Radding, this gene is now commonly known as *aur1*. In *S. cerevisiae*, AbA resistant mutants are characterised by single base alterations in *AUR1* resulting in the amino acid substitutions L137F, H157Y and F158Y (*103, 104*). In AbA sensitive yeast and fungi there are a number of reported cases where single amino acid mutations have rendered the Aur1 protein (Aur1p) resistant to AbA. As these mutations occur within close proximity to one another, this region must be important for AbA binding and it has been argued that either; the mutations cause a change in the binding site of Aur1p or that AbA still binds but the protein maintains its function.

It was demonstrated by Heidler and Radding that the partial deletion of the *AUR1* (*ABR1*) locus affects *S. cerevisiae* cell growth and division. A more detailed study by Hashida-Okado *et al.* showed that the dominant *S. cerevisiae* mutants were resistant to AbA concentrations greater than 25 μg/mL and analysis of the nucleotide sequence of *AUR1* predicted that the polypeptide is a hydrophobic protein, 401 amino acids in length, containing several possible transmembrane domains. Furthermore, they demonstrated that wild-type Aur1p is also a target for AbA, as cells containing a disrupted *AUR1* locus expressed morphological changes including the disappearance of microtubules and degradation of tubulin. This abnormality in microtubule organisation is similar to that observed in cells treated with AbA. This also suggests a possible role for Aur1p in microtubule organisation and stabilisation (*103, 104*).

In addition, mutations of *AUR1* resulting in an amino acid substitution have been observed in other fungi and also result in the production of an AbA resistant phenotype e.g. G240C in *S. pombe* and G275V in *A. nidulans* (corresponds to G240 in *S. pombe*) (*105, 106*). Moreover, Hashida-Okado *et al.* have also carried out a three base pair mutation in *S. cerevisiae AUR1* causing the amino acid substitution A240C. This mutant is named *AUR1-C* and has been manipulated for use as a selection marker, in combination with AbA, for use in a new transformation system not only with standard lab strains of *S. cerevisiae* but also with the industrial strain *S. carlsbergensis* (*107*). Hansen *et al.* have used this *AUR1-C* mutant, in addition to a *lacZ* reporter gene, to develop the pYC plasmid series thus expanding the possibilities available as alternatives to G418 resistance (*108*).

1.8.4 Location of Aur1p and IPC Synthase Activity

It was demonstrated by Hechtberger *et al.* (and subsequently by Leber *et al.*) that inositolphosphorylceramide (IPC) is highly enriched in the Golgi and vacuolar membranes of *S. cerevisiae* whereas most of the more complex mannosylated sphingolipids are located in the plasma membrane (*109, 110*). Hechtberger and Daum also showed that treatment of *S. cerevisiae* cells with the drugs cycloheximidine and nocodazole, which affect the ER to Golgi transport of IPC, have no effect on IPC biosynthesis. However, treatment with brefeldin A, which is known to cause disassembly of the Golgi in yeast, caused a decrease in IPC formation. Both studies hinted at the sub-cellular localisation of IPC synthase to the Golgi apparatus (*111*).

In addition to these early studies, the location of Aur1p and IPC synthase activity has been examined in an extensive series of experiments by Levine *et al.* (*112*). The incorporation of three copies of an HA epitope at the C-terminus of *AUR1* by homologous recombination was used to monitor the localisation of Aur1p *in vivo*. In a manner similar to that used in the identification of human SM synthase (section 1.8.1) immunofluorescence was used to

compare the localisation of HA tagged Aur1p with other membrane proteins of the Golgi. Anti-HA staining of Aur1p expressing cells showed co-localisation of the protein with mannosyltransferase, a medial Golgi marker. Membranes form Aur1p-HA expressing cells were fractionated using a velocity gradient and fractions assayed for IPC synthase activity. There was close correlation between fractions containing Aur1p-HA and those exhibiting IPC synthase activity.

Furthermore, an Aur1p-Protein A fusion was used to determine the cellular sub-location of the C-terminus. Cleavage of the protein A tag occurred in the absence of detergent, in comparison to Van1p-Protein A, a lumenal, type II Golgi enzyme, where detergent was required to cleave the protein A tag. From these studies it seems that the C-terminus of IPC synthase may reside on the cytoplasm face of the golgi membrane whereas the active site residues are located in the lumen. This is consistent with the location of the flourescently labelled ceramide (C_6-NBD-ceramide) product, which remains within the Golgi of live yeast cells rather than in the cytosol.

1.8.5 IPC synthase Solubilisation and Activity

There is at present, no structural information available for IPC synthase only predicted topologies. Based on the predicted molecular mass of the protein encoded by *AUR1* and the predicted topologies, the presence of 6/7 transmembrane domains is inferred suggesting that IPC synthase is an integral membrane protein. This makes its isolation, solublisation and characterisation very challenging.

Initially, Ko *et al.* showed that IPC synthase activity could be released from *S. cerevisiae* crude membrane extracts in the presence of the non-ionic detergent Triton X-100 and that IPC synthase activity was dependent upon surface concentrations of the substrates PI and ceramide in a Triton-X mixed micelle (*113*).

In an extensive study, Aeed *et al.* examined the effects of 26 membrane-perturbing agents on IPC synthase activity from *C. albicans* and found that CHAPS (zwitterionic detergent) treated membranes had significantly improved activity compared to crude membrane extracts. In this study Triton X-100 extracts were shown by size exclusion chromatography, to be large aggregates or complexes of between 1.5-20 x 10^6 Da. They were unable to determine whether these aggregates were comprised of discrete complexes formed by several enzyme molecules or a result of unspecific aggregation of enzyme and membrane lipids. The requirement for the addition of high concentrations of PI in the extraction buffer also makes this method of extraction unattractive. Aeed *et al.* also developed an assay which is almost completely dependent upon substrate concentration and were able to determine appropriate K_m values for C_6-NBD ceramide and PI which were 3.3 μM and 138 μM respectively (*114*). Since it appears that *C. albicans* IPC synthase contains two potential protein-protein interaction motifs, consisting of nine consecutive glutamic and aspartic acid residues towards the C-terminus and a cluster of 6 positively charged amino acids at the N-terminus, it may be that these sequences are responsible for the aggregation of IPC synthase molecules into large protein complexes (*115-117*).

1.9 Novel Antifungal Targets

There are a host of potential targets for the development of fungicidal agents for example, cell wall biosynthesis, plasma membrane biosynthesis, DNA and protein synthesis and signal transduction pathways (*118*). Under the umbrella of plasma membrane biosynthesis, extensive studies by Nagiec *et al.* have identified the sphingolipid pathway as a viable target for the development of novel anti-fungal agents (*119, 120*). However, enzymes early in the sphingolipid pathway, such as SPT, have mammalian homologues and are therefore less attractive targets in comparison to IPC synthase, for example, which is essential to fungi (and some fungal pathogens such as *Botrytis cinerea*, section 1.9.3) but absent in mammals

(*121*). Secondary metabolites, produced from many micro-organisms, provide a rich source of lead compounds for the development of novel anti-microbial agents (*122, 123*). However, most naturally occurring anti-fungal compounds possess a broad spectrum of activity and over decades of use have become less effective. This increased resistance to commonplace antiungal agents, such as the azoles (fluconazole and itraconazole) requires the development of novel compounds with high efficacies and specific modes of action (*124*). It has been suggested that efficient inhibitors of IPC synthase would fit these criteria.

1.9.1 Natural Product Inhibitors of SPT

Several natural product inhibitors of SPT have been isolated from various sources. These include the sphingofungins from the thermo-tolerant fungi *Aspergillus fumigatus* and *Paecilomyces variotii*, lipoxamycin from *Streptomyces virginiae* and myriocin from the fungus *Isaria sinclairii* (*125-127*). Although their mechanism of action remains unsolved their structures resemble that of sphingosine, **7**. This structural similarity suggests that their mode of action may be similar. Each group of antibiotics have broad-spectrum anti-fungal activity. However, since SPT is also present within mammalian cells, it does not provide a useful target for the development of new anti-fungal agents.

1.9.1.1 Myriocin

During a screening program for the identification of novel antifungal agents, antifungal activity was detected from the fermentation broth of the thermophillic fungus *Myriococcum albomyces*. Analysis of the broth revealed an active compound which was isolated and its structure determined, this antibiotic was named myriocin, **6** (*128*). Independently, the potent immunosuppressive compound ISP-1 was isolated from a culture of the fungus *Isalia sinclairii* and shown to be identical to that of myriocin (*129*).

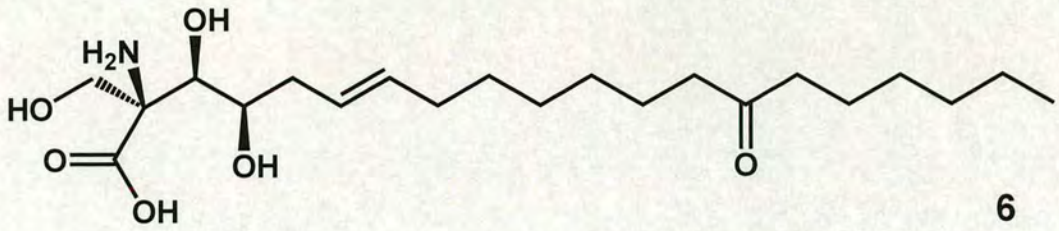

6

Subsequently, myriocin/ISP1 was shown by Miyake *et al.* to inhibit the proliferation of a murine IL-2 dependent cytotoxic T cell line (CTLL-2), with an IC_{50} of 15 nM. This growth inhibition could only be abolished by the addition of exogenous sphingosines. As a result they identified the primary target of myriocin as SPT and found that it inhibited the enzyme in a non-competitive manner with an apparent inhibition constant of 0.28 nM (*126*). Using a myriocin-containing affinity matrix, Chen *et al.* isolated LCB1 and LCB2 from the lysate of CTLL-2 cells (*130*).

Hanada *et al.* subsequently showed that 95 % inhibition of de novo sphingolipid biosynthesis, in CHO cells (L-YB/cLCB1), occurred in the presence of myriocin. Since growth inhibition could be rescued by the addition of exogenous sphingosine, this reinforces the suggestion that myriocin inhibits sphingolipid biosynthesis via inactivation of SPT (*131*). Myriocin was shown to competitively inhibit L-serine binding to *S. paucimobilis* SPT with a K_d^{app} of 1.3 μM, a 10^3 fold higher affinity, than the natural substrate L-serine (*132*). Since the structure of myriocin appears to mimic that of the condensation intermediate formed between L-serine and palmitoyl-CoA (**Fig. 9c**) it is possible to see why it binds so strongly to the enzyme.

1.9.1.2 The Sphingofungins

During screening tests for anti-fungal compounds from fungal sources, VanMiddlesworth *et al.* isolated and characterised four related compounds from cultures of *Aspergillus fumigatus*. These novel compunds were named sphingofungin A, B, C and D (**Fig. 11, 8-11**). Sphingofungins A-C exhibited a potent antifungal effect on *Cryptococcus neoformans*,

Saccharomyces cerevisiae and various *Candida* species with MIC values in the μg/mL range. Sphingofungin D exhibited less potent activity (*127*).

More detailed studies into the biological activity of sphingofungin B, **9** and C, **10** were carried out by Zweerink *et al.* in which the MIC values for *Saccharomyces cerevisiae* were determined to be 2 and 12 μg/mL respectively (*133*). Both compounds were observed to be lethal to growing cultures of *S. cerevisiae* with 99% lethality after 24 hours. In contrast, the antibiotics aculeacin and nystatin, which target cell wall/membrane biosynthesis, exhibited fungicidal activity after just 30 minutes. Since neither sphingofungin B or C had an effect on cell morphology and reversal of sphingofungin growth inhibition could be rescued by the addition of exogenous KDS, it was suggested that SPT is the target. Indeed, SPT activity from crude *S. cerevisiae* membrane extracts was inhibited by nanomolar levels of sphingofungin B and C, with sphingofungin B having a lower IC_{50} (20 nM) compared to sphingofungin C (100 nM) (*133*).

Horn *et al.* have identified two further sphingofungin compounds, sphingofungins E **12** and F **13** (**Fig. 11**) from *Paecilomyces variotii*, which share close structural resemblance, to myriocin. Their *in vitro* activity against SPT from crude *S. cerevisiae* membrane extracts was tested and compared to that of sphingofungin B (*134*). The IC_{50} values obtained are in the nanomolar range (7.2 and 57 nM respectively) however these were less potent than sphingofungin B. Sphingofungin F, **13** in which the CH_2OH at C2 is changed to CH_3 is distictively less potent than sphingofungin D, **11**.

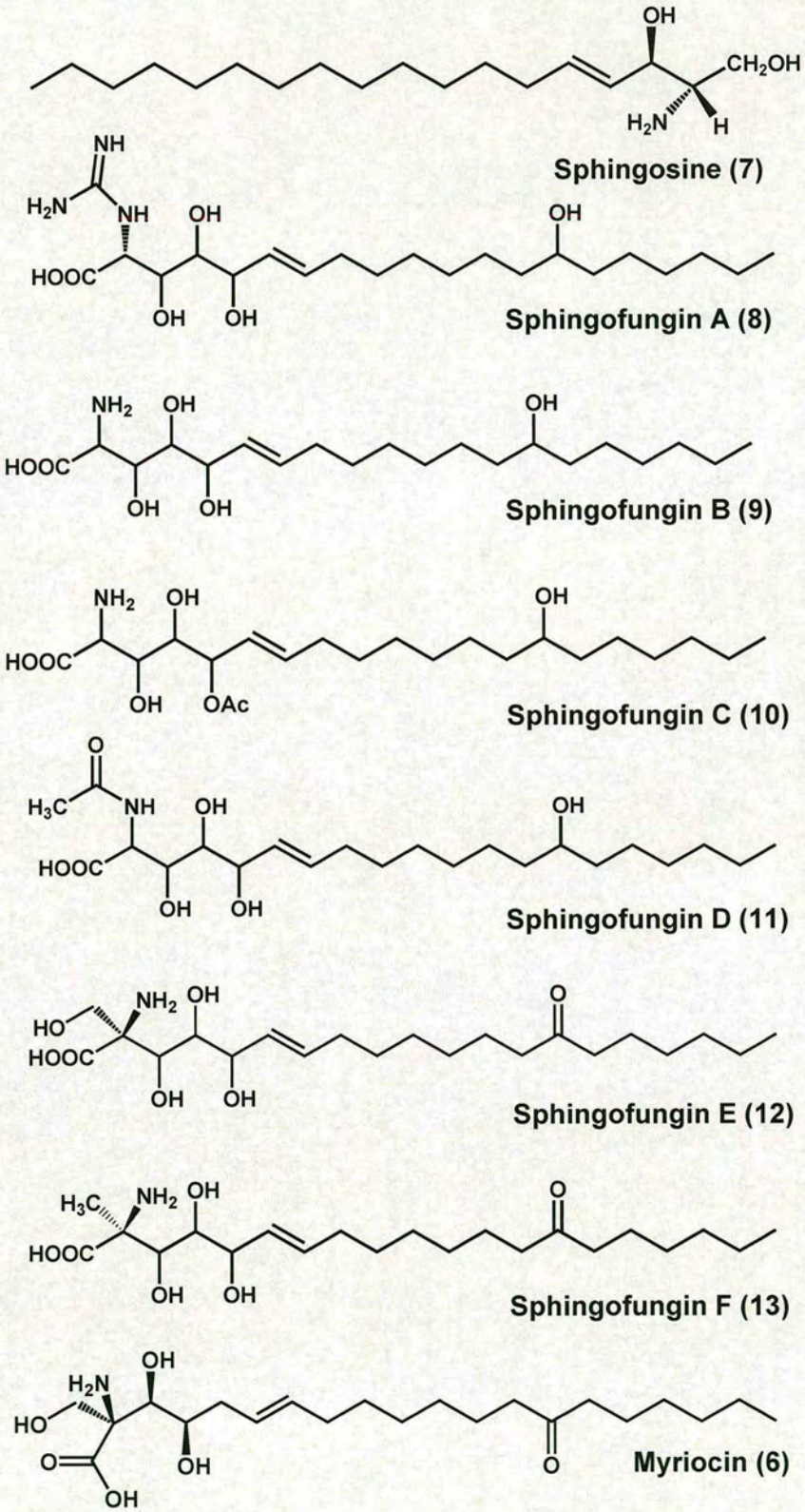

Figure 11: Structures of the Sphingofungins and Related Long Chain Bases
The sphingofungins (A-F, **8-13**) are sphingosine, 7 related molecules and bear a very close resemblance to myriocin, **6** therefore it is not surprising that they are able to bind to, and inhibit, SPT activity.

1.9.1.3 Sulfamisterin and Lipoxamycin

Recently, the novel inhibitor sulfamisterin, **14** has been identified from the fungus *Pycinidiella* strain AB5366. It is a naturally occurring α-substituted α-amino acid derivative possessing a sulfonated hydroxy function. An IC_{50} of 3 nM has been reported for this compound using a CHO cell-free lysate (*135*). To confirm that sulfamisterin inhibits sphingolipid biosynthesis by the inhibition of SPT, Yamaji-Hasegawa *et al.* monitored the incorporation of ^{14}C-serine and [^{3}H]-sphingosine/[^{3}H]-dihydrosphingosine into complex sphingolipids. In a cell-free system 100 nM sulfamisterin was required for the complete inhibition of SPT although a higher dose (10 μM) was required for the complete inhibition of sphingolipid biosynthesis in intact cells (*135*).

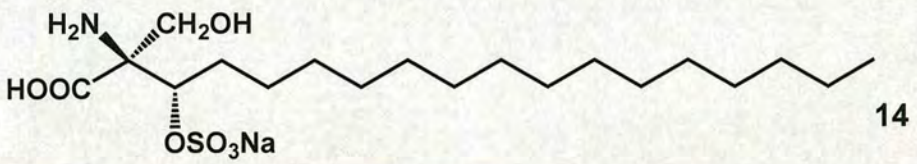

The total synthesis of sulfamisterin and a number of analogues was achieved by Sato *et al.* and these compounds were tested for their biological activity as described above. Interestingly, sulfonation of the hydroxyl group at position C3 is not essential for inhibition as desulfonated sulfamisterin also inhibits SPT activity (*136*). In addition, their studies show that the stereochemistry of this molecule at the C2 and C3 positions is vital for potent inhibitory activity. For example, the 2*R* compounds are ten-fold more active SPT inhibitors *in vitro* than the 2*S* compounds. Sphingolipid synthesis *in vivo* was also inhibited more significantly by the 2*R* compounds.

Lipoxamycin, **15** was originally isolated from *Streptomyces virginiae* var. *lipoxae* UC 5108. It was active against a range of fungi and yeast; the complete inhibition of *Candida albicans* and *Cryptococcus neoformans* growth was achieved at 10 and 1 μg/mL, respectively, but it proved less effective against bacteria with MIC values above 250 μg/mL. It was also found

to be intolerable to mice at concentrations above 10 mg/mL and was also ineffective against infections with *C. ablicans* and *C. neoformans* and some other pathogens in mice (*137*).

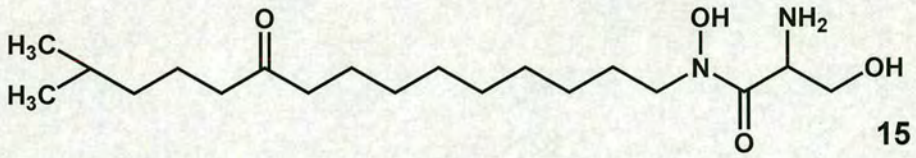

15

The structure of lipoxamycin was later determined by NMR and mass spectrometry (*138*). Although its structure contains a long alkyl chain and an amino containing polar head group, it does not resemble the sphingoid bases as closely as the sphingofungins. It does however exhibit comparable potency to the sphingofungins with an IC_{50} value of 21 nM *in vitro* against *S. cerevisiae* SPT. Its antifungal activity was also comparable with sphingofungin B against *Cryptococcus neoformans*, *Candida albicans* and *Aspergillus fumigatus*. Since the inhibition of lipoxamycin can be reversed by the addition of exogenous sphingolipid intermediates it was concluded that its mode of action is inhibition of SPT (*125*).

1.9.1.4 Cycloserine

Cycloserine, **16** (4-amino-3-isoxazolidinone, Seromycin) is a broad spectrum antibiotic used in combination with other antibiotics to treat tuberculosis. D-cycloserine is a natural product produced by *Streptomyces lavendulae* and *Streptomyces garyphalus* and acts on the PLP dependent enzymes alanine racemase and D-amino acid aminotransferase resulting in disruption of peptidoglycan biosynthesis (*139, 140*). In contrast, the L-isomer, originally isolated from the soil bacterium *Erwinia uredovora*, has been shown to inhibit SPT (*141-143*).

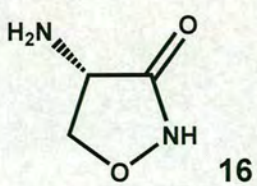

16

Studies have shown that the antibiotic L-cycloserine (LCS) has a potent inhibitory effect on SPT activity and hence sphingolipid production. Williams *et al.* have shown that KDS production in rabbit aorta was significantly inhibited by LCS; 50 % inhibition was obtained with 5 μM LCS and 50 μg of microsomal SPT protein (*144*). Additionally, Sundaram and Lev showed that growth of the anaerobic bacterium *Bacteroides levii* was significantly impaired in the presence of LCS. In particular, the activity of KDS synthetase was inhibited by 70% after one hour with 100 μg/mL LCS. Synthesis of phosphorylceramide containing lipids was also inhibited significantly as shown by the reduction of [^{32}P] incorporation (*142*). In a comparative inhibition study using mouse brain microsomes and SPT from *Bacteroides levii* they also demonstrated that LCS was the most potent inhibitor of KDS production (0.04 M caused a 50 % inhibition of SPT activity) *(145)*.

1.9.2 Inhibitors of IPC synthase

1.9.2.1 Aureobasidin A

The natural product Aureobasidin A (AbA, **17**) is the major aureobasidin isolated from *Aureobasidium pullulans* R106 (**Fig. 12**). It is a cyclic depsipeptide with potent, broad spectrum, antifungal activity targeted towards the inhibition of IPC synthase activity (*102, 146-148*).

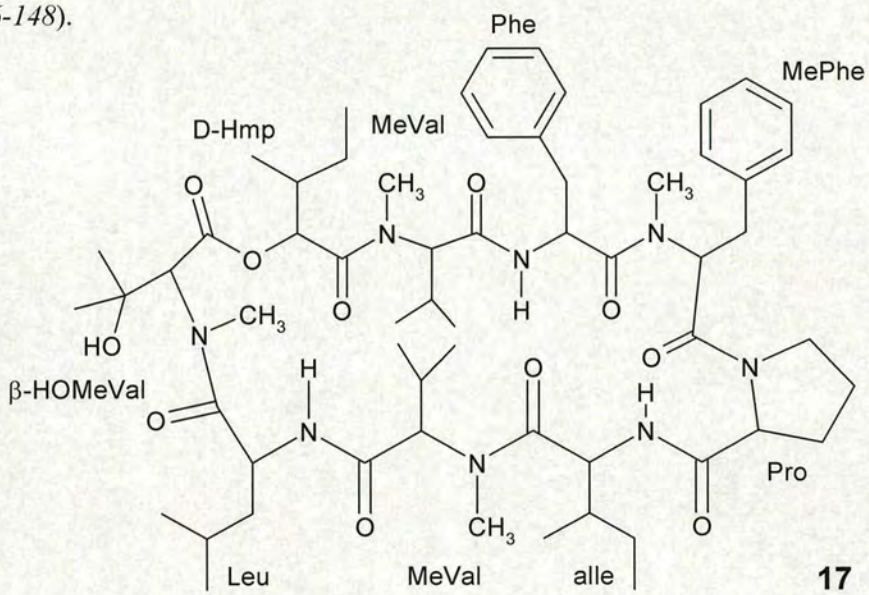

Figure 12: Structure of Aureobasidin A
Aureobasidin A, **17** is a cyclic depsipeptide, natural product inhibitor, isolated from *Aureobasidium pullulans* R106. Abbreviations; D-Hmp; 2(*R*)-hydroxy-3(*R*)-methylpentanoic acid, MeVal; *N*-methyl-L-valine, Phe; L-phenylalanine, MePhe; *N*-methyl-L-phenylalanine, Pro; L-proline, Leu; L-leucine, alle; L-allo-isoleucine, HOMeVal; β-hydroxy-N-methyl-L-valine.

AbA has been shown to exhibit potent antifungal activity against *S. cerevisiae* and is thought to affect the organisation of bud growth and the integrity of the cell membrane (*149*). In addition, AbA has been shown to inhibit the parasitic organisms *Leishmania Major* and *Toxoplasma gondii*. Studies by Denny *et al.* have shown that 20 μM AbA inhibited 90 % growth of *L. major* cultures (although the parasites remained viable) and pre-treatment cells with AbA significantly delayed infectivity (*88*). Sonda *et al.* showed that AbA blocked *T. gondii* replication without affecting host cell metabolism (*150*).

The pathogenic fungal species *Candida* and *Aspergillus* are also susceptible to AbA treatment although there may be a naturally resistant phenotype of *Aspergillus fumigatus* (*151*). The growth of all species tested from both genera of fungi were inhibited with IC_{50} values in the nanomolar range (2-6 ng/mL) however, tests with the *Aspergillus* strains showed variable MIC values from 0.8 to >50 μg/mL. This difference in resistance to AbA was investigated further by Zhong *et al.* in order to determine the cause. MIC values measured in the presence of verapamil, a mammalian multi-drug resistance (MDR) modulator, showed that a concentration of 200 μg/mL verapamil reduced the MIC value for *A. fumigatus* to 3 μg/mL, suggesting that the increased resistance observed is due to increased efflux of AbA through some form of transporter (*147*).

MDR transporters belong to the superfamily of ATP Binding Cassette (ABC) transporters of which the CFTR sub-group are also members. Both subgroups of transporters are often involved in the increased resistance to chemotherapeutic agents (*152*). ABC transporters are also present in *S. cerevisiae* where the mutant strain $aur3^R$ contains a recessive mutation in the pleotropic drug resistance gene *PDR1*. *PDR1* is a transcriptional regulator of two ABC transporter genes *YOR1*, a member of the CFTR subgroup and *PDR5* which belongs to the MDR group of transporters. AbA resistant phenotypes are produced when functional *YOR1* and mutated *PDR1* are both present, suggesting a potential interaction for AbA with multi-drug resistance transporters.

1.9.2.2 Rustmicin

Rustmicin, **18** also known as galbonolide A, is a 14-membered macrolide isolated from *Micromonospora sp.* which was discovered due to its potent antifungal activity against phytopathogenic fungi (*153*). It is a reversible inhibitor of sphingolipid biosynthesis and acts upon IPC synthase, resulting in the accumulation of ceramide and consequent loss of complex sphingolipid formation.

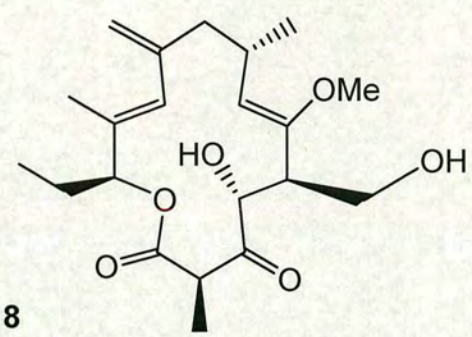

18

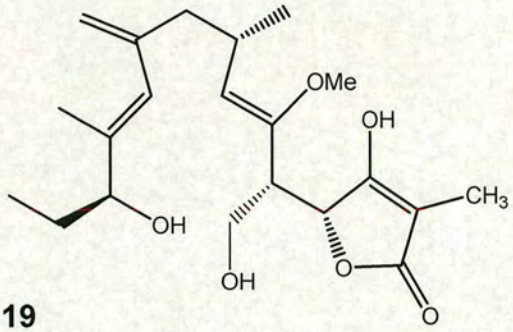

19

Rustmicin displays exceptional activity against *Cryptococcus neoformas*. Growth inhibition was achieved by Mandala *et al.* at concentrations below 1 ng/mL and IPC synthase was inhibited with an IC_{50} value of 70 pM (*154*). Its limitations for use as an antifungal agent lie mainly in its stability as it has been found to be less potent *in vivo* than expected from results achieved *in vitro*. This reduction in potency arises from a rearrangement of the structure in solution to produce the inactive γ-lactone derivative, **19**. An additional factor in reducing rustmicin's efficiency *in vivo* is that it is a good substrate for the MDR transporter *PDR5* mentioned previously (section 1.9.2.1).

1.9.2.3 Khafrefungin

Khafrefungin, **20** is a linear C_{22}-polyketide acid esterified with an aldonic acid. Like AbA and rustmicin, khafrefungin is active against *C. albicans*, *C. neoformans* and *S. cerevisiae* with MIC values of 2.0, 2.0 and 15.6 μg/mL respectively. Growth inhibition has been shown to result from the inhibition of sphingolipid biosynthesis, as khafrefungin is a potent inhibitor of IPC synthase (*155*).

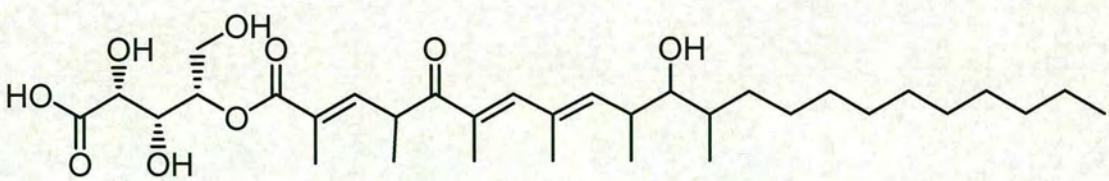

20

Inhibition of IPC synthase was shown, as in the case of rustmicin, to cause ceramide accumulation *in vivo* resulting in induced apoptosis of *S. cerevisiae* cells. In the same study by Mandala *et al.*, IC_{50} values of 0.09, 0.5 and 0.35 μg/mL were also obtained for the inhibition of IPC synthase from these organisms (*155*).

Wakabayashi *et al.* have shown that the stereochemistry of the hydroxyl groups of the aldonic acid moiety of khafrefungin is critical for antifungal activity as only the 2*R*, 3*R*, 4*S* compound, **20** exhibits antifungal activity. Their results have suggested that the mode of inhibition is mediated by the polar head group, which may mimic phosphoinositol (*156*).

1.9.2.4 The Pleofungins

The most recently discovered group of novel antifungal agents which are active against IPC synthase are the pleofungins, a group of depsipeptides isolated from a *Phoma sp.* fungus. Growth inhibition of *C. albicans*, *C. neoformans* and *A. fumigatus* by pleofungin A showed MIC values of 2.0, 0.3 and 0.5 μg/mL respectively. This molecule inhibited IPC synthase from *S. cerevisiae* and *A. fumigatus* with IC_{50} values of 16 and 1 ng/mL respectively (*157*).

1.9.3 Fungal Infections in Plants

In agriculture, the control of fungal infections is of great importance as fungal plant diseases are estimated to destroy approximately 20% of major food and cash crops worldwide (*158*). The plant pathogen *Botrytis cinerea* (grey mould) is one example as it causes serious pre- and post-harvest disease in economically important crops. It is a necrotrophic pathogen which affects plant cell viability by secreting toxins and host-degrading enzymes. In contrast to more specialised species, *B. cinerea* is indiscriminate in its phytopathogenicity and will therefore infect a range of plants and plant parts (*159*). This pathogen favours cool, moist conditions and is a weak parasite often found on injured or senescent plant tissue. The plants it can infect vary greatly in their biochemical defence mechanisms (*160*). *B. cinerea* infects

tissues by coordinating the expression of pathogenic enzymes, thus degrading the plant chemical defence systems and protective cell coatings (*161*).

In contrast to the agricultural problems it causes as a pathogen, under certain conditions *B. cinerea* infections can be beneficial. It is the causative organism of 'noble rot' which dries berries and causes the sugar and flavour to concentrate without affecting the acidity. This is exploited in the manufacture of dessert wines.

Studies by Ippolito *et al.* have shown that the yeast-like fungus *Aureobasidium pullulans* controls apple wound decay caused by *B. cinerea* (grey mould) and *Penicillium expansum* (blue mould). Typically, at the end of storage periods, *A. pullulans* had reduced decay from grey and blue mould by 89% and 67% respectively, compared to a water treated control (*162*). *A. pullulans* is thought to weaken the pathogen by out competing it for space and nutrients thus increasing their vulnerability to host secreted lytic enzymes and antibiotics. Since the antifungal agent aureobasidin A was originally isolated from the fermentation broth of *A. pullulans*, it is possible that *A. pullulans* suppresses the pathogenicity of *B. cinerea* through the action of AbA on IPC synthase. Furthermore, the IPC synthase inhibitor galbonolide A (rustmicin), isolated from *Streptomyces galbus* culture broth, possesses potent activity against *B. cinerea* amongst other pathogens (*163, 164*). The above studies indicate that *B. cinerea* may be a potential "model target" for further studies into IPC synthase inhibition.

1.10 Aims

Before the research described here was carried out, there was no structural information available for any enzyme involved in sphingolipid biosynthesis although enzyme isolation and biochemical characterisation studies were abundant. Since SPT catalyses the first and rate-limiting step of sphingolipid biosynthesis, it is an interesting target for structural studies. Since the structures of three members of the α-oxoamine synthase family of enzymes have been solved, comparative studies with SPT would be of significant interest (*71-73*).

Unfortunately, eukaryotic SPT is a membrane bound heterodimer and is extremely insoluble posing major technical difficulties for its isolation and characterisation. Fortunately however, a water soluble, bacterial homologue from *Sphingomonas paucimobilis* had been identified prior to this work providing a platform for structural studies (*49*).

The first aim in this research was the over-production, purification and crystallisation of wild-type *S. paucimobilis* SPT (*Sp* SPT). Naturally, if this could be crystallised in a form suitable for X-ray diffraction, it was hoped to solve the structure and to examine *Sp* SPT with substrates and/or inhibitors bound at the active site. It was expected that this structural information would provide an insight into the SPT mechanism.

Despite its importance as a target for antifungal agents, IPC synthase remains poorly characterised and therefore further studies into its isolation, over-production and biochemical characterisation need to be carried out. To date, no method for the over-production of IPC synthase has been reported and current wild-type IPC synthase isolation procedures are long and complicated processes these two areas need to be addressed (*113*). The second aim of this research therefore, was to optimise the over-production and purification of soluble IPC synthase from *S. cerevisiae*.

Although it would be relevant to agrochemical research to study IPC synthase from phytopathogenic fungi such as *Botrytis cinerea*, this fungus is more difficult to culture and manipulate compared to yeast. It seemed reasonable, therefore, to develop methods for IPC

synthase over-production and purification using the yeast enzyme. Isolation and characterisation of pure, soluble IPC synthase from either source should allow for further enzymatic studies and the availability of fungal IPC synthase for high-throughput screening would allow the identification of potentially useful inhibitors.

(1) McIlwain, H. (1975) The Second Thudichum Lecture. Cerebral isolates and neurochemical discovery. *Biochem Soc Trans 3*, 579-90.

(2) Spillane, J. D. (1974) 1874 - 1884: a memorable decade in the history of British neurology. *Trans Am Neurol Assoc 99*, 88-94.

(3) Levine, P., WA, Jacobs. (1912) On Sphingolipids. *The Journal of Biological Chemistry 11*, 547-554.

(4) Carter, H. E., and Humiston, C. G. (1951) Biochemistry of the sphingolipides. V. The structure of sphingine. *J Biol Chem 191*, 727-33.

(5) Carter, H. E., Nalbandov, O., and Tavormina, P. A. (1951) Biochemistry of the sphingolipides. VI. The o-methyl ethers of sphingosine. *J Biol Chem 192*, 197-207.

(6) Hakomori, S. I. (2007) Structure and function of glycosphingolipids and sphingolipids: Recollections and future trends. *Biochim Biophys Acta.*

(7) Fahy, E., Subramaniam, S., Brown, H. A., Glass, C. K., Merrill, A. H., Jr., Murphy, R. C., Raetz, C. R., Russell, D. W., Seyama, Y., Shaw, W., Shimizu, T., Spener, F., van Meer, G., VanNieuwenhze, M. S., White, S. H., Witztum, J. L., and Dennis, E. A. (2005) A comprehensive classification system for lipids. *J Lipid Res 46*, 839-61.

(8) Maceyka, M., Payne, S. G., Milstien, S., and Spiegel, S. (2002) Sphingosine kinase, sphingosine-1-phosphate, and apoptosis. *Biochim Biophys Acta 1585*, 193-201.

(9) Spiegel, S., and Milstien, S. (2002) Sphingosine 1-phosphate, a key cell signaling molecule. *J Biol Chem 277*, 25851-4.

(10) Dickson, R. C., and Lester, R. L. (2002) Sphingolipid functions in Saccharomyces cerevisiae. *Biochim Biophys Acta 1583*, 13-25.

(11) Sperling, P., and Heinz, E. (2003) Plant sphingolipids: structural diversity, biosynthesis, first genes and functions. *Biochimica et Biophysica Acta 1632*, 1-15.

(12) Huitema, K., van den Dikkenberg, J., Brouwers, J. F., and Holthuis, J. C. (2004) Identification of a family of animal sphingomyelin synthases. *Embo J 23*, 33-44.

(13) Hanada, K., Hara, T., and Nishijima, M. (2000) Purification of the serine palmitoyltransferase complex responsible for sphingoid base synthesis by using affinity peptide chromatography techniques. *J Biol Chem 275*, 8409-15.

(14) Linardic, C. M., and Hannun, Y. A. (1994) Identification of a distinct pool of sphingomyelin involved in the sphingomyelin cycle. *J Biol Chem 269*, 23530-7.

(15) Okazaki, T., Bell, R. M., and Hannun, Y. A. (1989) Sphingomyelin turnover induced by vitamin D3 in HL-60 cells. Role in cell differentiation. *J Biol Chem 264*, 19076-80.

(16) Grimm MO, G. H., Pätzold AJ, Zinser EG, Halonen R, Duering M, Tschäpe JA, De Strooper B, Müller U, Shen J, Hartmann T. (2005) Regulation of cholesterol and sphingomyelin metabolism by amyloid-beta and presenilin. *Nat Cell Biol 7*, 1118-1123.

(17) Kim, M. Y., Linardic, C., Obeid, L., and Hannun, Y. (1991) Identification of sphingomyelin turnover as an effector mechanism for the action of tumor necrosis factor alpha and gamma-interferon. Specific role in cell differentiation. *J Biol Chem 266*, 484-9.

(18) Colombaioni, L., and Garcia-Gil, M. (2004) Sphingolipid metabolites in neural signalling and function. *Brain Res Brain Res Rev 46*, 328-55.

(19) Ogretmen, B., and Hannun, Y. A. (2004) Biologically active sphingolipids in cancer pathogenesis and treatment. *Nat Rev Cancer 4*, 604-16.

(20) van Echten-Deckert, G., and Herget, T. (2006) Sphingolipid metabolism in neural cells. *Biochim Biophys Acta 1758*, 1978-94.

(21) Riboni, L., Tettamanti, G., and Viani, P. (2002) Ceramide in primary astrocytes from cerebellum: metabolism and role in cell proliferation. *Cerebellum 1*, 129-35.

(22) Huang, Y., Tanimukai, H., Liu, F., Iqbal, K., Grundke-Iqbal, I., and Gong, C. X. (2004) Elevation of the level and activity of acid ceramidase in Alzheimer's disease brain. *Eur J Neurosci 20*, 3489-97.

(23) Olivera, A., Kohama, T., Edsall, L., Nava, V., Cuvillier, O., Poulton, S., and Spiegel, S. (1999) Sphingosine kinase expression increases intracellular sphingosine-1-phosphate and promotes cell growth and survival. *J Cell Biol 147*, 545-58.

(24) Olivera, A., and Spiegel, S. (1993) Sphingosine-1-phosphate as second messenger in cell proliferation induced by PDGF and FCS mitogens. *Nature 365*, 557-60.

(25) Zhang, H., Desai, N. N., Olivera, A., Seki, T., Brooker, G., and Spiegel, S. (1991) Sphingosine-1-phosphate, a novel lipid, involved in cellular proliferation. *J Cell Biol 114*, 155-67.

(26) Radin, N. S. (2006) Preventing the binding of pathogens to the host by controlling sphingolipid metabolism. *Microbes Infect 8*, 938-45.

(27) Warnecke, D., and Heinz, E. (2003) Recently discovered functions of glucosylceramides in plants and fungi. *Cell Mol Life Sci 60*, 919-41.

(28) Tybulewicz VL, T. M., LaMarca ME, Willemsen R, Stubblefield BK, Winfield S, Zablocka B, Sidransky E, Martin BM, Huang SP, et al. (1994) Animal model of Gaucher's disease from targeted disruption of the mouse glucocerebrosidase gene. *Nature 357*, 407-410.

(29) Jacob, J. C., Kutty, K. M., Islam, M., Dominic, R. G., and Dawson, G. (1973) Krabbe's disease: globoid cell leukodystrophy. *Can Med Assoc J 108*, 1398-400.

(30) Wenger, D. A., Sattler, M., and Hiatt, W. (1974) Globoid cell leukodystrophy: deficiency of lactosyl ceramide beta-galactosidase. *Proc Natl Acad Sci U S A 71*, 854-7.

(31) Svennerholm, L. (1956) Composition of gangliosides from human brain. *Nature 177*, 524-5.

(32) Brown, D., E, London. (1998) Structure and origin of ordered lipid domains in biological membranes. *J. Membr. Biol. 164*, 103-114.

(33) Brown, D., E, London. (1998) Functions of lipid rafts in biological membranes. *Annu Rev Cell Dev Biol. 14*, 111-136.

(34) Riethmuller, J., Riehle, A., Grassme, H., and Gulbins, E. (2006) Membrane rafts in host-pathogen interactions. *Biochim Biophys Acta 1758*, 2139-47.

(35) Simons, K., and Ikonen, E. (1997) Functional rafts in cell membranes. *Nature 387*, 569-72.

(36) Ono, A., and Freed, E. O. (2001) Plasma membrane rafts play a critical role in HIV-1 assembly and release. *Proc Natl Acad Sci U S A 98*, 13925-30.

(37) Harouse, J. M., Bhat, S., Spitalnik, S. L., Laughlin, M., Stefano, K., Silberberg, D. H., and Gonzalez-Scarano, F. (1991) Inhibition of entry of HIV-1 in neural cell lines by antibodies against galactosyl ceramide. *Science 253*, 320-3.

(38) Kinjo, Y., Wu, D., Kim, G., Xing, G. W., Poles, M. A., Ho, D. D., Tsuji, M., Kawahara, K., Wong, C. H., and Kronenberg, M. (2005) Recognition of bacterial glycosphingolipids by natural killer T cells. *Nature 434*, 520-5.

(39) Wu, D., Xing, G. W., Poles, M. A., Horowitz, A., Kinjo, Y., Sullivan, B., Bodmer-Narkevitch, V., Plettenburg, O., Kronenberg, M., Tsuji, M., Ho, D. D., and Wong, C. H. (2005) Bacterial glycolipids and analogs as antigens for CD1d-restricted NKT cells. *Proc Natl Acad Sci U S A 102*, 1351-6.

(40) Kawahara, K., Seydel, U., Matsuura, M., Danbara, H., Rietschel, E. T., and Zahringer, U. (1991) Chemical structure of glycosphingolipids isolated from Sphingomonas paucimobilis. *FEBS Lett 292*, 107-10.

(41) Krziwon, C., Zahringer, U., Kawahara, K., Weidemann, B., Kusumoto, S., Rietschel, E. T., Flad, H. D., and Ulmer, A. J. (1995) Glycosphingolipids from Sphingomonas

paucimobilis induce monokine production in human mononuclear cells. *Infect Immun 63*, 2899-905.

(42) Lemaitre, D., Elaichouni, A., Hundhausen, M., Claeys, G., Vanhaesebrouck, P., Vaneechoutte, M., and Verschraegen, G. (1996) Tracheal colonization with Sphingomonas paucimobilis in mechanically ventilated neonates due to contaminated ventilator temperature probes. *J Hosp Infect 32*, 199-206.

(43) Perola, O., Nousiainen, T., Suomalainen, S., Aukee, S., Karkkainen, U. M., Kauppinen, J., Ojanen, T., and Katila, M. L. (2002) Recurrent Sphingomonas paucimobilis -bacteraemia associated with a multi-bacterial water-borne epidemic among neutropenic patients. *J Hosp Infect 50*, 196-201.

(44) Yabuuchi, E., Yano, I., Oyaizu, H., Hashimoto, Y., Ezaki, T., and Yamamoto, H. (1990) Proposals of Sphingomonas paucimobilis gen. nov. and comb. nov., Sphingomonas parapaucimobilis sp. nov., Sphingomonas yanoikuyae sp. nov., Sphingomonas adhaesiva sp. nov., Sphingomonas capsulata comb. nov., and two genospecies of the genus Sphingomonas. *Microbiol Immunol 34*, 99-119.

(45) Yamamoto, A., Yano, I., Masui, M., and Yabuuchi, E. (1978) Isolation of a novel sphingoglycolipid containing glucuronic acid and 2-hydroxy fatty acid from Flavobacterium devorans ATCC 10829. *J Biochem (Tokyo) 83*, 1213-6.

(46) Kawahara, K., Uchida, K., and Aida, K. (1982) Isolation of an unusual 'lipid A' type glycolipid from Pseudomonas paucimobilis. *Biochim Biophys Acta 712*, 571-5.

(47) Kawahara, K., Kuraishi, H., and Zahringer, U. (1999) Chemical structure and function of glycosphingolipids of Sphingomonas spp and their distribution among members of the alpha-4 subclass of Proteobacteria. *J Ind Microbiol Biotechnol 23*, 408-413.

(48) Alexander, C., and Rietschel, E. T. (2001) Bacterial lipopolysaccharides and innate immunity. *J Endotoxin Res 7*, 167-202.

(49) Ikushiro, H., Hayashi, H., and Kagamiyama, H. (2001) A water-soluble homodimeric serine palmitoyltransferase from Sphingomonas paucimobilis EY2395T strain. Purification, characterization, cloning, and overproduction. *J Biol Chem 276*, 18249-56.

(50) Ikushiro, H., Islam, M. M., Tojo, H., and Hayashi, H. (2007) Molecular characterization of membrane-associated soluble serine palmitoyltransferases from Sphingobacterium multivorum and Bdellovibrio stolpii. *J Bacteriol 189*, 5749-61.

(51) Weiss, B., and Stoffel, W. (1997) Human and murine serine-palmitoyl-CoA transferase--cloning, expression and characterization of the key enzyme in sphingolipid synthesis. *Eur J Biochem 249*, 239-47.

(52) Buede, R., Rinker-Schaffer, C., Pinto, W. J., Lester, R. L., and Dickson, R. C. (1991) Cloning and characterization of LCB1, a Saccharomyces gene required for biosynthesis of the long-chain base component of sphingolipids. *J Bacteriol 173*, 4325-32.

(53) Nagiec, M. M., Baltisberger, J. A., Wells, G. B., Lester, R. L., and Dickson, R. C. (1994) The LCB2 gene of Saccharomyces and the related LCB1 gene encode subunits of serine palmitoyltransferase, the initial enzyme in sphingolipid synthesis. *Proc Natl Acad Sci U S A 91*, 7899-902.

(54) Tamura, K., Nishiura, H., Mori, J., and Imai, H. (2000) Cloning and characterization of a cDNA encoding serine palmitoyltransferase in Arabidopsis thaliana. *Biochem Soc Trans 28*, 745-7.

(55) Han, G., Gable, K., Yan, L., Allen, M. J., Wilson, W. H., Moitra, P., Harmon, J. M., and Dunn, T. M. (2006) Expression of a novel marine viral single-chain serine palmitoyltransferase and construction of yeast and mammalian single-chain chimera. *J Biol Chem 281*, 39935-42.

(56) Wells, G. B., and Lester, R. L. (1983) The isolation and characterization of a mutant strain of Saccharomyces cerevisiae that requires a long chain base for growth and for synthesis of phosphosphingolipids. *J Biol Chem 258*, 10200-3.

(57) Pinto, W. J., Wells, G. W., and Lester, R. L. (1992) Characterization of enzymatic synthesis of sphingolipid long-chain bases in Saccharomyces cerevisiae: mutant strains exhibiting long-chain-base auxotrophy are deficient in serine palmitoyltransferase activity. *J Bacteriol 174*, 2575-81.

(58) Yasuda, S., Nishijima, M., and Hanada, K. (2003) Localization, topology, and function of the LCB1 subunit of serine palmitoyltransferase in mammalian cells. *J Biol Chem 278*, 4176-83.

(59) Gable, K., Slife, H., Bacikova, D., Monaghan, E., and Dunn, T. M. (2000) Tsc3p is an 80-amino acid protein associated with serine palmitoyltransferase and required for optimal enzyme activity. *J Biol Chem 275*, 7597-603.

(60) Wilson, W. H., Schroeder, D. C., Allen, M. J., Holden, M. T., Parkhill, J., Barrell, B. G., Churcher, C., Hamlin, N., Mungall, K., Norbertczak, H., Quail, M. A., Price, C., Rabbinowitsch, E., Walker, D., Craigon, M., Roy, D., and Ghazal, P. (2005) Complete genome sequence and lytic phase transcription profile of a Coccolithovirus. *Science 309*, 1090-2.

(61) Tamura, K., Mitsuhashi, N., Hara-Nishimura, I., and Imai, H. (2001) Characterization of an Arabidopsis cDNA encoding a subunit of serine palmitoyltransferase, the initial enzyme in sphingolipid biosynthesis. *Plant Cell Physiol 42*, 1274-81.

(62) Chen, M., Han, G., Dietrich, C. R., Dunn, T. M., and Cahoon, E. B. (2006) The essential nature of sphingolipids in plants as revealed by the functional identification and characterization of the Arabidopsis LCB1 subunit of serine palmitoyltransferase. *Plant Cell 18*, 3576-93.

(63) Yard, B. A., Carter, L. G., Johnson, K. A., Overton, I. M., Dorward, M., Liu, H., McMahon, S. A., Oke, M., Puech, D., Barton, G. J., Naismith, J. H., and Campopiano, D. J. (2007) The structure of serine palmitoyltransferase; gateway to sphingolipid biosynthesis. *J Mol Biol 370*, 870-86.

(64) Hornemann, T., Richard, S., Rutti, M. F., Wei, Y., and von Eckardstein, A. (2006) Cloning and initial characterization of a new subunit for mammalian serine-palmitoyltransferase. *J Biol Chem 281*, 37275-81.

(65) Hornemann, T., Wei, Y., and von Eckardstein, A. (2007) Is the mammalian serine palmitoyltransferase a high-molecular-mass complex? *Biochem J 405*, 157-64.

(66) Nicholson, G. A., Dawkins, J. L., Blair, I. P., Kennerson, M. L., Gordon, M. J., Cherryson, A. K., Nash, J., and Bananis, T. (1996) The gene for hereditary sensory neuropathy type I (HSN-I) maps to chromosome 9q22.1-q22.3. *Nat Genet 13*, 101-4.

(67) Bejaoui, K., Wu, C., Scheffler, M. D., Haan, G., Ashby, P., Wu, L., de Jong, P., and Brown, R. H., Jr. (2001) SPTLC1 is mutated in hereditary sensory neuropathy, type 1. *Nat Genet 27*, 261-2.

(68) Dawkins, J. L., Hulme, D. J., Brahmbhatt, S. B., Auer-Grumbach, M., and Nicholson, G. A. (2001) Mutations in SPTLC1, encoding serine palmitoyltransferase, long chain base subunit-1, cause hereditary sensory neuropathy type I. *Nat Genet 27*, 309-12.

(69) Bejaoui, K., Uchida, Y., Yasuda, S., Ho, M., Nishijima, M., Brown, R. H., Jr., Holleran, W. M., and Hanada, K. (2002) Hereditary sensory neuropathy type 1 mutations confer dominant negative effects on serine palmitoyltransferase, critical for sphingolipid synthesis. *J Clin Invest 110*, 1301-8.

(70) Dawkins, J. L., Brahmbhatt, S., Auer-Grumbach, M., Wagner, K., Hartung, H. P., Verhoeven, K., Timmerman, V., De Jonghe, P., Kennerson, M., LeGuern, E., and

Nicholson, G. A. (2002) Exclusion of serine palmitoyltransferase long chain base subunit 2 (SPTLC2) as a common cause for hereditary sensory neuropathy. *Neuromuscul Disord 12*, 656-8.

(71) Alexeev, D., Alexeeva, M., Baxter, R. L., Campopiano, D. J., Webster, S. P., and Sawyer, L. (1998) The crystal structure of 8-amino-7-oxononanoate synthase: a bacterial PLP-dependent, acyl-CoA-condensing enzyme. *J Mol Biol 284*, 401-19.

(72) Astner, I., Schulze, J. O., van den Heuvel, J., Jahn, D., Schubert, W. D., and Heinz, D. W. (2005) Crystal structure of 5-aminolevulinate synthase, the first enzyme of heme biosynthesis, and its link to XLSA in humans. *Embo J 24*, 3166-77.

(73) Schmidt, A., Sivaraman, J., Li, Y., Larocque, R., Barbosa, J. A., Smith, C., Matte, A., Schrag, J. D., and Cygler, M. (2001) Three-dimensional structure of 2-amino-3-ketobutyrate CoA ligase from Escherichia coli complexed with a PLP-substrate intermediate: inferred reaction mechanism. *Biochemistry 40*, 5151-60.

(74) Garneau-Tsodikova, S., Dorrestein P. C, Kelleher N. L and Walsh C. T. (2006) Protein assembly line components in prodigiosin biosynthesis:Characterisation of PigA,G,H,I,J. *J. Am. Chem. Soc. 128*, 12600-12601.

(75) Stanley, A., Walton L. J, Kourdi Zerikly M., Corre C. and Challis G. L. (2006) Elucidation of the *Streptomyces coelicolor* pathway to 4-methoxy-2,2'-bipyrrole-5-carboxaldehyde, an intermediate in prodiginine biosynthesis. *Chem. Commun.*, 3981-3983.

(76) Alexander, F. W., Sandmeier, E., Mehta, P. K., and Christen, P. (1994) Evolutionary relationships among pyridoxal-5'-phosphate-dependent enzymes. Regio-specific alpha, beta and gamma families. *Eur J Biochem 219*, 953-60.

(77) Grishin, N. V., Phillips, M. A., and Goldsmith, E. J. (1995) Modeling of the spatial structure of eukaryotic ornithine decarboxylases. *Protein Sci 4*, 1291-304.

(78) Jansonius, J. N. (1998) Structure, evolution and action of vitamin B6-dependent enzymes. *Curr Opin Struct Biol 8*, 759-69.

(79) Toney, M. D. (2005) Reaction specificty in pyridoxal phosphate enzymes. *Archives of Biochemistry and Biophysics 433*, 279-287.

(80) Hunter, G. A., and Ferreira, G. C. (1999) Lysine-313 of 5-Aminolevulinate Synthase Acts as a General Base during Formation of the Quinonoid Reaction Intermediates. *Biochemistry 38*, 12526.

(81) Lu, Z., Nagata, S., McPhie, P., and Miles, E. W. (1993) Lysine 87 in the beta subunit of tryptophan synthase that forms an internal aldimine with pyridoxal phosphate serves critical roles in transimination, catalysis, and product release. *J Biol Chem 268*, 8727-34.

(82) Toney, M. D., and Kirsch, J. F. (1993) Lysine 258 in aspartate aminotransferase: enforcer of the Circe effect for amino acid substrates and general-base catalyst for the 1,3-prototropic shift. *Biochemistry 32*, 1471-9.

(83) Webster, S. P., Alexeev, D., Campopiano, D. J., Watt, R. M., Alexeeva, M., Sawyer, L., and Baxter, R. L. (2000) Mechanism of 8-amino-7-oxononanoate synthase: spectroscopic, kinetic, and crystallographic studies. *Biochemistry 39*, 516-28.

(84) Toney, M. D., and Kirsch, J. F. (1991) The K258R mutant of aspartate aminotransferase stabilizes the quinonoid intermediate. *J Biol Chem 266*, 23900-3.

(85) Ploux, O., and Marquet, A. (1996) Mechanistic studies on the 8-amino-7-oxopelargonate synthase, a pyridoxal-5'-phosphate-dependent enzyme involved in biotin biosynthesis. *Eur J Biochem 236*, 301-8.

(86) Kerbarh, O., Campopiano, D. J., and Baxter, R. L. (2006) Mechanism of alpha-oxoamine synthases: identification of the intermediate Claisen product in the 8-amino-7-oxononanoate synthase reaction. *Chem Commun (Camb)*, 60-2.

(87) Becker, G. W., and Lester, R. L. (1980) Biosynthesis of phosphoinositol-containing sphingolipids from phosphatidylinositol by a membrane preparation from Saccharomyces cerevisiae. *J Bacteriol 142*, 747-54.

(88) Denny, P. W., Shams-Eldin, H., Price, H. P., Smith, D. F., and Schwarz, R. T. (2006) The protozoan inositol phosphorylceramide synthase: a novel drug target that defines a new class of sphingolipid synthase. *J Biol Chem 281*, 28200-9.

(89) Heidler, S. A., and Radding, J. A. (2000) Inositol phosphoryl transferases from human pathogenic fungi. *Biochim Biophys Acta 1500*, 147-52.

(90) Bromley, P. E., Li, Y. O., Murphy, S. M., Sumner, C. M., and Lynch, D. V. (2003) Complex sphingolipid synthesis in plants: characterization of inositolphosphorylceramide synthase activity in bean microsomes. *Arch Biochem Biophys 417*, 219-26.

(91) Luberto, C., Toffaletti, D. L., Wills, E. A., Tucker, S. C., Casadevall, A., Perfect, J. R., Hannun, Y. A., and Del Poeta, M. (2001) Roles for inositol-phosphoryl ceramide synthase 1 (IPC1) in pathogenesis of C. neoformans. *Genes Dev 15*, 201-12.

(92) Tafesse, F. G., Huitema, K., Hermansson, M., van der Poel, S., van den Dikkenberg, J., Uphoff, A., Somerharju, P., and Holthuis, J. C. (2007) Both sphingomyelin synthases SMS1 and SMS2 are required for sphingomyelin homeostasis and growth in human HeLa cells. *J Biol Chem 282*, 17537-47.

(93) Eastcott, E. V. (1928) Wildeirs' Bios. *J. Phys. Chem 32*, 1094-1111.

(94) Pennington, D., Sawyer, C. H., and Schmidt, J. (1951) The nature of the growth response of Saccharomyces cerevisiae to inositol. *J Bacteriol 62*, 677-83.

(95) Ghosh, A., Charalampous, F., Sison, Y., and Borer, R. (1960) Metabolic function of myo-inositol. I. Cytological and chemical alterations in yeast resulting from inositol deficiency. *J Biol Chem 235*, 2522-8.

(96) Eagle, H., Oyama, V. I., Levy, M., and Freeman, A. E. (1957) Myo-Inositol as an essential growth factor for normal and malignant human cells in tissue culture. *J Biol Chem 226*, 191-205.

(97) Steiner, S., and Lester, R. L. (1972) Studies on the diversity of inositol-containing yeast phospholipids: incorporation of 2-deoxyglucose into lipid. *J Bacteriol 109*, 81-8.

(98) Steiner, S., Smith, S., Waechter, C. J., and Lester, R. L. (1969) Isolation and partial characterization of a major inositol-containing lipid in baker's yeast, mannosyl-diinositol, diphosphoryl-ceramide. *Proc Natl Acad Sci U S A 64*, 1042-8.

(99) Lester, R. L., Smith, S. W., Wells, G. B., Rees, D. C., and Angus, W. W. (1974) The isolation and partial characterization of two novel sphingolipids from Neurospora crassa: di(inositolphosphoryl)ceramide and ((gal)3glu)ceramide. *J Biol Chem 249*, 3388-94.

(100) Hashida-Okado, T., Takeuchi R., Endo M., Takesako K. and Kato I., (1994) Cloning and characterisation of a gene conferring resistance to the antifungal antibiotic aureobasidin A (R106-1) in fission yeast. *In Abstracts of Annual Meeting of Japan Society of Molecular Biology.*

(101) Okado, T., Takesako K. and Kato L., (1995) Gene coding for a protein regulationg aureobasidin sensitivity. *European patent apllication 94303401.7. European Patent publication 0 644 262 A2.*

(102) Radding, J. and Heidler S. A., (1994) Identification and cloning of a mutant gene encoding dominant resistance to LY295337 (R106-1). *In Abstracts of the 5th International Mycology Congress, Vancouver, B.C*, 175.

(103) Hashida-Okado, T., Ogawa, A., Endo, M., Yasumoto, R., Takesako, K., and Kato, I. (1996) AUR1, a novel gene conferring aureobasidin resistance on Saccharomyces

cerevisiae: a study of defective morphologies in Aur1p-depleted cells. *Mol Gen Genet 251*, 236-44.

(104) Heidler, S. A., and Radding, J. A. (1995) The AUR1 gene in Saccharomyces cerevisiae encodes dominant resistance to the antifungal agent aureobasidin A (LY295337). *Antimicrob Agents Chemother 39*, 2765-9.

(105) Hashida-Okado, T., Yasumoto, R., Endo, M., Takesako, K., and Kato, I. (1998) Isolation and characterization of the aureobasidin A-resistant gene, aur1R, on Schizosaccharomyces pombe: roles of Aur1p+ in cell morphogenesis. *Curr Genet 33*, 38-45.

(106) Kuroda, M., Hashida-Okado, T., Yasumoto, R., Gomi, K., Kato, I., and Takesako, K. (1999) An aureobasidin A resistance gene isolated from Aspergillus is a homolog of yeast AUR1, a gene responsible for inositol phosphorylceramide (IPC) synthase activity. *Mol Gen Genet 261*, 290-6.

(107) Hashida-Okado, T., Ogawa, A., Kato, I., and Takesako, K. (1998) Transformation system for prototrophic industrial yeasts using the AUR1 gene as a dominant selection marker. *FEBS Lett 425*, 117-22.

(108) Hansen, J., Felding, T., Johannesen, P. F., Piskur, J., Christensen, C. L., and Olesen, K. (2003) Further development of the cassette-based pYC plasmid system by incorporation of the dominant hph, nat and AUR1-C gene markers and the lacZ reporter system. *FEMS Yeast Res 4*, 323-7.

(109) Hechtberger, P., Zinser, E., Saf, R., Hummel, K., Paltauf, F., and Daum, G. (1994) Characterization, quantification and subcellular localization of inositol-containing sphingolipids of the yeast, Saccharomyces cerevisiae. *Eur J Biochem 225*, 641-9.

(110) Leber, A., Hrastnik, C., and Daum, G. (1995) Phospholipid-synthesizing enzymes in Golgi membranes of the yeast, Saccharomyces cerevisiae. *FEBS Lett 377*, 271-4.

(111) Hechtberger, P., and Daum, G. (1995) Intracellular transport of inositol-containing sphingolipids in the yeast, Saccharomyces cerevisiae. *FEBS Lett 367*, 201-4.

(112) Levine, T. P., Wiggins, C. A., and Munro, S. (2000) Inositol phosphorylceramide synthase is located in the Golgi apparatus of Saccharomyces cerevisiae. *Mol Biol Cell 11*, 2267-81.

(113) Ko, J., Cheah S. and Fischl A. S., (1995) Solubilisation and characterisation of microsomal-associated phosphatidylinositol:ceramide phosphoinositol transferase from *Saccharomyces cerevisiae*. *Journal of Food Biochemistry 19*, 253-267.

(114) Aeed, P. A., Sperry, A. E., Young, C. L., Nagiec, M. M., and Elhammer, A. P. (2004) Effect of membrane perturbants on the activity and phase distribution of inositol phosphorylceramide synthase; development of a novel assay. *Biochemistry 43*, 8483-93.

(115) Hartmann, A. M., Nayler, O., Schwaiger, F. W., Obermeier, A., and Stamm, S. (1999) The interaction and colocalization of Sam68 with the splicing-associated factor YT521-B in nuclear dots is regulated by the Src family kinase p59(fyn). *Mol Biol Cell 10*, 3909-26.

(116) Nagai, A., Saijo, M., Kuraoka, I., Matsuda, T., Kodo, N., Nakatsu, Y., Mimaki, T., Mino, M., Biggerstaff, M., Wood, R. D., and et al. (1995) Enhancement of damage-specific DNA binding of XPA by interaction with the ERCC1 DNA repair protein. *Biochem Biophys Res Commun 211*, 960-6.

(117) Poetsch, A., Molday, L. L., and Molday, R. S. (2001) The cGMP-gated channel and related glutamic acid-rich proteins interact with peripherin-2 at the rim region of rod photoreceptor disc membranes. *J Biol Chem 276*, 48009-16.

(118) Groll, A. H., De Lucca, A. J., and Walsh, T. J. (1998) Emerging targets for the development of novel antifungal therapeutics. *Trends Microbiol 6*, 117-24.

(119) Nagiec, M. M., Nagiec, E. E., Baltisberger, J. A., Wells, G. B., Lester, R. L., and Dickson, R. C. (1997) Sphingolipid synthesis as a target for antifungal drugs. Complementation of the inositol phosphorylceramide synthase defect in a mutant strain of Saccharomyces cerevisiae by the AUR1 gene. *J Biol Chem 272*, 9809-17.

(120) Nagiec, M. M., Young, C. L., Zaworski, P. G., and Kobayashi, S. D. (2003) Yeast sphingolipid bypass mutants as indicators of antifungal agents selectively targeting sphingolipid synthesis. *Biochem Biophys Res Commun 307*, 369-74.

(121) Georgopapadakou, N. H. (2000) Antifungals targeted to sphingolipid synthesis: focus on inositol phosphorylceramide synthase. *Expert Opin Investig Drugs 9*, 1787-96.

(122) Fostel, J. M., and Lartey, P. A. (2000) Emerging novel antifungal agents. *Drug Discov Today 5*, 25-32.

(123) Vicente, M. F., Basilio, A., Cabello, A., and Pelaez, F. (2003) Microbial natural products as a source of antifungals. *Clin Microbiol Infect 9*, 15-32.

(124) Cartledge, J. D., Midgley, J., and Gazzard, B. G. (1997) Clinically significant azole cross-resistance in Candida isolates from HIV-positive patients with oral candidosis. *Aids 11*, 1839-44.

(125) Mandala, S. M., Frommer, B. R., Thornton, R. A., Kurtz, M. B., Young, N. M., Cabello, M. A., Genilloud, O., Liesch, J. M., Smith, J. L., and Horn, W. S. (1994) Inhibition of serine palmitoyl-transferase activity by lipoxamycin. *J Antibiot (Tokyo) 47*, 376-9.

(126) Miyake, Y., Kozutsumi, Y., Nakamura, S., Fujita, T., and Kawasaki, T. (1995) Serine palmitoyltransferase is the primary target of a sphingosine-like immunosuppressant, ISP-1/myriocin. *Biochem Biophys Res Commun 211*, 396-403.

(127) VanMiddlesworth, F., Giacobbe, R. A., Lopez, M., Garrity, G., Bland, J. A., Bartizal, K., Fromtling, R. A., Polishook, J., Zweerink, M., Edison, A. M., and et al. (1992) Sphingofungins A, B, C, and D; a new family of antifungal agents. I. Fermentation, isolation, and biological activity. *J Antibiot (Tokyo) 45*, 861-7.

(128) St-Jacques, M. (1973) Elucidation of structure and stereochemistry of myriocin. A novel antifungal antibiotic. *J Org Chem 38*, 1253-60.

(129) Fujita, T., Inoue, K., Yamamoto, S., Ikumoto, T., Sasaki, S., Toyama, R., Chiba, K., Hoshino, Y., and Okumoto, T. (1994) Fungal metabolites. Part 11. A potent immunosuppressive activity found in Isaria sinclairii metabolite. *J Antibiot (Tokyo) 47*, 208-15.

(130) Chen, J. K., Lane, W. S., and Schreiber, S. L. (1999) The identification of myriocin-binding proteins. *Chem Biol 6*, 221-35.

(131) Hanada, K., Nishijima, M., Fujita, T., and Kobayashi, S. (2000) Specificity of inhibitors of serine palmitoyltransferase (SPT), a key enzyme in sphingolipid biosynthesis, in intact cells. A novel evaluation system using an SPT-defective mammalian cell mutant. *Biochem Pharmacol 59*, 1211-6.

(132) Ikushiro, H., Hayashi, H., and Kagamiyama, H. (2004) Reactions of serine palmitoyltransferase with serine and molecular mechanisms of the actions of serine derivatives as inhibitors. *Biochemistry 43*, 1082-92.

(133) Zweerink, M. M., Edison, A. M., Wells, G. B., Pinto, W., and Lester, R. L. (1992) Characterization of a novel, potent, and specific inhibitor of serine palmitoyltransferase. *J Biol Chem 267*, 25032-8.

(134) Horn, W. S., Smith, J. L., Bills, G. F., Raghoobar, S. L., Helms, G. L., Kurtz, M. B., Marrinan, J. A., Frommer, B. R., Thornton, R. A., and Mandala, S. M. (1992) Sphingofungins E and F: novel serinepalmitoyl transferase inhibitors from Paecilomyces variotii. *J Antibiot (Tokyo) 45*, 1692-6.

(135) Yamaji-Hasegawa, A., Takahashi, A., Tetsuka, Y., Senoh, Y., and Kobayashi, T. (2005) Fungal metabolite sulfamisterin suppresses sphingolipid synthesis through inhibition of serine palmitoyltransferase. *Biochemistry 44*, 268-77.

(136) Sato, H., Maeba, T., Yanase, R., Yamaji-Hasegawa, A., Kobayashi, T., and Chida, N. (2005) Total synthesis and biological activities of (+)-sulfamisterin (AB5366) and its analogues. *J Antibiot (Tokyo) 58*, 37-49.

(137) Whaley, H. A., Sebek, O. K., and Lewis, C. (1970) Production, isolation, characterization, and evaluation of lipoxamycin, a new antifungal agent. *Antimicrobial Agents Chemother (Bethesda) 10*, 455-61.

(138) Whaley, H. A. (1971) The structure of lipoxamycin, a novel antifungal antibiotic. *J Am Chem Soc 93*, 3767-9.

(139) Noda, M., Matoba, Y., Kumagai, T., and Sugiyama, M. (2004) Structural evidence that alanine racemase from a D-cycloserine-producing microorganism exhibits resistance to its own product. *J Biol Chem 279*, 46153-61.

(140) Peisach, D., Chipman, D. M., Van Ophem, P. W., Manning, J. M., and Ringe, D. (1998) Crystallographic study of steps along the reaction pathway of D-amino acid aminotransferase. *Biochemistry 37*, 4958-67.

(141) Shoji, J., Hinoo, H., Masunaga, R., Hattori, T., Wakisaka, Y., and Kondo, E. (1984) Isolation of L-cycloserine from Erwinia uredovora. *J Antibiot (Tokyo) 37*, 1198-203.

(142) Sundaram, K. S., and Lev, M. (1984) L-cycloserine inhibition of sphingolipid synthesis in the anaerobic bacterium Bacteroides levii. *Biochem Biophys Res Commun 119*, 814-9.

(143) Sundaram, K. S., and Lev, M. (1985) Inhibition of cerebroside synthesis in the brains of mice treated with L-cycloserine. *J Lipid Res 26*, 473-7.

(144) Williams, R. D., Sgoutas, D. S., Zaatari, G. S., and Santoianni, R. A. (1987) Inhibition of serine palmitoyltransferase activity in rabbit aorta by L-cycloserine. *J Lipid Res 28*, 1478-81.

(145) Sundaram, K. S., and Lev, M. (1984) Comparative inhibition of bacterial and microsomal 3-ketodihydrosphingosine synthetases by L-cycloserine and other inhibitors. *Antimicrob Agents Chemother 26*, 211-3.

(146) Ikai, K., Takesako, K., Shiomi, K., Moriguchi, M., Umeda, Y., Yamamoto, J., Kato, I., and Naganawa, H. (1991) Structure of aureobasidin A. *J Antibiot (Tokyo) 44*, 925-33.

(147) Zhong, W., Jeffries, M. W., and Georgopapadakou, N. H. (2000) Inhibition of inositol phosphorylceramide synthase by aureobasidin A in Candida and Aspergillus species. *Antimicrob Agents Chemother 44*, 651-3.

(148) Zhong, W., Murphy, D. J., and Georgopapadakou, N. H. (1999) Inhibition of yeast inositol phosphorylceramide synthase by aureobasidin A measured by a fluorometric assay. *FEBS Lett 463*, 241-4.

(149) Endo, M., Takesako, K., Kato, I., and Yamaguchi, H. (1997) Fungicidal action of aureobasidin A, a cyclic depsipeptide antifungal antibiotic, against Saccharomyces cerevisiae. *Antimicrob Agents Chemother 41*, 672-6.

(150) Sonda, S., Sala, G., Ghidoni, R., Hemphill, A., and Pieters, J. (2005) Inhibitory effect of aureobasidin A on Toxoplasma gondii. *Antimicrob Agents Chemother 49*, 1794-801.

(151) Takesako, K., Kuroda, H., Inoue, T., Haruna, F., Yoshikawa, Y., Kato, I., Uchida, K., Hiratani, T., and Yamaguchi, H. (1993) Biological properties of aureobasidin A, a cyclic depsipeptide antifungal antibiotic. *J Antibiot (Tokyo) 46*, 1414-20.

(152) Ogawa, A., Hashida-Okado, T., Endo, M., Yoshioka, H., Tsuruo, T., Takesako, K., and Kato, I. (1998) Role of ABC transporters in aureobasidin A resistance. *Antimicrob Agents Chemother 42*, 755-61.

(153) Takatsu, T., Nakayama, H., Shimazu, A., Furihata, K., Ikeda, K., Furihata, K., Seto, H., and Otake, N. (1985) Rustmicin, a new macrolide antibiotic active against wheat stem rust fungus. *J Antibiot (Tokyo) 38*, 1806-9.

(154) Mandala, S. M., Thornton, R. A., Milligan, J., Rosenbach, M., Garcia-Calvo, M., Bull, H. G., Harris, G., Abruzzo, G. K., Flattery, A. M., Gill, C. J., Bartizal, K., Dreikorn, S., and Kurtz, M. B. (1998) Rustmicin, a potent antifungal agent, inhibits sphingolipid synthesis at inositol phosphoceramide synthase. *J Biol Chem 273*, 14942-9.

(155) Mandala, S. M., Thornton, R. A., Rosenbach, M., Milligan, J., Garcia-Calvo, M., Bull, H. G., and Kurtz, M. B. (1997) Khafrefungin, a novel inhibitor of sphingolipid synthesis. *J Biol Chem 272*, 32709-14.

(156) Wakabayashi, T., Mori, K., and Kobayashi, S. (2001) Total synthesis and structural elucidation of khafrefungin. *J Am Chem Soc 123*, 1372-5.

(157) Yano, T., Aoyagi, A., Kozuma, S., Kawamura, Y., Tanaka, I., Suzuki, Y., Takamatsu, Y., Takatsu, T., and Inukai, M. (2007) Pleofungins, novel inositol phosphorylceramide synthase inhibitors, from Phoma sp. SANK 13899. I. Taxonomy, fermentation, isolation, and biological activities. *J Antibiot (Tokyo) 60*, 136-42.

(158) Gullino, M., Leroux P. and Smith C. M., (2000) Uses and challenges of novel compounds for plant disease control. *Crop Protection 19*, 1-11.

(159) Babadoost, M. (2000) Report on plant disease: Gray-mould rot or Botrytis blight of vegetables. . 942.

(160) Manteau, S., Abouna S., Lambert B. and Legendre L., (2003) Differential regulation by ambient pH of putative virulence factor secretion by the phytopathogenic fungus *Botrytis cinerea*. *FEMS Microbiology Ecology 43*, 359-366.

(161) Staples, R. and Mayer A. M., (1995) Putative virulence factors of botrytis cinerea acting as a wound pathogen. *FEMS Microbiology Letters 134*, 1-7.

(162) Ippolito, A., El Ghaoth A., Wilson C. L. and Wisniewski M., (2000) Control of postharvest decay of apple fruit by *Aureobasidium pulluans* and induction of defense responses. *Postharvest Biology and Technology 19*, 265-272.

(163) Achenbach, H., Muhlenfeld H. and Zahner H., (1985) Galbonide A and galbonide B, 2 new non-glycosidic antifungal macrolides from *Streptomyces galbus*. *Tetrahedron letters 26*, 6167-6170.

(164) Fauth, U. (1986) Galbonide A and galbonide B, 2 nonglycosidid antifungal macrolides. *Journal of antibiotics 39*, 1760-1764.

Chapter 2: Serine Palmitoyltransferase (SPT)

2.1 Cloning and Over Expression of the Gene Encoding *S. paucimobilis* Serine palmitoyltransferase (SPT) in *E. coli*

2.1.1 Production of N-terminal Histidine-Tagged SPT; pET6HSPT

Previous work has been reported on wild type and recombinant serine palmitoyltransferase (SPT) from S*phingomonas paucimobilis* (1). Ikushiro *et al.* have isolated and purified both native SPT from *S. paucimobilis*, and a recombinant version from *E. coli* (BL21 (DE3) pLysS) cells. It is unclear in their paper whether their recombinant SPT protein contained a 6-histidine tag as purification using nickel-affinity chromatography was not reported. Despite concerns that the over-production of SPT, and hence an increase in the production of 3-ketosphinganine, could be toxic to *E. coli*, this was proven not to be the case.

Prior to the studies discussed in this thesis, the full length *spt* gene was amplified by PCR from *S. paucimobilis* strain 13361 using chromosomal DNA as a template and PCR forward and reverse primers based on the *spt* sequence deposited in the NCBI database by Ikushiro *et al.* (accession number AB055142). This DNA sequence was modified by insertion of the restriction endonuclease sites *BspH*I (5') and *BamH*I (3'), which allowed the gene to be inserted into the expression plasmid pET16b. Over-expression of pET16b*spt* produced untagged recombinant SPT protein however the isolation of untagged SPT was time-consuming, involving numerous chromatographic steps. In light of this, the gene encoding SPT was modified, by PCR, in an attempt to produce a N-terminal 6-histidine tagged protein. To do this, primers were designed to incorporate a *Nco*I restriction endonuclease site at the 5'- end of the *spt* gene allowing it to be excised from pET16b (*Nco*I/*BamH*I) and inserted into pET6H (an Edinburgh lab constructed plasmid).

Expression trials of pET6H*spt* were carried out, varying the following parameters: *E. coli* strain; HMS174 (DE3) and BL21 (DE3), temperature; 30°C and 37°C, induction time; 3, 4, 5, 6 hours and concentration of IPTG; 0.1, 0.25, 0.5 and 1 mM. Optimal expression was obtained from HMS174 (DE3) cells grown at 30°C and induced for 6 hours with 0.1 mM IPTG. While efficient over-production of pET6HSPT could routinely be obtained, purification proved more difficult as the protein bound very weakly to a His-Trap™ column (GE Healthcare) and as a result could be eluted with only 50mM imidazole.

To investigate this further, anion exchange chromatography was carried out as the untagged protein had also been purified in this way. Unfortunately, SPT did not bind to the anion exchange resin. As a result, it is feasible to suggest that over-production of SPT with a N-terminal tag had either; interfered with the correct folding of the protein or that the tag was inaccessible for purification. Initial crystallisation screens (Hampton Research) were set up with pET6HSPT however, no crystals could be obtained for structural studies.

The gene encoding SPT was also cloned into the plasmid pHISTEV ((lab constructed strain gifted by Dr. H. Liu, SSPF, St. Andrews) to produce recombinant SPT with a cleavable N-terminal histidine tag. However, again, the protein bound very weakly to a HisTrap™ column. Both results imply that tagging SPT at the N-terminus leads to an ineffective purification strategy.

2.1.2 Production of C-Terminal Histidine Tagged SPT; SPT-His_6

In light of the problems encountered with N-terminal tagged SPT, primers were designed to incorporate, by PCR, the restriction sites *Bsp*HI and *Xho*I at the 5' and 3' ends of the *spt* gene respectively. As a result, *spt* was cloned (by PCR) from pET6H with the restriction sites *Bsp*HI/*Xho*I which enabled the gene to be inserted into pET28a using the restriction sites *Nco*I/*Xho*I (**Fig. 13**). As *Nco*I and *Bsp*HI are complementary sequences, the N-terminal restriction site on the *spt* gene is lost upon insertion into pET28a.

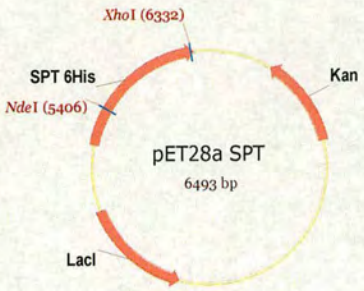

Figure 13: Expression Plasmid pET28a*spt*
The *S. paucimobilis spt* gene was inserted into pET28a using the *Bsp*HI and *Xho*I restriction sites. The resulting construct encodes a C-terminal 6-histidine (His_6)-tagged SPT protein.

Expression trials of pET28a*spt* were carried out as mentioned previously for pET6HSPT. The optimal conditions were similar, with the exception of time as it was found that similar levels of protein could be obtained after five, rather than six hours, of induction.

2.2 Purification and Characterisation of Recombinant SPT-His_6

Single step purification of SPT-His_6 was successful using a HisTrap™ column (GE Healthcare) and the protein was eluted with approximately 200mM imidazole. SPT-His_6 was subsequently purified by size exclusion chromatography and was eluted with 110-130 mL of size exclusion buffer. Using a standard curve, obtained from known molecular weight standards (GE Healthcare), the elution volume was used to calculate the approximate molecular weight of SPT- His_6 as 90-100 kDa. This suggests that SPT-His_6 was purified as a dimer in solution. This was confirmed by native gel PAGE of the elution fractions 12, 13 and 14 (**Fig. 14**).

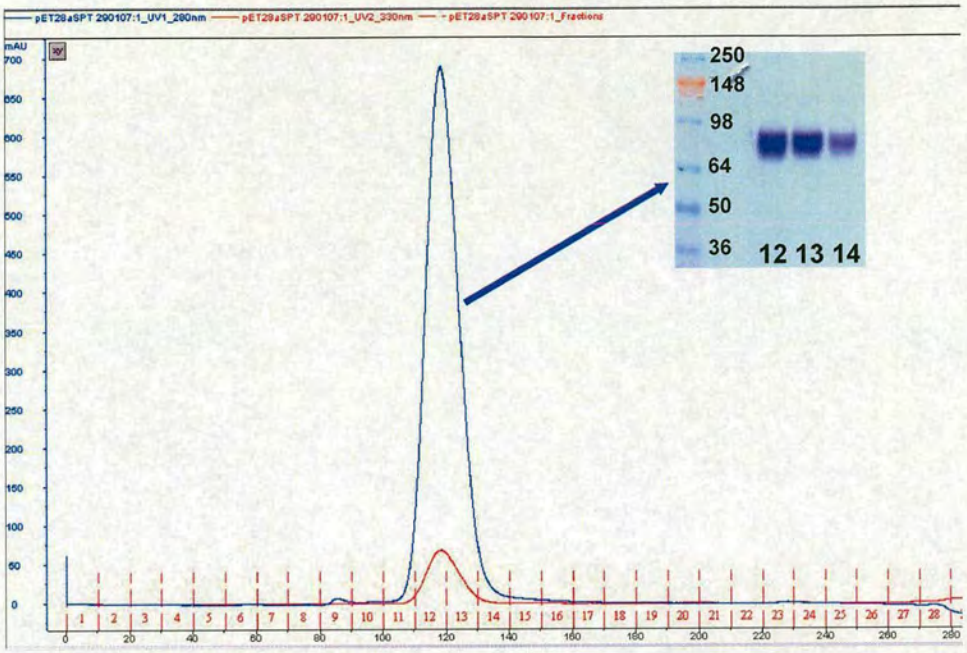

Figure 14: Size Exclusion and Native PAGE Analysis of SPT-His_6
Size exclusion purification and native gel PAGE analysis both suggest the presence of SPT-His_6 as a dimmer in solution with an approximate molecular weight of 90 kDa.

Electrospray ionisation mass spectrometry (ESI-MS) analysis of the purified protein indicated a monomer molecular weight of 45,969.64 ± 4.93 Da. This is consistent with the predicted mass of recombinant SPT (46,104 Da) from the gene sequence taking into account loss of the N-terminal methionine residue and the addition of the C-terminal 6-histidine affinity tag.

On average, purification yielded approximately 10 mg of protein per litre of cell culture. Although this yield was sufficient for biochemical and structural analyses, purification was optimised to give a higher yield of protein. This was accomplished by replacing the commercial pre-packed HiPrep™ column with Ni-NTA agarose (Invitrogen) to allow longer contact between the cell free extract and the chromatography media. Elution with 100 mM imidazole resulted in protein of a similar degree of purity and this protocol was optimised to yield 20 mg of protein per litre of cell culture (a two-fold increase compared with the pre-packed column method).

2.3 SPT Activity

2.3.1 Spectroscopic Analysis of holo-SPT

Since PLP is bound *via* Lys265, in holo-SPT, it gives the enzyme characteristic UV-visible absorptions (**Fig. 15**). Typically in PLP-dependent enzymes, the PLP moiety can exist in two tautomeric forms, an enolimine, **21** and ketoenamine, **22** which have different absorbance maxima at 336 and 425 nm respectively. These peaks represent the two different protonated states of PLP; the enolimine is formed when the oxygen is protonated and the ketoenamine when the imine nitrogen is protonated (*2*).

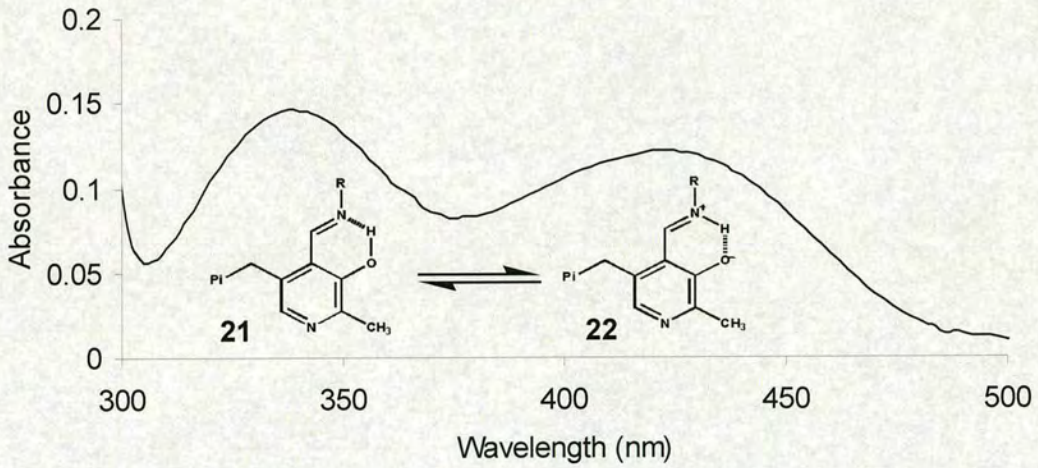

Figure 15: UV Visible Spectrum of holo-SPT
UV-visible spectrum of holo-SPT showing the characteristic peak of the enolimine, **21** (336 nm) and ketoenamine, **22** (425 nm) forms of the PLP.

2.3.2 Kinetic Analysis of L-serine Binding

Upon binding of L-serine to form the external aldimine complex, **23** (**Fig. 16**), there is a decrease in absorption at 336 nm with a concomitant increase at 425 nm. This is almost certainly due to the displacement of PLP from Lys265 by L-serine. The UV-visible spectra of SPT (20 μM) were measured in the presence of various L-serine concentrations (**Fig. 16**).

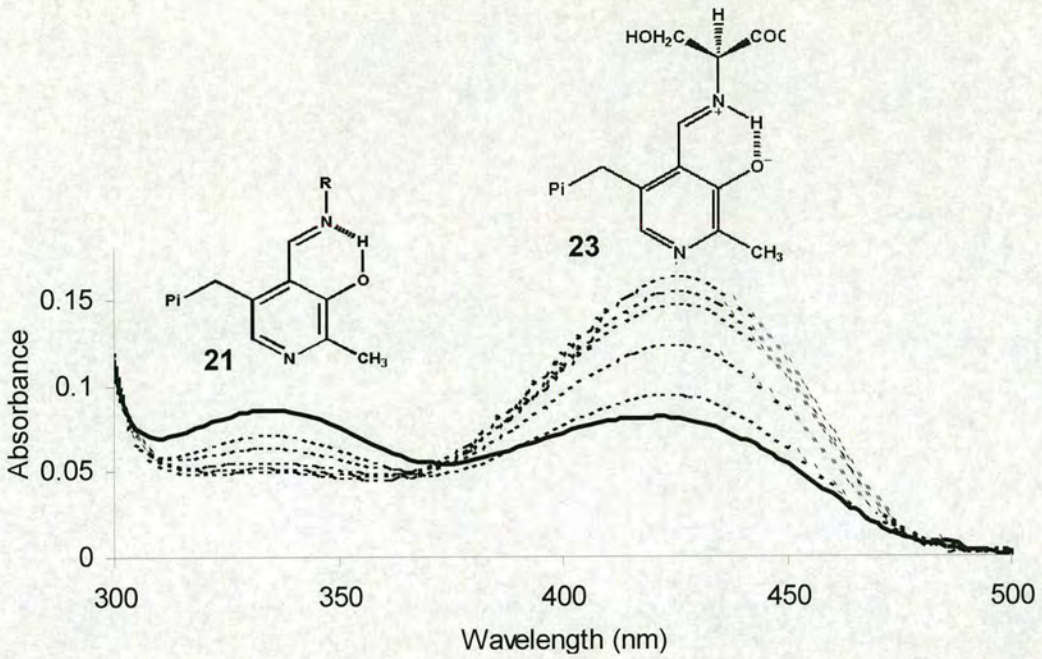

Figure 16: UV-visible Profile of L-serine External Aldimine Formation
The bold line represents holo-SPT and the dotted lines show the formation of the external aldimine, **23** upon incubation with increasing concentrations of L-serine. Assays were carried out in 20mM KPhos pH 7.5, 150 mM NaCl, 1mM EDTA with 20 μM SPT and increasing L-serine concentrations of 5, 10, 20, 30, 40 mM.

The spectral changes observed during L-serine binding showed a hyperbolic dependency on the concentration of L-serine (**Fig. 17a**). From this graph (of L-serine against the change in absorbance at 425 nm) the steady state apparent dissociation constant for external aldimine formation (K_2) was estimated as 1.65 ± 0.22 mM. This is comparable with the value of 1.40 mM reported by Ikushiro *et al.* for wild type SPT (*3*).

Pre-steady state measurements were performed and rate constants k_{obs} for the formation of the L-serine external aldimine were determined by monitoring the absorbance increase at 425 nm over time (**Fig. 17b**). The resultant traces (average of 4) were fitted to single exponential functions. Since the apparent rate constants (k_{app}) for changes in absorbance indicate saturation kinetics, it was assumed that the reaction followed **scheme 1** (E; SPT, S; L-serine, ES_1 and ES_2; SPT-L-serine complex species, K_1; L-serine binding to SPT, K_2; external aldimine formation).

$$E + S \underset{}{\overset{K_1}{\rightleftharpoons}} ES_1 \underset{k_{-2}}{\overset{K_2 \; k_{+2}}{\rightleftharpoons}} ES_2 \qquad (1)$$

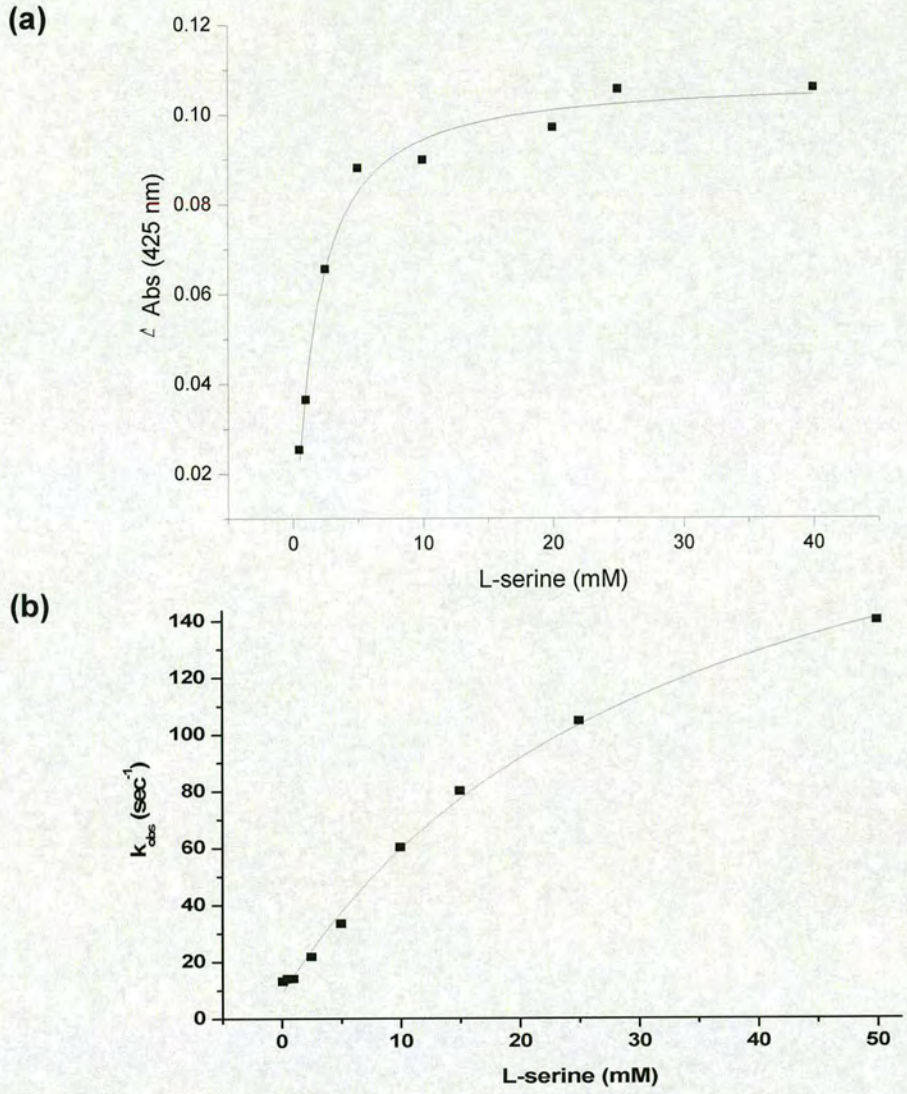

Figure 17: Kinetic Analysis of L-serine Binding

(a) The change in absorbance at 425 nm shows a hyperbolic dependency on L-serine concentration therefore L-serine concentration (0.5, 1, 2, 5, 10, 20, 40) was plotted against the change in absorbance at 425 nm and K_2 for external aldimine formation was estimated as 1.65 mM. (b) Rate constants for the formation of the external aldimine at increasing concentrations of L-serine (0.1, 0.5, 1, 2, 5, 10, 15, 25, 50 mM). All assays were carried out in 20mM KPhos pH 7.5, 150 mM NaCl, 1mM EDTA with 20μM SPT.

Kinetic parameters for L-serine binding were obtained by fitting the stopped flow data (**Fig. 17b**) to **equation 2**: $K_1 = 33.30 \pm 4.48$ mM, $k_{+2} = 220.70 \pm 14.01$ sec^{-1}, $k_{-2} = 8.92 \pm 1.71$ sec^{-1}. These parameters differ from the published results by Ikushiro *et al.*: $K_1 = 53.9 \pm 8.7$ mM, $k_{+2} = 1016.6 \pm 68.2$ s^{-1}, $k_{-2} = 32.6 \pm 11.2$ s^{-1} (*3*).

$$k_{app} = \frac{[S]}{K_1 + [S]} k_{+2} + k_{-2} \quad (2) \qquad K_2 = \frac{k_{-2}}{k_{+2} + k_{-2}} K_1 \quad (3)$$

K_2 was calculated as 1.30 mM using **equation 3** and is comparable with the experimental value (1.65 mM) obtained from steady-state spectroscopic analyses (**Fig. 17a**) and with that obtained by Ikushiro *et al.* (1.40 mM).

The rate of external aldimine formation (k_{+2}) for, recombinant SPT-His_6 is approximately 5-fold slower (220.70 ± 14.01 sec^{-1}) than the untagged, recombinant enzyme isolated by Ikushiro *et al.* (1016.6 ± 68.2 s^{-1}).

2.3.3 Confirmation of Product Identity

To confirm that purified SPT was active in the production of 3-ketodihydrosphingosine (KDS), a radioactive assay was developed. Purified holo-SPT was incubated with U-^{14}C labelled L-serine and palmitoyl-CoA. After incubation for 20 minutes at 37 °C, the lipids were extracted using chloroform:methanol (2:1, v/v). The aqueous (a) and organic (b) phases were separated and analysed by TLC, using a storage phosphor screen to detect radioactivity. ^{14}C labelled KDS was present in the organic phase (2) and absent, as expected, in the aqueous phase (1) (**Fig. 18**).

Control experiments were also carried out as follows; SPT and palmitoyl-CoA, SPT and L-[U-^{14}C] serine, L-[U-^{14}C] serine and palmitoyl-CoA (no SPT). In each experiment, no radioactivity was detected, by TLC, in the organic layer.

To confirm that the radioactive product was KDS, a non-radioactive standard (Matreya) was also analysed by TLC (as described in **Fig. 18**) and detected with ninhydrin. The R_f was measured as 0.61 for the non-radioactive standard and 0.64 for ^{14}C-labelled product suggesting that this radioactive spot corresponds to ^{14}C-KDS.

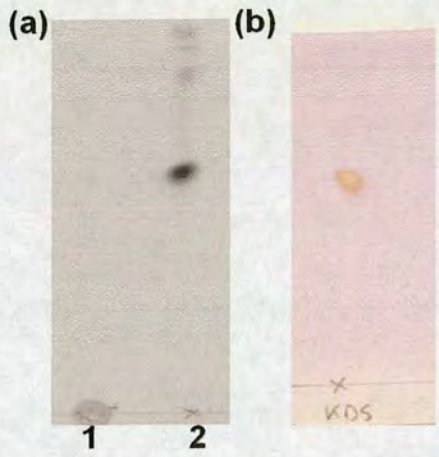

Figure 18: TLC Analysis of KDS Formation
(a) Autoradiographs showing that SPT (20 μM) is active in the conversion of L-[U-^{14}C] serine (2mM, 185kBq/mL) and palmitoyl-CoA (0.86mM) to KDS. 1: aqueous phase, 2: organic phase. (b) TLC of KDS standard (4 mM). KDS was detected with ninhydrin. Both TLCs were eluted with $CHCl_3$:CH_3OH:NH_4OH (40:10:1).

In an attempt to observe any turnover of the ^{14}C-KDS product, the assay mixture from **figure 18a** was incubated with a concentrated cell free extract from *S. paucimobilis*. The spot, suggested to be ^{14}C-KDS (**Fig. 19a**), is no longer present after incubation with *S. paucimobilis* cell free extract. Instead, at least four new radioactive spots are observed (**Fig. 19b**). The appearance of these new radioactive spots suggest that there are soluble enzymes, and perhaps additional substrates present, in the *S. paucimobilis* extract, which are capable of modifying KDS into new lipids.

In addition to ^{14}C-KDS formation (**Fig. 19a**), a radioactive spot is observed at the top of the TLC plate. This spot moves with the solvent front and, as yet, remains unidentified. Preliminary mass spectrometry analysis of this spot (carried out by Marine Raman) suggests that it may correspond to the KDS-PLP product external aldimine. As radioactivity from this spot is occasionally more intense than that for KDS, it is feasible to suggest that KDS-product release may be a rate-limiting factor in the SPT reaction.

The faint radioactive spot below KDS is currently uncharacterised however it has been observed during radioactivity assays carried out by Ikushiro *et al.* although no speculation has been cast upon its structure (*49, 50*).

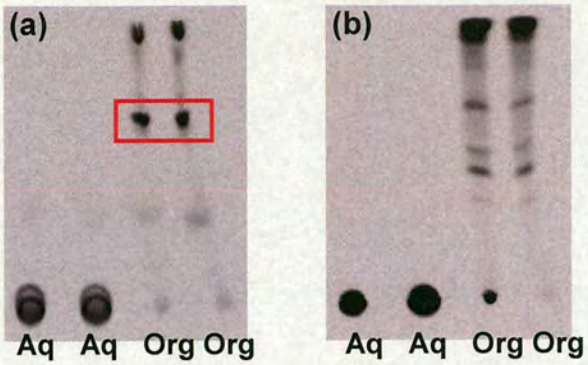

Figure 19: *S. Paucimobilis* Cell Free Extract Assay
(a) A standard assay is carried out to obtain ^{14}C-KDS (indicated by red box). 20 μM SPT, 2 mM L-[U-^{14}C] serine 9250 Bq/0.250μCi and 1.6 mM palmitoyl CoA were incubated for 1 hour at 37 °C before the addition of concentrated *S. paucimobilis* cell free extract. (b) The assay mixture was incubated for a further hour, at 37 °C, with *S. paucimobilis* cell free extract. The lipids were extracted and analysed as mentioned previously (**Fig. 18**).

2.4 Structural Biology of holo-SPT

All crystallographic analyses and discussion in this thesis were carried out in collaboration with Dr L Carter, Dr K Johnson and Prof J Naismith at the SSPF facility, University of St. Andrews. The bioinformatic data, discussed in section 2.5, were processed by Dr I Overton and Prof G Barton (University of Dundee) as part of the SSPF collaboration (*4*).

2.4.1 PLP-Internal Aldimine (holo-SPT)

Since SPT was active in the production of KDS, structural studies were carried out in an attempt to gain information about enzyme mechanism. Firstly, crystals of the apo-form of SPT were obtained from co-crystallisation experiments with myriocin, however they were of poor diffractive quality, with the "best" (highest diffracting) crystal only diffracting to 3.0 Å. In light of this, conditions were optimized to obtain the holo-form of the enzyme. SPT was crystallised in the presence of excess PLP and yellow crystals of holo-SPT were obtained, which diffracted to 1.30 Å. Using a homology model generated from the 2-amino-3-

ketobutyrate CoA ligase (KBL) monomer structure (PDB code: 1FC4), molecular replacement was used to solve the holo-SPT structure.

The first twenty N-terminal amino acids and the last nine C-terminal residues, including the histidine tag of SPT, are not visible in the electron density map hence the final model contains 391 of the 427 amino acids, from Arg22 to Ile419 inclusive. The rest of the 1.30 Å map is of a high quality and the PLP cofactor is clearly defined (**Fig. 20**).

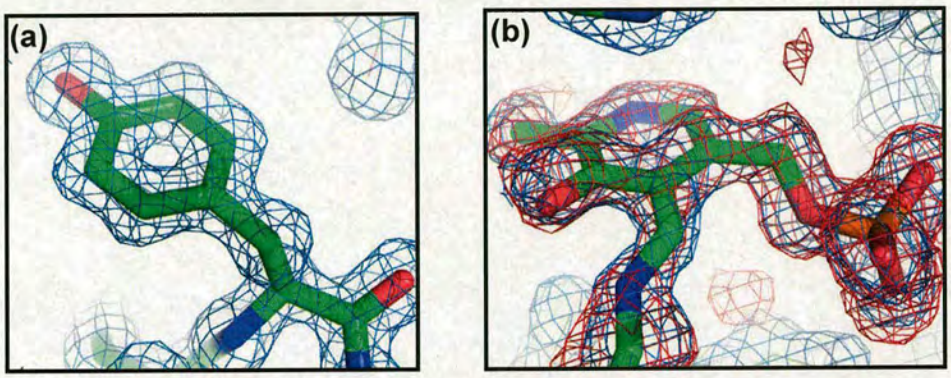

Figure 20: Density Maps of holo-SPT (1.30 Å)
(a) A 2fo-fc map is shown for Tyr123 at 1.0 sigma. (b) The internal aldimine bond between PLP and Lys265 is shown. The red density surrounding the PLP-Lys265 atoms is a 2fo-fc unbiased map contoured at 2 sigma and the blue density shows the 2fo-fc map of the refined structure contoured at 1 sigma.

2.4.2 Structural Comparison of the AOS Family

In common with the other members of the PLP-dependent enzyme superfamily, bacterial SPT is an intimate interlocked dimer. Both monomers of holo-SPT consist of three domains; N-terminal, central catalytic and C-terminal (**Fig. 21**). The N-terminal domain, of approximately 80 residues, is comprised of an α-helix followed by a three-stranded antiparallel β-sheet. This is linked to a larger central catalytic domain composed of a seven-stranded, mainly parallel, β-sheet domain of approximately 200 residues where the active site lysine (Lys265) resides. The C-terminal domain is comprised of approximately 100 amino acid residues which, make many interactions with residues from the N-terminal domain.

Figure 21: Overall Structure of the holo-SPT Homodimer
One monomer is coloured with the N-terminal domain shown in red, the central catalytic domain in green, and the C-terminal domain in yellow. The second subunit is shown in blue. PLP in each monomer is shown purple. Magnesium ions are shown in orange and are thought to be buffer derived.

The overall topology of SPT closely resembles that observed for structures of other members of the AOS family e.g. ALAS, KBL and AONS (**Fig. 22**). All of the structures have the same relative orientation of domains with the most obvious differences being observed in the orientation of the N-terminal helix and the position of loops connecting secondary structural elements remote from the active site (**Fig. 23b**).

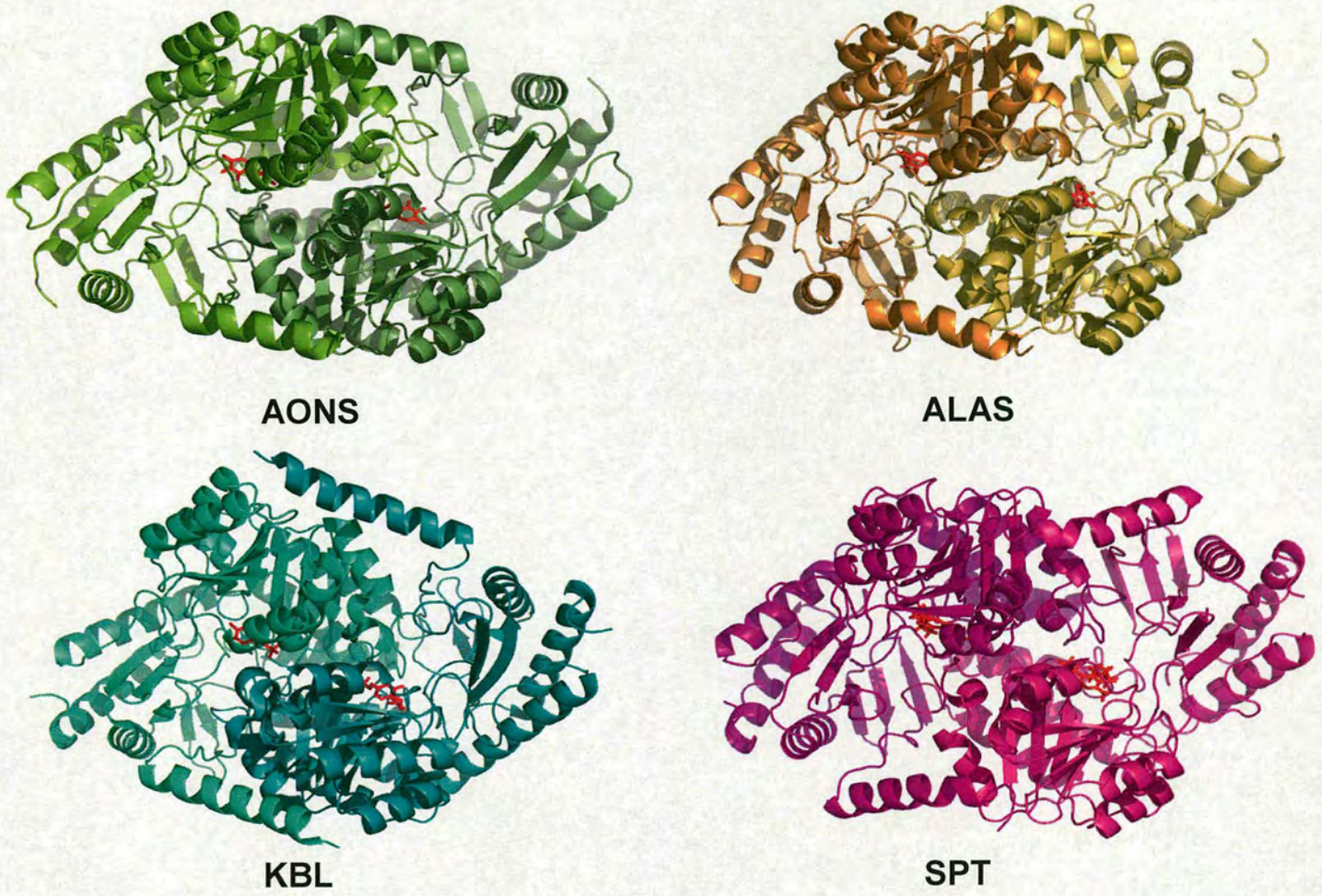

Figure 22: Crystal Structures of the AOS Family
The overall topology of AONS (PBD code: 1DJE), ALAS (2BWN), KBL (1FC4) and SPT (2JG2) are similar as each enzyme has the same relative orientation of domains.

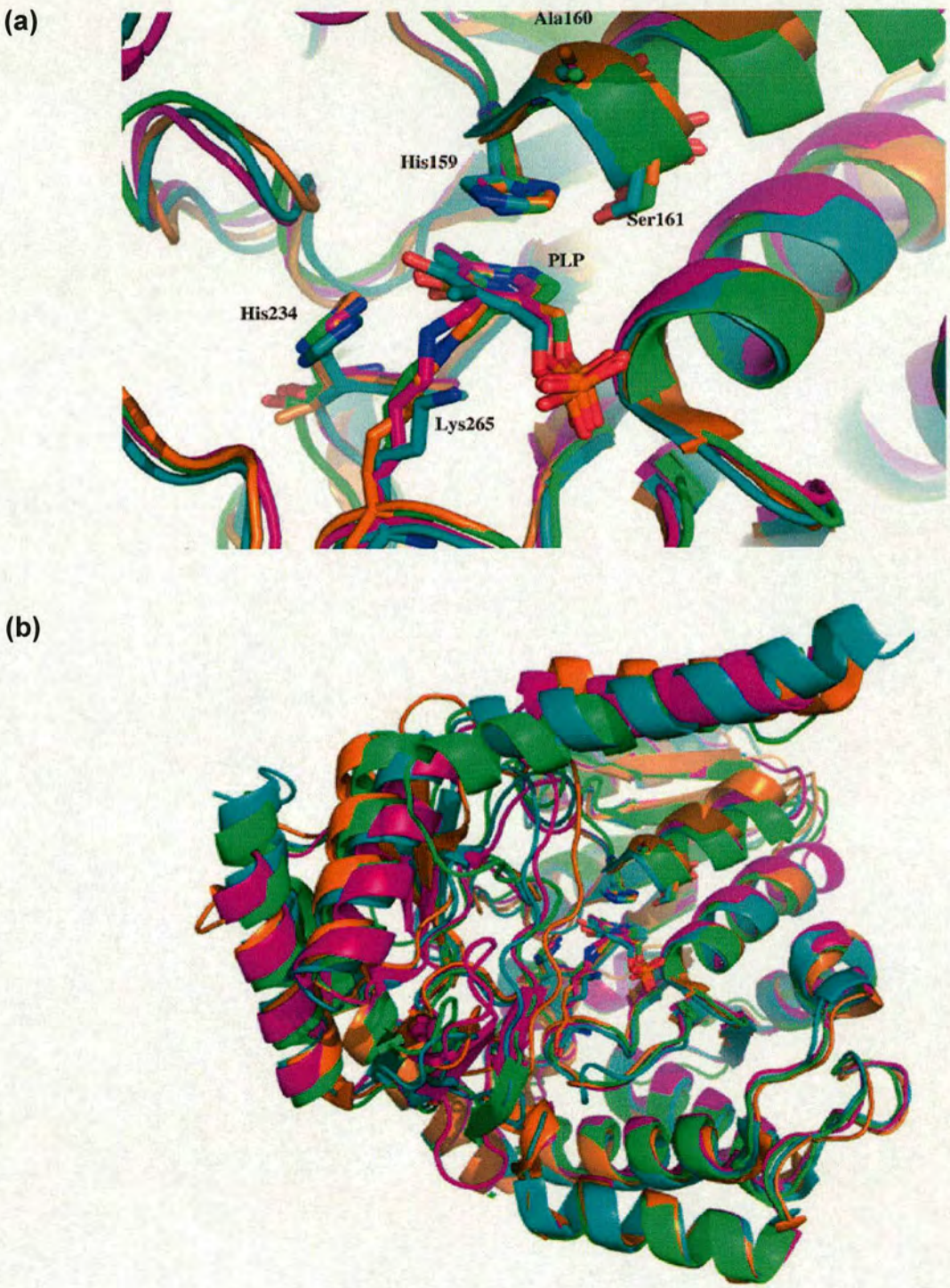

Figure 23: Structural Alignment of the AOS Family
(a) Overlay of key conserved residues involved in cofactor binding: His234, His159, Ala160, Ser161 and Lys265 (*S. paucimobilis* SPT numbering). The SPT structure is shown in green, the AONS in orange, ALAS in purple and KBL in blue. (b) An overall alignment of the monomers (same colouring scheme as (a).

Figure 24: Sequence Based Structure Alignment of the AOS family.
The structure-based sequence alignment of SPT, ALAS, KBL and AONS. The conserved (His, Ala, Ser) motif is shown in pink, the conserved Asp residue which interacts with N1 of PLP in turquoise, the conserved His involved in PLP binding is highlighted in green and the conserved active site Lys residue is shown in red.

2.4.3 The Co-factor Binding Site

The co-factor binding site is composed of residues from both monomers. For example, the side-chain of Asn100 from monomer B is located in close proximity to the backbone of Lys265 from monomer A providing further evidence of the inherent dimeric nature of SPT as a requirement for catalysis. Within the active site of SPT, PLP makes polar contacts with the side-chains of Asn138, Asp231, His234 and Thr262 and with the main chain residues Gly134 and Tyr135 (**Fig. 25**). Another important residue, His159, stacks above one face of the PLP ring. This residue is located at the beginning of a three-residue motif (His159, Ala160, Ser161) that is strictly conserved throughout the α-oxoamine synthase family (**Fig. 24**).

Other residues interact with the cofactor; the pyridinium nitrogen atom (N1) and the oxygen atom of Asp231 are 2.8 Å apart, suggesting that this carboxylic acid group may stabilise the protonated pyridinium form of the PLP by salt bridge formation. This acidic residue is also conserved throughout the family (**Fig. 24**) and a similar interaction has been observed between the N1 of PLP and the Asp204 residue of *E. coli* AONS, the Asp214 of *Rhodobacter capsulatus* ALAS and the Asp210 of *E. coli* KBL (*5-7*).

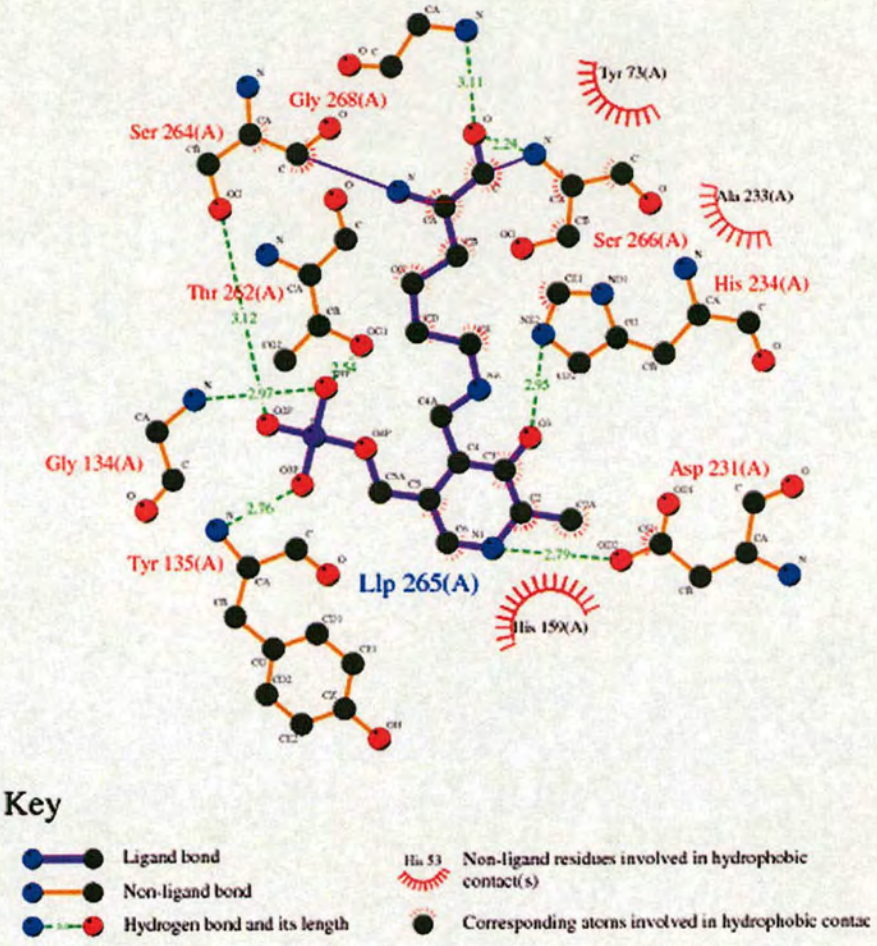

Figure 25: Ligplot Representation of the PLP Binding Site
This illustration shows the constellation of residues involved in cofactor binding. Llp265 refers to the PLP cofactor, covalently bound to the active site residue Lys265. (A) represents residues from monomer A.

2.4.4 Palmitoyl-CoA Binding Site

A complex of SPT with palmitoyl CoA could not be obtained during these studies, however the structure of the *R. capsulatus* holo-ALAS/succinyl-CoA complex (PDB code: 2BWO) was used to predict potential binding sites for palmitoyl CoA (*6*).

In the ALAS structure the density corresponding to the adenine part of the succinyl CoA is well defined. The base is bound within a hydrophobic pocket formed by a group of isoleucine residues on the surface of the enzyme. The adenine also makes a number of H-bond contacts with serine side-chains and the 3′-phosphoribose moiety interacts with a lysine

residue. Density for the phosphopantethene arm of CoA was not observed in the ALAS structure but the carboxylate of the succinate makes contact with an arginine residue (Arg21). A similar interaction has been observed in the AONS/AON-external aldimine structure where the carboxylate of the product also interacts directly with an arginine residue (Arg21) (*8*).

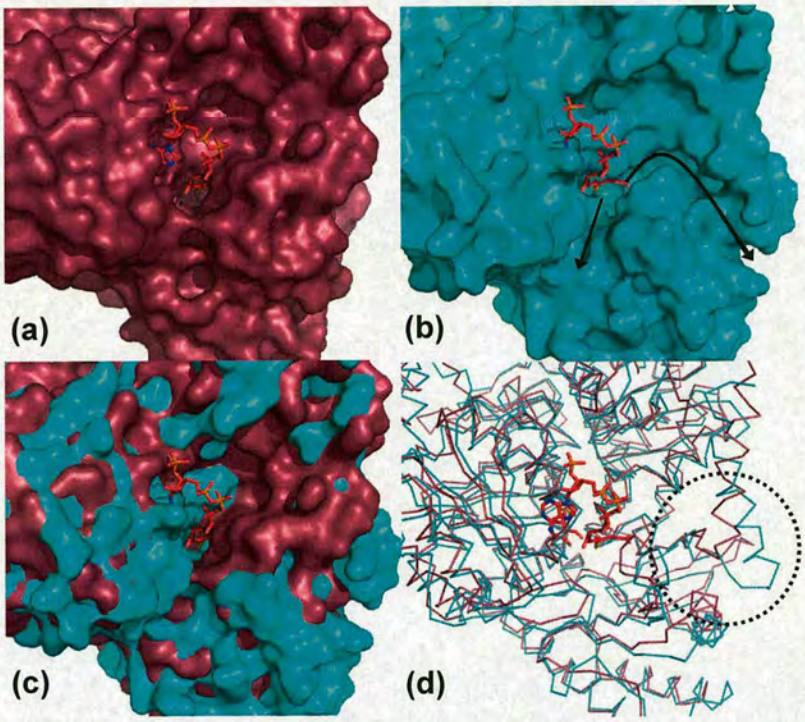

Figure 26: Analysis of Coenzyme-A Thioester Binding
(a) In purple, the space-fill structure of ALAS from *R. capsulatus* (2BWO) with the succinyl-CoA substrate shown as a ball and stick. (b) In blue, a space-fill for the *S. paucimobilis* SPT structure aligned to the ALAS structure (RMSD 2.2Å), showing where the succinyl-CoA is positioned after the structural alignment. Black arrows highlight the two putative channels where the additional carbons of palmitoyl-CoA may bind. (c) Shows an overlay of the ALAS and SPT space-fills, displaying how the first putative channel is foreshortened in the ALAS structure, possibly leading to specificity for succinyl-CoA. This specificity is mainly achieved by a rearrangement of the first helix, as shown circled by the dashed line, in (d).

These interactions were used to superimpose the holo-SPT structure onto the ALAS structure in an attempt to define a palmitoyl-CoA binding site. Two long hydrophobic channels where the C16 chain of palmitoyl-CoA could reside are illustrated in **figure 26b**. Since palmitoyl-CoA lacks a terminal carboxylate, SPT is devoid of a salt-bridge anchor, which delineates the end of the channel in ALAS.

2.5 Modelling of HSAN1 Mutations

2.5.1 Sequence Analysis of Bacterial and Human SPT

An update of the protein nomenclature arising from the sequencing of the human genome has meant that LCB1 is also known as SPT1 and LCB2 is known as SPT2. SPT1and SPT2 have been adopted for the analysis in this section. The *S. paucimobilis* SPT sequence (PubMed accession number AB055142) can be aligned reasonably well to the human SPT1 and SPT2 sequences (UniProt Primary accession numbers: O15269 and O15270 respectively). This includes the putative transmembrane sections of human SPT1/SPT2 (residues 16–36 and 67–87, respectively) and the first α-helix and first two β-strands of the bacterial structure.

Mapping of the putative *S. paucimobilis* SPT active site residues to SPT1 and SPT2 is shown in **table 1** below. It is notable that many of the SPT1 active site residues are markedly different to the bacterial and SPT2 residues. This suggests that substantial degradation of the ancestral active site may have taken place within the SPT1 subunit.

SPT	SPT1	SPT2	Suggested function
Y73	F106	Y176	Hydrophobic interactions with K265
G134	G167	G238	Interacts with phosphate of PLP
Y135	F168	F239	Interacts with phosphate of PLP
H159	C192	H263	Stacks above pyridinium ring of PLP
S161	A194	S265	Part of strictly conserved HAS motif
D231	E274	D344	Makes polar contacts to N1 of pyridinium ring
A233	S276	A346	Hydrophobic interactions with PLP
H234	L277	H347	Hydrogen bond to oxygen of pyridinium ring
T262	N306	T376	Interacts with phosphate of PLP
K265	N309	K379	Forms internal aldimine with PLP
G268	A312	G382	Hydrogen bond to backbone oxygen of Lys265
T294	S338	A408	Interacts with phosphate of PLP
A295	A339	A409	Interacts with phosphate of PLP

Table 1: Potential Functions of Active Site Residues
Active site residues were identified from the *S. paucimobilis* SPT structure and the homology model for the wild-type human SPT1/SPT2 heterodimer.

Analysis of a number of HSAN1 patients has revealed several mutations of the SPT1 subunit e.g. C133W, C133Y and V144D. These mutations cause alterations to SPT activity, resulting in a reduction of sphingolipid biosynthesis (*9, 10*). Currently, the role played by these mutations in HSAN1 remains unclear.

The *S. paucimobilis* SPT structure was used to make a homology model of the human SPT1/SPT2 heterodimer in order to examine the possible structural impacts of the HSAN1 mutations. The alignment of SPT1 and *S. paucimobilis* SPT maps residues Cys133 and Val144 of SPT1 to residues Asn100 and Asp111 of *S. paucimobilis* SPT (see **fig. 7, section 1.7.3** for alignment). Homology models for the human SPT1/SPT2 heterodimer, incorporating the C133W (SPT1) and V144D (SPT1) mutations, were built using the structure of the *S. paucimobilis* holo-SPT as a template.

2.5.2 Structural Impact of HSAN1 Mutations in *S. paucimobilis*

Residue Asn100 in the bacterial sequence maps to human SPT1 residue Cys133 and is located in the *S. paucimobilis* holo-SPT structure at the dimer interface. More importantly, it is found in close proximity to the active site (**Fig. 27**). The amino group of the Asn100 side-chain (monomer B) is within 2.63 Å of the backbone oxygen from the active site lysine residue (Lys265) of monomer A. Thus, it is reasonable to suggest that substitution of asparagine 100 by tryptophan or tyrosine will affect the active site geometry and perturb enzyme activity. **Figure 27** shows the N100W and N100Y mutant models of *S. paucimobilis* SPT where the side chain of tryptophan is within 0.52 Å and tyrosine 2.22 Å of the backbone oxygen of Lys265.

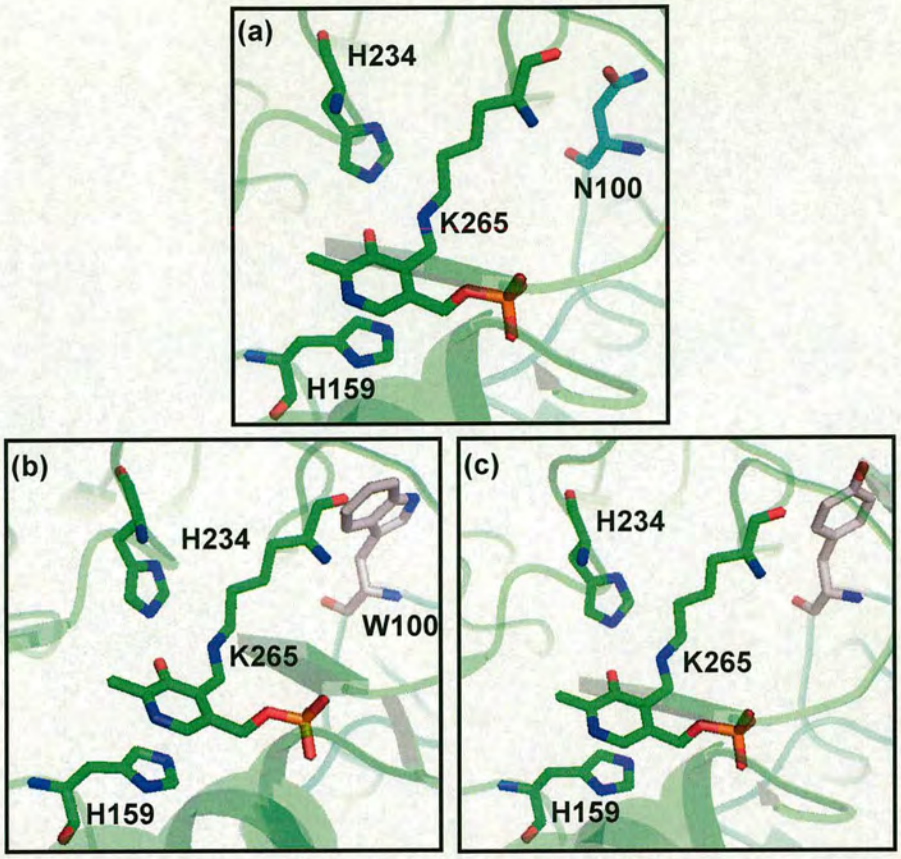

Figure 27: HSAN1 Models of *S. paucimobilis* SPT
(a) The distance of N100 (monomer B) to the backbone carbonyl oxygen of Lys265 (monomer A) is 2.63 Å. (b) The N100W mutant model highlights the close proximity of the tryptophan residue to the backbone of Lys265 (0.52 Å). (c) The N100Y mutant model shows tyrosine to be situated closer (2.22 Å) to Lys265 in comparison to the wild type asparagine residue (2.63 Å). Monomer A is represented in green and monomer B in cyan.

2.5.3 Structural Impact of Human HSAN1 Mutations

Figure 28 shows homology models of the human C133W and V144D mutations. These models provide insights into how mutations in the non-catalytic SPT1 subunit could affect the catalytically active SPT2 subunit and reduce SPT activity. The model for the C133W mutant (**Fig. 28b**) shows a steric clash between W133 and the backbone carbonyl oxygen of Lys265, which is not observed in the "wild-type" model (**Fig. 28a**). This suggests that the C133W mutation directly perturbs the active site geometry, which could consequently affect enzyme activity. In addition, the mutant model suggests that W133 contacts residue T378 of the SPT2 active site and may also affect Y176 *via* contact with N177.

The "wild-type" model reveals that V144 in α-helix3 (H3), packs together with several hydrophobic residues in α-helix9 (H9) (**Fig. 28d**). It could be postulated that V144 is important in stabilising the packing of H3 and H9. Indeed, the models predict that the N-terminal portion of H9 is composed of hydrophobic residues and interpretation of the V144D mutant model suggests that alterations to the H3-H9 packing may cause shifts in the neighbouring structure (**Fig. 28c**). The opposite face of H9 is seen to contact the C-terminal portion of α-helix 2 (H2), which is predicted to be adjacent in space to the region of the active site containing SPT2 residues S380 and G382. Furthermore, the H2-H3 loop (SPT1 residues 129–149) appears close to the cofactor and is the location of the pathogenic Cys133 mutations. It seems reasonable to suggest that movement of the H2 C-terminal region is likely to disturb the H2–H3 loop thus affecting the active site.

Figures 28c and 28d show that, despite being remote from the active site, the V144D mutation could conceivably disrupt the hydrogen bonding network and disturb the active site geometry by inducing rearrangements of H9, H3, H2, and the H2-H3 loop.

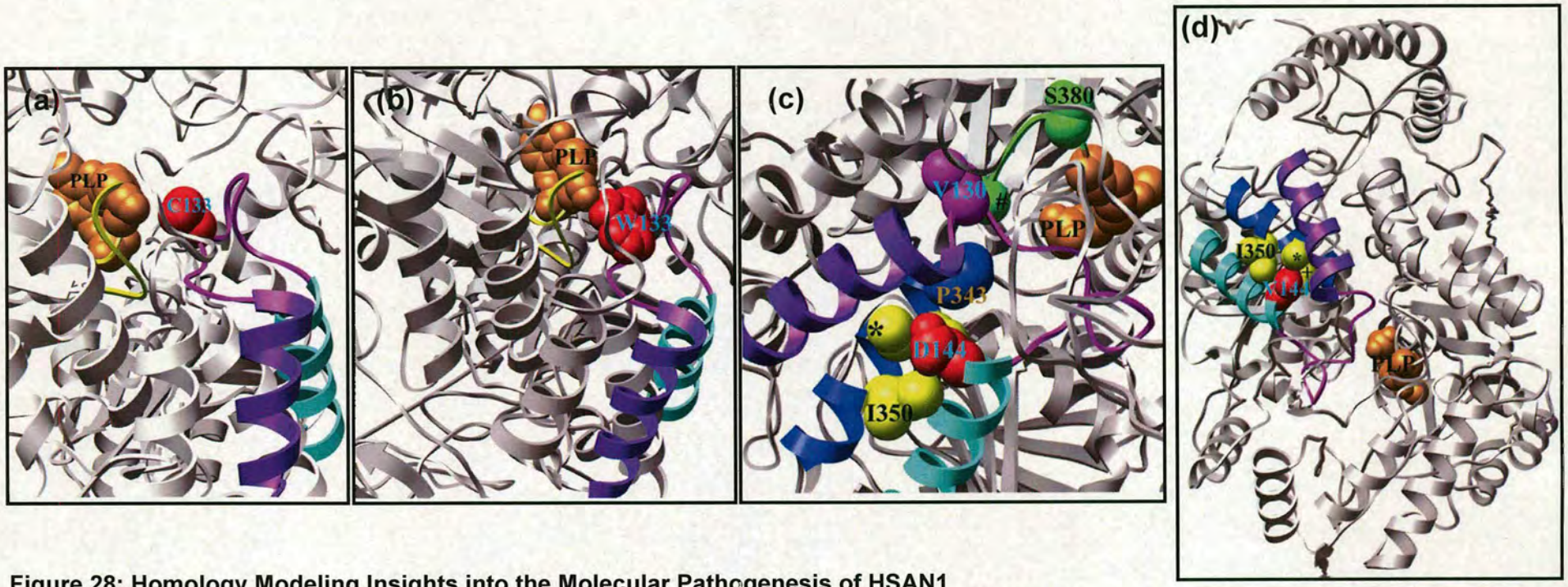

Figure 28: Homology Modeling Insights into the Molecular Pathogenesis of HSAN1

In all panels the PLP cofactor is shown in orange, α-helix 2 (H2) in purple, α-helix 3 (H3) in cyan, and the H2–H3 loop in magenta. Unless otherwise specified, residue numberings refer to SPT1. (a) The "wild-type" model with C133 (red) close to, but not contacting the cofactor. The S^{γ} atom of the C133 side-chain is closest to the phosphate oxygen of the PLP cofactor (van der Waals distance of 0.73 Å to the PLP O2P). (b) The C133W mutant model; the W133 (red) C^{δ} and N atoms clash with the backbone carbonyl oxygen of Lys265 which binds the PLP cofactor. The W133 C^{δ} has 0.65 Å van der Waals overlap with the Lys265 carbonyl oxygen. (c) The V144D mutant model; the Asp144 mutation appears to destabilise the H3-H9 packing and is likely to cause shifts in the neighbouring structure. Pro343 (blue) is highlighted at the N terminus of H9 as disturbance of this, and other residues, by perturbations of the H3–H9–H2 interactions is postulated to affect the H2–H3 loop (magenta). The Cβ atom of the D144 side-chain is closest to the PLP cofactor (van der Waals distance of 14.1 Å from the PLP O2P). (d) The "wild type" model; Val144 (red) packing with Ile350, Ala346 and Ala347 (all shown in yellow). These residues form part of α-helix 9 (H9), shown in blue. The C^{γ} atom of the V144 side-chain is the closest to the PLP cofactor (van der Waals distance of 13.6 Å from the PLP O2P).

2.6 Crystal Structure of the L-serine External Aldimine

To obtain the SPT-L-serine external aldimine, holo-SPT crystals were soaked for in buffer containing L-serine. The highest diffractive quality crystal obtained, produced a dataset to 1.5 Å resolution. In the structure, the first twenty N-terminal amino acids and the last eight C-terminal residues, including the histidine tag, are not visible hence, the final model contains 392 of the 427 amino acids from Arg22 to Gly420 inclusive. Examination of the active site shows, as expected, that Lys265 has been displaced (3.87 Å) from PLP by L-serine to form the external aldimine. Since it is no longer bound to PLP, Lys265 is free and makes hydrogen bond contacts (2.95 Å) with the hydroxyl of the L-serine side chain.

Overall, there are no dramatic alterations to the dimeric structure of SPT. The main difference between the internal and external aldimine structures is the shift of a loop region within the C-terminal domain, by 5.37 Å. This causes new hydrogen bond interactions to occur between Arg378 and the carboxylate group of L-serine (**Fig. 29**). This arginine is from the same monomer as the active site lysine residue.

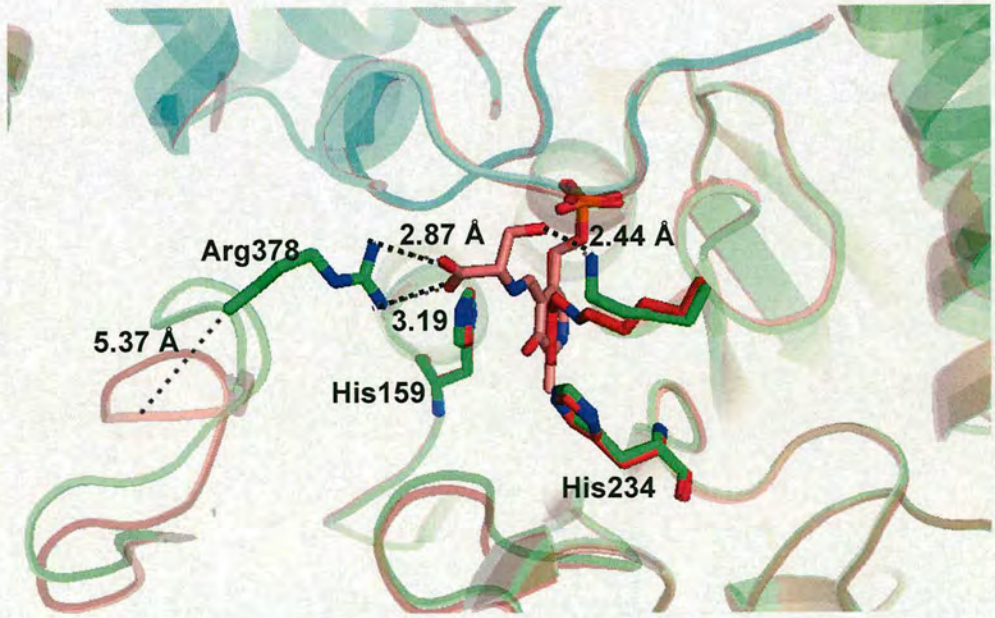

Figure 29: Structural Comparison of the Internal and External Aldimine
A large shift (5.37 Å) of a loop region within the C-terminal domain occurs during L-serine binding. This results in the formation of new hydrogen bond interactions between Arg378 and the carboxylate side group of L-serine. The internal aldimine is shown in red and the external in green/pink.

There do not appear to be any other significant movements among the constellation of residues within the active site. For example, the conserved histidine residues, His 159 and His234, remain in the similar positions. However, the orientation of the plane of the PLP ring has changed slightly; the N1 nitrogen has moved by 1.09 Å towards Lys265 (**Fig. 30**).

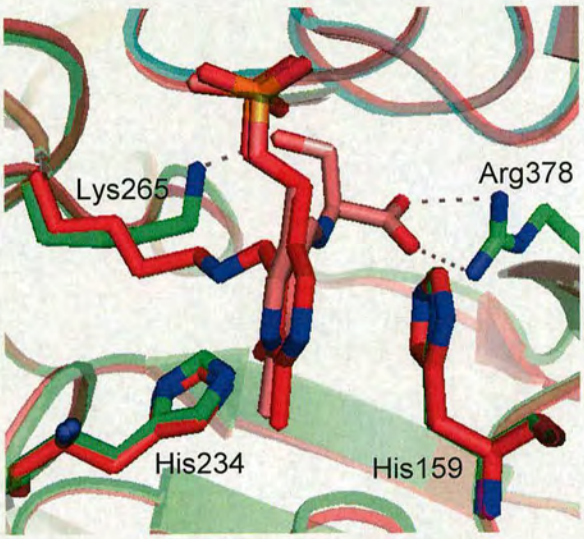

Figure 30: Overlay of the Internal and External Aldimine Active Sites
The orientation of the pyridinium ring of PLP differs between the internal and external aldimine structures by 1.09 Å. Internal aldimine structure is shown in green and the external in red.

It is interesting to note, that Arg378 of *S. paucimobilis* SPT does not align with an arginine residue in SPT1 or SPT2. However, it does align with Arg349 of AONS from *E. coli* and is located before the conserved PXXP motif found in the SPT and AONS sequences (PATP; SPT and PTVP; AONS). It has been noted by Webster and colleagues, that this motif forms a flexible loop in the AONS structure which moves by 5.5 Å toward the C-terminal catalytic domain upon substrate binding. In particular, the threonine residue (Thr352) of this loop is mobile, providing contacts with the AON product (*8*).

The PATP motif is conserved between *S. paucimobilis* SPT and human SPT2 however it is completely lost in the human SPT1 sequence, being replaced by the residues RSIA. Again, this highlights the dramatic differences between SPT1 and SPT2, which result in the SPT1/SPT2 dimer having a single active site. It is also interesting to note that mutations in the SPT2 "PATP" motif destroy SPT1/SPT2 activity (Prof. Teresa Dunn, personal communication).

2.7 Inhibition by Cycloserine

2.7.1 Mechanisms of Inhibition

The natural products, L-cycloserine (LCS) and D-cycloserine (DCS) are enantiomers of an interesting drug molecule that it used to treat *Mycobacterium tuberculosis*. The mechanisms of cycloserine inhibition of PLP-dependent enzymes (**Fig. 31** and **32**) have been studied previously (*11-15*). The first step involves displacement of the internal aldimine lysine residue, from the holo-enzyme, by cycloserine. The resultant external aldimine commonly undergoes deprotonation to form a resonance stabilised ketimine adduct, **24** (see **Fig. 31a**).

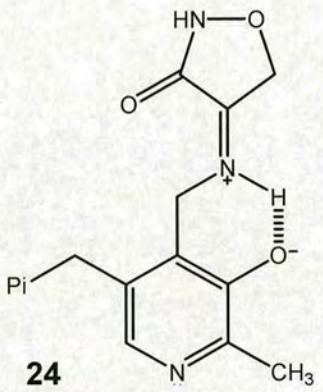

24

The structure of this non-covalently bound adduct has been determined by the crystallisation of cycloserine with the PLP-dependent enzymes ArnB aminotransferase and dialkylglycine decarboxylase, amongst others, and has been observed with both enantiomers of cycloserine (*12, 14*).

Breakdown of the PLP-cycloserine imine appears to occur by two distinct routes. The simplest is hydrolysis of the imine to give pyridoxamine 5'-phosphate (PMP, **26**) and a β-ketoacid, **27** (pathway (a), **Fig. 31**) whereas the second involves participation of an enzyme derived nucleophile within the active site (pathway (b), **Fig. 31**).

The second mechanism has been suggested by Rando as a result of his studies on alanine racemase (*16*). Isomerisation of the Schiff base occurs to form a ketimine intermediate, **25** as before, which is then followed by the nucleophilic attack of the cycloserine amide bond, possibly by an active site residue, to form a covalently bound adduct. Subsequent hydrolysis

yields PMP, **26** and an acylated enzyme adduct and further hydrolysis of the acyl-adduct may also occur to release a β-ketoacid, from the enzyme. However, liquid chromatography-mass spectrometry analysis of SPT after incubation with L-cycloserine showed that the molecular mass of the enzyme was unchanged, suggesting that if an enzyme bound adduct had formed it was easily hydrolysed.

Another mechanism for the inhibition of SPT by L-cycloserine has been suggested by Ikushiro *et al.* and is shown in **figure 32a** (*3*). In comparison to the formation of the non-covalent adduct, **25** discussed above, it has been suggested that after external aldimine formation, the L-cycloserine ring is hydrolysed to form a ring-opened intermediate, **28**. It is suggested that this intermediate then rearranges *via* rapid ring closure and reopening to form an oxime intermediate, **29**. In addition, the ring-opened species, **28** can undergo 1,3-proton transfer to form an unstable imine that is hydrolysed to form PMP, **26** and β-oxyaminopyruvate, **27**. While these mechanistic theories are attractive, it is noteworthy that to date, no structural information has been published on L-cycloserine inhibition of SPT and no published results are available on the isolation of the β-ketoacid.

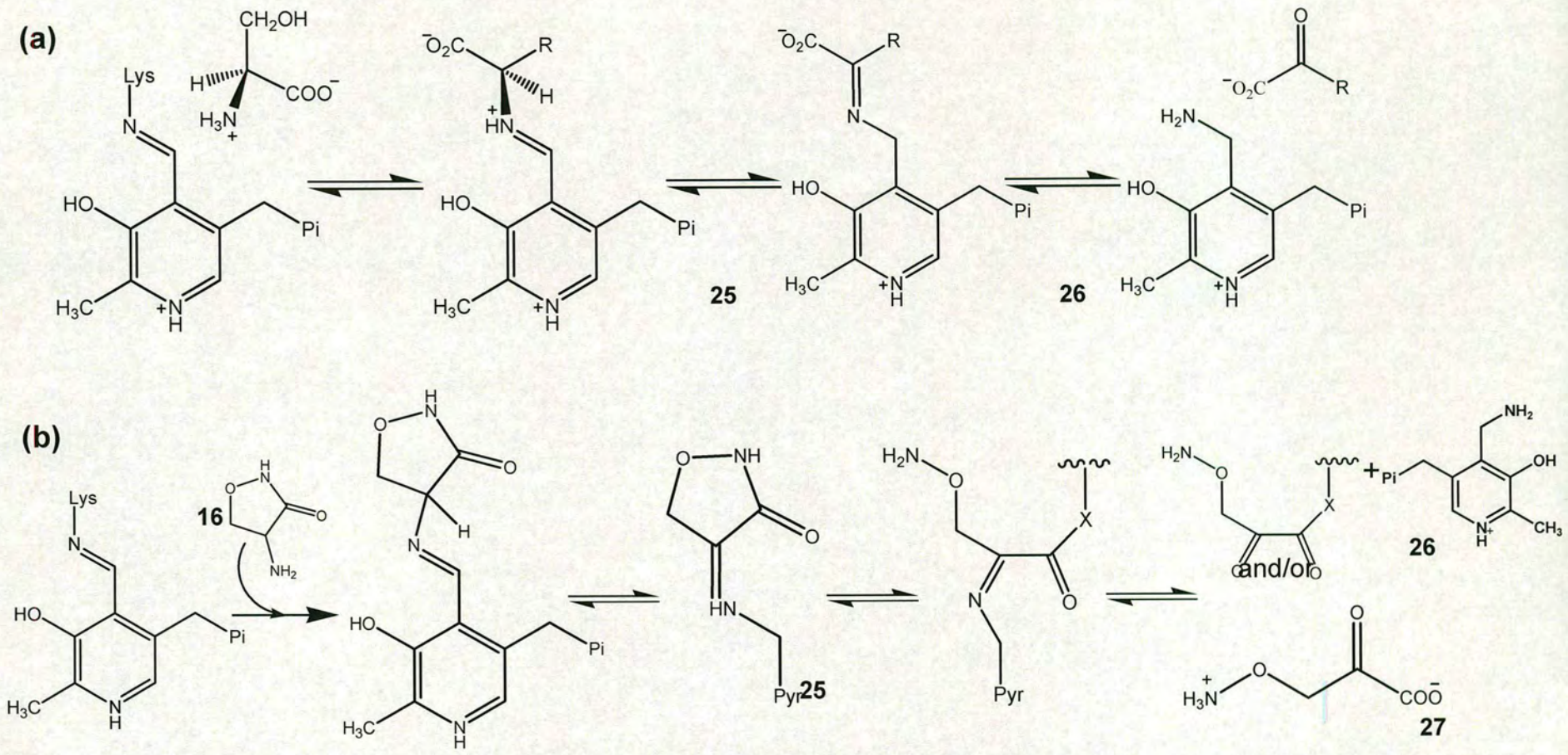

Figure 31: Hydrolysis Mechanisms for Cycloserine Inhibition: (a) Amino acid conversion proceeds *via* a ketimine intermediate, **25** which is subsequently hydrolysed to the corresponding β-keto acid, and PMP, **26.** (b) Cycloserine inhibition of alanine racemase (as proposed by Rando) involves an enzyme derived nucleophile and hydrolysis of cycloserine to produce PMP, **26** and an enzyme bound diketone adduct and/or the β-ketoacid; β-oxyaminopyruvate, **27** (*16*).

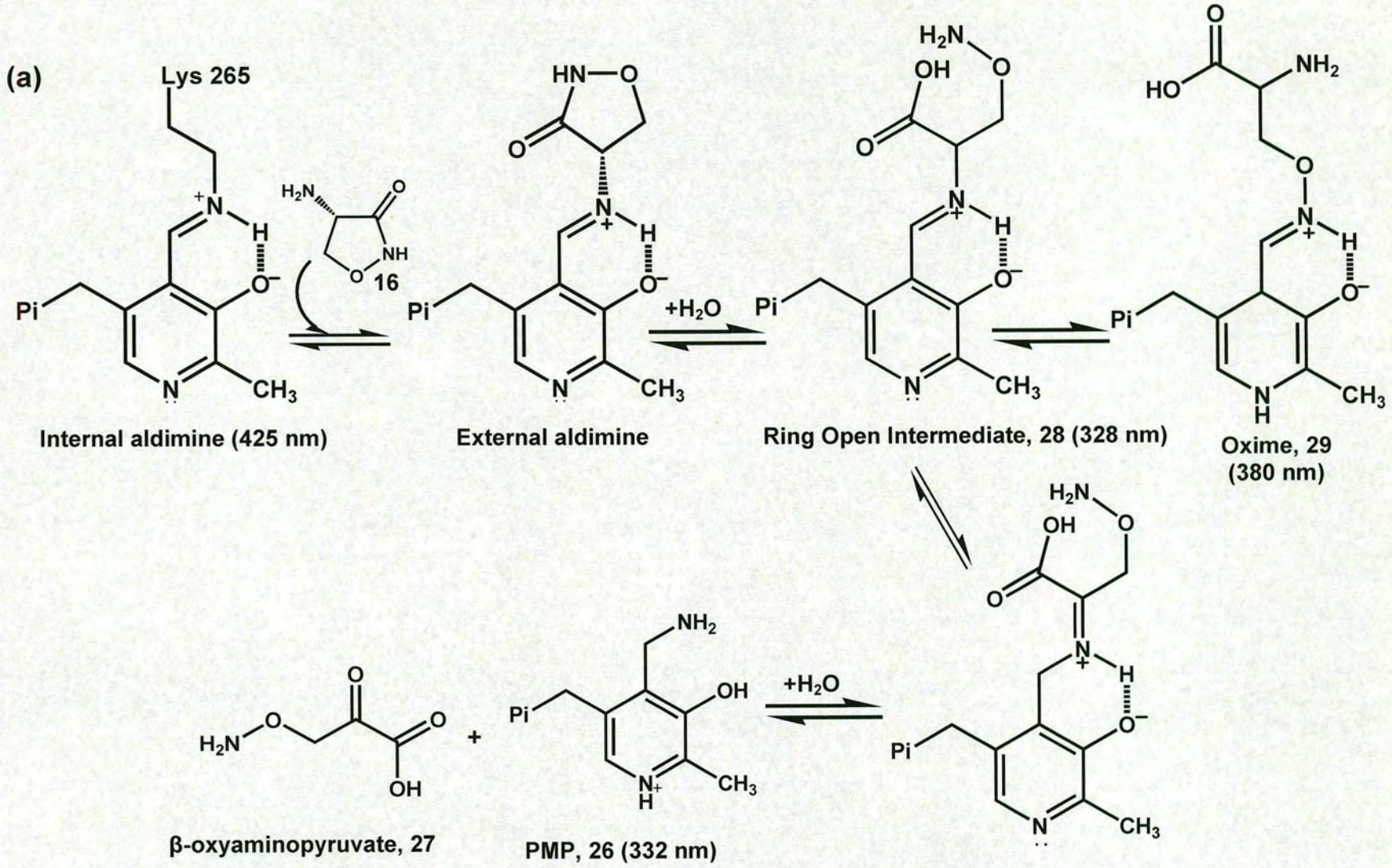
(a)
Lys 265
16
+H2O
Internal aldimine (425 nm)
External aldimine
Ring Open Intermediate, 28 (328 nm)
Oxime, 29
(380 nm)
β-oxyaminopyruvate, 27
PMP, 26 (332 nm)
+H2O

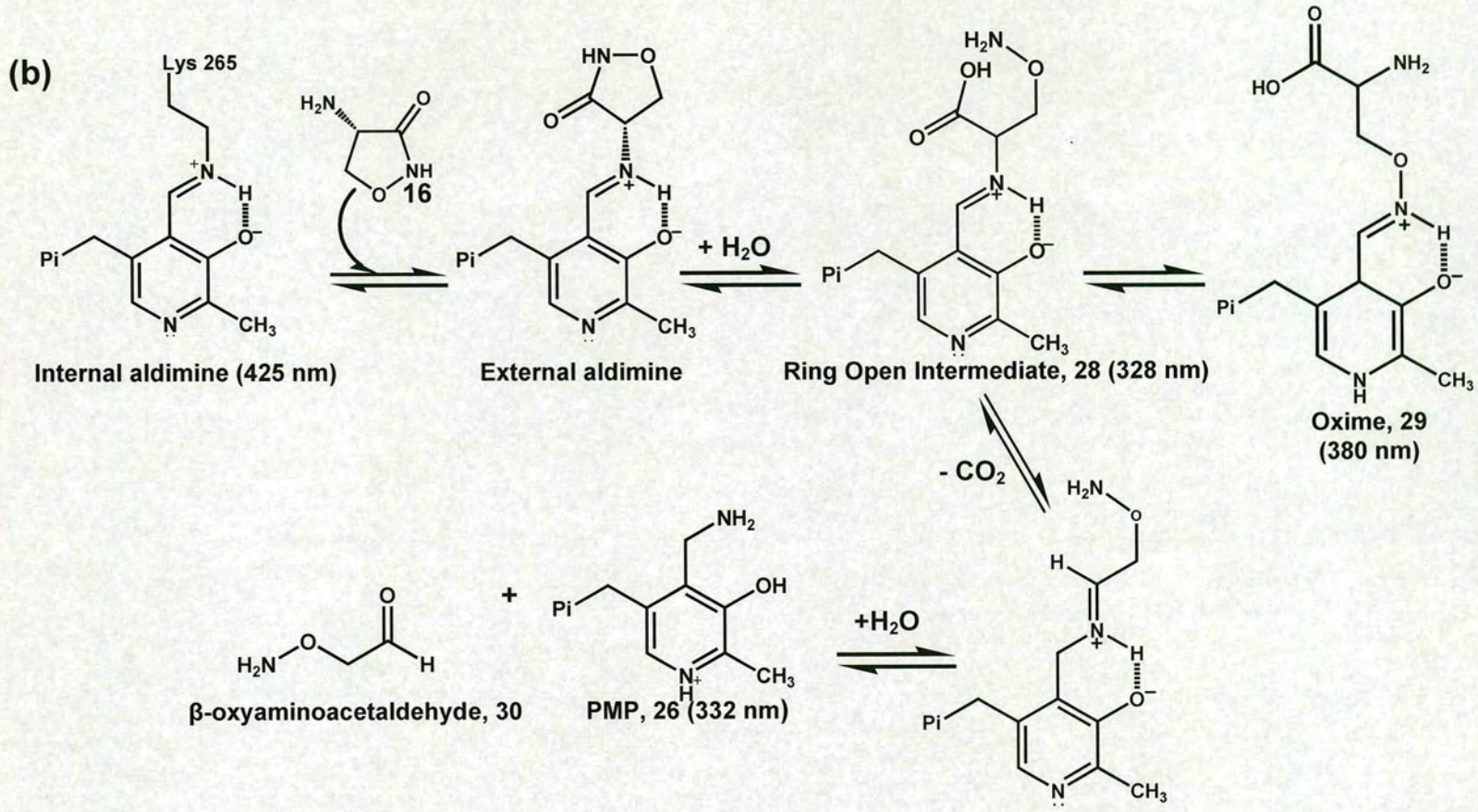

Figure 32: Proposed Mechanisms of SPT Inhibition by L-cycloserine (*3*)

L-cycloserine (LCS, **16**) binds to SPT to form an external aldimine where the LCS ring remains intact. Subsequent hydrolysis, possibly enzyme catalysed due to the speed of the reaction, produces a species which absorbs at 328 nm. This species is postulated to be the ring opened intermediate, **28**. This intermediate rearranges to form an oxime species, **29** with a λ_{max} of 380 nm. (a) The ring open intermediate can undergo 1,3-proton transfer to form an unstable imine that is susceptible to hydrolysis. The final step suggested by Ikushiro *et al.* involves the slow hydrolysis of the unstable imine to form PMP **26**, which can be observed spectroscopically at 332 nm and β-oxyaminopyruvate, **27**. (b) In contrast, the ring open intermediate may undergo decarboxylation before hydrolysis occurs, releasing PMP, **26** and β-oxyaminoacetaldehyde, **30.**

2.7.2 Inhibition of SPT Activity by L-cycloserine

Studies by Sundaram and Lev, and Williams *et al.* have shown that L-cycloserine inhibits SPT activity. Radioactive assays were used to investigate the inhibition; Sundaram and Lev monitored the incorporation of DL-[3-^{14}C]serine into 3-ketosphinganine (KDS) by TLC and autoradiography and Williams *et al.* monitored the incorporation of water soluble [^{3}H]-serine into chloroform soluble KDS (*17, 18*). In light of these studies, a radioactive assay was also used to observe L-cycloserine inhibition of *S. paucimobilis* SPT. The assay was carried out as previously described for holo-SPT (section 2.3.2) however, prior to incubation with L-[U-^{14}C-]serine, SPT was incubated with L-cycloserine (1 mM). **Figure 33** shows that KDS production is significantly decreased when SPT is pre-incubated with L-cycloserine.

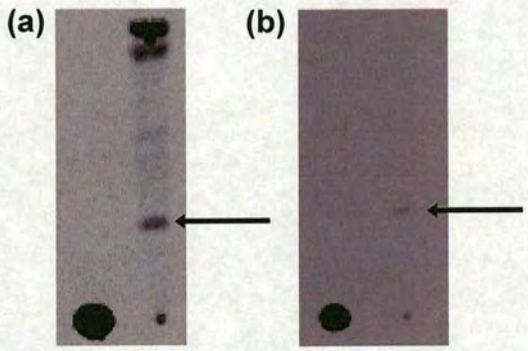

Figure 33: Inhibition of KDS Production by L-cycloserine
(a) Control assay: SPT (20 μM), palmitoyl-CoA (1.6 mM) and L-[U-^{14}C-] serine (10 mM) were incubated for 1 hour at 37 ^{o}C. (b) Inhibition by L-cycloserine: SPT (20 μM), palmitoyl-CoA (1.6 mM) and 1 mM L-cycloserine were incubated for 1 hour at 37 ^{o}C after which L-[U-^{14}C-] serine (10 mM) was added and incubated for a further hour. Arrows indicate the presence of KDS.

It is relevant to note, that a large radioactive spot is observed at the top of the TLC plate as seen in previously in **figure 19**. In addition to the inhibition of KDS formation, this spot is also missing from the post-inhibition TLC. This would make it feasible to suggest that formation of the unidentified radioactive spot is SPT-dependent.

It is also relevant that *S. paucimobilis* growth was inhibited in a dose-dependent manner when incubated with L-cycloserine (**Fig. 34**). It seems likely that interruption of sphingolipid biosynthesis, by inhibition of SPT, has an adverse effect on cell growth. Sphingolipids have

been shown to be essential components of the eukaryotic plasma membrane and, although they are not present in most bacteria, may be important in stabilisation of the membrane structure in *S. paucimobilis* (*19, 20*). It should be noted that cycloserine may also inhibit many other PLP-dependent enzymes required for bacterial growth.

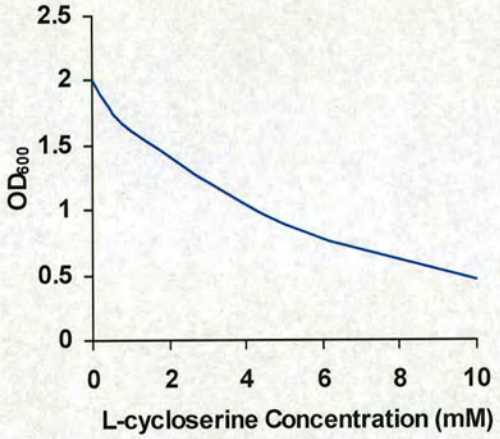

Figure 34: L-cycloserine Inhibition of *S. paucimobilis* Growth
S. paucimobilis were grown overnight at 37 °C in LB broth before being diluted to an OD_{600} of 0.4 in LB containing L-cycloserine (0.5, 1, 5 and 10 mM). Cells were incubated at 37 °C for a further 4 hours and the OD_{600} recorded. It was observed that the cell density decreased as the concentration of L-cycloserine increased.

2.7.3 Spectroscopic and Crystallographic Analyses of L-cycloserine Inhibition

Manohar and co-workers have shown that, upon binding of D-cycloserine to serine hydroxymethyl transferase, there is an immediate decrease in absorbance at 425 nm with the appearance of a shoulder at 330 nm. This reaction appears to proceed *via* a transient intermediate which absorbs at 340 nm. It has been suggested that this is the tetrahedral intermediate adduct between the internal and external aldimines (*21*). L-cycloserine inhibition of ArnB amino transferase results in loss of the internal aldimine peak at 430 nm and the appearance of a new species at 334 nm (*14*). Reaction of D-cycloserine with this enzyme is extremely rapid and irreversible.

Spectroscopic analysis of L-cycloserine binding to SPT shows complex changes in the UV visible spectra (**Fig. 35**). Approximately 20 seconds after the addition of L-cycloserine, there is a decrease in absorbance at 425 nm and consequently, the characteristic yellow appearance of SPT is lost. It is reasonable to imply that this decrease at 425 nm results from the loss of conjugation within the PLP molecule. It might also be suggested that disappearance of the internal aldimine and formation of two new species absorbing at 328 and 380 nm respectively, could be responsible for the loss in colour. Over approximately 24 hours, both these species disappear and instead, a new peak at 332 nm is observed which is characteristic of PMP.

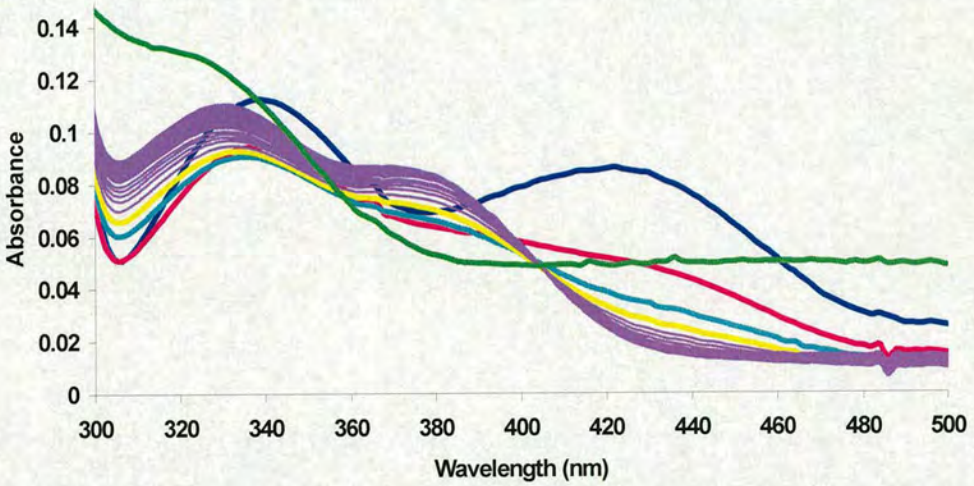

Figure 35: UV visible Spectral Analysis of SPT Inhibition by L-cycloserine
Blue; holo-SPT (20 μM), magenta; 5 seconds after addition of LCS (1 mM) there is rapid disappearance of the internal aldimine, cyan; 10 seconds after addition, yellow; 20 seconds after addition, lilac; 30 seconds - 30 minutes after incubation there is formation of two species which have absorbance maxima of 328 and 380 nm, green; 20 hours after addition of LCS there is formation of a new species which absorbs at 332 nm. The assay was carried out in 20 mM KPhos pH 7.5, 150 mM NaCl, 1mM EDTA.

Since D-cycloserine (DCS) is a rigid analogue of D-alanine, it is known to targ*et al.*anine racemase. In the crystal structure of the DCS-inhibited enzyme the density at the active site is consistent with a planar cycloserine ring and a saturated, hybridised C4' of PLP. In the structure of the L-cycloserine inhibited enzyme, it is unclear from the density whether the ring is planar, however it has been suggested that an aromatic 3-hydroxyisoxazole-PMP adduct (tautomer of **24**) may be formed (*22*). It is also worthy to note that in the crystal

structure of DCS inhibited D-amino acid amino transferase there are no covalent interactions between the DCS and the enzyme. Instead, the intact cycloserine ring tautomerises to form a stable, cyclic adduct with PLP. As there are no covalent interactions between the enzyme and PLP-inhibitor adduct, D-amino acid amino transferase could be reactivated slowly by dialysis against PLP (*15*).

SPT displayed similar behaviour after incubation with L-cycloserine, as Liquid chromatography-mass spectrometry (LC-MS) analysis of SPT after dialysis against PLP suggested no covalent modifications had taken place within the enzyme.

Holo-SPT, obtained from the dialysis experiment, was re-incubated with L-cycloserine and UV-visible spectra were recorded (**Fig. 36**). The characteristic decrease at 425 nm, upon addition of L-cycloserine and concomitant increases in absorbance at 380 and 330 nm respectively were observed.

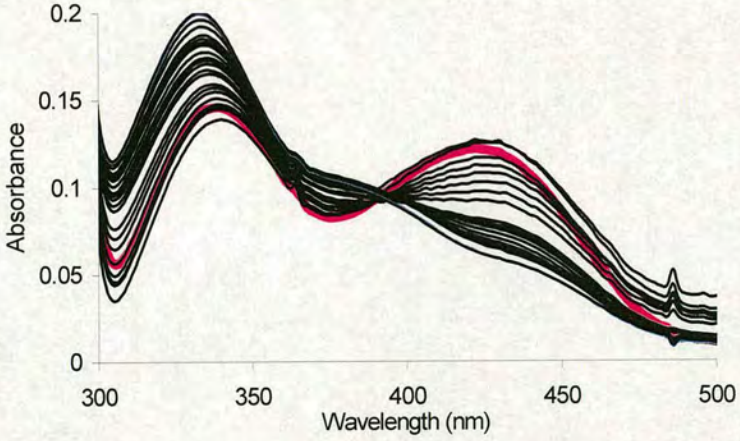

Figure 36: UV Visible Spectrum After Incubation of "Re-loaded" SPT with L-cycloserine

SPT (20 μM) was incubated with L-cycloserine (1 mM) and the UV-visible spectra recorded over 15 minutes. The characteristic decrease in absorbance at 425 nm is observed together with the appearance of two new peaks at 330 and 380 nm. The magenta line represents reloaded SPT (20 μM).

The UV-visible spectra of SPT, before incubation with L-cycloserine, and after dialysis against PLP, were overlaid (**Fig. 37**). Even after incubation with L-cycloserine, gel filtration and dialysis, SPT still exhibited the same spectroscopic properties as the original purified holo-enzyme indicating that no changes to the enzyme had occurred.

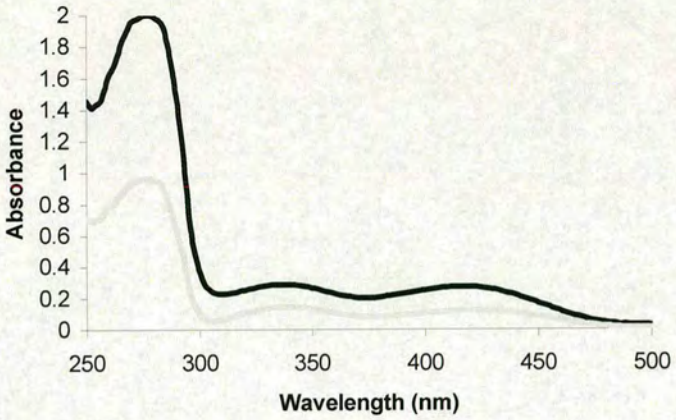

Figure 37: UV-Visible Spectra of SPT Before and After Inhibition With L-cycloserine

Overlay of holo-SPT (20 μM) before incubation with L-cycloserine (bold line) and holo-SPT (10 μM) after gel filtration and dialysis against PLP (dotted line).

2.7.4 Breakdown of L-cycloserine

In an attempt to identify the intermediate(s) formed during the breakdown of L-cycloserine (LCS), SPT (after incubation with LCS) was denatured with urea and the UV-visible spectra of the solution were recorded over a four hour period (**Fig. 38**). Initially, a shift in absorbance is observed from 425 to 400 nm. This could result from the presence of the LCS external aldimine where the LCS ring is still intact. In addition, there is the appearance of a new species with an absorbance maximum at 328 nm. The appearance of this peak is accompanied by a decrease in absorbance at 400 nm. It is reasonable to suggest that the decrease at 400 nm results from hydrolysis of the LCS ring to form a ring-opened L-cycloserine-PLP adduct, **28** which absorbs at 328 nm.

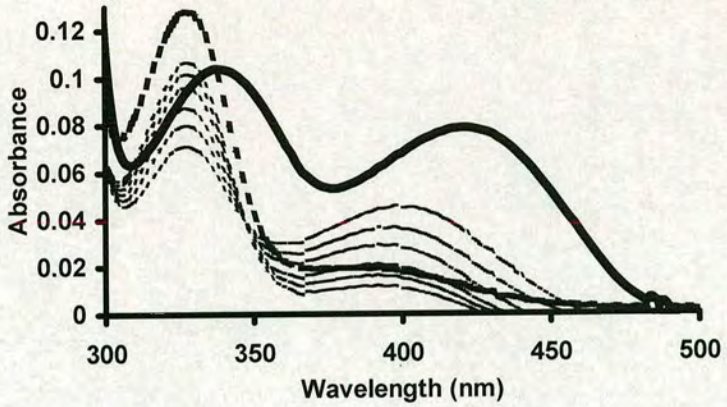

Figure 38: UV-Visible Spectra of a Solution Containing L-cycloserine After Denaturation of SPT

SPT (20 μM) was incubated with L-cycloserine (1 mM) and the protein denatured with Urea (final concentration 4 M). UV visible spectra were recorded 15, 20, 30, 40, 60, 120 and 240 minutes after denaturation. A new species was detected in solution at 328 nm. Bold line: holo-SPT, dotted lines: formation of a species which absorbs at 328 nm.

SPT was also incubated with O-methyl-DL-serine, a structural analogue of the hydrolysed L-cycloserine-PLP intermediate. After denaturation of SPT, the UV-visible spectra were recorded. As no visible changes were observed after 10 minutes the solution was incubated further and the UV-visible spectrum was recorded after 24 hours. During this time a new species, which could be the O-methyl–DL-serine-PLP external aldimine **31**, was observed with an absorbance maximum at 328 nm (**Fig. 39**).

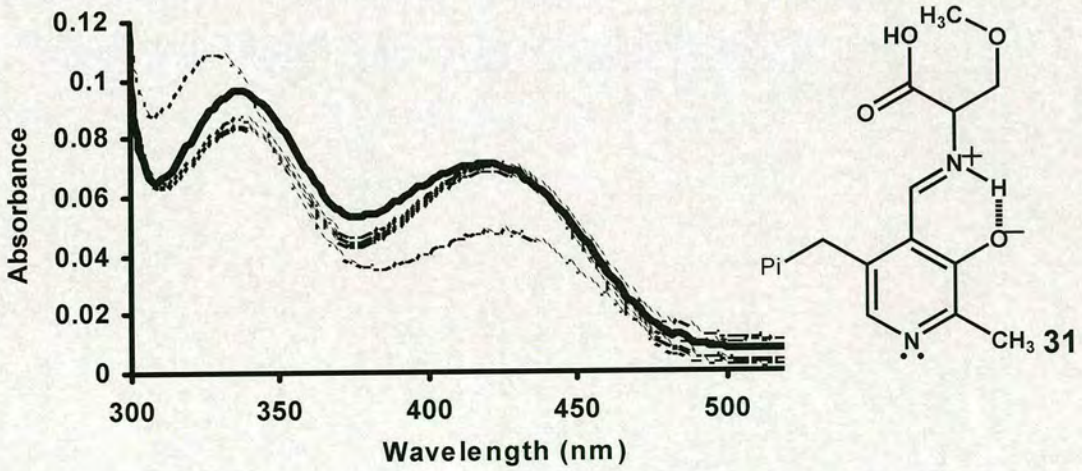

Figure 39: UV-Visible Profile of Solution Containing O-methyl-DL-serine After Denaturation of SPT

SPT (20 μM) was incubated with O-Me-DL-serine (10 mM) and the UV visible spectra recorded after 5, 60, 300, 600 seconds and 24 hours. The species remaining in solution after denaturation of SPT also absorbs at 328 nm. The bold line represents holo-SPT and the dotted lines the formation of the O-Me-DL-serine-PLP external aldimine, **31**.

2.7.5 Crystal Structure of SPT and L-cycloserine

In an attempt to obtain the structure of L-cycloserine inhibited SPT, the protein was co-crystallised in the presence of 1 mM L-cycloserine. Colourless crystals were obtained and data was collected on the highest diffractive quality crystal to 1.45 Å resolution. Refinement of the data showed that two L-cycloserine hydrolysis products were bound at the active site (**Fig. 40a**). The electron density of one of these products was sufficiently defined to identify it as pyridoxamine 5'-phosphate, PMP. It is apparent that the active site lysine (Lys265) is retracted away from the pyridine ring of PMP in a manner similar to that seen in the L-serine external aldimine structure.

The highly conserved residue His159, which forms part of the HAS motif conserved amongst the AOS family, remains stacked above the pyridine ring of PMP as seen in the holo-SPT and L-serine external aldimine structures (**Fig. 40b**). As with holo-SPT (see table 1, section 2.5.1) Thr262 (monomer A), Ser264 (monomer A) and Thr294 (monomer B) provide hydrogen bond contacts to the phosphate of PMP and His234 also remains in a similar position, providing hydrogen bond contacts to the oxygen of PMP.

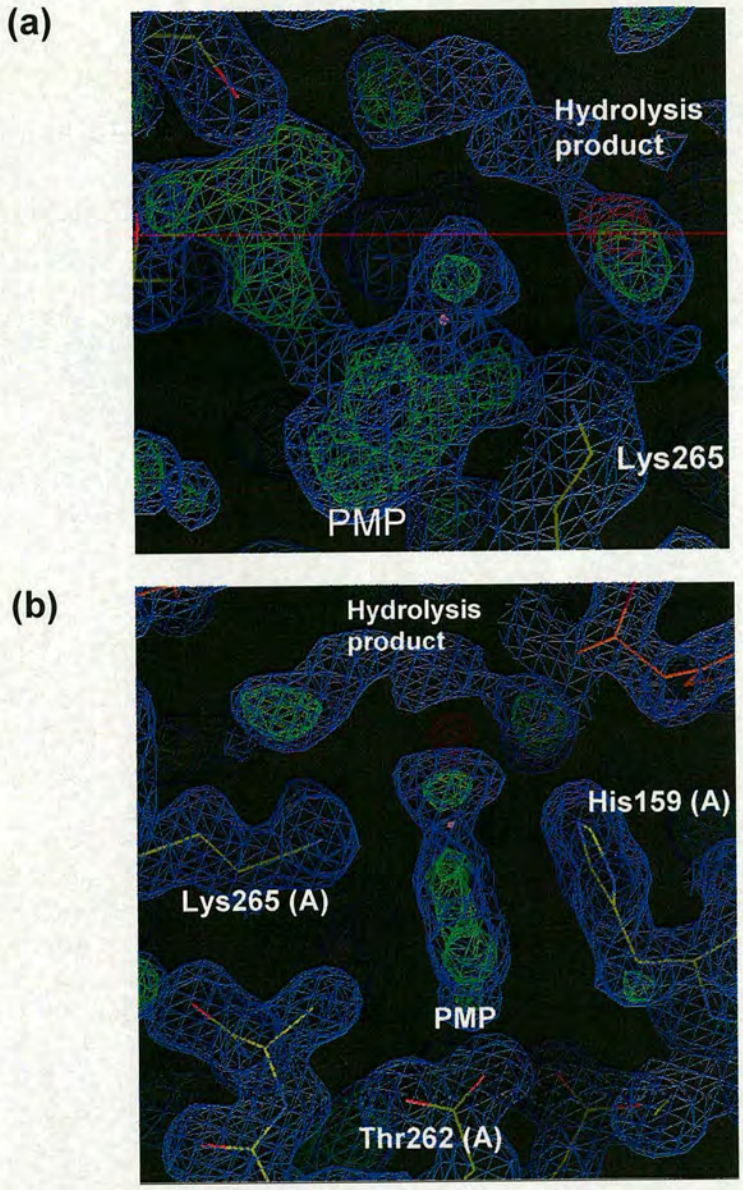

Figure 40: Electron Density Showing the L-cycloserine Hydrolysis Products Within the Active Site of SPT

(a) Two hydrolysis products were observed at the active site of SPT after co-crystallisation with L-cycloserine (1 mM). One of these products has been identified as PMP. The active site lysine (Lys265) is retracted away from the pyridine ring of PMP. (b) The highly conserved histidine residue (His159) remains stacked above the pyridine ring of PMP. In addition, Thr262(A), Ser264(A) and Thr294(B) provide hydrogen bond contacts to the phosphate of PMP, as seen in the holo-SPT and L-serine external aldimine structures.

The density representing the additional LCS-hydrolysis product shown in figure 40, orthogonal to the plane of the PMP ring, is ambiguous and it is difficult to ascertain what this density represents. It appears to be too short to be β-oxyaminopyruvate and therefore may

correspond to a truncated species. It is feasible to suggest that this truncated species is the decarboxylated β-ketoacid derivative β-oxyaminoacetaldehyde, 30 as SPT is a decarboxylating enzyme (Fig. 32b, section 2.7.1). In fact, Ser264 is located at one end of this density suggesting that it may be providing hydrogen bond contacts, possibly with an amino group, of the small molecule. In contrast, His159 is located at the opposite end of the electron density and it could be suggested that this may provide a docking site for the carboxylate (aldehyde) group of the small molecule.

2.8 Conclusions

The holo-SPT and L-serine external aldimine structures are the first to be solved of a SPT from any organism. In addition to the crystal structures, bioinformatic analysis of bacterial and human SPT has not only provided insight into enzyme function but also how mutations may affect enzyme behaviour e.g. mutations associated with hereditary sensory and autonomic neuropathy type I (HSAN1). The crystal structure of L-cycloserine inhibited SPT has opened a gateway for the analysis of inhibition and although the mechanism for cycloserine inhibition of PLP-dependent enzymes is hypothesised in many publications, a specific mechanism for the inhibition of SPT remains unclear (*15-18, 24, 25*). Many experiments are therefore required in order to confirm the identity of reaction intermediates and hence solve the mechanism of L-cycloserine inhibition.

(1) Ikushiro, H., Hayashi, H., and Kagamiyama, H. (2001) A water-soluble homodimeric serine palmitoyltransferase from Sphingomonas paucimobilis EY2395T strain. Purification, characterization, cloning, and overproduction. *J Biol Chem 276*, 18249-56.

(2) Toney, M. D. (2005) Reaction specificty in pyridoxal phosphate enzymes. *Archives of Biochemistry and Biophysics 433*, 279-287.

(3) Ikushiro, H., Hayashi, H., and Kagamiyama, H. (2004) Reactions of serine palmitoyltransferase with serine and molecular mechanisms of the actions of serine derivatives as inhibitors. *Biochemistry 43*, 1082-92.

(4) Yard, B. A., Carter, L. G., Johnson, K. A., Overton, I. M., Dorward, M., Liu, H., McMahon, S. A., Oke, M., Puech, D., Barton, G. J., Naismith, J. H., and Campopiano, D. J. (2007) The structure of serine palmitoyltransferase; gateway to sphingolipid biosynthesis. *J Mol Biol 370*, 870-86.

(5) Alexeev, D., Alexeeva, M., Baxter, R. L., Campopiano, D. J., Webster, S. P., and Sawyer, L. (1998) The crystal structure of 8-amino-7-oxononanoate synthase: a bacterial PLP-dependent, acyl-CoA-condensing enzyme. *J Mol Biol 284*, 401-19.

(6) Astner, I., Schulze, J. O., van den Heuvel, J., Jahn, D., Schubert, W. D., and Heinz, D. W. (2005) Crystal structure of 5-aminolevulinate synthase, the first enzyme of heme biosynthesis, and its link to XLSA in humans. *Embo J 24*, 3166-77.

(7) Schmidt, A., Sivaraman, J., Li, Y., Larocque, R., Barbosa, J. A., Smith, C., Matte, A., Schrag, J. D., and Cygler, M. (2001) Three-dimensional structure of 2-amino-3-ketobutyrate CoA ligase from Escherichia coli complexed with a PLP-substrate intermediate: inferred reaction mechanism. *Biochemistry 40*, 5151-60.

(8) Webster, S. P., Alexeev, D., Campopiano, D. J., Watt, R. M., Alexeeva, M., Sawyer, L., and Baxter, R. L. (2000) Mechanism of 8-amino-7-oxononanoate synthase: spectroscopic, kinetic, and crystallographic studies. *Biochemistry 39*, 516-28.

(9) Bejaoui, K., Uchida, Y., Yasuda, S., Ho, M., Nishijima, M., Brown, R. H., Jr., Holleran, W. M., and Hanada, K. (2002) Hereditary sensory neuropathy type 1 mutations confer dominant negative effects on serine palmitoyltransferase, critical for sphingolipid synthesis. *J Clin Invest 110*, 1301-8.

(10) McCampbell, A., D, Truong, DC, Broom, A, Allchorne, K, Gable, RG, Cutler, et al. . (2005) Mutant SPTLC1 dominantly inhibits serine palmitoyltransferase activity in vivo and confers an age-dependent neuropathy. *Hum. Mol. Genet. 14*, 3507-3521.

(11) Feng, Z., and Barletta, R. G. (2003) Roles of Mycobacterium smegmatis D-alanine:D-alanine ligase and D-alanine racemase in the mechanisms of action of and resistance to the peptidoglycan inhibitor D-cycloserine. *Antimicrob Agents Chemother 47*, 283-91.

(12) Malashkevich, V. N., Strop, P., Keller, J. W., Jansonius, J. N., and Toney, M. D. (1999) Crystal structures of dialkylglycine decarboxylase inhibitor complexes. *J Mol Biol 294*, 193-200.

(13) Noda, M., Matoba, Y., Kumagai, T., and Sugiyama, M. (2004) Structural evidence that alanine racemase from a D-cycloserine-producing microorganism exhibits resistance to its own product. *J Biol Chem 279*, 46153-61.

(14) Noland, B. W., Newman, J. M., Hendle, J., Badger, J., Christopher, J. A., Tresser, J., Buchanan, M. D., Wright, T. A., Rutter, M. E., Sanderson, W. E., Muller-Dieckmann, H. J., Gajiwala, K. S., and Buchanan, S. G. (2002) Structural studies of Salmonella typhimurium ArnB (PmrH) aminotransferase: a 4-amino-4-deoxy-L-arabinose lipopolysaccharide-modifying enzyme. *Structure 10*, 1569-80.

(15) Peisach, D., Chipman, D. M., Van Ophem, P. W., Manning, J. M., and Ringe, D. (1998) Crystallographic study of steps along the reaction pathway of D-amino acid aminotransferase. *Biochemistry 37*, 4958-67.

(16) Rando, R. (1975) On the mechanisms of action of antibiotics which act as irreversible enzyme inhibitors. *Biochemical Pharmacology 24*, 1153-60.

(17) Sundaram, K. S., and Lev, M. (1984) Comparative inhibition of bacterial and microsomal 3-ketodihydrosphingosine synthetases by L-cycloserine and other inhibitors. *Antimicrob Agents Chemother 26*, 211-3.

(18) Williams, R. D., Sgoutas, D. S., Zaatari, G. S., and Santoianni, R. A. (1987) Inhibition of serine palmitoyltransferase activity in rabbit aorta by L-cycloserine. *J Lipid Res 28*, 1478-81.

(19) Obeid, L. M., Okamoto, Y., and Mao, C. (2002) Yeast sphingolipids: metabolism and biology. *Biochim Biophys Acta 1585*, 163-71.

(20) van Meer, G., and Holthuis, J. C. (2000) Sphingolipid transport in eukaryotic cells. *Biochim Biophys Acta 1486*, 145-70.

(21) Manohar, R., Rao, A. G., and Rao, N. A. (1984) Kinetic mechanism of the interaction of D-cycloserine with serine hydroxymethyltransferase. *Biochemistry 23*, 4116-22.

(22) Fenn, T., GF Stamper, AA Morollo and D Ringe. (2003) A side reaction of alanine racemase: Transamination of cycloserine. *Biochemsitry 42*, 5775-5783.

(23) Olson, G., M Fu, S Lau, KL Rinehart and RB Silverman. (1998) An aromatisation mechanism of inactiviation of γ-aminobutyric acid aminotransferase for the antibiotic L-cycloserine. *J. Am. Chem. Soc 120*, 2256-2267.

Chapter 3: Inositol Phosphorylceramide Synthase

3.1 Production of Recombinant Aur1p

Previous attempts to obtain soluble, active Inositol Phosphorylceramide Synthase (Aur1p) were carried out by Dr. Rachel Breen (2005, PhD Thesis, University of Edinburgh). These included cloning *AUR1* with 6-hisitidine and GST tags for expression and purification in *E. coli.* In summary, both methods were unsuccessful due to the toxicity of *AUR1* to *E. coli.* Hence, insoluble inclusion bodies were formed. Isolation and refolding of insoluble Aur1p was not attempted and since *E. coli* also lack the appropriate post-translational modification machinery found in eukaryotic organisms, this expression system was not optimised further. Instead, the eukaryotic host *Pichia pastoris* and the expression vector pPICZαA were used. This produced a His_6 tagged Aur1p with a c-myc tag for Western blot detection and an α-signal sequence for secretion into the media (**Fig. 41**).

Figure 41: Recombinant *AUR1* gene constructed in pPICZαA
AUR1 was cloned into the expression vector pPICZαA. This produced a C-terminally tagged Aur1p construct which contained an α-signal sequence for secretion into the media.

Positive *P. pastoris* transformants were selected using the antibiotic zeocin (100 μg/mL) however this is a relatively expensive method of selection in comparison to ampicillin and kanamycin used for the selection of bacterial transformants. Induction of recombinant *AUR1* expression was carried out using methanol due to the presence of the *AOX1* promoter. Since *AOX1* is tightly regulated at the transcriptional level, the presence of glucose represses transcription even in the presence of methanol. As a result, *P. pastoris* cells had to be grown in glucose-free media. Induction of pPICZαA*AUR1* expression was a lengthy procedure lasting four days and required the addition of methanol every 24 hours to compensate for metabolism and evaporation. Limited information was obtained from analysis of the media as both the cells containing pPICZαA*AUR1* and the controls appeared to exhibit Aur1p activity. As a result, an extensive library of constructs was created in an attempt to obtain

over-expression of *AUR1*. These clones included truncated and full-length forms of *AUR1* from *S. cerevisiae* and *B. cinerea*. The clone taken forward as the best candidate for further investigation in this thesis (by personal communication with Dr Breen) was pPICZ*AUR1*ScKozak.

Ni-NTA purification of Aur1p-His_6 was carried out from the cell free extract of *P. pastoris* containing pPICZ*AUR1*ScKozak. SDS-PAGE analysis of the Ni-NTA elution fraction produced 4 bands consistent with previous purifications carried out by Dr Breen (**Fig. 42**).

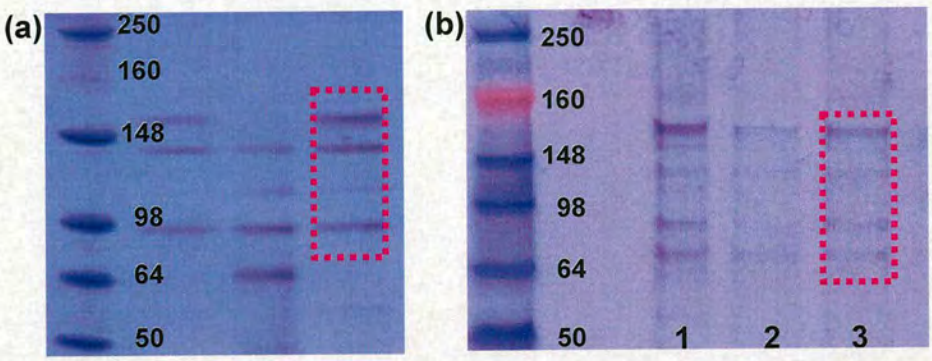

Figure 42: SDS Analysis After Ni-NTA Purification of Aur1p-His_6
(a) Ni-NTA elutions of Aur1p constructs, carried out by Dr Breen. The Ni-NTA elution of pPICZ*aur1*ScKozak is highlighted (b) SDS analysis of Ni-NTA purification carried out during these studies. 1; flow through from load onto Ni-NTA column, 2; wash (5 mM imidazole), 3; elution (500 mM imidazole). The Ni-NTA elution is highlighted. SeeBlue plus2 pre-stained marker (Invitrogen) was used for both gels.

The bands highlighted in **figure 42b** were subjected to proteolytic digest with trypsin and the fragments analysed by Matrix Associated Laser Desorption Ionisation Time of Flight (MALDI-ToF) mass spectrometry in an attempt to identify Aur1p. Unfortunately, no conclusive data was obtained from this experiment. As it remained unclear if these bands corresponded to Aur1p and its aggregates/degradation products, an alternative expression strategy was required to obtain Aur1p for structural studies.

3.2 TAP-tagged Aur1p from *S. cerevisiae*

3.2.1 Cloning of pKW804*AUR1*

This approach involved tagging AUR1p with a Tandem Affinity Purification (TAP) tag using homologous recombination, which allowed the insertion of a gene encoding tagged Aur1p into the chromosome of *S. cerevisiae* thus replacing the wild type gene. For this to occur, the C-terminus (3' end) of *AUR1* had to be cloned to include DNA encoding the TAP tag. This was carried out using the pKW804 binding cassette which is identical to the pFA6a-GFP-kanMX6 cassette developed by Longtine *et al.* except for the GFP moiety, which has been replaced by the ZZ-TEV-S tandem affinity tag via the restriction sites PacI/AscI (**Fig. 43**) (*1*).

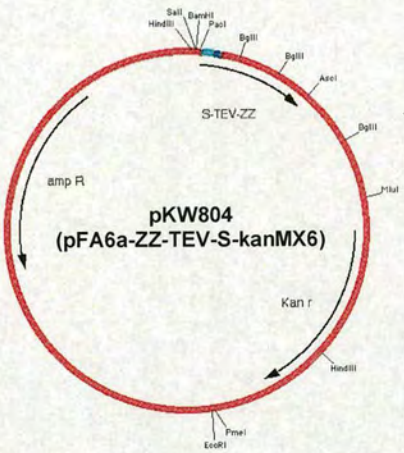

Figure 43: pKW804 Binding Cassette
The ZZ-TEV-S region encodes an affinity tag that is comprised of a ZZ domain containing two IgG binding domains from *Staphylococcus aureus*, a TEV protease cleavage site and an S peptide. The tag also confers resistance to the aminoglycoside anti-biotic G418.

Once the ZZ-TEV-S sequence had been incorporated onto the 3'-end of *AUR1*, the DNA was used to transform the *S. cerevisiae* strain JB811 (the genetically modified JB811 cells were renamed JB811_BY). This strain was selected as it is protease deficient thus it was hoped that the degradation of Aur1p during purification would be prevented. The presence of G418 resistance provided a cheaper method of selection in comparison to zeocin resistance as discussed above. However, the over-expression of *AUR1-ZZ-TEV-S* was unattainable due to

the lack of an inducible promoter sequence. Identification of positive transformants was achieved by PCR using transformed *S. cerevisiae* JB811_BY genomic DNA as a template and primers specific for *AUR1-ZZ-TEV-S* (section 4.2.1.2). The forward primer (*AUR1* TAP for) was designed to bind to the N-terminus of wild type *AUR1* as no modifications had been made to the 5'-end of the gene. In contrast, the reverse primer (*AUR1* TAP rev) was specific to the ZZ-TEV-S tag-encoding region and consequently only bound to the 3'-end of recombinant *AUR1*. A single band of 3573 bp, corresponding to *AUR1-ZZ-TEV-S* (**Fig. 44**).

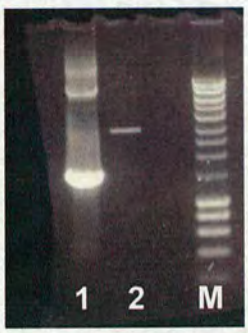

Figure 44: PCR of *S. cerevisiae* (JB811_BY) Genomic Preparation
Lane 1; negative control, 2; *AUR1-ZZ-TEV-S*, M; Hyperladder 1 (New England Biolabs). A band is observed in lane 2 at approximately 3.5 kbp which corresponds to the *AUR1-ZZ-TEV-S* PCR product.

3.2.2 Purification of Recombinant TAP-tagged Aur1p

A small-scale preparation (1 litre) was achieved using *JB811_BY* cells containing *AUR1-ZZ-TEV-S*. An IgG "pull down" with IgG sepharose (Amersham) was used in the first purification step of Aur1p-ZZ-TEV-S from the *JB811_BY* cell free extract. Samples were collected at each step of purification for analysis by SDS-PAGE (**Fig. 45a**) and Western blot (**Fig. 45b**) using peroxidase anti-peroxidase (PAP) antibodies which bind specifically to the ZZ region of the affinity tag. Similar to the results obtained by Ni-NTA purification of His-tagged Aur1p, four bands were observed by SDS-PAGE and Western blot after IgG sepharose purification (lanes 6 and 7, **Fig. 45**). These bands were analysed by MALDI-ToF mass spectrometry however, again, no conclusive evidence was obtained which allowed them to be assigned as Aur1p and/or its aggregation/degradation products.

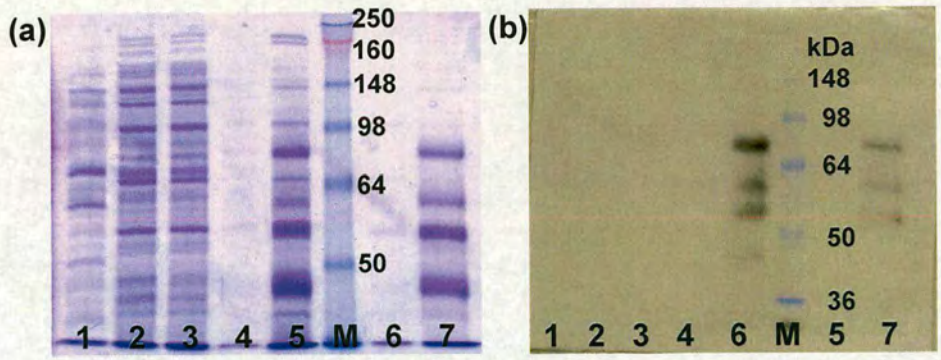

Figure 45: SDS-PAGE and Western Blot Analysis of IgG Sepharose Purification

(a) SDS PAGE analysis of IgG purification. Lane 1; negative control (JB811 CFE), 2; cell free extract before incubation with IgG, 3; supernatant (s/n) after centrifugation, 4; s/n after wash, 5; IgG sepahrose after wash, 6; s/n after incubation with TEV protease, 7; IgG sepharose after incubation with TEV protease. (b) Western Blot using peroxidase anti-peroxidase (PAP) antibodies. Lanes are the same as (a). M; SeeBlue plus2 pre-stained marker (Invitrogen).

The predicted molecular weight of Aur1pZZ-TEV-S is 61,502 Da. A band below 64 kDa is observed in lanes 6 and 7 (**Fig. 45a** and **45b**) and may correspond to Aur1pZZ-TEV-S. However, there are additional bands with higher and lower molecular weights suggesting the presence of modified/degraded forms of Aur1p-ZZ-TEV-S. This evidence suggests that although a protease deficient strain and protease inhibitors were used during purification, Aur1p-ZZ-TEV-S has still become truncated in some way. Since no mass spectrometry data could be obtained, it is difficult to assign the identity of the proteins in these bands. In addition, the bands obtained after IgG purification do not correlate to previous purification of pPICZαAAur1p by Ni-NTA chromatography thus highlighting the difficulties of purifying Aur1p to homogeneity (**Fig. 46**). In light of this, another method was required to obtain pure, recombinant Aur1p.

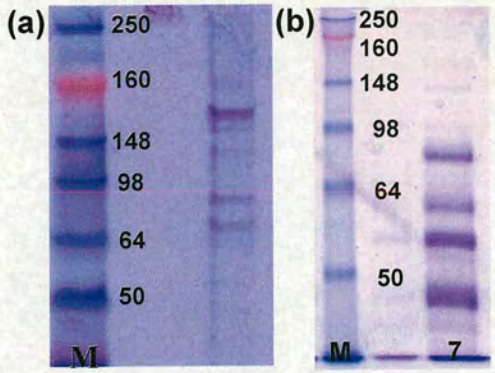

Figure 46: Comparison of pPICZαAAur1p and AUR1-ZZ-TEV-S Purifications
(a) Ni-NTA purification of pPICZαAAur1p. Lane 1; Ni-NTA elution. (b) IgG sepharose purification of Aur1p-ZZ-TEV-S. Lane 7; IgG sepharose after TEV protease cleavage. M; SeeBlue plus2 pre-stained marker (Invitrogen).

3.3 Production of a C-Terminal His_6-tagged Aur1p from *S. cerevisiae*

3.3.1 Manipulation of pAUR123

In contrast to ZZ-TEV-S (TAP) tagged Aur1p, attempts were made to obtain a histidine tagged Aur1p (Aur1p-His_6) in *S. cerevisiae*. Although this had failed previously in *E. coli*, *S. cerevisiae* was used with the rationale that this would be a more suitable host since it already contains a copy of wild-type *AUR1*. Initially, *AUR1-C* was cloned, by PCR, from the pAUR123 expression vector and inserted into pGEM. The pAUR123 expression vector is a non-integrating episomal plasmid that can be used to transform both *E. coli* and *S. cerevisiae* (**Fig. 47**). Sequencing of the *AUR1-C* gene in pGEM identified two point mutations, F158Y and A240C which are responsible for resistance to aureobasidin A (AbA). To confirm this, pAUR123 was used to transform the *S. cerevisiae* strains W303 and JB811, which were subsequently tested, together with wild type cells, on YPD agar containing AbA. Wild type JB811 and W303 cells did not grow in the presence of AbA however the growth of those cells transformed with pAUR123 was not affected.

Although there is an effective selection procedure for pAUR123, the over-expression of *AUR1-C* is not possible, nor are there any specific methods for the purification and detection of Aur1-C protein. In light of this, attempts were made to tag Aur1-C protein with a histidine tag however, after extensive amounts of cloning, codons encoding only three histidine residues were added successfully onto the 3'-end of *AUR1-C* and this method was not optimised further.

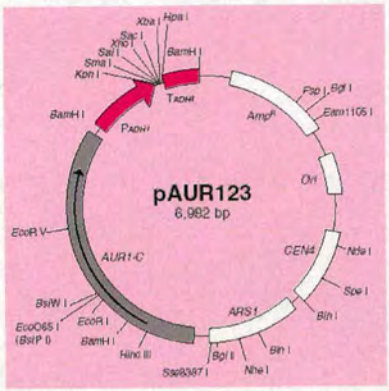

Figure 47: pAUR123 Expression Vector
aur-C; AbA resistance gene in *S. cerevisiae*, ARS; replication origin in *S. cerevisiae,* CEN; centromere in *S. cerevisiae,* Amp^R; selective marker in *E. coli,* Ori; replication origin in *E. coli,* PADH1; promoter of ADH1 gene.

3.3.2 Cloning of *AUR1-C*-His_6 using pYES2/CT/*LacZ*

As numerous attempts to obtain histidine-tagged *AUR1-C* were unsuccessful, *AUR1-C* was cloned with a 3'- *Xho*I restriction site to allow the gene to be excised from the pAUR123 plasmid. The *AUR1-C* gene was excised from pAUR123 (*Hind*III/*Xho*I) and subsequently cloned into pGEM. Sequencing of pGEM*AUR1-C* confirmed the presence of the point mutations F158Y and A240C therefore the gene could still be selected for using AbA. After sequencing, *AUR1-C* was excised from pGEM (*Hind*III/*Xho*I) and ligated into pYES2/CT/*LacZ* to produce pYES2/CT/*AUR1-C* (**Fig. 48**).

The pYES™ vector (Invitrogen) has similar properties to the pAUR123 vector (Takara) as it is a shuttle vector which allows cloning in *E. coli* and expression in yeast. However, pYES contains the *GAL1* promoter for protein over-expression in *S. cerevisiae* and also encodes a

C-terminal 6-histidine tag, followed by a V5-epitope, to allow purification by Ni-NTA chromatography and detection with anti-V5 antibodies. It also contains the *URA3* selection marker for selection of positive transformants with –uracil minimal media.

INVSc1 cells (*S. cerevisiae* auxotrophic for uracil) were used for the transformation with pYES2/CT/*AUR1-C* and positive transformants were selected for on –uracil minimal media agar. Galactose was added to the agar to induce expression of *AUR1-C* and the resistance conferred by Aur1p to AbA, provided an additional selection procedure for the identification of positive transformants.

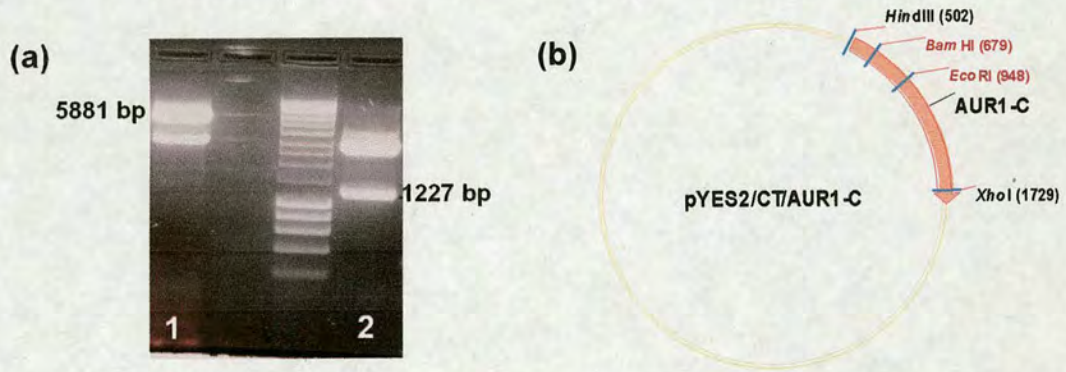

Figure 48: Cloning of pYES2/CT/*AUR1-C*
(a) Restriction digest of 1: pYES2/CT/LacZ and 2: pGEM*aur1-C* with *Hind*III and *Xho*I produced bands corresponding to the pYES2/CT plasmid (5881 bp) and *aur1-C* (1227 bp). (b) The digested *AUR1-C* gene was ligated into pYES2/CT using the *Hind*III/*Xho*I restriction sites to give pYES2/CT/*AUR1-C*.

3.3.3 Selection for Aur1-C-His$_6$ With Aureobasidin A

S. cerevisiae INVSc1 cells, were tested for their sensitivity to AbA and were killed at a concentration of 1 µg/mL. These cells were transformed with pYES2/CT/LacZ (negative control) and pYES2/CT/*AUR1-C* before being spread onto –uracil minimal agar containing 2% galactose and 1 µg/mL AbA. Cells transformed with pYES2/CT/*AUR1-C* grew in the presence of AbA however those cells containing the negative control plasmid were killed (**Fig. 49**).

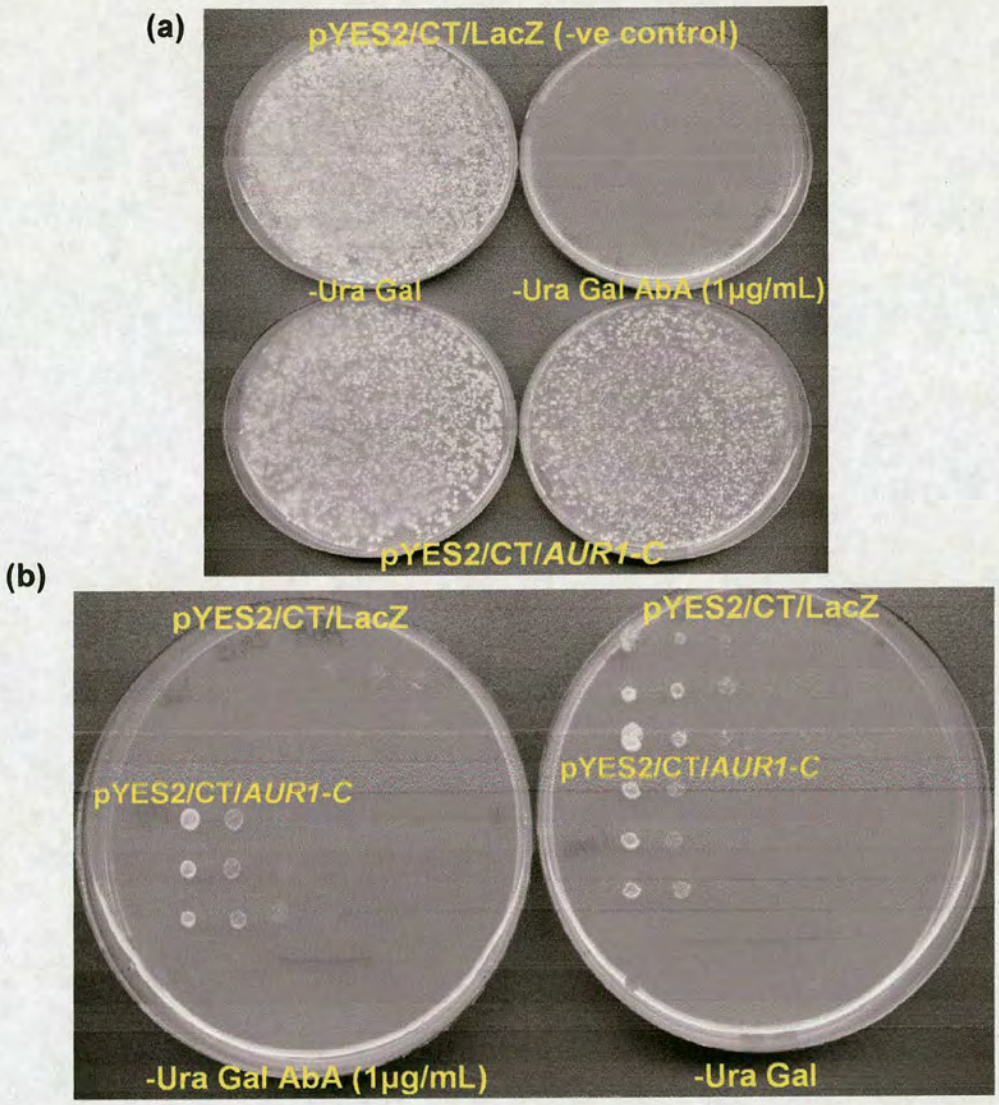

Figure 49: Selection for Aur1-C His_6 Using Aureobasidin A
(a) *S. cerevisiae* containing pYES2/CT/LacZ did not grow on minimal agar containing Aureobasidin A (AbA). However cells containing pYES2/CT/*AUR1-C* were stable in the presence of 1 µg/mL AbA. (b) Microtitre plates containing ten fold dilutions of transformed *S. cerevisiae* overnight cultures were spotted onto minimal agar containing 2% galactose with and without AbA. The cells expressing *aur1-C* grew in the presence of AbA.

Small-scale induction of pYES2/CT/*AUR1-C* expression was carried out over a 12 hour period using 2% galactose and samples were taken at 2 hour intervals for analysis by Western blot. Expression of Aur1-C-His_6 was observed after 2-4 hours of induction however significant expression was obtained after 8-12 hours. Since the level of Aur1-C-His_6

expression after 12 hours was not significantly more than after 8, an induction time of 8 hours was chosen (**Fig. 50**).

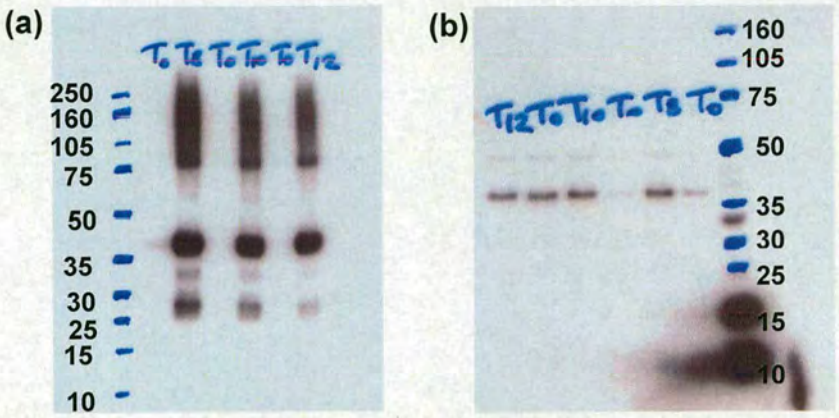

Figure 50: Galactose Induction of pYES2/CT/*AUR1-C*
(a) Detection of Aur1-C-His_6 with anti-V5 antibodies. (b) Detection of Aur1-C_His_6 with anti-C-terminal 6 His antibodies. Samples were taken after 8, 10 and 12 hours of induction at 30°C. T_0; before induction, Tn; after induction.

3.3.4 Detection of Aur1-C-His_6 by Western Blot

Detection of Aur1-C-His_6 expression was carried out using anti-V5 (1:1000) and anti-C-terminal 6His (1:5000) antibodies. Both antibodies detected a band at approximately 40 kDa, however the predicted molecular weight of Aur1-C-His_6 is 48,694 Da suggesting that post-translational modification could have taken place e.g. the cleavage of an N-terminal signal sequence. An additional band at approximately 75 kDa is observed by anti-V5 detection (**Fig. 50a**). The smear observed above 75 kDa is indicative of glycosylation, often observed during analysis of eukaryotic proteins. To test the specificity of the anti-V5 antibody the LacZ protein (expressed from the pYES2/CT/LacZ plasmid) was used as a control. Analysis of an INVSc1 cell free extract detected a band between 75 and 160 kDa (**Fig. 51**) and corresponds to the predicted molecular weight of the LacZ protein (119,678 Da).

Figure 51: Detection of Aur1-C-His$_6$ From a *S. cerevisiae* Cell Free Extract
Anti-V5 detection of pYES2/CT/*AUR1-C* and pYES2/CT/LacZ from an INVSc1 cell free extract after 8, 10 and 12 hours of induction.

3.3.5 Isolation and Purification of Aur1-C-His$_6$

As Aur1p is an integral membrane protein of the Golgi apparatus, isolation of soluble microsomal protein has previously been problematic. Encouraged by the expression observed from the pYES2/CT/*AUR1-C* construct it was decided to increase the scale of induction from 1 to 10 litres and attempt to isolate soluble, recombinant Aur1p. After mechanical disruption of INVSc1 cells expressing pYES2/CT/*AUR1-C*, the cell free extract was centrifuged as described by Ko *et al.* (*2*). Firstly, the mitochondrial fraction was removed and secondly the microsomal fraction was obtained. The microsomal fraction was subsequently solubilised using the non-ionic detergent Triton X-100 as this had been shown by Aeed *et al.* to retain Inositol Phosphorylceramide Synthase activity (*3*). The solubilsed fraction was incubated with Ni-NTA agarose and soluble, recombinant Aur1p was eluted using imidazole (300 mM).

All wash and elution fractions from the purification were analysed by SDS-PAGE and Western blot using anti-V5 antibodies (**Fig. 52**). A single band was observed at approximately 40 kDa in both the solubilised microsomal fraction (lane 6) and the Ni-NTA elution fractions (lanes 10-13).

Although this result is promising, it can be seen from **figure 52** (lanes 2-5) that most of the recombinant Aur1p protein remained in the insoluble, membrane fractions suggesting that further optimisation of the solubilisation procedure is required. Furthermore, recombinant Aur1p could not be detected by Coomassie staining suggesting that the isolated yield was very low.

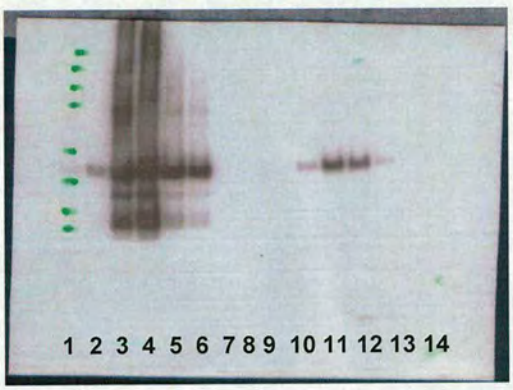

Figure 52: Detection of Aur1-C-His$_6$ After Ni-NTA Purification
Anti-V5 Western blot detection of Aur1-C-His$_6$ after Ni-NTA purification. Lane 1; marker, 2; blank, 3; cell debris, 4; cell free extract, 5; insoluble fraction, 6; solubilised microsomes, 7; 5 mM imidazole wash, 8; 20 mM imidazole wash, 9-14; 300 mM imidazole elutions. The marker is indicated by the green lines and represents the following molecular weights, in descending order, from the top of the gel; 250, 160, 105, 75, 50, 35, 30, 25 kDa.

3.4 Conclusions

After numerous attempts to obtain recombinantly tagged Aur1p protein (N-terminal 6HisAur1p, TAP-tagged Aur1p, C-terminal Aur1pHis$_6$), pure, soluble protein was acheived using the pYES2/CT expression vector. This allowed the galactose induced over-expression of a C-terminal His$_6$ tagged Aur1p which could be purified, in one step, by Ni-NTA chromatography. The presence of a V5-epitope, located before the His$_6$ tag, allowed the detection of Aur1-C-His$_6$ by Western blot. Optimisation of the Western blot procedure for detection of Aur1-C-His$_6$ was beneficial as the low yields of protein, obtained from Ni-NTA purification, were not visible by Coomassie staining. Both aims outlined in section 1.10 have been successfully achieved and will now allow future work to focus on methods to increase the yield of protein to facilitate biochemical and structural studies.

(1) Longtine, M., Mckenzie, A., Demarini, D. J., Shah, N.G., Wach, A, Brachat, A., Philippsen, P. and Pringle, J. R., (1998) Additional molecules for versatile and economical PCR-based gene deletion and modification in *S. cerevisiae*. *Yeast 14*, 953-961.

(2) Ko, J., Cheah, S.and Fischl, A. S., (1995) Solubilisation and characterisation of microsomal-associated phosphatidylinositol:ceramide phosphoinositol transferase from *Saccharomyces cerevisiae*. *Journal of Food Biochemistry 19*, 253-267.

(3) Aeed, P. A., Sperry, A. E., Young, C. L., Nagiec, M. M., and Elhammer, A. P. (2004) Effect of membrane perturbants on the activity and phase distribution of inositol phosphorylceramide synthase; development of a novel assay. *Biochemistry 43*, 8483-93.

Chapter 4: Materials and Methods

4.1 MATERIALS

All reagents, chemicals and media were purchased from either Sigma, Aldrich, Fisher, Biorad, Pharmacia or Oxoid unless otherwise stated and all primers were purchased from Sigma Genosys. All competent cells and pET plasmids were purchased from Novagen and all chromatography columns were from GE Healthcare unless otherwise indicated. The pET16bSPT plasmid was constructed in the lab, prior to this work, by Dr Rachel Breen. The pAUR123 plasmid was purchased from TaKaRa Bio. Inc. *via* Cambrex Bioscience Wokingham Ltd., the pYES2/CT/LacZ plasmid and INVSc1 strain were purchased from Invitrogen and the pKW804 and pFA6a-TRP1-pGAL1 plasmids, together with the *S. cerevisiae* strains W303 and JB811 were gifted by Dr Kevin Hardwick, Wellcome Trust Centre for Cell Biology, University of Edinburgh.

4.1.1 Competent *E. coli* Cell Lines

Table 2

Species	Cell line	Genotype	Application
E. coli	BL21 DE3 (Novagen)	F^- *ompT* *hsd*S_B (r_B^- m_B^-) *gal dcm* (DE3)	Transformation, expression host.
E. coli	DH5α™ (Invitrogen)	F^- φ80d*lacZ*ΔM15 Δ(*lac*2YA-*arg*F) U169 *rec*A1 *end*A1 *hsd*R17 (r_K^-, m_K^-) *pho*A *sup*E44λ^- *thi*-1 *gyr*A96 *rel*A1	Transformation, plasmid storage.
E. coli	HMS174 DE3 (Novagen)	F^- *rec*A1 *hsd*R (r_{K12}^-, m_{K12}^+) (DE3) (RIF^R)	Transformation, expression host.
E. coli	One Shot® Top 10 (Invitrogen)	F^- *mcr*A Δ(*mrr-hsd*RMS-*mcr*BC) φ80*lacZ*ΔM15 Δ*lac*x74 *rec*A1 *ara*Δ139 Δ(*ara-leu*)7697 *gal*U *gal*K *rps*L (Str^R) *end*A1 *nup*G	Transformation of ligations, plasmid storage.
E. coli	JM109 (Promega)	*end*A1, *rec*A1, *gyr*A96, *thi*, *hsd*R17 (r_k^-, m_k^+), *rel*A1, *sup*E44, Δ(*lac-pro*AB), [F′ *tra*D36, *pro*AB, *laq*I^qZΔM15].	Transformation of ligations, plasmid storage.

4.1.2 *Saccharomyces cerevisiae* Cell Stocks

The *S. cerevisiae* strains W303, JB811 and INVSc1 were plated onto YPD agar and grown for 2 days at 30°C. A single colony was used to inoculate YPD (5 mL) under sterile conditions since the broth contained no antibiotic at this stage. The inoculant was grown for at least 24 hours at 30°C with agitation. Glycerol was added to a final concentration of 30% and allowed to equilibrate into the membrane for 20 minutes. The cell stock was subsequently flash frozen in liquid nitrogen prior to storage at -80°C.

4.1.3 Growth Media

All media were dissolved in distilled water and the pH adjusted to 7.5 where required. All were autoclaved for 20 minutes at 120°C, 15 psi before use unless otherwise stated and if required to be stored, were kept at 4°C.

2YT: Bacto-tryptone (16 g/L), bacto-yeast extract (10 g/L), sodium chloride (5 g/L).

Luria Bertani (LB): Bacto-tryptone (10 g/L), bacto-yeast extract (5 g/L), sodium chloride (10 g/L).

Minimal Glycerol Medium, MGM: Yeast Nitrogen Base without amino acids (13.4% w/v), glycerol (10% w/v) and biotin (0.02% w/v) were added to autoclaved, sterile water.

Minimal Methanol Medium, MM: Yeast Nitrogen Base (13.4% w/v), methanol (1 %) and biotin (0.02%) were added to autoclaved, sterile water.

SOC: Bacto-tryptone (20 g/L), bacto-yeast extract (5 g/L), sodium chloride (10 mM), potassium chloride (2.5 mM), magnesium chloride (10 mM), magnesium sulfate (10 mM), glucose (2 % w/v).

YPD: Bacto-tryptone (20 g/L) and bacto-yeast extract (10 g/L) were dissolved in sterile water and autoclaved. Glucose (20%, 0.2 μm filtered) was added to a final concentration of 2% on cooling.

4.1.4 Agar

LB: Bacto-agar (15 g/L) was added to LB media and autoclaved for 20 minutes at 120 °C, 15 psi. Antibiotic was added on cooling (approximately 50°C) to the required concentration. Plates were allowed to dry before being stored at 4 °C with a shelf life of 1-2 months, however those containing antibiotic generally have a shorter shelf life of a few weeks.

YPD: Bacto agar (20g/L) was added to YPD media and autoclaved for 20 minutes at 120 °C, 15 psi. Antibiotic was added on cooling (approximately 50°C) to the required concentration. Plates were allowed to dry before being stored at 4°C with a shelf life of 2-3 months, however those containing antibiotic generally have a shorter shelf life of approximately 1 month.

Sc Minimal Selection: Bacto agar (20g/L), Yeast Nitrogen Base (7g/L) and -Ura drop out mix (0.77g/L) were added to sterile water and autoclaved for 20 minutes at 120 °C, 15 psi. Glucose was added to a final concentration of 2% on cooling.

Sc Minimal Induction: Bacto agar (20g/L), Yeast Nitrogen Base (7g/L) and -Ura drop out mix (0.77g/L) were added to sterile water and autoclaved for 20 minutes at 120 °C, 15 psi. Galactose was added to a final concentration of 2% on cooling.

4.1.5 Antibiotic Stock Solutions

All antibiotic stocks were sterile filtered (0.2 μm) and stored at 4°C.

Ampicillin: A 100 mg/mL stock solution was made and the required volume added to media to give a final concentration of 100 μg/mL.

Aureobasidin A: A 5 mg/mL stock solution was made and the required volume added to media to a final concentration of 1 or 5 μg/mL. (*S. cerevisiae* cells were tested for their sensitivity to AbA on YPD agar containing 1 and 5 μg/mL AbA. Those that did not grow in

the presence of 1 μg/mL were consequently classed as AbA sensitive and were used for future transformation procedures.)

G418: A 100 mg/L solution was made and the required volume added to media to give a final concentration of 200 μg/mL.

Kanamycin: A 30 mg/mL stock solution was made and the required volume added to media to give a final concentration of 30 μg/mL.

Zeocin™: A 100 mg/mL stock solution was made and the required volume added to media to a final concentration of 100 μg/mL.

4.1.6 Solutions and Buffers

Each buffer was made by dissolving the components described below in sterile water. All buffers were 0.2 μm filtered and degassed prior to chromatography. All buffer stocks were stored at 4°C.

0.5 M Potassium Phosphate, KPhos pH7.5: Dibasic potassium phosphate, K_2HPO_4 (0.470 moles/L), monobasic potassium phosphate, KH_2PO_4 (0.0299 moles/L).

IPC synthase Binding Buffer: 20 mM Tris-HCl pH 7.4, 10% glycerol, 0.5 M NaCl, 5 mM β-mercaptoethanol, 0.05% Triton X-100, 5 mM imidazole.

IPC synthase Elution Buffer: 20 mM TrisHCl pH 7.4, 10% glycerol, 0.5 M NaCl, 5 mM β-mercaptoethanol, 0.05% Triton X-100, 500 mM imidazole.

IPC synthase Lysis buffer: 50 mM Tris-HCl pH 7.0, 0.3 M sucrose, 10 mM β-mercaptoethanol, 1 mM EDTA, 1 mini protease tablet per 50 mL.

IPC synthase Solubilisation Buffer: 50 mM Bis-Tris-Cl pH 6.0, 10% glycerol, 5 mM β-mercaptoethanol, 1 mM manganese chloride, 1% Triton X-100, 1 mini protease tablet per 20 mL of buffer.

Lithium Acetate Mix: 100 mM LiOAc, 10 mM Tris pH 7.4, 1 mM EDTA were made up to the required volume using distilled water.

PEG Mix: 40% PEG (2800), 100 mM LiOAc, 10 mM Tris pH 7.4, 1 mM EDTA were made up to the required volume using distilled water.

Ni-NTA Binding buffer: 20 mM KPhos pH 7.5, 25 μM PLP, 10 mM imidazole, 150 mM NaCl, 1 protease inhibitor cocktail tablet per 50 mL of buffer.

Ni-NTA Elution buffer: 20 mM KPhos pH 7.5, 25 μM PLP, 100 mM imidazole, 150 mM NaCl.

Size Exclusion Chromatography Buffer: 20 mM KPhos pH 7.5, 25 μM PLP, 2 mM EDTA, 150 mM NaCl.

SPT Assay Buffer: 50 mM KPhos pH 7.5, 150 mM NaCl, 0.1 mM EDTA.

4.2 METHODS

4.2.1 DNA Manipulation

4.2.1.1 Cloning and Expression Plasmids

Table 3

Plasmid	Cloning/ Expression	Application
pCR2.1-TOPO (Invitrogen)	Cloning in *E. coli*	Provides stock of DNA available for manipulation into various expression vectors.
pGEM®-T Easy (Promega)	Cloning in *E. coli*	Provides stock of DNA available for manipulation into various expression vectors.
pET-16b	Expression in *E. coli*	Expression of an untagged protein.
pET-28a	Expression in *E. coli*	Expression of a C-terminal His_6-tagged protein.
pET-6H	Expression in *E. coli*	Expression of a N-terminal 6His-tagged protein.
pHISTEV30a	Expression in *E. coli*	Expression of a cleavable N-terminal 6His-tagged protein.
pAUR123 (Takara)	Cloning in *E. coli* and expression in *S. cerevisiae*	Allows cloning of target gene in *E. coli* and expression of an untagged protein in *S. cerevisiae*.
pYES2/CT/LacZ (Invitrogen)	Cloning in *E. coli* and expression in *S. cerevisiae*	Allows cloning of target gene in *E. coli* and expression of a C-terminal His_6-tagged protein in *S. cerevisiae*.

4.2.1.2 Oligonucleotide Primers

Table 4

Primer	Sequence (5'- 3')
3HisAUR123 for	AATCATTCCTTTGCGTATGGCACACCACCACAACCCT TTTTCGAGATGG
3HisAUR123 rev	CCATCTCGAAAAAGGGTTGTGGTGGTGTGCCATACG CAAAGGAATGATT
AUR1 TAP for	CCTTCGTTATTTGATGGATCTACTTCTGTTTCTCGTTC GTCCGCCACGTCTATAACGTCACTAGGTGTAAAGAG GGCTCGGATCCCCGGGTTAAT
AUR1 TAP rev	TATAAAATTCTAAAGATAATCAGTGGTATGTGATTAA ATAAACTACATGTATATTATGCTAAACGACAATCCTG ACTAAGGAATTCGAGCTCGTTTAAAC
pAUR123 seq for	GTTGCGGTTTTCATA
pAUR123 seq rev	TATCCGTAATTGCA
pAUR123 XhoI rev	CTCGAGAGCCCTCTTTACACCT
pYES2/CT/*AUR1-C* for seq	ACTACTAGCAGCTGTAATAC
pYES2/CT/*AUR1-C* rev seq	GTAAGCGTGACATAACTAAT
SPT BspHI for	GGACACCGTCATGACCGAAGCC
SPT XhoI rev	GATCCTCGAGGCCGATGACGCCGACCGCGCGGC

4.2.1.3 Transformation of Competent *E. coli*

Plasmid DNA (1 μL) was added to competent *E. coli* cells (20 μL) and incubated for 30 minutes on ice. The cells were then heat shocked for 30 seconds at 42°C before being incubated on ice for a further 2 minutes. SOC medium (80 μL) was added and the cells were agitated (250 rpm) for 1 hour at 37 °C. Cells (50 μL) were spread onto LB agar containing the appropriate antibiotic and incubated overnight at 37°C. Subsequently, 1 colony was used to inoculate 2YT broth (10 mL) containing antibiotic and grown overnight at 37°C with shaking (250 rpm).

4.2.1.4 Transformation of *Saccharomyces cerevisiae*: Lithium Acetate Method

Cells (from glycerol stock) were streaked onto YPD agar and incubated at 30°C for 2-3 days. One colony was used to inoculate YPD broth (5 mL) and was grown overnight at 30°C with shaking (250 rpm). This inoculant (2 mL) was diluted into YPD (50 mL) and grown to an OD_{660} of approximately 0.5 before the cells were harvested by centrifugation (1500 rpm for 3 minutes). The cells were washed with lithium acetate mix (LiOAc, 1 mL) and transferred to a 1.5 mL epindorf. They were subsequently centrifuged for 10 seconds using a bench top centrifuge and the supernatant removed. This wash step was repeated using 0.5 mL LiOAc. Carrier DNA (15 µL, 10 mg/mL single stranded salmon sperm DNA) was mixed with the DNA to be transformed (1-5 µg) in a separate 1.5 mL epindorf to which 100 µL of cells in LiOAc (containing 700 µL of PEG mix) were added. The mixture was incubated at room temperature for 30 minutes before being heat shocked at 42°C for 15 minutes. The cells were harvested using a bench top centrifuge and resuspended in YPD (200 µL) before being spread onto YPD agar and incubated for 2 days at 30°C. The colonies obtained were replica plated onto YPD agar containing the appropriate selection agent and incubated for a further 2 days at 30°C.

4.2.1.5 Polymerase Chain Reaction (PCR): Taq Polymerase Beads (GE Healthcare)

Generally, each PCR reaction contained; template DNA (5 µL), forward primer (5 µL), reverse primer (5 µL) and puRe Taq Ready-To-Go PCR beads (x2, GE Healthcare). Each PCR bead was reconstituted to a final volume of 25 µL to yield the following concentration of reactants; dNTPs (200 µM in 10 mM Tris-HCL, pH 9 at room temperature), potassium

chloride (50 mM) and magnesium chloride (1.5 mM). The final reaction volume (50 µL) was made with sterile water and subsequently covered with a layer of mineral oil.

A general PCR reaction consisted of 30 temperature cycles; denaturation (94°C, 60 seconds), annealing (54°C, 30 seconds), elongation (72°C, 90 seconds) followed by an additional extension period (72°C, 10 minutes). The reaction was terminated by the addition of DNA loading dye (6x, Novagen) and the mixture was separated by electrophoresis.

The purified PCR product could then be cloned using the pCR2.1-TOPO® vector (Invitrogen) or pGEM-Teasy (Promega) according to manufacturers instructions. All cloned DNA was transformed into Top10 competent cells (25 µL) and cultures were grown on S-Gal agar plates containing ampicillin (100 µg/mL) thus providing blue/white screening for the identification of viable clones.

4.2.1.6 Polymerase Chain Reaction: Expand Polymerase (Roche)

Generally each reaction contained, forward primer (300 mM), reverse primer (300 mM), dNTP (350 µM), Buffer 1 (5 µL, 10x), template DNA (1.75 mM) and Expand long template enzyme mix (0.75 µL). The reaction was made up to 50 µL with sterile water. The general thermal cycling procedure consisted of the following steps: step1, initial denaturation (94°C, 2 minutes), steps 2-31, denaturation (94°C, 15 seconds), annealing (45-65°C, 30 seconds) and elongation (72°C, 2 minutes). This was followed by a final extension step for 10 minutes at 72°C.

4.2.1.7 Polymerase Chain Reaction: QuickChange® Site-Directed Mutagenesis (Stratagene).

Generally, each reaction contained forward primer (125 ng), reverse primer (125 ng), dNTP (1 µL), reaction buffer (5 µL, 10x), double stranded template DNA (5-50 ng) and *PfuTurbo* DNA polymerase (1µL). The reaction was made up to 50 µL with sterile water.

The general thermal cycling procedure consisted of the following steps; step 1, initial denaturation (95°C, 30 seconds), steps 2-19, denaturation (95°C, 30 seconds), step 20, annealing (55°C, 1 minute) and elongation (68°C, 1 minute/kbp).

Following thermal cycling, the reaction mixture was cooled to 37°C before adding the restriction endonulease DpnI (1 μL) to remove any dam methylated/parental DNA. This solution was mixed using a pipette and centrifuged for 1 minute at 13,000 rpm before being incubated for 1 hour at 37°C. After digestion with DpnI, the DNA mixture (2 μL) was transformed into TOP10 competent cells as mentioned in section 4.2.1.3.

4.2.1.8 Ligation Into An Expression Vector

Ligations were carried out using the gene of interest (3 μL), the restricted plasmid (14 μL), T4 ligase (1 μL, $1x10^6$ ligations/unit, New England Bio-labs) T4 ligase buffer (2 μL, 10x, New England Bio-labs). The ligation was incubated overnight at room temperature and subsequently, 2 μL was transformed into TOP10 competent cells (25 μL) as described in section 4.2.1.3.

4.2.1.9 Cloning Using pFA6a-ZZ-TEV-S-kanMX6

The binding cassette pKW804 was used for this procedure. It is identical to pFA6a-GFP-kanMX6 used by Longtine *et al.* except for the GFP moiety (*1*). The GFP part has been replaced by the S-TEV-ZZ (S peptide; binds S protein, TEV; TEV protease cleavage site, ZZ; 2x IgG binding domains from *Stapholococcus aureus*) tandem affinity tag using the restriction sites PacI/AscI.

The forward primer (AUR1 TAP for) contained 80 bp homologous to the 5'-end of the AUR1 gene followed by the F2 C-terminal tagging sequence acquired from Longtine *et al.* *(1)*. The reverse primer (AUR1 TAP rev) contained 80 bp homologous to part of chromosome XI (downstream of the AUR1 gene) followed by the R1 Deletion/C-terminal

tagging sequence acquired from Longtine *et al. (1)*. These primers were used for PCR in combination with Expand DNA polymerase and the PKW804 cassette according to section 4.2.1.6. The PCR was analysed by electrophoresis and where successful, a product of approximately 2.5 kbp was obtained. The reaction was scaled up to 500 µL (10 x 50 µL reactions) after which, all reactions were pooled and extracted using phenol:chloroform:isoamyl alcohol (25:24:1, v/v) see section 4.2.1.10.

4.2.1.10 Solvent Extraction of sTAP DNA

All PCR reactions were pooled and to them was added an equal volume of phenol:chloroform:isoamyl alcohol (25:24:1, v/v). The mixture was vortexed vigorously before being centrifuged for 5 minutes at 13,000 rpm. The upper aqueous layer was removed and the DNA precipitated using 2.5 volumes of ethanol (ice cold). The mixture was centrifuged again, as before, and the ethanol removed by evaporation at room temperature overnight. The precipitated DNA was resuspended in sterile water (10-20 µL) and transformed into JB811 cells using the lithium acetate method described in section 4.2.1.4.

4.2.2 DNA PURIFICATION

4.2.2.1 Mini-Prep: QIAprep® Spin Miniprep Kit (QIAGEN)

This procedure was carried out according to the manufacturers instructions, provided with the kit and is summarised below.

An overnight culture (1.5 mL) was transferred to a sterile epindorf (1.5 mL) and centrifuged (13,000 rpm, 2 minutes) using a bench-top centrifuge. The supernatant was discarded and the procedure repeated with a further 1.5 mL of culture. The pellet was resuspended in P1 buffer (250 µL) and to this, P2 buffer (250 µL) was added. This was followed by immediate invertion of the epindorf 4-6 times. Subsequently, N3 buffer (350 µL) was added and the mixture inverted immediately (4-6 times). The resultant cloudy mixture was centrifuged (13,000rpm, 10 minutes) after which, the supernatant was transferred to a QIAprep spin column and centrifuged (13,000rpm, 1 minute). The flow through was discarded and the spin column washed with PB buffer (500 µL) and centrifuged (13,000rpm, 1 minute). The column was washed further with PB buffer (750 µL) and centrifuged (13,000rpm, 1 minute). The column was centrifuged for a further minute to remove any residual wash buffer before the purified DNA was eluted with sterile water (100 µL) and stored at -20°C until required.

4.2.2.2 Gel Extraction –QIAquick ® Gel Extraction Kit (QIAGEN)

DNA was excised from an agarose gel (1%) and purified according to the manufacturers instructions, which are summarised below.

Agarose containing the DNA, was covered in sufficient QG buffer (600 µL – 1 mL) and incubated at 50°C until the agarose had completely dissolved. This solution was transferred to a spin column and centrifuged (13,000 rpm, 1 minute). The supernatant was discarded and QG buffer (500 µL) was added to the column and centrifuged (13,000 rpm, 1 minute). The supernatant was discarded and PE buffer (750 µL) added to the column and incubated for 2-

5 minutes. The column was centrifuged (13,000 rpm, 1 minute), the supernatant discarded, and the column centrifuged again to remove any residual buffer. The purified DNA was eluted with sterile water (30 μL) and stored at -20°C until required.

4.2.3 DNA ANALYSIS

4.2.3.1 Digestion by Restriction Endonuclease

Generally, a single restriction digest contained the following; template DNA (8 μL), restriction buffer (1 μL, 10x, New England Biolabs) and restriction endonuclease (1 μL, New England Bio-labs). This mixture was incubated at 37°C for 3 hours and the reaction was terminated by the addition of DNA loading dye (2 μL, 6x, Novagen). The digestion mixture was loaded onto an agarose gel (1%) and separated by electrophoresis (section 4.2.3.2).

4.2.3.2 Electrophoresis

Agarose (1.0 g) was added to TAE buffer (100 mL, Bio-Rad) and boiled until the agarose had completely dissolved. On cooling, to approximately 50°C, ethidium bromide was added to a final concentration of 0.5 μg/mL and the solution swirled to ensure complete mixing. The molten agarose solution was transferred to the casting mould and allowed to set at room temperature. DNA loading dye (6x, Novagen) was added to the DNA samples (2 μL to small samples of approximately 10 μL and 10 μL to larger samples of approximately 50 μL). The gel was immersed in TAE buffer and run at a constant voltage of 100 volts until good separation between bands was observed.

4.2.3.3 Sequencing PCR

To prepare a DNA sample for sequencing the DNA source (5 μL) was added to sequencing buffer (2 μL, 5x, Applied Bioscience) containing Big Dye version 3.1 (2 μL) and sequencing primer (1 μL forward or reverse). Primers (**table 5**) were provided as 100 ng/μL stocks however, 3.2 pM/μL stocks were made as 3.2 pM was required for each sequencing reaction. Only one primer, forward or reverse, was required for each sequencing reaction. The general

sequencing program consisted of 25 cycles of the following steps; 95°C for 30 seconds, 50°C for 20 seconds and 60°C for 4 minutes.

Primer	Plasmid	Sequence
pCR2.1 M13 Rev (forward primer)	pCR2.1	**5'** CAGCAAACAGCTATGAC **3'**
pCR2.1 M31 For (reverse primer)	pCR2.1	**5'** GTAAAACGACGGCCAG **3'**
pGem T7 For (forward primer)	pGem	**5'** TAATACGACTCACTATAGGG **3'**
pGem T7 Rev (reverse primer)	pGem	**5'** ATTTAGGTGACACTATAGAA **3'**

Table 5: Sequencing Primers

4.2.4 PROTEIN PRODUCTION AND ISOLATION

4.2.4.1 Large Scale Over-expression in *E. coli*

One colony was used to inoculate 2YT broth (500 mL) containing the appropriate antibiotic and was grown overnight at 37 °C with shaking (250 rpm). This inoculant was sub-cultured into 2YT broth (4 litres containing antibiotic) and grown to an OD_{600} of 0.6, at 37 °C before being induced with IPTG (0.1 mM). Induction was carried out at 30 °C for 5 hours.

4.2.4.2 Expression of pPICZαA*AUR1Sc* in *Pichia pastoris*

Cells were streaked onto YPD-agar containing Zeocin (100 μg/ml) and incubated for 2 days at 30°C. A single colony was used to inoculate MGM broth (10 mL) containing zeocin (100 μg/mL) and was incubated at 30°C, with shaking (250 rpm), until an OD_{600} of 2-6 had been reached. This culture was then used to inoculate MGM broth (1.5 litres) and was grown at 30°C to an OD_{600} 2-6 before the cells were harvested by centrifugation (3000 rpm, 10 minutes, 4°C). The cell pellet was resuspended in MM (500 mL) to an OD_{600} of 20-40 and agitated (250 rpm) for 4 days at 30°C. To compensate for metabolism and evaporation, methanol was added to a final concentration of 1% (v/v) every 24 hours. The cells were harvested by centrifugation (3000 rpm, 4°C, 10 minutes) and flash frozen in liquid nitrogen before being stored at -80°C.

4.2.4.3 Cell Lysis by Sonication

All steps were performed on ice. The cell pellet was resuspended in resuspension buffer (40 mL, 4:1 v/w) containing 1 protease inhibitor cocktail tablet (Roche) and sonicated for 15 cycles (30 seconds on, 30 seconds off) using a soniprep 150. The cell debris was harvested by centrifugation (15,000 rpm, 20 minutes, 4°C) and the supernatant retained for purification.was

4.2.4.4 Cell Lysis by Mechanical Disruption: Bead Beater

The outer chamber of the bead beater (Biospec Products Inc.) was filled to ¾ of its capacity with ice which, was subsequently immersed in a solution of ethanol:water (50:50 v/v). The inner chamber was filled to approximately 50% with acid washed glass beads (Sigma) to which, the thawed cell pellet was added. The pellet and beads were mixed to expel any air before any remaining space within the chamber was filled with lysis buffer. Lysis was carried out at 4°C with 5 cycles (30 seconds on, 30 seconds off) and the cell debris removed by centrifugation (11,000 rpm, 20 minutes, 4°C).

4.2.4.5 Solubilisation of the Microsomal Fraction

A *S. cerevisiae* cell free extract was centrifuged (15,000 rpm, 25 minutes, 4°C) to remove the mitochondrial fraction and the supernatant subsequently centrifuged (30,000 rpm, 45 minutes, 4°C,) to obtain the microsomal fraction. The microsomal pellet was resuspended in solubilisation buffer and agitated slowly for 90 minutes at 4°C. The insoluble fraction was removed by centrifugation (30,000 rpm, 4°C, 45 minutes) and the supernatant aliquoted and stored immediately at -80°C until required.

4.2.5 PROTEIN PURIFICATION

4.2.5.1 Ni-NTA Agarose

On average, each purification using a HiPrep™ column yielded approximately 10 mg of protein per litre of cell culture. Although this yield is sufficient for biochemical and structural analyses, purification was optimised further to give a higher yield of protein. The prepacked HiPrep™ column (GE Healthcare) was replaced with Ni-NTA agarose (Invitrogen). This method was subsequently used routinely, in the purification of pET28aSPT for crystallisation.

The cell free extract (approximately 40 mL) was incubated with pre-equilibrated Ni-NTA agarose (2 mL, 5-10 mg protein/mL beads) at 4°C for 1 hour prior to packing the beads into an empty polyprep column (5 mL, QIAGEN) by gentle suction. This method allowed longer contact between the cell free extract and the chromatography media thus allowing more time for the 6-histidine tag of the protein to interact with the Ni-NTA of the agarose. The beads were packed and washed with 10 column volumes of Ni-NTA binding buffer, under gentle suction, and the protein eluted with 5 column volumes of Ni-NTA elution buffer. The protein was eluted with 100 mM imidazole in comparison to the Hiprep™ method which required 200 mM.

It appeared that the Ni-NTA agarose beads were being over loaded with protein, as a large amount of recombinant SPT was observed by SDS PAGE analysis of the flow through. To prevent over loading, half the volume (20 mL of cell free extract) was used per 2 mL of agarose. This modification yielded a two-fold increase in protein production (approximately 20 mg of protein per Litre of cell culture).

4.2.5.2 Size Exclusion Chromatography

A HiPrep™ 26/60 Sephacryl™ S-200 (318 ml) size exclusion column was pre-equilibrated with 1 column volume of gel filtration buffer. Before loading, the protein sample was 0.45 μm filtered and concentrated to 3-5% of the total column volume. It was eluted over 1 isocratic column volume and 10 mL fractions were collected. The approximate molecular mass of purified protein was calculated using a calibration curve obtained from known molecular weight standards (GE Healthcare).

4.2.5.3 IgG "Pull Down"

An initial "pull-down" purification of *AUR1-C*STEVZZ was attempted using IgG Sepharose6 (fast flow) resin (GE Healthcare). The cell free extract (40 mL) was incubated with IgG resin (100 μL) for 2 hours at 4°C. The beads were harvested by centrifugation and washed with lysis buffer containing one protease inhibitor cocktail tablet. The beads were incubated in the presence of TEV protease (100 units) at 4°C overnight to remove the ZZ-domain and release Aur1p from the resin.

4.2.6 PROTEIN ANALYSIS

4.2.6.1 Sodium Dodecyl Sulfate-Polyacrylamide Gel Electrophoresis (SDS-PAGE)

An average gel (10 mL) consisted of a 12% running gel (H_2O, 30 % acrylamide, 1.5 M Tris pH 8.8, 10 % SDS, 50 mg/mL ammonium persulfate and 15 µL TEMED) and a 4 % stacking gel (H_2O, 30% acrylamide, 0.5 M Tris pH 6.8, 10% SDS, 50 mg/mL ammonium persulfate and 15 µL TEMED). All protein samples were denatured by the addition of SDS-loading buffer (1.5 M TrisHCl pH 6.8, 5 % v/v glycerol, 10 % w/v SDS, 0.4 mL β-mercaptoethanol and 0.05% w/v bromophenol blue) and boiled for 10 minutes. The mixture was centrifuged (13.000 rpm, 5 minutes) prior to loading the gel.

The gel was run for approximately 50 minutes at a constant voltage of 180 volts. Subsequently, it was immersed in Coomassie stain (H_2O, 0.1% w/v Coomassie brilliant blue R250, 40% v/v methanol and 10% v/v acetic acid) and incubated for 20 minutes at 37°C. The gel was destained (H_2O, 40% v/v methanol and 10% v/v acetic acid) until all excess stain had been removed.

An approximate protein molecular mass was obtained using the pre-stained protein molecular weight markers SeeBlue Plus2 (Invitrogen) or Low Molecular Weight Marker (GE Healthcare).

4.2.6.2 Non-Denaturing (Native) Gel

A pre-cast Tris-Glycine gel (10%, Invitrogen) was used for the detection of non-denatured protein. Native loading buffer (25 µL, Invitrogen) was added to each protein sample (25 µL) which was loaded onto the gel without boiling. The gel was run for 90 minutes at a constant voltage of 100 volts and was stained as mentioned in section 4.2.6.1.

4.2.6.3 Semi-Dry Western Blot

After SDS-PAGE (section 4.2.6.1), Hybond™ ECL nitrocelluose membrane (GE Healthcare) was cut to fit the gel. Both the gel and the membrane were equilibrated in transfer buffer (25 mM Tris, 150 mM glycine, 10% methanol) for 15 minutes at room temperature. Three pieces of Whatman filter paper slightly larger than the membrane were soaked in transfer buffer before being transferred onto a Trans-blot SD semi-dry transfer cell (Biorad). The membrane was placed onto the filter paper followed by the gel and finally another three sheets of filter paper, pre-soaked in transfer buffer. At each stage, care was taken to ensure that no air bubbles were present between each layer. The protein was transferred for 1 hour at a constant voltage of 15 volts.

The membrane was blocked for 90 minutes at room temperature (or overnight at 4°C) in blocking solution (5% w/v skimmed dried milk powder in PBS-Tween) with gentle agitation and then washed with PBS-Tween for 2 x 5 minutes, 2 x 10 minutes, 1 x 20 minutes. It was subsequently incubated with antibody solution (blocking solution containing antibody to desired dilution) at room temperature for 90 minutes before being washed as described above. The ECL Plus™ (GE Healthcare) reaction was carried out according to manufacturers instructions and the membrane was exposed to Kodak® X-Omat AR film, XAR-5, 18 cm x 24 cm for the amount of time required for adequate detection of protein. The film was developed using Konica SRX-101A.

Exposure time is protein dependent and optimisation is often required for each individual protein detected.

4.2.6.4 BCA™ Protein Assay (PIERCE)

This method utilises bicinchoninic acid for the colourimetric detection and quantitation of total protein in solution. The assay relies on the proteinaceous reduction of Cu^{2+} to Cu^{1+} in an

alkaline medium. The Cu^{1+} is consequently detected by the bicinchoninic acid in a ratio of 1:2, thus producing a colour change from green to purple which can be detected spectrophotometrically at 562 nm.

2 mL of working reagent (50:1 v/v, solution A: solution B) was added to a clean, dry test tube, containing the protein sample (100 µL) and incubated for 30 minutes at 37 °C. A standard curve was produced from serial dilutions (**table 6**) of a known stock concentration of BSA (2 mg/mL) and the concentration of protein calculated according to this standard curve. Each sample was carried out in duplicate.

STANDARD	CONCENTRATION (mg/mL)
A	2.00
B	1.50
C	1.00
D	0.75
E	0.50
F	0.25
G	0.125
H	0.025
I	0.00

Table 6: Standard Curve Concentrations

4.2.7 PROTEIN AND SMALL MOLECULE CHARACTERISATION

4.2.7.1 Liquid Chromatography-Mass Spectrometry of Proteins

Mass spectrometry was performed on a Micromass Platform equipped with an electrospray ion source. The spectrometer cone voltage was ramped from 40 to 70 volts and source temperature set to 140°C. Protein samples were separated with a Waters HPLC 2690 with a Jupiter C5 reverse phase column (5μm, 250 x 4.6mm, Phenomenex) directly connected to the spectrophotometer. Proteins were eluted from the column with a 5-95% acetonitrile gradient using an acetonitrile/water/TFA (0.01%v/v) solvent system (flow rate 0.4ml/min). The total ion count in the range 500 to 2000 m/z was scanned at 0.1s intervals. The scans were accumulated, the spectra combined and the molecular mass was determined by the MaxEnt and Transform algorithms of the Mass Lynx software (MicroMass).

4.2.7.2 Liquid Chromatography-Mass Spectrometry of Small Molecules

Mass spectrometry was performed on a Micromass Platform equipped with an electrospray ion source. The spectrometer cone voltage was ramped from 40 to 70 volts and source temperature set to 140°C. Protein samples were separated with a Waters HPLC 2690 with Phenomenex C_{18} reverse phase column directly connected to the spectrometer. The small molecules were eluted from the column with a 30-60% acetonitrile gradient using an acetonitrile/ water/ TFA (0.01%v/v) solvent system (flow rate 0.1ml/min). The total ion count in the range 200 to 800 m/z was scanned at 0.1s intervals. The scans were accumulated, the spectra combined and masses were determined by the MaxEnt and Transform algorithms of the Mass Lynx software (MicroMass).

4.2.8 PROTEIN CHEMISTRY

All assays in this section refer to pET28aSPT unless otherwise stated. All UV-visible spectra were recorded on a single-beam Hewlett-Packard 8452A diode array spectrophotometer and analysed using UV-Visible ChemStation software (Agilent). All assays were carried out on a 500 μL scale at 25 °C unless otherwise stated.

4.2.8.1 Spectroscopic Measurements

To convert apo-SPT to holo-SPT, the enzyme was dialysed for 1 hour at 4°C against 20 mM potassium phosphate pH 7.5 containing 150 mM NaCl, 25 μM PLP and 1 mM EDTA. Excess PLP was removed using a PD-10 (Sephadex G-25M) desalting column (GE Healthcare) before any spectrophotometric measurements were taken. The concentration of recombinant SPT was 20 μM in all assays unless otherwise stated and the spectrophotometer was blanked with 20 mM potassium phosphate pH 7.5, 150 mM NaCl and 1 mM EDTA.

For measurements involving L-serine or L-cycloserine fresh stock solutions (10x) were made prior to use by dissolving the required mass of substrate in sterile water.

4.2.8.2 Stopped Flow Measurements of L-serine Binding

Data were obtained using a SX.15MV stopped-flow spectrophotometer (Applied Photophysics) at 25 ± 1 °C. Data were analysed with Origin 7 (Microcal) and average traces from four or more measurements were used for analysis. The buffer used for all stopped-flow experiments was 20 mM Khos pH 7.5, 150 mM NaCl. A 2x solution of protein and substrate were loaded into separate chambers and the protein mixed in a 1:1 ratio with substrate within the reaction vessel to give a final concentration of 20 μM. The reaction was monitored by the increase in absorbance (428 nm) at various L-serine concentrations (0.1 to 50 mM).

4.2.8.3 Detection of 3-ketosphinganine

A radioactivity assay, which monitors the incorporation of ^{14}C-serine into ^{14}C-labelled 3-ketodihydrosphingosine, was used for the detection of 3-ketodihydrosphingosine produced by recombinant SPT.

A typical assay contained 20 μM SPT (in 20mM KPhos pH 7.5, 150 mM NaCl and 1mM EDTA), 20 mM L-[U-^{14}C] serine (9250 Bq/0.250 μCi) and 1.6 mM palmitoyl-CoA. The reaction was incubated at 37°C for 20 minutes and terminated by the addition of 0.4 M NH_4OH. The lipid portion was extracted with an equal volume of $CHCl_3$:CH_3OH (2:1 v/v) and the sample centrifuged. The aqueous layer was removed and the organic solvent evaporated overnight. The lipid residue was resuspended in 15 μL of $CHCl_3$:CH_3OH (2:1 v/v) and spotted onto a Silica Gel 60 TLC plate. The lipids were separated with $CHCl_3$:CH_3OH:NH_4OH (40:10:1 v/v) and the TLC was incubated with a Storage Phosphor Screen (GE Healthcare) for 5 days at room temperature. The screen was developed using a Storm Phosphor Imager (GE Healthcare) and the image visualised using ImageJ software.

For comparison, a reference sample of 3-ketodihydrosphingosine (Matreya) was analysed on a Silica Gel 60 TLC plate as above and detected using ninhydrin.

For incubation with *S. paucimobilis* cell free extract, the assay described above was incubated for 1 hour at 37 °C before addition of a concentrated *S. paucimobilis* cell free extract. This mixture was incubated for a further hour at 37 °C and extracted as above.

4.2.8.4 L-cycloserine Inhibition of Recombinant SPT

Inhibition of recombinant SPT by L-cycloserine was monitored using the method previously described (section 4.2.8.3) with the following modifications: 20 μM SPT (in 20 mM KPhos pH 7.5, 150 mM NaCl), 1.6mM palmitoyl-CoA and 1mM L-cycloserine were incubated for 1 hour at 37 °C, before 10mM L-[U-^{14}C] serine (9250 Bq/0.250 μCi) was added. This was incubated for a further hour at 37 °C.

4.2.8.5 Denaturation with Urea

SPT (20uM) was incubated with L-cycloserine (1 mM) and the protein denatured with Urea (final concentration 4 M) at time points 15, 30, 40, 60, 120 and 240 minutes. The UV-visible spectra were recorded before after denaturation.

4.2.9 STRUCTURAL BIOLOGY

4.2.9.1 Apo-SPT

pET28aSPT was screened for suitable crystallisation conditions using the high throughput facilities at the Scottish Structural Proteomics Facility (SSPF), University of St. Andrews. The crystallisation conditions were screened using a nano-drop crystallisation robot (Cartesian Honeybee, Genomic Solutions) as part of the Hamilton-Thermo Rhombix system. Over 700 conditions were tested from commercially available sparse-matrix screens, using sitting-drop vapour-diffusion, with a well volume of 100 µL in 96 well plates (Griener 3-square) at 293 K. Drops containing 0.2 µL of protein and 0.1 µL of well solution were used. Several conditions produced initial crystals and these were optimised using the Rhombix system. Small (< 0.05mm x 0.05 x 0.2mm) colourless, cubic crystals were produced by adding 0.1 µL of SPT (24 mg/mL in 10 mM Tris pH 7.5, 150 mM NaCl, 25 µM PLP) and 5 µL myriocin to 0.1 µL of well solution (100 mM Tris pH 6.5, 10% PEG 8K, 170 mM $MgCl_2$).

The crystals were mounted in cryoloops (Hampton Research) and cryoprotected by passing them through a mixture of 20% glycerol and well solution. Crystals were then frozen by rapid immersion in liquid nitrogen, and transferred to sample changer baskets (Molecular Dimensions). Multiple crystals were screened at Beam Line BM14, Grenoble, ESRF using the sample changer, and a low-resolution dataset (3.0 Å) was collected from the highest diffraction resolution, single crystal at 100K. Data were indexed and scaled with DENZO and SCALEPACK as implemented in the CCP4 suite (*2*). Initial phases were determined using molecular replacement, with a homology model generated from the KBL (PDB code: 1FC4) monomer structure and confirmed a dimer. The molecular replacement model was built using the CASPR server (*3*).

4.2.9.2 Holo-SPT

The initial hits were further optimized with screens generated using the Crystools server (*3*). The protein was dialysed in the presence of excess PLP to ensure complete reloading. Contrary to preparation of the apo-SPT, excess PLP was not removed by size exclusion chromatography prior to crystallisation. Sitting drop plates (EasyXtal DG-CrystalSupport; QIAGEN) were used for trials in which, a large yellow crystal (~0.8mm x 0.2 x 0.2mm) grew in a 2 µL drop, consisting of 1 µL SPT (20 mg/mL in 10 mM Tris pH 7.5, 150 mM NaCl and 25 µM PLP) and 1 µL of well solution (100 mM HEPES pH 6.5, 230 mM $MgCl_2$, and 25% PEG 3350). The crystal was mounted in a cryoloop and cryoprotected in 22% PEG3350, 100 mM HEPES pH 6.5, 120 mM $MgCl_2$, 20% PEG400.

The crystal was subsequently frozen and shipped to the ESRF where a 1.3 Å dataset was collected on BM14 at 100 K. Data were processed with MOSFLM and SCALA. Phases were calculated with Phaser (*4, 5*) using the partially refined apo- structure as a starting model. Automated model building in ArpWarp successfully built 391 residues out of 427, and produced an initial model with an R-factor of 19.5% and a Rfree of 23.2% (*6*). Both apo- and holo- models were refined using Refmac5 (*7*) and manually adjusted by Coot (*8*). The apo-structure was refined using isotropic B factors, with tight non-crystallographic restraints applied between the two monomers for the whole of the refinement process. The holo-structure was refined with anisotropic B factors, with TLS refinement used in the later rounds of refinement. Waters were added and checked using Coot. Structure quality was checked using the tools with Molprobity (*9*). The final model statistics are shown in table 1, section 2.4.1.

4.2.9.3 L-serine External Aldimine

Crystallisation trials were set up in sitting drop plates (EasyXtal DG-CrystalSupport, Qiagen). Holo-SPT crystals grew in a 2 µl drop, consisting of 1 µl of 20 mg/ml SPT (in 10

mM Tris pH 7.5, 150 mM NaCl and 25 μM PLP and 1 μl of well solution (22% PEG 3350, 100 mM HEPES pH 6.5, 120 mM $MgCl_2$). A single holo-SPT crystal was soaked for 10 minutes at room temperature in 22% PEG3350, 120 mM $MgCl_2$, 100 mM HEPES pH6.5 containing 5mM serine before being mounted in a cryo-loop and cryo-protected in 22% PEG3350, 120 mM $MgCl_2$, 100 mM HEPES pH6.5, 20% PEG400. The crystal was frozen and shipped to the ESRF where a 1.5 Å dataset was collected on beamline ID23-2 (wavelength=0.873Å) at 100 K.

4.2.9.4 SPT and L-cycloserine

A 10 mM stock solution of L-cycloserine was prepared. This was added to holo-SPT (20 μM) to a final concentration of 1 mM. After incubation overnight at 4 °C, the protein was concentrated to 20 mg/ml and this solution was used in co-crystallisation experiments. SPT-L-cycloserine crystals grew from a 2 μl drop, consisting of 1 μl of 20 mg/ml SPT/L-cycloserine (in 10 mM Tris pH 7.5, 150 mM NaCl and 25 μM PLP) and 1 μl of well solution (100 mM HEPES pH 6.5, 110 mM $MgCl_2$, 21.5% PEG 3350). A single, colourless crystal was mounted in a cryo-loop and cryo-protected in 22% PEG3350, 120 mM $MgCl_2$, 100 mM HEPES pH6.5, 20% PEG400. The crystal was frozen and shipped to the ESRF where a 1.45 Å dataset was collected on beamline ID14-1 (wavelength=0.934 Å) at 100 K.

(1) Longtine, M., A, Mckenzie, DJ, Demarini, NG, Shah, A, Wach, A, Brachat, P, Philippsen P., and Pringle J. R., (1998) Additional molecules for versatile and economical PCR-based gene deletion and modification in *S. cerevisiae*. *Yeast 14*, 953-961.

(2) (1994) The CCP4 suite: programs for protein crystallography. *Acta Crystallogr D Biol Crystallogr 50*, 760-3.

(3) Segelke, B. W. (2001) Efficiency Analysis of Screening Protocols Used in Protein Crystallization. . *J. Crystal Growth*, 553-562.

(4) Storoni, L. C., McCoy, A. J., and Read, R. J., (2004) Likelihood-enhanced fast rotation functions. *Acta Crystallogr D Biol Crystallogr 60*, 432-8.

(5) McCoy, A. J., Grosse-Kunstleve, R. W., Storoni, L. C., and Read, R. J., (2005) Likelihood-enhanced fast translation functions. *Acta Crystallogr D Biol Crystallogr 61*, 458-64.

(6) Morris, R. J., Perrakis, A. and Lamzin, V. S. (2002) ARP/wARP's modelbuilding algorithms. I. The main chain. . *Acta Cryst. D.*, 432-438.

(7) Murshudov, G. N., Vagin, A. A., Lebedev, A., Wilson, K. S., and Dodson, E. J., (1990) Efficient anisotropic refinement of macromolecular structures using FFT. *Acta Crystallographica Section D-Biological Crystallography.*, 247-255.

(8) Emsley, P., and Cowtan K., (2004) Coot: model-building tools for molecular graphics. *Acta Crystallographica Section D 60*, 2126-2132.

(9) Davis, I. W., Murray, L. W., Richardson, J. S. and Richardson, D. C., (2004) MOLPROBITY: structure validation and all-atom contact analysis for nucleic acids and their complexes. *Nucleic Acids Res.*, W615-619.

Chapter 5: Conclusions and Future Work

The high-resolution structural information produced from these studies will facilitate a more detailed investigation into the mechanism and inhibition of SPT.

The holo-SPT and L-serine external aldimine structures, presented in this thesis, are the first to be solved of a SPT from any organism. In addition to the crystal structures, bioinformatic analysis of bacterial and human SPT have not only provided insights into enzyme function but have also shown how mutations may affect enzyme behaviour e.g. mutations associated with hereditary sensory and autonomic neuropathy type I (HSAN1).

Mutations of human SPT (C133W, C133Y and V144D) have been shown to directly affect enzyme activity and cause a range of neuropathological defects leading to the condition HSAN1. Since *S. paucimobilis* SPT shows sufficient sequence conservation with human SPT, it has allowed us, in collaboration with the SSPF St. Andrews, to generate homology models of the human SPT1/SPT2 heterodimer. This has facilitated the analysis of how mutations of SPT may be involved in the pathology of HSAN1 (see section 2.5) ***(4)***.
Two *S. paucimobilis* SPT N100W and N100Y mutants were obtained shortly after conclusion of these studies. The high-resolution crystal structures of both mutants have been determined, in collaboration with the SSPF, St. Andrews (Dr K Johnson and Marine Raman) and both appear to have impaired L-serine binding efficiencies. However, further kinetic and structural analyses are essential in order to provide details of how these mutations affect SPT activity.

In addition to holo-SPT and the L-serine external aldimine, the crystal structure of L-cycloserine inhibited SPT provides a basis for the further analysis of inhibition. To date, although mechanisms for the cycloserine inhibition of PLP-dependent enzymes are hypothesised in many publications, no specific mechanism has been determined (*13-16, 22,*

23). The results shown in this thesis appear to agree with the mechanism proposed by Ikushiro *et al.* (*3*). However, mass spectrometry analysis is required to determine the intermediates formed during the L-cycloserine inhibition of SPT and, together with further biochemical and crystallographic experiments, should provide a detailed mechanism of inhibition.

After numerous attempts to obtain soluble Aur1p, insertion of the *AUR1* gene into the expression vector pYES2/CT (Invitrogen) was successful. The pYES2/CT/*AUR1-C* construct allowed the (galactose induced) over-expression of a C-terminal histidine tagged Aur1-C-His_6 protein which could be purified in one step, by Ni-NTA chromatography.

Unfortunately, time did not permit further optimisation of the purification protocol for Aur1-C-His_6. As the yield of protein from 10 litres of *S. cerevisiae* cell culture was significantly low (could not be detected by colloidal coomassie staining), production of a higher cell mass, by fermentation, would have been advantageous at this point. It is hoped that purification of Aur1-C-His_6 from a larger volume of *S. cerevisiae* cell culture would provide sufficient protein for identification by Coomassie staining and mass spectrometry. Alternatively, future work focusing on the screening of a range of detergents, in order to increase the amount of soluble material isolated would also be beneficial.

Biochemical and kinetic analysis of substrate binding are also important considerations. The availability of fluorescently labelled ceramide substrates, such as C_6NBD and C_{12}NBD-ceramide, will enable the production of fluorescently labelled inositol phosphorylceramide to be monitored.

The successful cloning, over-expression, purification and detection procedures from these studies (section 3.3) may now be applied to the *AUR1* gene from the fungal pathogen *B. cinerea* in order to isolate and characterise this important target enzyme.

To date, there is no data to suggest that the over-production of a soluble, histidine tagged Aur1p has been achieved. In addition, no biochemical analysis can be found on recombinant Aur1p-His_6. Therefore, the results reported in this thesis, may facilitate the progression of this field toward obtaining biochemical, and possibly structural, information about this important fungicidal target.

Appendix 1: PostgraduateStudent Training Record

1. PERSONAL DETAILS

Name	Beverley Yard
Date of Registration	01/09/2004
Sources of Funding	University of Edinburgh/Syngenta
Universities Attended	St Andrews University
Qualifications and Dates	BSc Honours (2.1) Cell Biology and Pathology, May 2004
Ph.D. Supervisors	Dr D Campopiano and Prof. R Baxter
Field of Study	Chemical Biology

2. TRAINING

2.1 Biophysical Postgraduate Student Seminar Programmes Attended 2004-2007

2.2 Oral Presentations to Biophysical Section

1st year: Isolation and characterisation of enzymes involved in sphingolipid biosynthesis, 15 mins. 2nd year: Essential enzymes of sphingolipid biosynthesis, 20 mins. 3rd year "chalk and talk": The Structure of Serine Palmitoyltransferase, 30 mins, Final 3rd talk Firbush: Serine Palmitoyltransferase: Gateway to sphingolipid biosynthesis, 45 minutes.

2.3 Demonstrating Duties

1st year; Biological Chemistry 1 ~45 hours, 2nd year; Biological Chemistry 1 ~72 hours, 3rd year; Biological Chemistry 1 ~45 hours and CLS2 ~20 hours

2.4 Delegated Assistant in the Supervision of Specified Honours Project Student(s)

Peter; BSc Hons student, 20 hours/week (10 weeks), Natalia; Masters student, 25 hours/week (16 weeks), Anna; Masters student, 20 hours/week (~6 weeks), Daniel; summer student, 35 hours/week (8 weeks), Scott; BScHons student 20 hours/week (16 weeks), Alex; Masters student, 15 hours/week (~3 weeks).

2.5 Training Undertaken in Safety

General safety, Fire safety, GMO safety, Radiation Protection

2.6 Conferences Attended and Work Presented

Poster presentation at the CASE students day; Syngenta (1 day, 2004), attended the RSc Chemistry and Biology of Natural Product Biosynthesis; University of Bristol, (2005, 1 day), attended the GE Healthcare Challenging Proteins European Workshop; Paris (Oct 17-18th 2005), attended the 158th SGM Meeting; University of Warwick (3-4th April 2006), attended the 6th Annual CID symposium; University of Edinburgh (16th May 2006), won prize for best oral contribution titled "Serine palmitoyltransferase: Gateway to sphingolipid biosynthesis at the RSc BOG meeting; University of Manchester (18th Dec 2006), poster presentation at the 159th annual SGM meeting; University of Manchester (26th-29th March 2007), oral presentation at the RSc Chemistry and Biology of Natural Product Biosynthesis III Meeting; University of Bristol (20th June), poster presentation at the Protein Society Meeting "Proteins form Birth to Death", Boston MA (21-25th June 2007).

2.7 Other Relevant Training Activities

I was granted beam-time on ID14-2 at the European Synchrotron Radiation Facility, Grenoble. I was shown how to collect data and use the "microspec" equipment which was set up on the beam-line. This equipment was only available for use 4 times throughout the year therefore this was an invaluable experience.

Appendix 2: The Structure of Serine Palmitoyltransferase: Gateway to Sphingolipid Biosynthesis

doi:10.1016/j.jmb.2007.04.086 J. Mol. Biol. (2007) 370, 870–886

JMB

Available online at www.sciencedirect.com

ScienceDirect

ELSEVIER

The Structure of Serine Palmitoyltransferase; Gateway to Sphingolipid Biosynthesis

Beverley A. Yard[1]†, Lester G. Carter[2]†, Kenneth A. Johnson[2] Ian M. Overton[3], Mark Dorward[2], Huanting Liu[2], Stephen A. McMahon[2] Muse Oke[2], Daphné Puech[2], Geoffrey J. Barton[3] James H. Naismith[2] and Dominic J. Campopiano[1]*

[1]*School of Chemistry EaStCHEM, The University of Edinburgh, West Mains Road Edinburgh, EH9 3JJ Scotland, UK*

[2]*Centre for Biomolecular Sciences, Scottish Structural Proteomics Facility The University of St. Andrews Fife KY16 9ST, Scotland, UK*

[3]*School of Life Sciences Research University of Dundee Dow Street, Dundee DD1 5EH, Scotland, UK*

**Corresponding author*

Sphingolipid biosynthesis commences with the condensation of L-serine and palmitoyl-CoA to produce 3-ketodihydrosphingosine (KDS). This reaction is catalysed by the PLP-dependent enzyme serine palmitoyltransferase (SPT; EC 2.3.1.50), which is a membrane-bound heterodimer (SPT1/SPT2) in eukaryotes such as humans and yeast and a cytoplasmic homodimer in the Gram-negative bacterium *Sphingomonas paucimobilis*. Unusually, the outer membrane of *S. paucimobilis* contains glycosphingolipid (GSL) instead of lipopolysaccharide (LPS), and SPT catalyses the first step of the GSL biosynthetic pathway in this organism. We report here the crystal structure of the holo-form of *S. paucimobilis* SPT at 1.3 Å resolution. The enzyme is a symmetrical homodimer with two active sites and a monomeric tertiary structure consisting of three domains. The PLP cofactor is bound covalently to a lysine residue (Lys265) as an internal aldimine/Schiff base and the active site is composed of residues from both subunits, located at the bottom of a deep cleft. Models of the human SPT1/SPT2 heterodimer were generated from the bacterial structure by bioinformatics analysis. Mutations in the human SPT1-encoding subunit have been shown to cause a neuropathological disease known as hereditary sensory and autonomic neuropathy type I (HSAN1). Our models provide an understanding of how these mutations may affect the activity of the enzyme.

Keywords: serine palmitoyltransferase; sphingolipids; X-ray crystallography; bioinformatics; hereditary sensory and autonomic neuropathy type I

Introduction

Sphingolipids are essential components of eukaryotic cells where they play important roles in intracellular signalling and in membrane structure.[1–4] All sphingolipids are composed of a long-chain base (LCB), a fatty acid and à polar head group. The sphingoid bases (containing 1,3-dihydroxy-2-aminoalkane and its derivatives) were first isolated by Thudichum who characterised the brain alkaloid "sphingosin" over a century ago.[5] The chemical structure of the family of sphingolipids was subsequently characterised by Carter and colleagues over five decades later.[6] Serine palmitoyltransferase (SPT; EC 2.3.1.50) catalyses the first and rate-limiting step of the sphingolipid biosynthetic pathway in all organisms studied to date.[7] This reaction is a

† B.A.Y. and L.G.C. contributed equally to this work.

Abbreviations used: ALAS, 5-aminolevulinate synthase; AONS, 8-amino-7-oxononanoate synthase; AOS, α-oxoamine synthase; CoA, coenzyme A; GSL, glycosphingolipid; HSAN1, hereditary sensory and autonomic neuropathy type I; KBL, 2-amino-3-ketobutyrate CoA ligase; KDS, 3-ketodihydrosphingosine; LCB, long-chain base; LPS, lipopolysaccharide; PLP, pyridoxal 5′-phosphate; RMSD, root-mean-square deviation; SPT, serine palmitoyltransferase.

E-mail address of the corresponding author: Dominic.Campopiano@ed.ac.uk

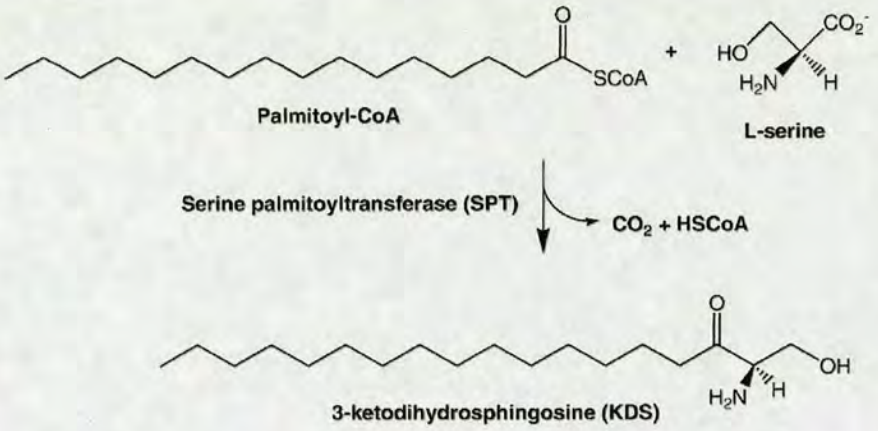

Figure 1. The reaction catalysed by serine palmitoyltransferase (SPT).

pyridoxal 5′-phosphate (PLP)-dependent, decarboxylative, Claisen condensation of the amino acid L-serine and the long-chain (C16) fatty acid palmitoyl-CoA, which produces the sphingolipid precursor, 3-ketodihydrosphingosine (KDS; Figure 1).

SPT belongs to the small family of enzymes called the α-oxoamine synthases (AOS) which catalyse the condensation of specific amino acid and acyl-CoA thioester substrates.[8] This family is classified under the larger α-division, fold type I enzymes within the PLP-dependent enzyme superfamily.[9,10] Other members of this family include; 8-amino-7-oxononanoate synthase (AONS)[11,12] from the biotin biosynthetic pathway, 5-aminolevulinate synthase (ALAS)[13–15] which catalyses the first step in tetrapyrrole biosynthesis and 2-amino-3-ketobutyrate CoA ligase (KBL)[16] involved in threonine metabolism. A consensus catalytic mechanism has emerged for those enzymes catalysing the decarboxylation of an amino acid substrate (SPT, AONS and ALAS) (Figure 2).[7,12,17–20] Briefly, the catalytic pathway is comprised of the following steps: formation of an external aldimine *via* displacement of the lysine-PLP internal aldimine (holo-SPT) by the incoming amino acid substrate; formation of a quinonoid intermediate by abstraction of the α-proton from the PLP-amino acid external aldimine; a Claisen condensation with the fatty acid-CoA substrate followed by displacement of the CoA to form a β-ketoacid; decarboxylation of this species to form a product quinonoid; protonation of this quinonoid to form the product external aldimine and finally release of the α-oxoamine product and regeneration of the enzyme PLP-internal aldimine. The factors governing differences in substrate specificity that distinguish each member within the family have still to be resolved.

Early studies of sphingolipid biosynthesis in eukaryotes revealed serine palmitoyltransferase activity in rat liver and yeast extracts.[21,22] Eukaryotic SPT is located in the endoplasmic reticulum (ER) and consists of at least two heterologous monomer subunits, long chain base 1 and 2 (LCB1/LCB2, also known as SPT1 and SPT2, respectively), encoded by separate genes (*lcb*1 and *lcb*2).[21,23–25] Sequence analysis of the encoded *Saccharomyces cerevisiae* SPT1 and SPT2 subunits revealed that SPT2 contains an active site lysine residue required for PLP-binding which is conserved amongst other members of the AOS family. In contrast, SPT1 lacks this lysine (and other key residues) and it has been suggested that it plays a regulatory role in the SPT dimer.[21,24] Both of these subunits are essential to produce the functionally active, heterodimeric SPT; however, both are membrane-associated and this has made their isolation and characterisation particularly challenging. Nevertheless, small amounts of active SPT have been isolated from yeast and mammalian cells.[26–30] Curiously, a small protein, of unknown activity (Tsc3p) has been shown to be required for optimal SPT activity in *S. cerevisiae*; however, a homologous protein has yet to be identified in other species.[31]

Despite the apparent non-catalytic role of SPT1 within the mammalian heterodimer, it has been shown that single amino acid mutations within a highly conserved region of this subunit down-regulate SPT activity leading to the condition known as hereditary sensory and autonomic neuropathy type I (HSAN1).[32,33] Analysis of HSAN1 patients has revealed two mutational hotspots in SPT1 at Cys133 (C133W or C133Y) and Val144 (V144D). Corresponding mutations in the SPT1 subunit of *S. cerevisiae* cause reduced SPT activity, though they do not affect the ability of the SPT1 mutant to dimerise with SPT2.[26]

Topological studies of the eukaryotic SPT1 subunit from Chinese hamster ovary (CHO) cells identified a single non-essential, membrane-spanning, N-terminal domain. In comparison, SPT1 from *S. cerevisiae* has two additional membrane-spanning domains near to the predicted PLP-binding region of the protein which, when deleted, affected membrane binding and SPT activity.[27,34] In order to overcome the solubility problems encountered with membrane-associated SPTs, Ikushiro *et al.* isolated a water soluble, homodimeric form of the enzyme from the Gram-negative, aerobic bacteria

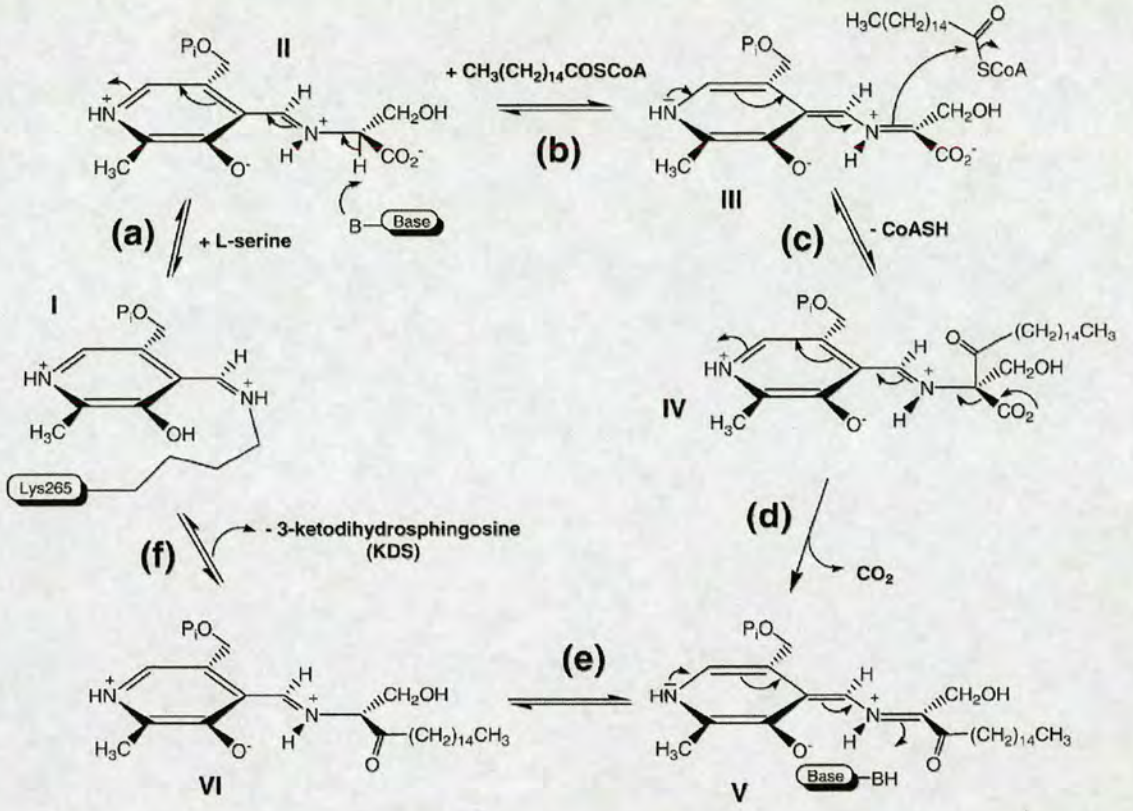

Figure 2. Proposed reaction mechanism of SPT. (a) Transaldimination of internal aldimine (holo-SPT), **I** with L-serine to form external aldimine, **II**; (b) deprotonation of C^{α} by base to form quinonoid, **III**; (c) Claisen condensation to form putative β-ketoacid-aldimine complex, **IV**; (d) decarboxylation to form product quinonoid, **V**; (e) reprotonation of quinonoid to form product external aldimine, **VI** (f) release of product 3-ketodihydrosphingosine (KDS) and regeneration of **I**.

Sphingomonas paucimobilis EY2395.[35,36] This organism possesses an unusual feature, its outer membrane is composed solely of glycosphingolipids (GSLs) whereas most other Gram-negative bacteria have lipopolysaccharides (LPS, also known as endotoxins) in their outer leaflets.[37] Currently, there is no high-resolution structural information available for a SPT from any organism. Here, we present the crystal structure the holo-form of *S. paucimobilis* SPT. The holo-SPT structure reported here is the first high-resolution structure of an enzyme from the sphingolipid biosynthetic pathway.

Results and Discussion

Purification and characterisation

S. paucimobilis SPT was expressed in *Escherichia coli* from plasmid pET-28a as a six-histidine, C-terminal fusion (a corresponding N-terminal, six-histidine fusion was unsuitable for structural studies; data not shown). A rapid, two-step purification procedure using immobilised nickel affinity and size-exclusion chromatography was carried out. This enabled the isolation of milligram amounts of both the apo and holo-forms of the enzyme. Increased amounts of the holo-form were obtained by incubation of the predominantly apo-form with excess PLP. The purified holo-enzyme was dimeric in solution (based on size-exclusion chromatography and native gel electrophoresis; data not shown) and its UV-visible spectrum showed characteristic peaks at 336 nm and 425 nm which correspond to the enolimine and ketoenamine forms of the PLP-bound enzyme, respectively (Figure 3(a)).[8] The recombinant holo-SPT was active in the conversion of serine and palmitoyl-CoA to form KDS (Figure 3(b)) and displayed similar catalytic properties to those reported previously (data not shown).[36] Electrospray ionisation mass spectrometry (ESI-MS) analysis gave a molecular mass consistent with the predicted mass of recombinant *S. paucimobilis* SPT from the gene sequence. This takes into account loss of the N-terminal methionine residue and the addition of the C-terminal histidine affinity tag.

Structures of *S. paucimobilis* SPT

Our discussion focuses on the higher-resolution holo-enzyme structure. The first 20 N-terminal amino acids and the last nine C-terminal residues,

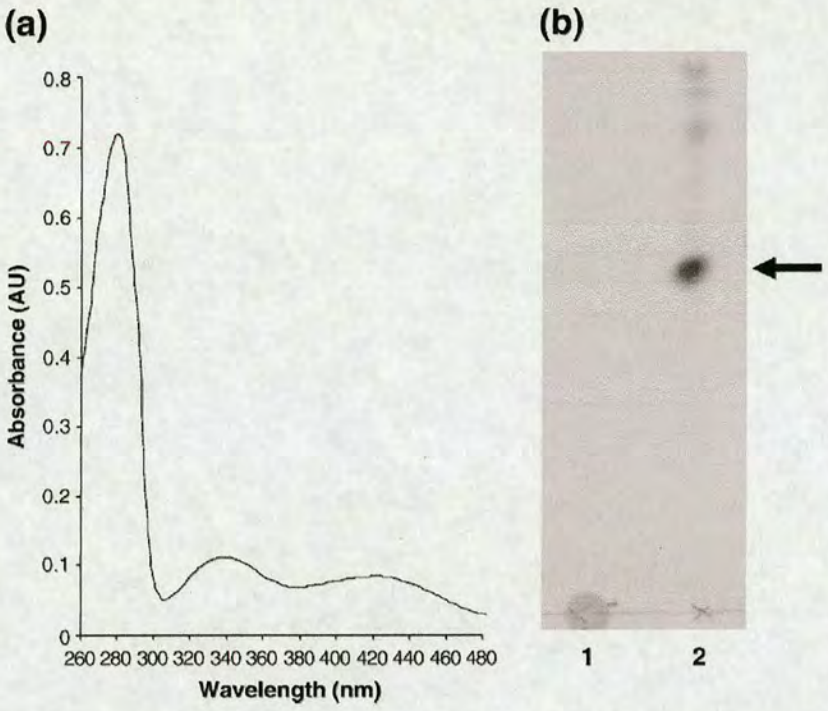

Figure 3. (a) UV-visible spectrum of SPT used in this study. Purified SPT (20 μM) shows the characteristic peaks for the PLP-bound (holo-) internal aldimine form of the enzyme with absorbance maxima at 336 nm and 425 nm. (b) Autoradiograph showing SPT is active in the conversion of L-serine and palmitoyl-CoA to 3-ketodihydrosphingosine (KDS). Recombinant holo-SPT was incubated with (U-^{14}C)- labelled L-serine and palmitoyl-CoA for 20 min at 37 °C and the assay was extracted with an equal volume of chloroform/methanol (2:1, v/v). The aqueous (1) and organic (2) phases were analysed by TLC and compared with authentic standards. The arrow marks the position of the product KDS.

including the histidine tag, are not visible and therefore our final model contains 391 of the 427 amino acids from Arg22 to Ile419 inclusive. The 1.3 Å map is of a high quality and the cofactor is clearly defined (Supplementary Data). The monomer of the holo-SPT form consists of three domains (N-terminal, central catalytic and C-terminal) and is shown in Figure 4. The overall topology of SPT

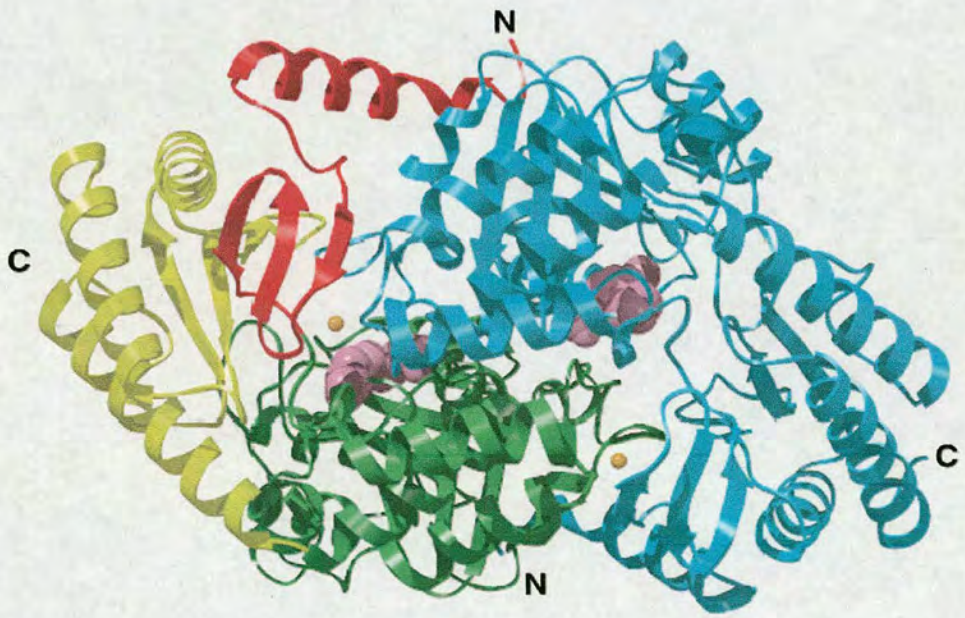

Figure 4. Overall structure of the holo SPT homodimer. One monomer is coloured with the N-terminal domain shown in red, the central catalytic domain in green, and the C-terminal domain in yellow. The second subunit is shown in blue and the N and C terminii are labelled. The PLP in each monomer is shown as a purple space-fill and magnesium ions are shown in orange. This Figure was produced using Chimera.[66]

closely resembles that observed for structures of the other members of the α-oxoamine synthase (AOS) family; ALAS (PDB code 2BWN), KBL (PDB code 1FC4) and AONS (PDB code 1DJE) (Figure 5). The C^{α} RMSD values for SPT relative to these structures are 1.5 Å over 372 residues with ALAS, 1.4 Å over 364 residues with KBL and 1.6 Å over 357 residues with AONS. All of the structures have the same relative orientation of domains, the most obvious differences are in the orientation of the N-terminal helix and the position of loops connecting secondary structural elements remote from the active site. The N-terminal domain of ~80 residues comprises an α-helix followed by a three-stranded, antiparallel β-sheet. This is linked to a larger central catalytic domain composed of a seven-stranded, mainly parallel, β-sheet domain of ~200 residues where the active site lysine (Lys265) resides. The C-terminal domain comprises ~100 amino acid residues which make many interactions with residues of the N-terminal domain.

In common with the other members of the PLP-dependent superfamily, bacterial SPT is an intimate, interlocked, dimer (Figure 4). In the holo-SPT structure the dimer is produced by applying -X,Y,-Z+1/2 crystallographic symmetry of the $C222_1$ space group to the monomer in the asymmetric unit. The buried interface area (composed of residues from the central domain of one monomer and the N-terminal domain of the other) is 3880 $Å^2$

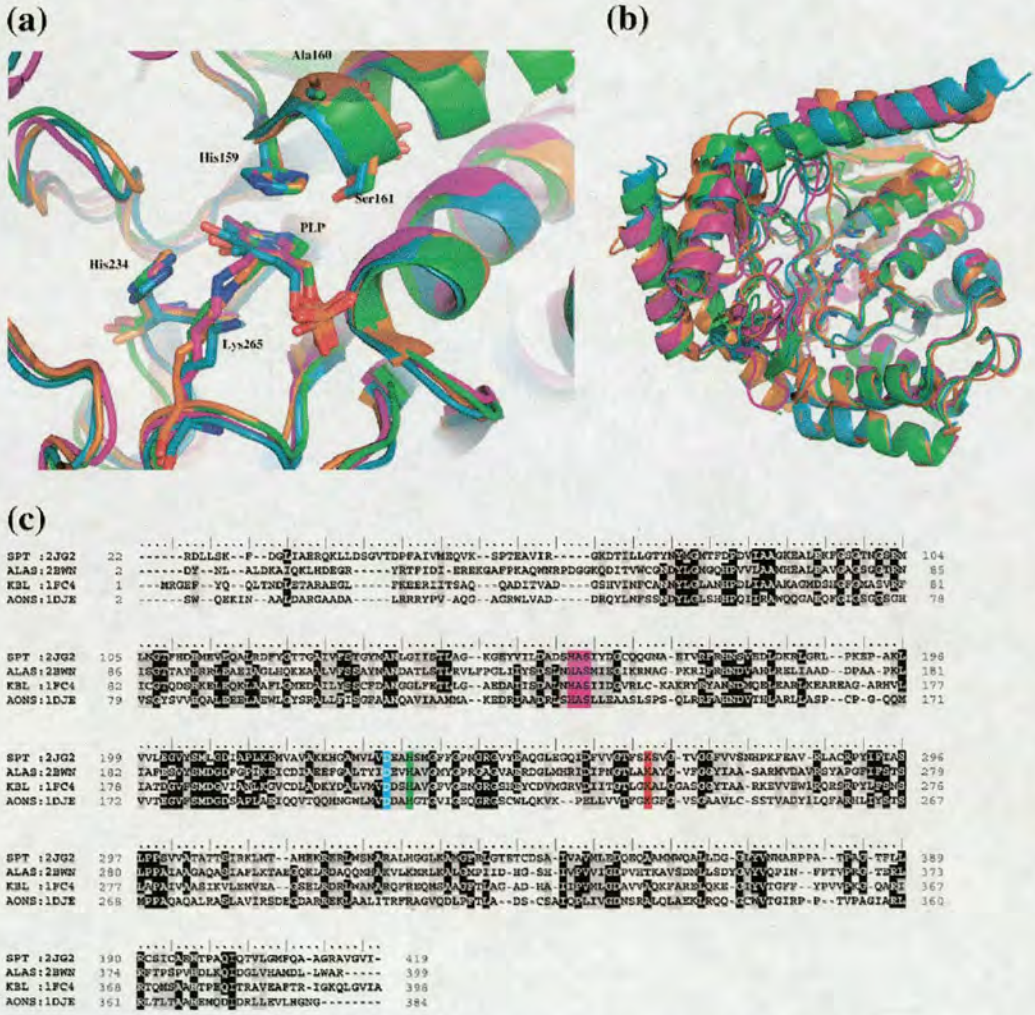

Figure 5. Structural alignment of the members of the AOS family. (a) Overlay of key conserved residues involved in cofactor binding: His234, His159, Ala160, Ser161, and Lys265 (SPT numbering). The SPT (2JG2) structure is shown in green, the AONS (1DJE) is shown in orange, the ALAS (2BWN) structure is shown in purple, and the KBL (1FC4) structure is shown in blue. (b) An overall alignment of the monomers (same colouring scheme as in (a)). (c) The structure-based sequence alignment of these four enzymes. The conserved (His, Ala, Ser) motif is shown in pink, the conserved residue Asp231 which interacts with N1 of PLP in turquoise, the conserved His involved in PLP binding is highlighted in green, and the conserved active site Lys residue is shown in red.

per monomer, which is approximately 22% of the monomer surface area.

The active site

In the holo-SPT structure the PLP cofactor is bound to Lys265 as an internal aldimine (Schiff base). Although all PLP-dependent enzymes require formation of an imine *via* a conserved lysine, the PLP binding sites are varied with respect to the surrounding protein environment.[38] In SPT, the PLP makes polar contacts with the side-chains of Asn138, Asp231, His234 and Thr262 and with the main-chain of Gly134 and Tyr135 (Figure 6). We also observe His159 stacking above one face of the pyridinium ring of PLP (Figure 7). This residue is located at the beginning of a three-residue motif (His159, Ala160, Ser161) that is strictly conserved throughout the AOS family (Figure 5(c)). The cofactor binding site is composed of residues from both monomers. Importantly, the side-chain of Asn100 from monomer B is in close proximity to the backbone of Lys265 from monomer A (Figure 7). This provides an example of the inherent dimeric nature of the functional enzyme and also gives insight into how mutations in the human "non-catalytic" SPT1 subunit may influence the activity of the heterodimer.

Other residues which interact with the cofactor are clearly observed; the pyridinium nitrogen atom (N1) and the oxygen atom of Asp231 are 2.8 Å apart, suggesting that this carboxylic acid group may stabilise a protonated pyridinium form of the PLP by salt bridge formation.[39] This acidic residue is conserved throughout the family (Figure 5(c)) and a similar salt bridge has been observed between the N1 of PLP and the Asp204 residue of *E. coli* AONS, the Asp214 of *Rhodobacter capsulatus* ALAS and the Asp210 of *E. coli* KBL.[11,15,16]

Since we were unable to obtain a complex of SPT with palmitoyl-CoA, we used the structure of the *R. capsulatus* ALAS/PLP-external aldimine/succinyl-CoA complex to predict potential binding sites (PDB code 2BWO).[15] In the ALAS structure the density corresponding to the adenine part of the succinyl-CoA is well defined, and the base is bound within a hydrophobic pocket formed by a group of isoleucine residues on the surface of the enzyme. The adenine also makes a number of H-bond contacts with serine side-chains and the 3′-phosphoribose moiety interacts with a lysine residue. Density for the phosphopantethene arm of CoA was not observed in the ALAS structure but the carboxylate of the succinate makes contact with Arg21. A similar salt-bridge interaction was previously observed in the AONS/AON external aldimine structure where the AON carboxylate interacts directly with the Arg21 residue of the product AON.[12] We used this information to superimpose the holo-SPT structure onto the ALAS

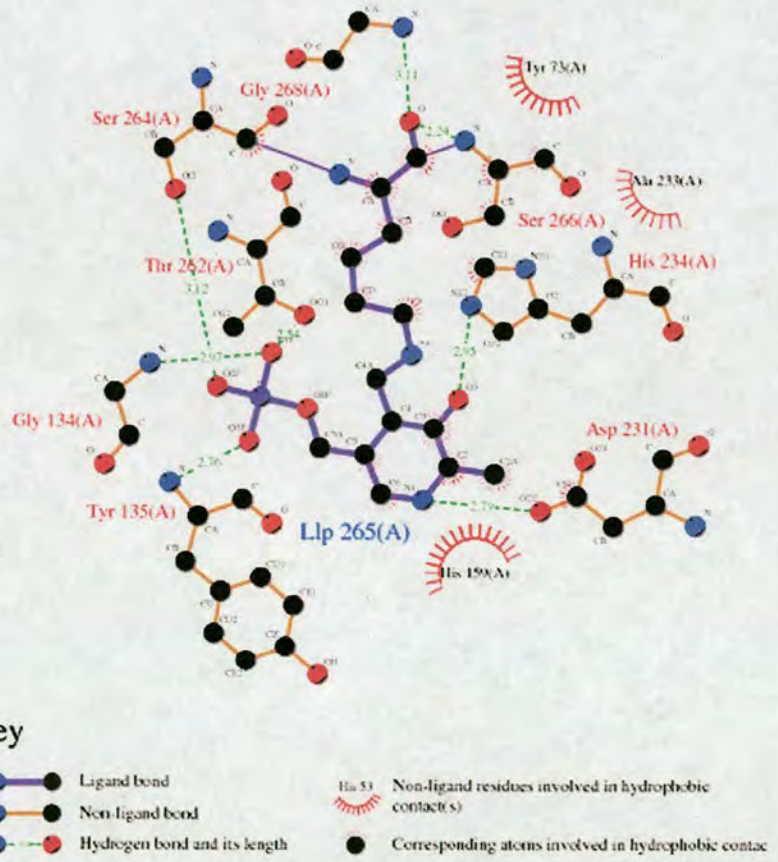

Figure 6. A Ligplot representation of the PLP binding site showing the constellation of residues involved in cofactor binding. Llp265 refers to the PLP cofactor covalently bound to the active site residue Lys265. (A) represents residues from monomer A.

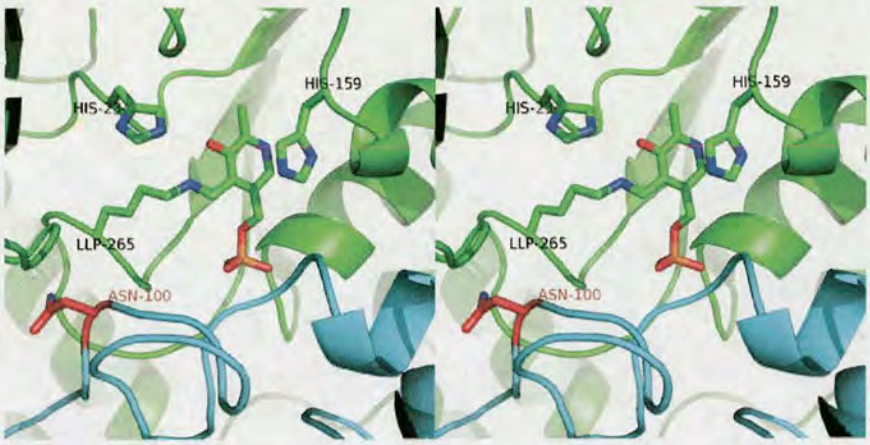

Figure 7. Stereo view showing the proximity of the Asn100 residue of monomer B to the PLP cofactor of monomer A in the *S. paucimobilis* SPT homodimer. Monomer A is drawn in green and monomer B is drawn in blue. Asn100 of monomer B is shown in CPK. Using the sequence alignment in Figure 9, the *S. paucimobilis* SPT Asn100 residue maps to residue Cys133 on the SPT1 subunit of human SPT. Mutations at this residue C133W and C133Y are known to cause the autosomal disease hereditary sensory and autonomic neuropathy type I (HSAN1). The conserved residues His159 and His234 which interact directly with the PLP cofactor are also highlighted.

structure in an attempt to define a palmitoyl-CoA binding site. Two long hydrophobic channels where the C16 palmitic acid chain could reside are illustrated in Figure 8. Since palmitoyl-CoA lacks a terminal carboxylate, SPT is devoid of a salt-bridge anchor, which would delineate the end of either channel.

The cofactor binding site

The high resolution of the holo-SPT structure has provided an insight into the relative juxtaposition of the planar PLP ring with the imine bond which links it to Lys265 (see Supplementary Data). PLP-dependent enzymes catalyse a variety of reactions and the stereoelectronic control of the reactivity of the cofactor was proposed by Dunathan.[40] This "Dunathan hypothesis" requires the imine and PLP ring to be co-planar and suggests that rotation about the α-carbon to nitrogen bond in the external aldimine form of the enzyme controls which bond is activated towards cleavage. The bond to be broken is therefore placed perpendicular to the PLP ring. In the SPT mechanism, this would be the C^{α}-H of the serine-PLP external aldimine (intermediate II; Figure 2). The nature of the protonation state of the imine nitrogen (NZ) and PLP oxygen are also thought to influence the rate of catalysis.[8,38] In the crystal structure of holo-SPT reported here, we note that the PLP ring is not co-planar with the imine (offset by 47°, around C3-C4-C4′-NZ), suggesting that the oxygen of the PLP is protonated (intermediate I; Figure 2). Further evidence for this comes from the observation of additional density at this oxygen. We attribute this to a water molecule H-bonded to the O-H. This water molecule is surrounded by a network of others and may be displaced upon binding of serine and formation of the external aldimine. This phenomenon was also observed in the structure of the alanine racemase from *Mycobacterium tuberculosis*.[41] It is known that large conformational changes occur during the catalytic cycle of the enzymes from the AOS family thus enabling them to control the bond breaking and forming steps.[11,12,15]

Structural impact of human HSAN1 mutations

A number of human diseases have been discovered that are caused by defects in sphingolipid catabolism. The hereditary sensory and autonomic neuropathies (HSAN) are a clinically and genetically heterogeneous group of disorders, which are currently classified into five types.[42] HSAN type I (HSAN1) is an autosomal dominant (AD) neuropathy characterised by marked sensory impairment and degeneration of peripheral nerves. The HSAN1 locus was mapped using genetic linkage analysis to human chromosome 9 (9q22.1–q22.3), specifically to missense mutations in the *lcb1* gene of SPT.[32] Analysis of a number of HSAN1 patients has revealed several mutations of the SPT1 subunit: C133W, C133Y, V144D and G387A. These mutations confer dominant negative effects on SPT activity, resulting in down-regulation of sphingolipid synthesis.[43,44]

A recent study used a transgenic mouse model containing the SPT1 C133W mutation to investigate its impact on SPT activity and resulting molecular pathophysiology. Mice expressing the C133W mutation had impaired activity confirming that this mutation dominantly inhibits the SPT enzyme *in vivo*. These mice developed mild sensory and motor deficiency by ten months of age and also displayed myelin thinning and morphological changes of the root ganglia.[44] Surprisingly, the authors noted that although the composition of the ceramide pool was altered, the total ceramide levels in these mice were unaffected. This suggests a compensatory mechanism may be present which regulates cellular ceramide production. The role played by these SPT1 mutations in HSAN1 remain unclear; however, they

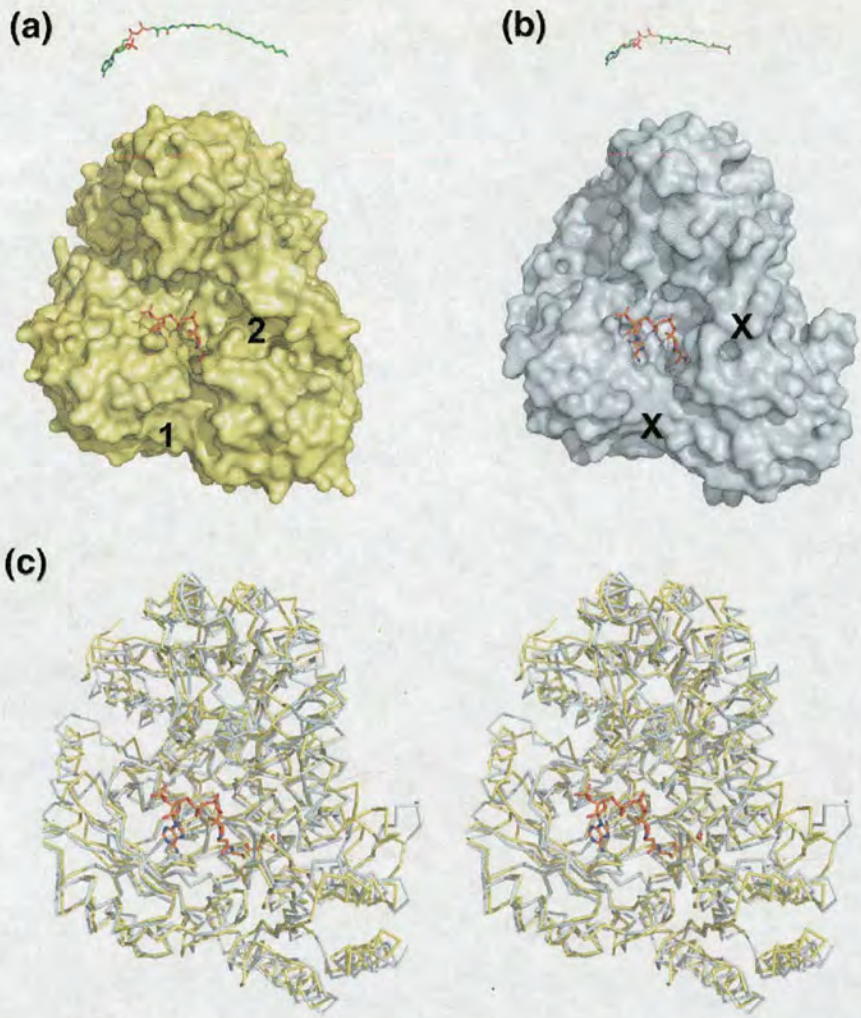

Figure 8. Analysis of coenzyme A thioester binding. (a) In yellow a space-fill of the structure of the *S. paucimobilis* SPT structure aligned to the ALAS structure (PDB code 2BWO; RMSD 2.2 Å), and with the ALAS succinyl-CoA substrate shown in ball and stick. Above the SPT structure the true substrate palmitoyl-CoA is shown, with the fatty acid thioester bond of CoA highlighted. The two putative channels where the additional carbons of the SPT substrate palmitoyl-CoA may bind are labelled 1 and 2. (b) The ALAS structure and the location of succinyl-CoA binding site (succinyl-CoA is also shown above the structure, allowing the relative lengths of the two CoA substrates to be appreciated). The positions of the channels, which are absent in ALAS are highlighted with crosses. (c) A stereo view of the alignment of the ALAS and SPT structures as wireframes, displaying how channel 2 is foreshortened in the ALAS structure, by a rearrangement of the first helix (circled), possibly leading to specificity for the shorter succinyl-CoA substrate.

may lead to toxic accumulation of misfolded proteins which is a mechanism commonly associated with neurodegenerative diseases.

To examine the possible structural impacts of human SPT1 mutations we have used our *S. paucimobilis* SPT structure to model the human SPT1/SPT2 dimer. BLAST alignment[45] of *S. paucimobilis* SPT to human SPT1 and SPT2 finds pairwise percentage identities of 28% and 32%, respectively. The alignment of SPT1 and *S. paucimobilis* SPT maps SPT1 residues Cys133, Val144, and Gly387 to *S. paucimobilis* SPT residues Asn100, Asp111 and Thr342, respectively (Figure 9). Mapping of the SPT active site residues to SPT1 and SPT2 is shown in Table 1. It is notable that many of the SPT1 active site residues are markedly different to the bacterial and SPT2 residues, indicating substantial degradation of the ancestral active site formed within the SPT1 subunit. Homology models for the human SPT1/SPT2 heterodimer "wild-type" (WT) and incorporating the mutated SPT1 residues C133W, V144D and G387A were built using the structure of the *S. paucimobilis* holo-SPT as a template. The WT model is generally similar to the bacterial holoenzyme structure; STAMP[46] alignment of the bacterial monomer to SPT1 of the WT model finds a mean C^{α} RMSD of 0.52 Å over 352 residues.

Figure 10 shows modelled snapshots of the molecular mechanisms by which the mutations C133W and V144D may affect the SPT1/SPT2 structure and provide insights into how mutations in the "inactive" SPT1 subunit have a dominant

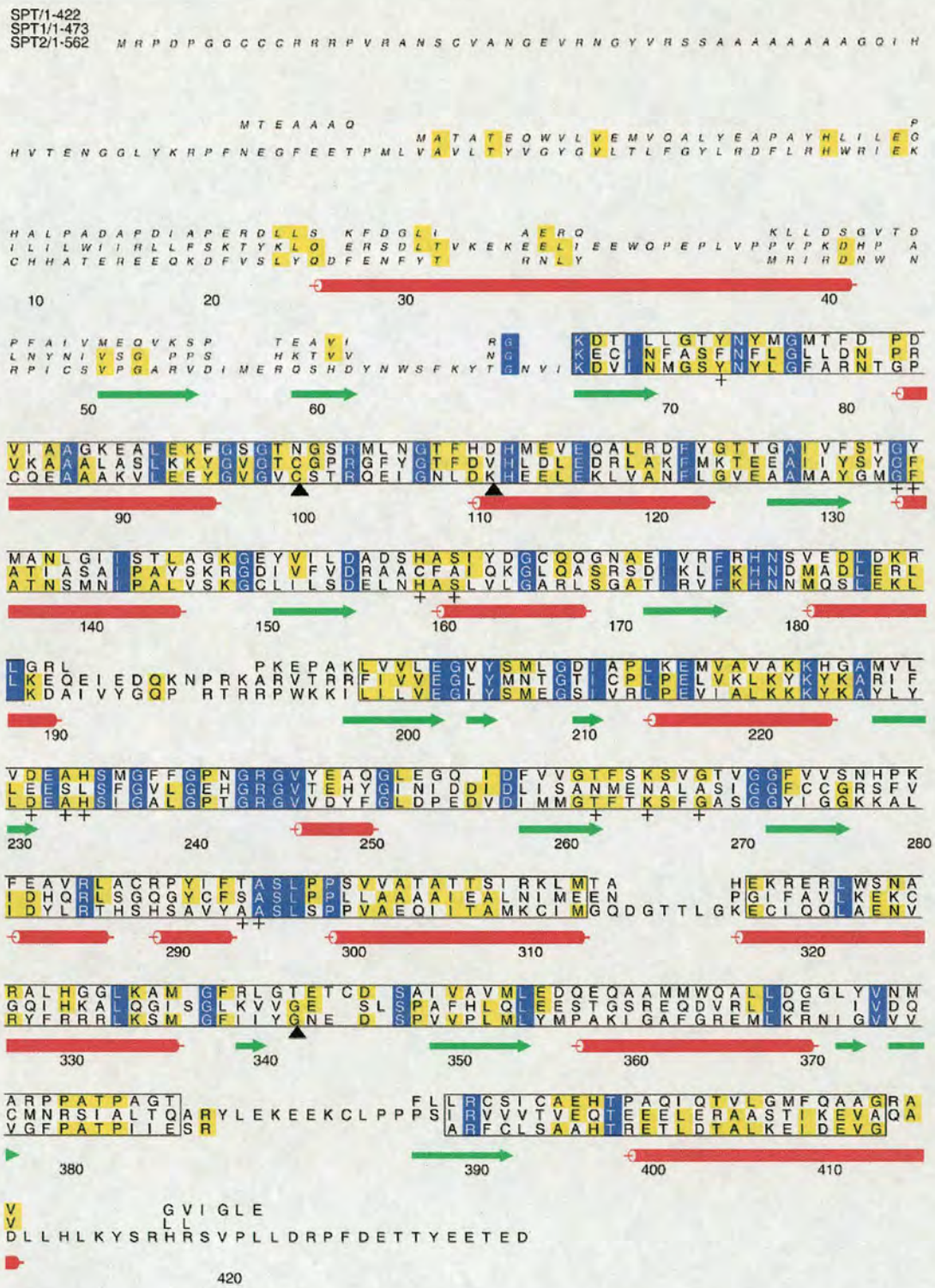

Figure 9. Alignment of *S. paucimobilis* SPT (Pubmed accession number: AB055142) to human SPT1 and SPT2 (UniProt Primary accession numbers: O15269, LCB1_Human and O15270, LCB2_Human, respectively). Residues are coloured to indicate conservation, numbering refers to the *S. paucimobilis* SPT sequence; + symbols denote important active site residues identified by examination of the SPT structure (also see Table 1). The secondary structure elements were identified with STRIDE[65] using the bacterial SPT structure. In general, SPT can be aligned relatively well to the human sequences. However, a region at the N terminus is more difficult to align, including the putative transmembrane sections of SPT1 and SPT2 (residues 16–36 and 67–87, respectively), as well as the first α-helix and the first two β-strands in the bacterial structure; this difficult alignment region is shown in smaller, italicised font. Regions considered to be relatively well-aligned are boxed. This Figure was produced using Alscript.[73]

Table 1. Active site residues identified by Ligplot and analyses in Chimera of the *S. paucimobilis* holo-SPT (SPT) structure as well as the homology model for the wild-type human SPT1/SPT2 heterodimer

SPT	SPT1	SPT2	Suggested function
Y73	F106	Y176 (496)	Hydrophobic interactions with Lys265
G134	G167	G238 (558)	Interacts with phosphate of PLP
Y135	F168	F239 (559)	Interacts with phosphate of PLP
H159	C192	H263 (583)	Stacks above pyridinium ring of PLP
S161	A194	S265 (585)	Part of strictly conserved HAS motif
D231	E274	D344 (664)	Makes polar contacts to N1 of pyridinium ring
A233	S276	A346 (666)	Hydrophobic interactions with PLP
H234	L277	H347 (667)	Hydrogen bond to oxygen of pyridinium ring
T262	N306	T376 (696)	Interacts with phosphate of PLP
S264	E308	T378 (698)	Unknown
K265	N309	K379 (699)	Forms an internal aldimine with PLP
S266	A310	S380 (700)	Unknown
V267	L311	F381 (701)	Unknown
G268	A312	G382 (702)	Hydrogen bond to backbone oxygen of Lys265
T294	S338 (296)	A408	Interacts with phosphate of PLP
A295	A339 (297)	A409	Interacts with phosphate of PLP

Numbers given in parentheses refer to the numbering in the homology model and also serve to distinguish residues that are thought to participate in the active site.

effect on the "active" SPT2 subunit, and on SPT activity as a whole. Residue Asn100 in the bacterial sequence maps to human SPT1 Cys133, and is located in the *S. paucimobilis* holo-SPT structure at the dimer interface and more importantly close to the active site (Figure 7). The amino group of the side-chain of Asn100 from monomer B is within hydrogen bonding distance of the backbone oxygen from the active site residue (Lys265) of monomer A. Thus, substitution by Trp or Tyr would be expected to affect the enzyme activity. The homology model for the HSAN1 C133W mutant shows a steric clash between Trp133 and the backbone carbonyl oxygen of the active site lysine residue which anchors the PLP cofactor (Figure 10(b)), suggesting that this mutation exerts direct perturbations to the geometry of the active site and consequently affects the enzyme activity. Indeed, in the WT model Cys133 does not contact the cofactor (Figure 10(a)). Additionally, the mutant model suggests that Trp133 contacts SPT2 active site residue Thr378, as well as being likely to affect SPT2 active site residue Tyr176 *via* contact with residue Asn177.

The WT model reveals V144 in α-helix3 (H3), packing with several hydrophobic residues in α-helix9 (H9) (Figure 10(c)). We postulate that V144 could be important in stabilising the packing of these two helices. Indeed, the models predict the N-terminal half of H9 to be composed of hydrophobic residues; interpretation of the V144D mutant model suggest that alterations to the H3-H9 packing may cause shifts in the neighbouring structure (Figure 10(d)). The opposite face of H9 is seen to contact the C-terminal portion of α-helix 2 (H2), which is predicted to be adjacent in space to the region of the active site containing SPT2 residues Ser380 and Gly382. Furthermore, the loop between H2 and H3 (SPT1 residues 129–149) appears close to the cofactor and is the location of the pathogenic Cys133 mutations. Therefore movement of the C terminus of H2 is likely to disturb the H2–H3 loop and be communicated to the active site. Thus, the V144D mutation may conceivably disturb the active site geometry by inducing rearrangements of H9, H3, H2, and the H2-H3 loop. Indeed, in the V144D mutant model the active site geometry is altered, and we suggest that the cofactor encounters steric clashes, causing disruption of hydrogen bonding when compared to the WT model. Therefore, analysis of the models suggests that the HSAN1 V144D mutation, despite being remote from the cofactor, can still influence the active site geometry and lead to a reduction in enzyme activity.

Conclusion

The high-resolution structure presented here is not only the first structure of a SPT, but is also the first crystal structure reported for any enzyme involved in sphingolipid biosynthesis. SPT catalyses the first and rate-limiting step of this pathway and our work now allows an in-depth analysis of the structure and mechanism of this important enzyme. Mutations of human SPT have been shown to directly affect enzyme activity and cause a range of neuropathological defects leading to the condition known as hereditary sensory and autonomic neuropathy (HSAN). The homodimeric, bacterial enzyme shows sufficient sequence conservation with the human SPT1/SPT2 heterodimer to allow generation of models and our study provides some insight into the molecular mechanisms of the human disease HSAN1.

Materials and Methods

Plasmids and competent *E. coli* cells were purchased from Novagen, all chromatography columns were from GE Healthcare, restriction endonucleases and DNA ligase were purchased from New England Biolabs. All buffers and reagents were from Sigma unless stated otherwise. Palmitoyl-CoA was from Roche, [U-^{14}C]serine (specific activity 1.85 MBq/ml) was from GE Healthcare. The *S. paucimobilis* strain 13361 was from the National Collection of Industrial and Marine Bacteria (NCIMB), Aberdeen, and is also known as strain DSM1098 (NCTC 11030).

Cloning and expression of *S. paucimobilis* SPT in *E. coli*

The full length *spt* gene was amplified by PCR from *S. paucimobilis* strain 13361 using chromosomal DNA as a template and PCR forward and reverse primers based on

the *spt* sequence deposited by Ikushiro *et al.* in the NCBI database with the accession number AB055142.[35] Primers were designed to incorporate BspHI and XhoI restriction enzyme sites at the 5′ and 3′ end of the gene, respectively (SPT BspHI forward: 5′ GGACACCGTCATGACC-GAAGCC 3′, SPT XhoI reverse: 5′ GATCCTCGAGGCC-GATGACGCCGACCGCGCGGCCC 3′). The BspHI site spanned the start codon and the XhoI site removed the stop codon and allowed the gene to be cloned as a C-terminal six-histidine tagged fusion. The PCR product of 1263 bp was cloned into pCR2.1 (Invitrogen) and positive clones were isolated and sequenced to confirm the identity of the *spt* gene and the incorporation of the restriction enzyme sites. A positive pCR2.1/SPT clone was digested with BspHI and XhoI and the isolated *spt* gene ligated into pET-28a cut with the restriction enzymes NcoI and XhoI. Positive clones were isolated and identified by restriction enzyme analysis, sequenced to confirm the fidelity of the clone and consequently named pET-28a SPT. The sequence of the SPT used in our study from *S. paucimobilis* strain 13361 is 100 % identical to that isolated from *S. paucimobilis* strain EY2395.[35]

Plasmid pET-28a SPT was used to transform *E. coli* HMS 174 (DE3) competent cells and selection was carried out on LB agar containing 30 μg/ml of kanamycin. A single colony was used to innoculate 500 ml of 2YT broth (16 g/l Bacto-tryptone, 10 g/l Bacto-yeast extract, 5 g/l sodium chloride (pH 7.5)) which was shaken at 250 rpm overnight at 37 °C. The overnight culture was added to 4 l of 2YT broth supplemented with kanamycin and grown at 37 °C to an A_{600} of 0.6. Protein expression was induced by the addition of IPTG to give a final concentration of 0.1 mM and growth was continued for 6 h at 30 °C. The cells were harvested (Sorvall RC5-B centrifuge) by centrifugation at 3500 rpm for 20 min at 4 °C.

Purification of pET-28a SPT

All purification steps were carried out at 4 °C. The cell pellet (~10 g) was resuspended in Ni-NTA binding buffer 4:1 (v/w) (20 mM potassium phosphate (pH 7.5), 25 μM PLP, 150 mM NaCl, 10 mM imidazole and one EDTA-free protease tablet (Roche)) before being disrupted by sonication (Soniprep 150) for 15 cycles (30 s on, 30 s off) on ice. The cell debris was harvested by centrifugation at 16,000 rpm for 30 min. The cell-free extract was filtered (0.45 μm syringe filter) before being loaded onto a 5 mL HisTrap™ column at 0.5 ml/min. The column was washed with binding buffer until all unbound proteins had been eluted and then a linear gradient of 10 mM–500 mM imidazole gradient was applied over 20 column volumes (100 ml). Fractions containing the SPT protein were analysed by SDS–PAGE before being combined for dialysis against three changes of buffer (20 mM potassium phosphate (pH 7.5), 150 mM NaCl, 25 μM PLP, 2 mM EDTA). This sample was then loaded onto a previously calibrated HiPrep™ 26/60 Sephacryl™ S-200 size exclusion column. Recombinant SPT was eluted at a flow rate of 1 ml/min in buffer (10 mM Tris (pH 7.5), 150 mM NaCl, 25 μM PLP, 1 mM EDTA). The presence of a SPT dimer was calculated using the calibration curve of known molecular mass standards (GE Healthcare).

The purity of the SPT from the size exclusion column was analysed by SDS–PAGE and the protein concentration was measured using the BCA™ protein assay kit (Pierce) giving a yield of ~10 mg protein per litre of initial *E. coli* cell culture. The enzyme was dialysed against 10 mM Tris (pH 7.5), 150 mM NaCl, 25 μM PLP at 4 °C in preparation for crystallisation. Initially, excess PLP was removed using a PD10 column (GE Healthcare) before being concentrated, routinely to 20 mg/ml, using a VivaSpin 10 kDa cut-off concentration filter.

Structural biology

The protein was screened for suitable crystallisation conditions using the high-throughput facilities at the Scottish Structural Proteomics Facility (SSPF). The crystallisation conditions were screened using a nano-drop crystallisation robot (Cartesian Honeybee, Genomic Solutions) as part of the Hamilton-Thermo Rhombix system. Over 700 conditions were tested from commercially available sparse-matrix screens, using sitting-drop vapour-diffusion with a well volume of 100 μl in 96 well plates (Griener; 3-square) at 20 °C. Drop sizes of 0.2 μl (containing 0.1 μl of protein and 0.1 μl well solution) and 0.3 μl (containing 0.2 μl of protein and 0.1 μl well solution) were used. Several conditions produced initial crystals and these were optimised using the Rhombix system. Small (<0.05 mm × 0.05 × 0.2 mm) colourless cubic crystals were produced by adding 0.1 μl of 24 mg/ml SPT in 10 mM Tris (pH 7.5), 150 mM NaCl, 25 μM PLP, 5 μl of myriocin, to 0.1 μl of 10% PEG 8000, 0.17 M $MgCl_2$, 0.1 M Tris (pH 6.5) well solution. These crystals were mounted in cryo-loops (Hampton Research) and then cryo-protected by passing the crystals through a mixture of 20% (v/v) glycerol and well solution. Crystals were then frozen by rapid immersion in liquid nitrogen, and transferred to sample changer baskets (Molecular Dimensions). Multiple crystals were screened at Beam Line BM14, Grenoble, ESRF using the sample changer, and a low-resolution dataset (3.0 Å) was collected from the "best" (highest diffraction resolution) single crystal at 100 K.

Data were indexed and scaled with DENZO and SCALEPACK as implemented in the CCP4 suite[47] (statistics are shown in Table 2). Analysis of the solvent content suggested that there were two molecules in the asymmetric unit (50% solvent; Matthew's coefficient[48] 2.5). Initial phases were determined using molecular replacement, with a homology model generated from the KBL (PDB code 1FC4) monomer structure and confirmed a dimer. The molecular replacement model was built using the CASPR server.[49] Initial analysis of the density showed that this crystal did not have PLP bound in either subunit; in one subunit a water molecule was observed in the active site. This indicated we had crystallized the apo-form of the enzyme from the solution (or at least predominantly apo-form), despite the presence of PLP in the crystallisation solution. There was also no observable density for myriocin.

The initial hits were further optimized using screens generated using the Crystools server.[50] The protein was dialysed in the presence of excess PLP to ensure complete reloading prior to crytallisation. Contrary to preparation of the apo-SPT, excess PLP was not removed by size exclusion using a PD10 column. Crystallisation trials were set up in sitting drop plates (EasyXtal DG-CrystalSupport; Qiagen). A large yellow crystal (~0.8 mm × 0.2 × 0.2 mm) grew in a 2 μl drop, consisting of 1 μl 20 mg/ml SPT in 10 mM Tris (pH 7.5), 150 mM NaCl and 25 μM PLP and 1 μl of the well solution (0.11M $MgCl_2$, 21% (w/v) PEG3350, 0.10M Hepes (pH 6.5)). The crystal was mounted in a cryo-loop and cryo-protected in a solution containing 22% PEG 3350, 100 mM Hepes (pH 6.5), 120 mM $MgCl_2$, 20% PEG 400.

The crystal was then frozen and shipped to the ESRF where a 1.3 Å dataset was collected at BM14 at 100 K. Data were processed with MOSFLM and SCALA and are

shown in Table 2. Analysis of the solvent content suggested that there was one molecule in the asymmetric unit (33% solvent; Matthew's coefficient, 1.9 Da Å^3). Phases were calculated with Phaser,[51,52] using the partially refined apo structure as a starting model. Automated model building in ArpWarp[53] successfully built 391 residues out of 427, and produced an initial model with an *R*-factor of 19.5% and a R_{free} of 23.2%.

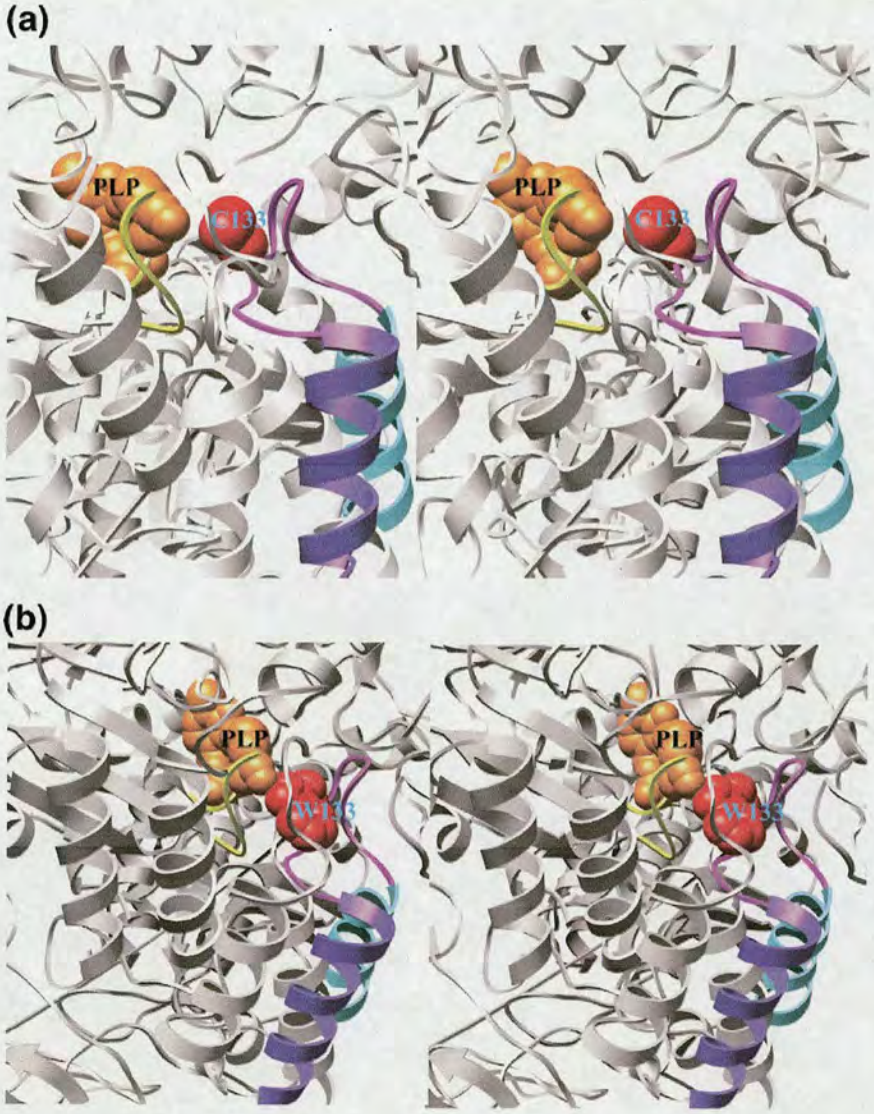

Figure 10. Homology modelling insights into the molecular pathogenesis of human SPT1 C133W and V144D mutations found in HSAN1. In all panels the PLP cofactor is shown in orange, α-helix 2 (H2) in purple, α-helix 3 (H3) in cyan, and the H2–H3 loop in magenta. Unless otherwise specified, residue numberings refer to SPT1. All panels are rendered in stereo view. (a) The wild-type (WT) model with C133 (red) close to, but not contacting the cofactor. The S^{γ} atom of the C133 side-chain is closest to the phosphate oxygen of the PLP cofactor (van der Waals distance of 0.73 Å to the PLP O2P). (b) The C133W mutant model, the W133 (red) C^{δ} and N atoms clash with the backbone carbonyl oxygen of Lys265 which binds the PLP cofactor. The W133 C^{δ} has 0.65 Å van der Waals overlap with the Lys265 carbonyl oxygen. (c) The WT model, with Val144 (red) packing with Ile350, Ala346 and Ala347 (all shown in yellow). These residues form part of α-helix 9 (H9), shown in blue. The C^{γ} atom of the V144 side-chain is the closest to the PLP cofactor (van der Waals distance of 13.6 Å from the PLP O2P). (d) The V144D mutant model, the Asp144 mutation appears to destabilise the H3-H9 packing and is likely to cause shifts in the neighbouring structure. We highlight Pro343 (blue) at the N terminus of H9, disturbance of this and other residues by perturbations of the H3–H9–H2 interactions is postulated to affect the H2–H3 loop (magenta). For example, Val130 (magenta) on the H2–H3 loop contacts SPT2 residues associated with the active site Ala383 and Gly382 (green); SPT2 Ser380 (green) is also likely disturbed by movements in these residues. Moreover, the H2–H3 loop is the site of the C133W mutation, thus perturbations in the H2-H3 structure are likely to disturb the active site geometry. The C^{β} atom of the D144 side-chain is closest to the PLP cofactor (van der Waals distance of 14.1 Å from the PLP O2P). This Figure was produced using Chimera,[66] GIMP [http://www.gimp.org/] and Adobe Illustrator [http://www.adobe.com/products/illustrator/].

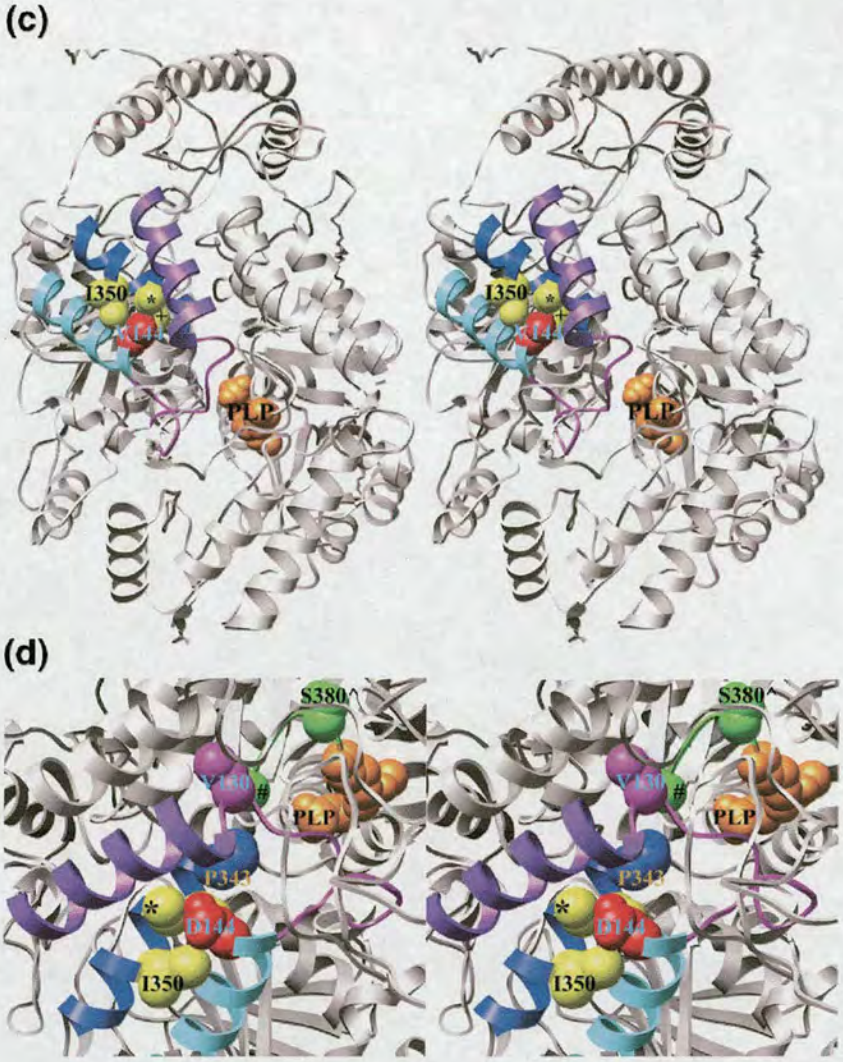

Figure 10 (*legend on previous page*)

Analysis of the density revealed that the PLP was covalently bound to Lys265, confirming we had obtained the holo-form of the protein. Both apo and holo models were refined using Refmac5[54] and manually adjusted by Coot.[55] The apo structure was refined using isotropic *B* factors, with tight non-crystallographic restraints applied between the two monomers for the whole of the refinement process.

The process of completing the apo structure was greatly helped by using the 1.3 Å holo-SPT structure as a guide. The holo structure was refined with anisotropic *B* factors, with TLS refinement used in the later rounds of the refinement process. Waters were added and checked using Coot.[55] Structure quality was checked using tools within Molprobity.[56] The final model statistics are shown in Table 2. In the holo-SPT structure the first 21 residues and the C-terminal tag are disordered. Superpositions were carried out using the SSM algorithm implemented in CCP4.[47] The root-mean-square deviation (RMSD) between chain A of the apo and holo structures is 1.0 Å over 355 C^{α} atoms. The largest differences occur in a number of flexible loops, which are poorly ordered in the apo structure. There is no evidence of large domain movements between the apo and holo structures. There is a slight rigid body movement of the monomers with respect to each other in the apo compared to holo-SPT dimer. Whether this affect is caused by PLP binding or is a result of crystal packing is unclear.

Spectroscopic measurements

All UV-visible spectra were recorded on a single-beam Hewlett-Packard 8452A diode array spectrophotometer and analysed using UV-Visible ChemStation software (Agilent). To convert the apo-SPT to holo-SPT the enzyme was dialysed for 1 h at 4 °C against 20 mM potassium phosphate (pH 7.5) containing 150 mM NaCl, 25 μM PLP and 2.0 mM EDTA. Excess PLP was removed by passing the protein through a PD-10 (Sephadex G-25M) desalting column (GE Healthcare) before any spectrophotometric measurements were taken (Figure 3(a)). The concentration of recombinant SPT was 20 μM

Table 2. X-ray crystallographic data

Data details	apo-SPT	holo-SPT
Integration software	Denzo	Mosflm
Scaling software	Scalepack	Scala
Space group	$C222_1$	$C222_1$
Unit cell parameters (Å)	a=93.87, b=109.54, c=187	a=74.2, b=107.6, c=90.32
Matthew's coefficient	2.6	1.9
Solvent content (%)	53	35
Monomers in asymmetric unit	2	1
Wavelength (Å)	0.976	0.9785
Observations	152,432	692,849
Resolution range (Å)	50–3.0 (3.11–3.0)	30–1.3 (1.37–1.3)
Number of reflections	19,635 (1927)	88,217 (12,783)
Completeness (%)	99.5 (99.9)	99.7 (100.0)
Mean $I/\sum(I)$	21 (5)	19.7 (2.9)
R_{merge} [a]	0.08 (0.49)	0.07 (0.50)
Redundancy	7.8 (8.2)	7.9 (5.2)
Refinement statistics		
Resolution range (Å)	20–3.0 (3.07–3.00)	18.8–1.3 (1.33–1.30)
Number of reflections (working)	18,544 (1325)	83,750 (6020)
Number of reflections (test)	996 (57)	4422 (355)
Completeness (% total)	99.6 (99.42)	99.57 (98)
$R_{working}$ [b] (%)	25 (31)	15 (27)
R_{free} [b] (%)	28 (38)	18 (32)
Mean B Factor (Å)	85	13.65
Stereochemical parameters		
Bond length (RMS observed) (Å)	0.008	0.002
Bond angle (RMS observed) (deg.)	1.3	1.2
Protein residues	720	397
Water molecules	39	415
Magnesium molecules	0	1
Total atoms	5563	3470
Ramachandran plot Favoured/ allowed/outliers (%)	99.3/94/0.6	97.8/100/0
PDB code	2jgt	2jg2

[a] $R_{merge}=\sum_{hkl}\sum_i|I_{hkl,\,i}-\langle I_{hkl}\rangle| / \sum_{hkl}\langle I_{hkl}\rangle$, where $I_{hkl,\,i}$ is the intensity of the ith measurement and $\langle I_{hkl}\rangle$ is the weighted mean of all measurements of I_{hkl}.

[b] $R_{working}$ (and R_{free})$=\sum||F_o|-|F_c|| / \sum|F_o|$, where F_o and F_c are the observed and calculated structure factors.

and the spectrophotometer was blanked with 20 mM potassium phosphate (pH 7.5) containing 2.0 mM EDTA and 150 mM NaCl.

Mass spectrometry

Protein masses were determined by high-pressure liquid chromatography electrospray mass spectrometry (HPLC ESI-MS). These were carried out on a MicroMass Platform II quadrupole mass spectrometer equipped with an electrospray ion source. Protein samples were separated with a Waters HPLC 2690 fitted with a Phenomenex C5 reverse phase column. Data were acquired and analysed using MassLynx software (V4.0). The experimentally determined mass of recombinant *S. paucimobilis* SPT (45,969.64 (±4.93) Da) is in good agreement with the expected mass of 46,104 Da for apo-SPT (428 amino acids, which includes the C-terminal LEHHHHHH fusion affinity tag). The mass obtained represents SPT having lost the N-terminal methionine residue (expected mass without N-terminal methionine is 45,973 Da).

Assay of recombinant SPT activity

The activity of the purified SPT enzyme was based on a published radioactive assay which monitors the condensation of L-[U-^{14}C]serine and palmitoyl-CoA to produce the ^{14}C-labelled 3-ketodihydrosphingosine (KDS) product.[35] A typical assay was carried out on a 500 µl scale and contained 20 µM SPT in 50 mM Hepes (pH 7.5), 150 mM KCl, 0.1 mM EDTA, 20 mM L-[U-^{14}C]serine (9250 Bq/0.250 µCi; GE Healthcare) and 1.6 mM palmitoyl-CoA. The reaction was incubated at 37 °C for 20 min and terminated by the addition of 2.0 M NH_4OH to a final concentration of 0.4 M. The lipid portion was extracted with an equal volume of $CHCl_3/CH_3OH$ (2:1, v/v). The sample was centrifuged and the aqueous layer was removed before the organic solvent was allowed to evaporate in air. The lipid residue was resuspended in 15 µl of $CHCl_3/CH_3OH$ (2:1, v/v) and spotted onto a Silica Gel 60 TLC plate. The lipids were separated with $CHCl_3/CH_3OH/NH_4OH$ (40:10:1, by vol.) and the TLC was exposed to a Storage Phosphor Screen (GE Healthcare) for five days at room temperature. The screen was developed using a Storm Phosphor Imager (GE Healthcare) and the image visualised using ImageJ software (Figure 3(b)). For comparison, a reference sample of 3-ketodihydrosphingosine (KDS; Avanti Polar Lipids) was analysed on a Silica Gel 60 TLC plate as described above. The KDS was detected using a ninhydrin spray and its *Rf* value agrees with published values.

Multiple sequence alignments for homology modelling

Multiple sequence alignment (MSA) can be more accurate when more related sequences are aligned.[57] Additionally, an MSA of many related sequences is useful for identifying core, relatively reliable, alignment regions. Evaluation of the alignment quality is a key factor in assessing the reliability of analysis based on the associated homology models. The *S. paucimobilis* SPT sequence (Pubmed accession number AB055142) formed the basis to search for sequences to include in the first MSA. The BLASTP[45] top hit from a search of the COG[58] database identified COG0156, thus the 78 sequences from this COG were included. Also included were 347 sequences found *via* PSIBLAST searching (five iterations, default settings) the SEG[59] and Helixfilt (D. Jones, unpublished results) filtered UniRef100[60] database. Additionally the Ensembl[61] human SPT1 (UniProt Primary accession number O15269; LCB1_Human) and human SPT2 (UniProt Primary accession number O15270; LCB2_Human) isoforms were included. Magicmatch[62] was used to filter out identical sequences leaving a total of 411 sequences for the first of several rounds of MSA using Mafft6.234‡[63] with the "linsi" setting (iterative refinement for maximum accuracy). Jalview[64] was employed to examine this alignment annotated with the STRIDE[65] secondary structure assignments and Chimera[66] assigned inter-monomer contacts of the *S. paucimobilis* SPT holo-enzyme homodimer, as well as the Jnet[67] predicted secondary structure for the human SPT1 and SPT2 sequences. Visual inspection drawing on this information as well as the Swissprot[68] annotation for

‡ http://align.bmr.kyushu-u.ac.jp/Mafft/software/

human SPT1 and SPT2 then allowed the exclusion of divergent sequences for the next round of MSA using Mafft. Two further rounds of MSA and visual inspection were conducted, leading to the exclusion of 23 sequences. Then the Pfam00155 seed alignment (48 sequences)[69] was aligned to this alignment using Mafft; this Pfam family provides substantial coverage of the sequences of interest (residues 98–464 and 168–528 of the human SPT1 and SPT2 sequences, respectively). A further round of visual inspection excluded a further two sequences leaving a final set of 434 sequences; this final alignment was then edited with consideration of the alignment of the *S. paucimobilis* SPT structure/sequence to the human SPT1 and SPT2 sequences. Figure 9 shows the final alignment of these three sequences, which was used as the starting point for homology modelling. Structural visualisation was performed with both Chimera and RASMOL.[70]

Homology modelling

Several rounds of homology modelling were performed using Modeller,[71] with selective removal of restraints according to inspection of the Modeller probability densities (temperature factor estimates) and the MSA. The *S. paucimobilis* SPT homodimer holo structure was used as a template for modelling the human SPT1 and SPT2 sequences as a heterodimer with the cofactor included as a block residue. Modeller parameters for the final rounds of modelling were set to obtain high-quality models (model at level 3 and refine at level 5), with a total of 15 models attempted per Modeller run (three models, each with five loop models). The model with the lowest value of the Modeller objective function was selected and then side-chain rebuilding was performed using SCWRL.[72]

Protein Data Bank accession number

The coordinates can be downloaded from the RCSB PDB using accession codes 2JGT for apo-SPT and 2JG2 for holo-SPT.

Acknowledgements

We are grateful to the UK BBSRC (Biotechnology and Biological Sciences Research Council) for funding the SSPF SPORT facility (Scottish Structural Proteomics Facility Structural Proteomics Of Rational Targets) initiative (grant BBS/B/14434). J.H.N. is a Career Development Fellow of the BBSRC. B.A.Y. thanks The School of Chemistry, University of Edinburgh and Syngenta Agrochemicals for their support. D.J.C. thanks the Royal Society of Edinburgh for the award of a RSE/Scottish Executive Personal Research Fellowship and the Big Lottery and Cystic Fibrosis Trust for support. Thanks to Dr J. Procter for advice on using Modeller and Dr T. Walsh for computational assistance. I.M.O. and G.J.B. acknowledge financial support from the SSPF SPORT initiative. We thank Professor Bob Baxter for his enthusiastic support of this work and for his critical reading of the manuscript and Dr Andy Corran (Syngenta) for his support throughout this project.

Supplementary Data

Supplementary data associated with this article can be found, in the online version, at doi:10.1016/j.jmb.2007.04.086

References

1. Futerman, A. H. & Hannun, Y. A. (2004). The complex life of simple sphingolipids. *EMBO Rep.* **5**, 777–782.
2. Kobayashi, T., Takahashi, M., Nagatsuka, Y. & Hirabayashi, Y. (2006). Lipid rafts: new tools and a new component. *Biol. Pharm. Bull.* **29**, 1526–1531.
3. Merrill, A. H. (2002). De Novo sphingolipid biosynthesis: a necessary, but dangerous, pathway? *J. Biol. Chem.* **277**, 25843–25846.
4. Hirabayashi, Y., Igarashi, Y. & Merrill, A. H. (2006). *Sphingolipid Biology*, 1st edit., Springer-Verlag, Tokyo.
5. Thudichum, J. L. (1884). *A Treatise on the Chemical Constitution of the Brain*. Bailliere, Tindall and Cox, London.
6. Carter, H. E., Haines, H. W., Ledyard, W. E. & Norris, W. P. (1947). Biochemistry of the sphingolipides. *J. Biol. Chem.* **169**, 77–82.
7. Hanada, K. (2003). Serine palmitoyltransferase, a key enzyme of sphingolipid metabolism. *Biochim. Biophys. Acta*, **1632**, 16–30.
8. Eliot, A. C. & Kirsch, J. F. (2004). Pyridoxal phosphate enzymes: mechanistic, structural, and evolutionary considerations. *Annu. Rev. Biochem.* **73**, 383–415.
9. Mehta, P. K. & Christen, P. (2000). The molecular evolution of pyridoxal-5′-phosphate-dependent enzymes. *Adv. Enzymol. Relat. Areas Mol. Biol.* **74**, 129–184.
10. Schneider, G., Kack, H. & Lindqvist, Y. (2000). The manifold of vitamin B6 dependent enzymes. *Struct. Fold. Des.* **8**, R1–R6.
11. Alexeev, D., Alexeeva, M., Baxter, R. L., Campopiano, D. J., Webster, S. P. & Sawyer, L. (1998). The crystal structure of 8-amino-7-oxononanoate synthase: a bacterial PLP-dependent, acyl-CoA-condensing enzyme. *J. Mol. Biol.* **284**, 401–419.
12. Webster, S. P., Alexeev, D., Campopiano, D. J., Watt, R. M., Alexeeva, M., Sawyer, L. & Baxter, R. L. (2000). Mechanism of 8-amino-7-oxononanoate synthase: spectroscopic, kinetic, and crystallographic studies. *Biochemistry*, **39**, 516–528.
13. Jordan, P. M. & Shemin, D. (1972). 5-Aminolevulinic acid synthase. In *The Enzymes* (Boyer, P. D., ed.), 3rd edit., vol. 7, pp. 339–356. Academic Press, London.
14. Ferreira, G. C. & Gong, J. (1995). 5-Aminolevulinate synthase and the first step of heme biosynthesis. *J. Bioenerg. Biomembr.* **27**, 151–159.
15. Astner, A., Schulze, J. O., van den Heuvel, J., Jahn, D., Schubert, W. D. & Heinz, D. W. (2005). Crystal structure of 5-aminolevulinate synthase, the first enzyme of heme biosynthesis, and its link to XLSA in humans. *EMBO J.* **24**, 3166–3177.
16. Schmidt, A., Sivaraman, J., Li, Y., Larocque, R., Barbosa, J. A., Smith, C. *et al.* (2001). Three-dimensional structure of 2-amino-3-ketobutyrate CoA ligase from *Escherichia coli* complexed with a PLP-substrate

intermediate: inferred reaction mechanism. *Biochemistry*, **40**, 5151–5160.
17. Hunter, G. A. & Ferreira, G. C. (1999). Lysine-313 of 5-aminolevulinate synthase acts as a general base during formation of the quinonoid reaction intermediates. *Biochemistry*, **38**, 3711–3718.
18. Zaman, Z., Jordan, P. M. & Akhtar, M. (1973). Mechanism and stereochemistry of the 5-aminolaevulinate synthetase reaction. *Biochem. J.* **135**, 257–263.
19. Alexeev, D., Baxter, R. L., Campopiano, D. J., Kerbarh, O., Sawyer, L., Tomczyk, N. *et al.* (2006). Suicide inhibition of alpha-oxamine synthases: structures of the covalent adducts of 8-amino-7-oxononanoate synthase with trifluoroalanine. *Org. Biomol. Chem.* **4**, 1209–1212.
20. Kerbarh, O., Campopiano, D. J. & Baxter, R. L. (2006). Mechanism of alpha-oxoamine synthases: identification of the intermediate Claisen product in the 8-amino-7-oxononanoate synthase reaction. *Chem. Commun.*, 60–62.
21. Buede, R., Rinker-Schaffer, C., Pinto, W. J., Lester, R. L. & Dickson, R. C. (1991). Cloning and characterization of LCB1, a *Saccharomyces* gene required for biosynthesis of the long-chain base component of sphingolipids. *J. Bacteriol.* **173**, 4325–4332.
22. Williams, R. D., Wang, E. & Merrill, A. H., Jr (1984). Enzymology of long-chain base synthesis by liver: characterization of serine palmitoyltransferase in rat liver microsomes. *Arch. Biochem. Biophys.* **228**, 282–291.
23. Hanada, K., Hara, T., Nishijima, M., Kuge, O., Dickson, R. C. & Nagiec, M. M. (1997). A mammalian homolog of the yeast LCB1 encodes a component of serine palmitoyltransferase, the enzyme catalyzing the first step in sphingolipid synthesis. *J. Biol. Chem.* **272**, 32108–32114.
24. Nagiec, M. M., Baltisberger, J. A., Wells, G. B., Lester, R. L. & Dickson, R. C. (1994). The LCB2 gene of *Saccharomyces* and the related LCB1 gene encode subunits of serine palmitoyltransferase, the initial enzyme in sphingolipid synthesis. *Proc. Natl Acad. Sci. USA*, **91**, 7899–7902.
25. Nagiec, M. M., Lester, R. L. & Dickson, R. C. (1996). Sphingolipid synthesis: identification and characterization of mammalian cDNAs encoding the Lcb2 subunit of serine palmitoyltransferase. *Gene*, **177**, 237–241.
26. Gable, K., Han, G., Monaghan, E., Bacikova, D., Natarajan, M., Williams, R. & Dunn, T. M. (2002). Mutations in the yeast LCB1 and LCB2 genes, including those corresponding to the hereditary sensory neuropathy type I mutations, dominantly inactivate serine palmitoyltransferase. *J. Biol. Chem.* **277**, 10194–10200.
27. Han, G., Gable, K., Yan, L., Natarajan, M., Krishnamurthy, J., Gupta, S. D. *et al.* (2004). The topology of the Lcb1p subunit of yeast serine palmitoyltransferase. *J. Biol. Chem.* **279**, 53707–53716.
28. Hanada, K., Hara, T., Fukasawa, M., Yamaji, A., Umeda, M. & Nishijima, M. (1998). Mammalian cell mutants resistant to a sphingomyelin-directed cytolysin. Genetic and biochemical evidence for complex formation of the LCB1 protein with the LCB2 protein for serine palmitoyltransferase. *J. Biol. Chem.* **273**, 33787–33794.
29. Hanada, K., Hara, T. & Nishijima, M. (2000). Purification of the serine palmitoyltransferase complex responsible for sphingoid base synthesis by using affinity peptide chromatography techniques. *J. Biol. Chem.* **275**, 8409–8415.
30. Chen, J. K., Lane, W. S. & Schreiber, S. L. (1999). The identification of myriocin-binding proteins. *Chem. Biol.* **6**, 221–235.
31. Gable, K., Slife, H., Bacikova, D., Monaghan, E. & Dunn, T. M. (2000). Tsc3p is an 80-amino acid protein associated with serine palmitoyltransferase and required for optimal enzyme activity. *J. Biol. Chem.* **275**, 7597–7603.
32. Bejaoui, K., Wu, C., Scheffler, M. D., Haan, G., Ashby, P., Wu, L. *et al.* (2001). SPTLC1 is mutated in hereditary sensory neuropathy, type 1. *Nature Genet.* **27**, 261–262.
33. Dawkins, J. L., Hulme, D. J., Brahmbhatt, S. B., Auer-Grumbach, M. & Nicholson, G. A. (2001). Mutations in SPTLC1, encoding serine palmitoyltransferase, long chain base subunit-1, cause hereditary sensory neuropathy type I. *Nature Genet.* **27**, 309–312.
34. Yasuda, S., Nishijima, M. & Hanada, K. (2003). Localization, topology, and function of the LCB1 subunit of serine palmitoyltransferase in mammalian cells. *J. Biol. Chem.* **278**, 4176–4183.
35. Ikushiro, H., Hayashi, H. & Kagamiyama, H. (2001). A water-soluble homodimeric serine palmitoyltransferase from *Sphingomonas paucimobilis* EY2395T strain. Purification, characterization, cloning, and overproduction. *J. Biol. Chem.* **276**, 18249–18256.
36. Ikushiro, H., Hayashi, H. & Kagamiyama, H. (2004). Reactions of serine palmitoyltransferase with serine and molecular mechanisms of the actions of serine derivatives as inhibitors. *Biochemistry*, **43**, 1082–1092.
37. Kawahara, K., Seydel, U., Matsuura, M., Danbara, H., Rietschel, E. T. & Zahringer, U. (1991). Chemical structure of glycosphingolipids isolated from *Sphingomonas paucimobilis*. *FEBS Letters*, **292**, 107–110.
38. Toney, M. D. (2005). Reaction specificity in pyridoxal phosphate enzymes. *Arch. Biochem. Biophys.* **433**, 279–287.
39. Hunter, G. A. & Ferreira, G. C. (1999). Pre-steady-state reaction of 5-aminolevulinate synthase. Evidence for a rate-determining product release. *J. Biol Chem.* **274**, 12222–12228.
40. Dunathan, H. C. (1966). Conformation and reaction specificity in pyridoxal phosphate enzymes. *Proc. Natl Acad. Sci. USA*, **55**, 712–716.
41. LeMagueres, P., Im, H., Ebalunode, J., Strych, U., Benedik, M. J., Briggs, J. M. *et al.* (2005). The 1.9 Å crystal structure of alanine racemase from *Mycobacterium tuberculosis* contains a conserved entryway into the active site. *Biochemistry*, **44**, 1471–1481.
42. Houlden, H., Blake, J. & Reilly, M. (2004). Hereditary sensory neuropathies. *Curr. Opin. Neurol.* **17**, 569–577.
43. Bejaoui, K., Uchida, Y., Yasuda, S., Ho, M., Nishijima, M., Brown, R. H., Jr *et al.* (2002). Hereditary sensory neuropathy type 1 mutations confer dominant negative effects on serine palmitoyltransferase, critical for sphingolipid synthesis. *J. Clin. Invest.* **110**, 1301–1308.
44. McCampbell, A., Truong, D., Broom, D. C., Allchorne, A., Gable, K., Cutler, R. G. *et al.* (2005). Mutant SPTLC1 dominantly inhibits serine palmitoyltransferase activity in vivo and confers an age-dependent neuropathy. *Hum. Mol. Genet.* **14**, 3507–3521.
45. Altschul, S. F., Madden, T. L., Schaffer, A. A., Zhang, J., Zhang, Z., Miller, W. & Lipman, D. L. (1997). Gapped BLAST and PSI-BLAST: a new generation of protein database search programs.. *Nucl. Acids Res.* **25**, 3389–3402.
46. Russell, R. B. & Barton, G. J. (1992). Multiple protein sequence alignment from tertiary structure comparison:

assignment of global and residue confidence levels. *Proteins: Struct. Funct. Genet.* **14**, 309–323.
47. CCP4 (1994). The CCP4 suite: programs for protein crystallography. *Acta Crystallog. sect. D*, **50**, 760–763.
48. Matthews, B. W. (1968). Solvent content of protein crystals. *J. Mol. Biol.* **33**, 491–497.
49. Claude, J. B., Suhre, K., Notredame, C., Claverie, J. M. & Abergel, C. (2004). CaspR: a web server for automated molecular replacement using homology modelling. *Nucl. Acids Res.* **32**, W606–W609.
50. Segelke, B. W. (2001). Efficiency Analysis of Screening Protocols Used in Protein Crystallization. *J. Crystal Growth*, **232**, 553–562.
51. CoyMc, A. J., Grosse-Kunstleve, R. W., Storoni, L. C. & Read, R. J. (2005). Likelihood-enhanced fast translation functions. *Acta Crystallog. sect. D*, **61**, 458–464.
52. Storoni, L. C., McCoy, A. J. & Read, R. J. (2004). Likelihood-enhanced fast rotation functions. *Acta Crystallog. sect. D*, **60**, 432–438.
53. Morris, R. J., Perrakis, A. & Lamzin, V. S. (2002). ARP/wARP's model-building algorithms. I. The main chain. *Acta Crystallog. sect. D*, **58**, 968–975F.
54. Murshudov, G. N., Vagin, A. A., Lebedev, A., Wilson, K. S. & Dodson, E. J. (1990). Efficient anisotropic refinement of macromolecular structures using FFT. *Acta Crystallog. sect. D*, **55**, 247–255.
55. Emsley, P. & Cowtan, K. (2004). Coot: model-building tools for molecular graphics. *Acta Crystallog. sect. D*, **60**, 2126–2132.
56. Davis, I. W., Murray, L. W., Richardson, J. S. & Richardson, D. C. (2004). MOLPROBITY: structure validation and all-atom contact analysis for nucleic acids and their complexes. *Nucl. Acids Res.* **32**, W615–W619.
57. Raghava, G. P. S., Searle, S. M. J., Audley, P. C., Barber, J. D. & Barton, G. J. (2003). OXBench: a benchmark for evaluation of protein multiple sequence alignment accuracy. *BMC Bioinformatics*, **4**, 47.
58. Tatusov, R. L., Fedorova, N. D., Jackson, J. D., Jacobs, A. R., Kiryutin, B., Koonin, E. V. *et al.* (2003). The COG database: an updated version includes eukaryotes. *BMC Bioinformatics*, **4**, 41.
59. Wooton, J. C. (1994). Non-globular domains in protein sequences: automated segmentation using complexity measures. *Comput. Chem.* **18**, 269–285.
60. Apweiler, R., Bairoch, A., Wu, C. H., Barker, W. C., Boeckmann, B., Ferro, S. *et al.* (2004). UniProt: the Universal Protein knowledgebase. *Nucl. Acids Res.* **32**, D115–D119.
61. Birney, E., Andrews, T. D., Bevan, P., Caccamo, M., Chen, Y., Clarke, L. *et al.* (2004). An overview of Ensembl. *Genome Res.* **14**, 925–928.
62. Smith, M., Kunin, V., Goldovsky, L., Enright, A. J. & Ouzounis, C. A. (2004). MagicMatch–cross-referencing sequence identifiers across databases. *Bioinformatics*, **21**, 3429–3430.
63. Katoh, K., Misawa, K., Kuma, K. & Miyata, T. (2002). MAFFT: a novel method for rapid multiple sequence alignment based on fast Fourier transform. *Nucl. Acids Res.* **30**, 3059–3066.
64. Clamp, M., Cuff, J., Searle, S. M. & Barton, G. J. (2004). The Jalview Java alignment editor. *Bioinformatics*, **20**, 426–427.
65. Frishman, D. & Argos, P. (1995). Knowledge-based protein secondary structure assignment. *Proteins: Struct. Funct. Genet.* **23**, 566–579.
66. Pettersen, E. F., Goddard, T. D., Huang, C. C., Couch, G. S., Greenblatt, D. M., Meng, E. C. & Ferrin, T. E. (2004). UCSF Chimera–a visualization system for exploratory research and analysis. *J. Comput. Chem.* **25**, 1605–1612.
67. Cuff, J. & Barton, G. J. (2000). Application of multiple sequence alignment profiles to improve protein secondary structure prediction. *Proteins: Struct. Funct. Genet.* **40**, 502–511.
68. Boeckmann, B., Bairoch, A., Apweiler, R., Blatter, M. C., Estreicher, A., Gasteiger, E. *et al.* (2003). The SWISS-PROT protein knowledgebase and its supplement TrEMBL in 2003. *Nucl. Acids Res.* **31**, 365–370.
69. Finn, R. D., Mistry, J., Schuster-Bockler, B., Griffiths-Jones, S., Hollich, V., Lassmann, T. *et al.* (2006). Pfam: clans, web tools and services. *Nucl. Acids Res.* **34**, D247–D251.
70. Sayle, R. A. & Milner-White, E. J. (1995). RASMOL: biomolecular graphics for all. *Trends Biochem. Sci.* **20**, 374–376.
71. Sali, A. & Blundell, T. L. (1993). Comparative protein modelling by satisfaction of spatial restraints. *J. Mol. Biol.* **234**, 779–815.
72. Canutescu, A. A., Shelenkov, A. A. & Dunbrack, R. L. J. (2003). A graph-theory algorithm for rapid protein side-chain prediction. *Protein Sci.* **12**, 2001–2014.
73. Barton, G. J. (1993). ALSCRIPT - a tool to format multiple sequence alignments. *Protein Eng.* **6**, 37–40.

Edited by R. Huber

(Received 22 February 2007; received in revised form 12 April 2007; accepted 18 April 2007)
Available online 10 May 2007